Ministry of Higher Education and Scientific Research

Monastir University

THESIS

Presented to fulfill the doctor degree requirements from the

National Engineering School of Monastir

In Energy Engineering

By Riheb Mabrouk

Sensible and Latent Heat Storage in porous media

Publicly defended on December 25, 2021

Jury Members

Mr. Abdallah Mhimid	**Professor**	**ENIM, Monastir**	**Chair**
Mr. Ammar Hidouri	**Associate-Professor**	**Faculté de science de Gafsa, Gafsa**	**Reviewer**
Mr. Walid Hassan	**Associate-Professor**	**ENIM, Monastir**	**Reviewer**
Mr. Hassane Naji	**Professor**	**Univ Artois, Univ Lille, France**	**Examinator**
Mr. Khalifa Slimi	**Professor**	**ENIM, Monastir**	**Examinator**
Mr. Hacen Dhahri	**Professor**	**ENIM, Monastir**	**Supervisor**

Laboratoire d'Etudes des Systèmes Thermiques et Energétiques (LESTE) LR99ES31

Acknowlagement

I wish to express deep gratitude to my supervisor **Hacen Dhahri**, Professor at ENIM University of Monastir, Tunisia, for his invaluable supervision and insight throughout the research process and for all the patience and support you gave me since the first day of my thesis completion. His consistent trust during my thesis work is greatly appreciated.

I would like to thank **Hassane Naji**, Professor at University of Artois and University of Lille, France, for accepting me as a visitor scholar and researcher in his Laboratory and the useful advice and support, for co-supervising, generously providing guidance and for all the patience and support you gave me. He was always there to lend a helping hand in this thesis.

I would like to thank **Abdallah Mhimid**, Professor at ENIM, University of Monastir, who has kindly accepted to be the president of the jury evaluating my thesis work.

I would thank also my committee members **Ammar Hidouri** Associate-Professor at Gafsa science faculty, University of Gafsa, and **Walid Hassan** Associate-Professor at ENIM, University of Monastir, for accepting to review my thesis. Their critical reviews and evaluations of my work resulted in the success of this PhD thesis.

Many thanks are also addressed to **Hassane Naji**, Professor at University of Artois and University of Lille, France, and **Khalifa Slimi**, Professor at ENIM, University of Monastir, Tunisia, for accepting to examine this thesis.

A special thanks to my family, words cannot express how grateful I am to my parents **Moktar** and **Salwa** for unconditional support, prayers for me all the time and encouragement to pursue my interests. This thesis is dedicated to them. No dedication can express the love, esteem, dedication and respect that I have always had for you. Nothing in the world is worth the efforts provided day and night for my education and my well-being. This work is the fruit of your sacrifices that you have made for my education and training.

I am deeply thankful to my brothers **Adnene** and **Ilyes** and my sister **Insaf** for their supports, sacrifices and help throughout my life. You have always been a major source of support when things would get a discouraging.

Without family kind support, it would be impossible for me to complete my PhD.

SOMMAIRE

General introduction

The population rate and economy are increasing exponentially, which has caused a massive growth in the demand and consumption of energy around the world, thus playing an important role in triggering serious environmental impacts. According to the statistics published by Eurostat in 2015, the member states of the European Union have experienced a remarkable raise in their energy demand that achieved around 1084 million tons of oil equivalent (Mtoe) where 422 Mtoe were used in building sectors which corresponds to 39% of the total energy demand [1]. For example the building sector, being the most consumer sector of energy, represents more than 33.33% of global energy consumption and is equally responsible for an important amount of CO2 emission [2]. Moreover, heating, ventilating, and air-conditioning (HVAC) systems accounts for over 50% of energy consumption in building sectors. Thereby an increase in renewables has made it possible to meet a large part of the demand. In the light of this purpose, policy makers and researchers are looking for new policies to have more sustainable and energy-efficient buildings, promoting crucial solutions to improve both energy saving and energy storage in order to dissuade the crisis of global warming.

Finding a novel strategy to promote and maintain energy efficiency in different sectors has been a major problem for governments and societies whose goal is to reduce energy consumption while ensuring thermal comfort whatever the weather conditions. The implementation of thermal energy storage (TES) technique allows attenuating of peak loads, eliminating of issues produced by the coupling between energy demand and its availability, integrating of renewables and ensuring efficient management of thermal energy, thereby enhancing energy efficiency. According to Sharma et al. [3] TES technologies are divided into thermal or thermochemical categories. The thermal approach consists of sensible and latent heat storage methods, which will remain our focus in this report. Yet, the thermochemical category is still limited in its applications due to its high cost, unavailability and ambiguous life span [3].

Latent heat storage (LHS) systems have received considerable attention in different applications due to their large energy storage density and the ability of phase change materials (PCMs) to store thermal energy during phase transition period at a constant temperature. An extensive TES technology related to heating and/or cooling enhancement by mitigating the energy demand is the integration of PCMs into applications, which have gained great attention and have become a topic of large interest over the last decade. PCMs are able to bridge the gap between energy supply and demand by storing and releasing energy, therefore

making it a promising solution. Currently, the use of PCMs covers various domains (such as building temperature regulation, waste heat recovery, compact heat exchangers, solar energy storage, concentrating solar plants, etc) including applications with a large temperature range (from 20 °C to 200 °C). However, the low thermal conductivity of PCMs is one of their weaknesses because it restricts thermal transport by giving rise to slow heat dissipation during charging/discharging processes. Wherefore, the use of metallic foams with PCMs is nowadays increasingly utilized as porous media to overcome this defect owing to their high thermal conductivity and their low cost. Indeed, this approach has recently attracted more attention which leads to an increase in the specific surface area of heat exchange and thus, to a rapid heat diffusion.

In the same research axis, the sensible heat storage (SHS) method depicts the most simple and economical mode of thermal storage where sensible heat storage materials (SHSMs) do not undergo any phase change during the storage cycle. The most common issue with liquid SHSMs is that they require large storage reservoir volume for heat transfer fluid (HTF) and expensive heat exchangers. Thereby, important studies have been carried out on SHS units using several solid SHSMs. Nevertheless, for all SHS devices, storage and recuperation processes must be performed efficiently to achieve high capacity performance. Therefore, SHS systems should meet the following criteria: low cost, large energy density, high interstitial heat transfer between HTF and storage medium, and reversible charging/discharging periods after multiple cycles. For this, it is important to investigate such parameters to enhance thermal performances of SHS systems and encourage their participation in the markets. On such a topic, the use of porous medium is one of the most promising solutions for improving the SHS efficiency.

Generally, as indicated above, each TES system presents certain benefits and drawbacks. Particularly, this study's attention is in LHS and SHS technologies using a porous metallic structure as a green and promising solution to meet energy demand and enhance thermal performances of systems. Therefore, the main object of this work is to define the new challenges in storing the sensible and latent energy through the use of porous materials and provide investigations of different parameters in order to identify the optimum conditions for storing the maximum of energy, by using a numerical analysis method: Lattice Boltzmann method (LBM).

This thesis is laid out as follows:

Chapter 1. A review on sensible and latent heat thermal energy storage systems in porous media.

This chapter covers the subject of SHS and LHS applications in different sectors in several respects. The integration of porous metallic structure in these methods is reviewed to explain this strategy. In addition, to numerically handle these physical phenomena, the LBM approach at the representative elementary volume (REV)-scale and pore-scale approaches is described based on results published in literature.

Chapter 2. Lattice Boltzmann simulation of forced convection melting of a composite phase change material with heat dissipation through an open-ended channel.

This chapter performs a numerical assessment of Reynolds number ($100 \le \mathrm{Re} \le 600$), Eckert number ($0 \le Ec \le 10$) and porosity ($0.4 \le \varepsilon \le 0.8$) effects on heat transfer under forced convection in an open-ended horizontal channel filled with a porous structure (metal foam) and a phase change material (PCM: paraffin). Simulations are achieved via the single relaxation time thermal lattice Boltzmann method (SRT-TLBM) at the REV scale using three distribution functions to handle the phase change phenomenon during charging and discharging periods

Chapter 3. Numerical investigation of metal foam pore density effect on sensible and latent heats storage through an enthalpy-based REV-scale lattice Boltzmann method.

In this chapter, the two-dimensional laminar flow and heat transfer in an open-ended rectangular porous channel (metal foam) including either a phase change material (LHS case) or water (SHS case) have been numerically investigated. The SRT-TLBM with triple distribution function has been employed at the REV scale to perform the pores per inch density ($10 \le PPI \le 60$) effects of the metal foam on the storage of sensible and latent heat during charging/discharging processes at two Re numbers of 200 and 400.

Chapter 4. Pulsating flow effects on phase change phenomenon in a porous channel using the Lattice Boltzmann method.

In this chapter, an LHS system composed of porous metal foams with PCM subjected to pulsating fluid flow was proposed and it was compared to the model developed in the first chapter. The effect of three porosities (0.7, 0.8 and 0.9), pulsating amplitude, A (=0.1, 0.5 and 0.9), and Strouhal number, St (=0.5 and 1) were investigated using the SRT-LBM at the REV scale.

References

[1] Olivieri, L., Tenorio, J. A., Revuelta, D., Navarro, L., Cabeza, L. F. (2018). Developing a PCM-enhanced mortar for thermally active precast walls. Const. Build. Mater., 181, 638-649.

[2] Devaux, P., Farid, M. M. (2017). Benefits of PCM underfloor heating with PCM wallboards for space heating in winter. Appl. Energy, 191, 593-602.

[3] Sharma, A., Tyagi, V. V., Chen, C. R., Buddhi, D. (2009). Review on thermal energy storage with phase change materials and applications. Ren. Sust. Energy Rev., 13 (2), 318-345.

Chapter 1

A review on sensible and latent heat thermal energy storage systems in porous media

Abstract

Sharing of renewables, reduction of energy consumption and optimization of energy management as an attempt to limit environmental problems (air pollution, global warming, acid rain etc.) has become the genuine concern for current advancing scientific engineering research. Furthermore, with the drastic growth in requirements in building and industrial sectors worldwide, the need for proper technique that allows enhancement in thermal performance of systems is addressed. Using sensible and latent heat storage materials (SHSMs and PCMs) for thermal energy storage mechanisms can meet the requirements such as thermal comfort in buildings when selected correctly. However, as the operating temperature changes, a series of complex technical issues arise, such as challenging heat transfer problems, leakage, corrosion, subcooling, supercooling etc. This work reviews the most recent research advances in sensible and latent heat storage using porous media strategy as potential technology from a technical point of view and supplies helpful information for researchers and engineers in the domain of energy storage. In this research paper, the status and challenges of PCMs incorporation methods are introduced. An up-to-date database of research documents was provided and their findings regarding the sensible and latent heat storage in porous medium, their field of application and their impact on energy consumption were discussed. It has been found that the implementation of porous matrix improves thermal performances of systems, reduces energy consumption, reduces CO2 emissions and assures thermal comfort in buildings. In addition, the lattice Boltzmann method (LBM) is reviewed from the aspect of different computational fluid dynamics (CFD) methods. LBM at the representative elementary volume (REV)-scale and pore-scale approaches are compared based on results published in literature. The robust ability of LBM at the REV and pore scale simulations to handle the phase change heat transfer mechanisms and sensible heat storage process in porous medium has been revealed. Finally, the prospects of sensible and latent energy storage technologies are summarized.

1. Introduction

Nowadays, energy storage sector figures as a fundamental technology facing to the rapid development of industrialization and urbanization. Thereby, over the years, energy storage systems (ESSs) technology has been widely developed to ensure the sustainability of

renewable energy resources and to balance the gap between energy demand and supply [1]. Throughout history, as the human population increases, the worldwide energy consumption augments more and more. This is clearly observed from figure. 1, energy use has increased faster than population size [2]. Yet, it is noteworthy to highlight the industrialization and welfare level as the factors responsible for the enormous energy consumption.

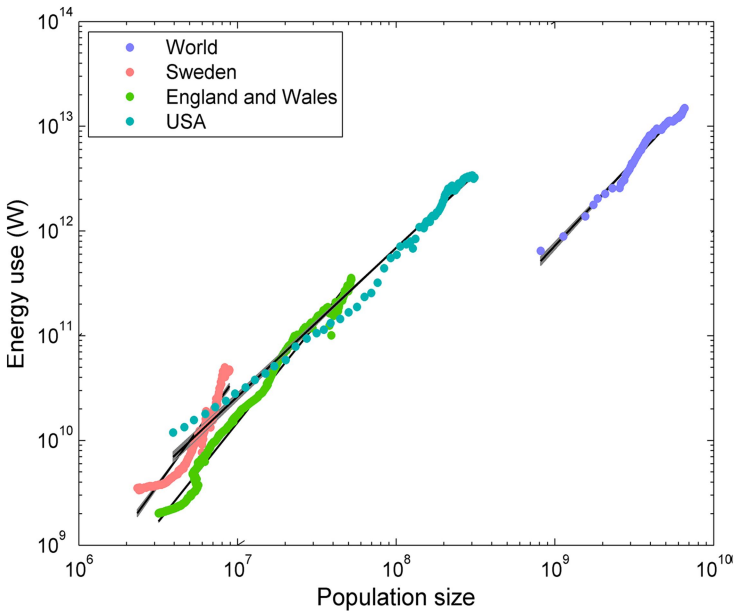

Figure 1. Energy use (W) profiles vs. population size for different regions through time [2].

Inevitably, it is crucial to implement ESS into energy systems not only to limit the intermittency of renewables, but also to facilitate the flexibility of energy systems rising their efficiency. Generally, the use of ESSs aims at matching the energy demand and supply. As illustrated in Table 1, there are different methods of ESSs that are used in various engineering applications [3].

Table 1. Energy Storage (ES) Methods [3].

Energy Storage Methods				
Thermal	**Mechanical**	**Electromechanical**	**Electrical**	**Chemical**
Sensible thermal	Pumped hydro	Electrochemical capacitors	Capacitors	Hydrogen storage
Latent thermal	Compressed air	Batteries	Super capacitors	Synthetic natural gas
Thermo-chemical	Flywheel	Fuel cells	Super conducting magnetic ES (SCMES)	

Among several ES methods, thermal energy storage (TES) appears as one of the emerging technologies that can bridge the intermittency gap in renewables such as solar energy [4],

save energy and promote environmental respect (greener world). TES systems consist of a storage medium, exploited to store thermal energy (heat and/or cold) that is reserved for a defined period, so as to use it when and where it is needed [4, 5]. Thereby, the applications of these systems (TES) are in building (air conditioning, thermal comfort, domestic hot water, etc.) and industrial sectors (chemical industry, food industry, etc.) [6]. It is important to underline that the estimated yearly potential energy savings at the European Union (EU) were 7.5% as a result of implementing these technologies: TES systems [7]. As for the environmental savings, the annual potential CO2 emissions were reduced by about 5.5% in the EU [7]. Later on, a 90% of the CO2 emissions mitigation is expected by 2050 according to the international renewable energy agency (IRENA) owing to the TES systems application (figure 2) [8]. Thus, this mechanism has attracted strong attention through an economic and environmental analysis in several sectors (figure 2).

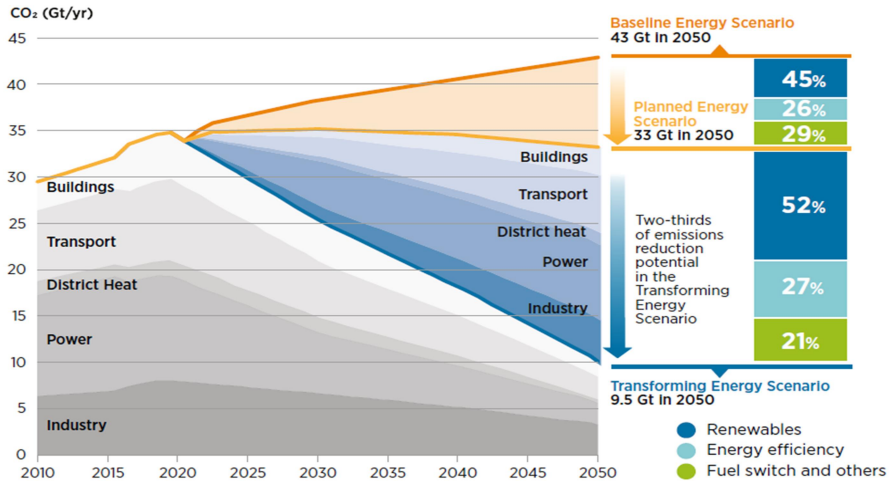

Figure 2. Yearly CO2 emissions related to different sectors of energy, 2010-2050 [8].

In the last decade, the scientific research on TES had achieved a record in numbers of published documents, which results more than 14.000 publications as indicated by Calderon et al. [9]. However, the choice of an appropriate TES system depends on various factors, basically depending on the field of application, technical conditions (volume, temperature span...etc), storage time and the economic aspect (marketability and cost-effectiveness) [10]. Considering the characteristics of the storage period, there are two types of TES systems called short-term storage systems and long-term storage systems. The first concept, short-term storage, has a storage cycle of a few hours and it is renowned as diurnal heat storage [11]. While the second concept, long-term storage, has a long charge and discharge periods that persist for several months and it is well known as seasonal heat storage [12]. In this context, as an example the storage of the solar thermal energy, seasonal TES (STES) stores heat

collected in summer last up to more than three months (charge period) using central solar heating plants and it is therefore used in winter (discharge period) [13]. Yet, the reverse process can also be applied [13]. Hence, this second category of TES systems (STES) has a significant contribution to the efficient use of renewables in building applications such as decarbonization and district heating [14, 15]. It is important to highlight that the STES systems are in competition with other large-scale techniques such as natural gas storage, pumped storage hydropower system and power-to-heat methods. Yet, sector coupling remains as the most important challenge for the future energy concepts. Furthermore, large scale TES systems are needed for the conception of any other technology. Thus, TES does not compete; but, it ensures the stability and resilience to the system.

Moreover, considering the characteristics of the energy storage method, TES solutions can be categorized into three methods of sensible heat storage (SHS), latent heat storage (LHS) (also known as phase change material (PCM)) and thermo-chemical energy storage (TCHS). Besides, these three categories may be implemented in active or passive buildings applications [16, 17]. In the passive building technology, only SHS and LHS methods are used. Nonetheless, this technology allows to enhance thermal comfort thanks to the use of materials with high thermal inertia without being affected by external conditions [16, 18]. While in the active building concept, TCHS method is used. This concept allows to augment renewables contributions such as solar and aero-thermal energy [17, 18]. In addition, it improves the systems' efficiency by regulating the process range for example using frequent start/stop in order to reduce discontinuous input [17, 18]. Furthermore, active technology enables to mitigate the peak load [17, 18]. In this context, Ben Romdhane et al. [19] documented a review on passive building applications based on the LHS method. Authors compared both methods LHS and SHS, and then reported that LHS technique stores 5–14 times more heat than SHS one. Further, Rathore and Shukla [20] presented a review of different TES types used in building and then, a great attention was paid to LHS materials. Also, a detailed description of several LHS designs has been carried out. The study indicated that a promising period of time can be obtained by implementing LHS material especially, macroencapsulated phase change material (MPCM). Therefore, this period will mitigate the reliance on heaters and cooling and thereby, save energy. In addition, Lizana et al. [18] reviewed the development and applications of Thermal Energy Storage materials for the building sector, mainly oriented towards zero energy buildings (ZEBs). Different properties, design and classification of sensible, latent and thermochemical TES materials are described and compared according to the recent scientific research, most known international projects and commercial systems. Thereby, they revealed that there exists a shortage of available

materials for TCHS solution. Otherwise, the thermochemical method requires well-maintained tanks and heat exchangers for small-scale processes. So far, it needs additional efforts to optimize the technical and economical concept of TCHS systems. Moreover, Navarro et al. [17] carried out a comprehensive review about the TES technologies integrated into active building applications. The two types of active systems: direct and indirect systems are followed this work. In a direct technology, the storage medium is the heat transfer fluid (HTF) while, in an indirect one, to store the heat a second medium is required. They declared that the active systems design requires a proper maintenance to accomplish an appropriate incorporation, considering various conditions and requirements such as climatic, aesthetical and operational. Each TES type has its benefits and drawbacks and the operation principle is absolutely dependent on the application and its requirements, like the capacity or power. So, surveys related to the several categories of TES are described by various research trends. A comparison of some parameters of TES methods is reported in Table 2 [21].

Table 2. Comparison of TES solutions [21].

TES technique	Capacity [kWh/t]	Power [MW]	Efficiency [%]	Storage time [h,d,m]	Cost [€/kWh]
Sensible heat	10-50	0.001-10	50-90	d/m	0.1-10
Latent heat	50-150	0.001-1	75-90	h/m	10-50
Thermo-chemical heat	120-250	0.01-1	75-100	h/d	8-100

To study the influence of such scientific topic in literature, a bibliometric analysis was recently known as an appropriate tool that can analyze a huge quantity of scientific data and supply critical insights into the most relevant achievements in a domain. Recently, many articles talking about energy storage appeared based on this methodology to define research trends and to map the state of the art [22-26]. In that sense, Gabeza et al. [27] released a bibliometric analysis using the software VOSviewer to develop the research related to the TES categories and to pick out the research gaps. This literature study was achieved analyzing the keywords' co-occurrence found with the software that, for TES topics, is illustrated in figure 3. In this case, the pertinence in terms can be identified from the dimension of the circles, for example, the biggest circle identifies the topic with more studies. On the other hand, the research gaps were identified by smaller circles or the absence of keywords. As shown in figure 3 and indicated in reference [28], the TES category (red circle) had a high relevance as well as the LHS method (known as PCM) (purple circle) meaning that they were the topics with more published documents.

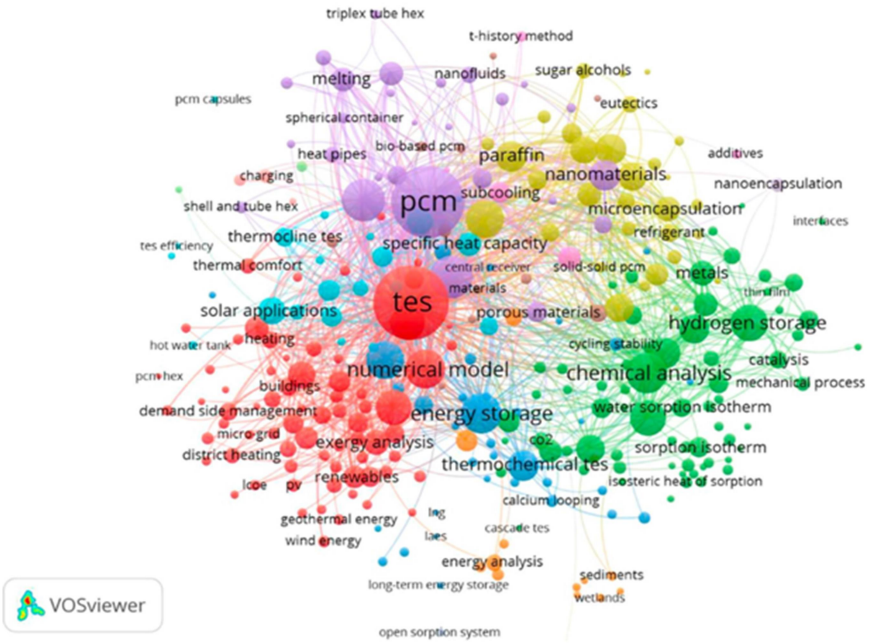

Figure 3. Keywords' co-occurrence for the storage sector [27].

This general overview is as well expected to participate as a guide for the readers for the decision-making process in the progress of TES solutions for different sectors.

1.1 Aim and scope of the review paper

The aim of this paper is to give a general overview on the state-of-the-art of TES technologies. A great attention is focused on SHS and LHS systems and their applications in various sectors. This review covers the subject of phase change heat transfer phenomenon and sensible energy storage process in porous medium. The Lattice Boltzmann method (LBM) at the REV and pore scale approaches are reviewed to show its robust ability to handle these mechanisms. This document includes six sections including the state-of-the art of different TES technologies in the introduction. In addition, a comprehensive analysis of the sensible energy storage technique is provided by reviewing the different sensible heat storage materials and the effect of porous medium on this method (Section 2). Technical conception, economic properties and many other characteristics of latent energy storage technologies (Section 3) are introduced. The phase change heat transfer in porous structure is discussed (Section 3) and then a comparison between SHS and LHS options is done (Section 4). The LBM at REV and pore scale methods, including new solutions of simulating heat transfer mechanisms in porous supports and recent developments, are covered (Section 5). Finally, the article ends with summary and critical recommendations.

2. Sensible heat storage (SHS) method

Sensible heat storage (SHS) is the most traditional, mature and widely applied TES solution owing to its simple operation and reasonable costs, however, its energy storage density is the lowest compared with the two other options of TES (LHS and TCHS) [28]. Here, the storage mechanism consists of changing the temperature (through heat transfer) of a liquid or solid storage medium (water, air, oil, sand, rock beds, bricks etc). Figure 4 depicts the typical diagram of SHS (e.g. during sensible heating or cooling) [3, 29]. Thus, the storage material does not undergo phase transition during the process (heating or cooling).

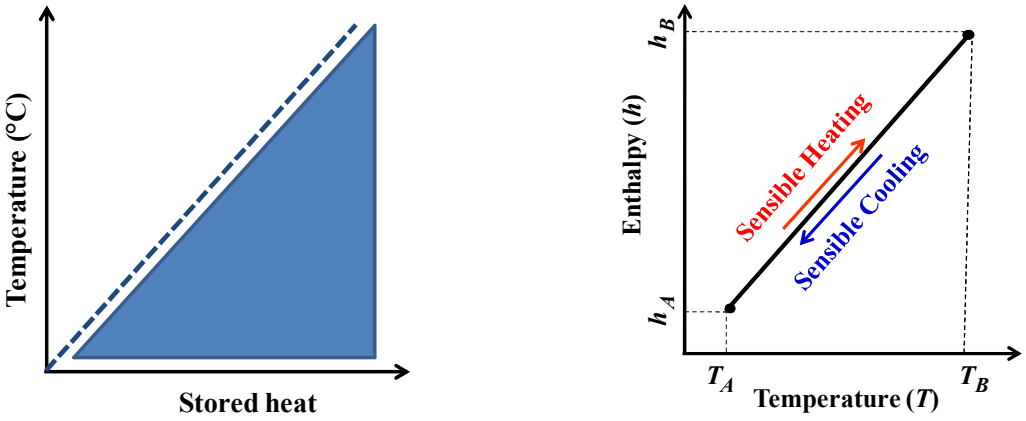

Figure 4. Diagram of temperature change during sensible heat storage [3, 29].

An advantage of this mode is that the storage and release of the accumulated heat (charging and discharging cycle) can be repeated without any problem, so a large volume is required to meet the needs [30]. Generally, this method takes advantage of some properties of the storage material such as its high specific heat and large difference in temperature [31]. In other words, the amount of stored sensible heat (Q) depends on mass (m), heat capacity (c_p) and temperature gradient (ΔT) as given in Eq. (1) [31]:

$$Q = \int_{T1}^{T2} mc_p dT \tag{1}$$

where, subscripts 1 and 2 denote the inlet and outlet temperature of the heat transferred.

Thereby, two main features of SHS materials (SHSMs) should be pursued to increase the volumetric storage capacity (MJ/m^3) that are high specific heat and density. For example, in the case of water which is the most available and practical SHSM, for a thermal gradient of 60°C, the sensible heat storage capacity is estimated at 250 MJ/m^3 [18]. Fernandez et al. [32] presented a bar chart that includes a specific characteristic plotted for all SHSMs so as to identify and classify materials.

On the other hand, thermal conductivity, thermal diffusivity and flow rate play a key role in charging/discharging cycles, which ensure the stratification ability. High thermal stratification facilitates the release of heat, as it permits a bass temperature thermal energy source to be transferred to the cooler areas during charging period, and thus, higher exergy (quality energy) is promptly obtained from the warmer zones during discharging cycle [33].

Likewise, the thermal effusivity parameter appears as the principle influencing variable on thermal inertia when talking about passive building applications as carried out by Ståhl [34]. This parameter characterizes the ability of a material to exchange and absorb heat as defined in Eq. (2) [18]:

$$\text{thermal effusivity} = \sqrt{\lambda \rho c_p} \tag{2}$$

Consequently, the increase in thermal effusivity, increases the heat stored quantity and then, reduces the energy consumption [18].

Besides, availability, cost, toxicity and volume change are promising criteria for selection for sustainable SHSM [18]. So, the main disadvantages of SHSMs are their limited energy density and self-discharge of the device especially for short-period storage [35].

To evaluate the performance of a SHS system, González-Roubaud et al. [36] have emphasized the following:

- Energy storage capacity: energy accumulated in the device that relies on the storage mode, the features of the material and the dimension of the system;
- Power: to control the speed of the charging and discharging processes;
- Efficiency: It estimates the energy losses and gains;
- Time of charging/discharging cycles: It defines the time needed to accomplish the two periods
- Cost: It includes the cost of the SHSM, the heat exchanger and the thermal energy storage enclosure.

According to Gabeza et al. [27] SHS method was strongly used in solar applications (concentrated solar power (CSP) [37] plants or desalination [38]), which was mostly modeled numerically. For example, the water-based SHS tool is one of the most widely used solar TES systems in residential applications. Such an application is sketched in Figure 5 [3]. During daytime, solar energy captured by a solar collector is transferred as thermal energy to the

water in the storage tank through a working fluid. The pump maintains a constant flow rate when the working fluid is subjected to forced convection.

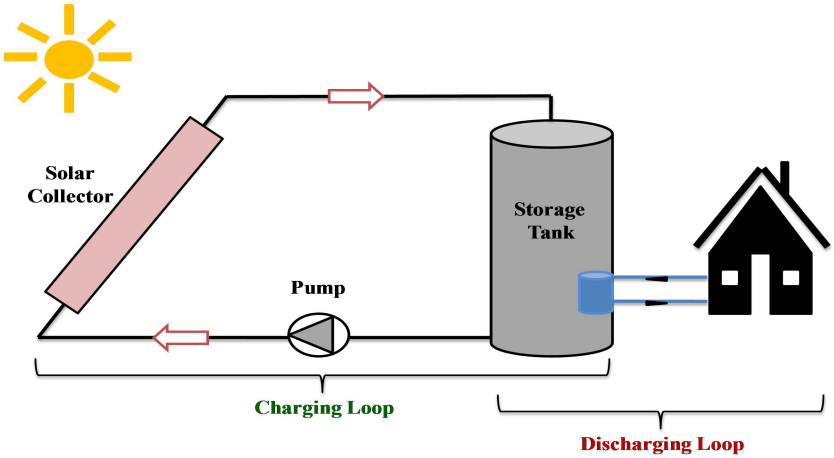

Figure 5. Simple solar application: solar-based water heating device [3].

There are numerous feasible conceptions for a SHS device. Therefore, numerical studies and experiments are carried out to define optimum parameters in order to enhance the system performance. SHS technologies are gathered in table 3.

Table 3. SHS techniques and their classification [39].

SHS techniques	**Classification**			
Underground thermal energy storage	Aquifer thermal energy storage	Borehole thermal energy storage	Tank thermal energy storage	Pit thermal energy storage
Thermal energy storage in tanks	Vertical (Thermocline)		Horizontal	
Thermal energy storage in packed bed	Stationary beds		Fluidized beds	
Thermal energy storage in building structures				

For this purpose, Koçak et al. [39] published a comprehensive review paper on SHS systems and materials that are available and applied in solar heat industrial applications. According to temperature range, they pointed out that there are three groups of solar industrial processes: low temperature applications ($\prec 150°C$), medium temperature processes (between 150 and 400°C) and high temperature procedures ($\succ 400°C$). Indeed, they concluded that packed bed thermocline technique is the most economic and widely used method for sustainable solar applications regardless of the temperature range.

2.1 Sensible heat storage materials (SHSMs)

There are various reviews related to TES solutions that handle the thermo-physical characteristics of commonly used SHSMs and compare its several parameters (such as

physical, chemical, thermal, environmental, economic aspects...) in order to satisfy all the requirements for building and/or industrial applications. These SHSMs are classified into solid and liquid storage materials [3, 18]. Generally, water and oils are the most often used liquids, whereas solids are numerous such as rocks, bricks, metals... [3, 18]. Fernandez et al. [32] presented an overview of the SHSMs in the temperatures range 150–200 °C. They used the method developed by Prof. Ashby [40, 41] for materials selection in order to find suitable and potential materials for long and short term cycles for the SHS method. According to the authors, solid SHSMs are classified into four groups: metals and alloys, ceramics and glasses, polymers and elastomers and hybrids. The thermo-physical properties of some commonly used SHSMs are listed in Table 4 [3, 18, 19, 42].

Table 4. Thermo-physical properties of some commonly used SHSMs [3, 18, 19, 42].

SHSM	Type	Density (kg/m^3)	Thermal conductivity (W/mK)	Specific heat (kJ/kgK)
Water (80 °C)	Liquid	970	0.67	4.19
Water (40 °C)	Liquid	990	0.63	4.19
Water (10 °C)	Liquid	1000	0.6	4.19
Oil	Liquid	880	0.14	1.88
Ethanol	Liquid	790	0.171	2.4
Propanol	Liquid	800	0.161	2.5
Butanol	Liquid	809	0.167	2.4
Ceramic brick	Solid	1800	0.73	0.92
Rock	Solid	2800-1500	3.5-0.85	1
Concrete	Solid	2000	1.35	1
Wood	Solid	700-450	0.18-0.12	1.6
Aluminum	Solid	2707	204	0.896
Copper	Solid	8954	385	0.383
Granite	Solid	2640	4.0-1.7	0.82
Sand and gravel	Solid	2200-1700	2	1.18-0.91
Clay or silt	Solid	1800-1200	1.5	2.5-1.67
Limestone	Solid	2600-1600	2.3-0.85	1
Cement mortar	Solid	1800	1	1
Brick	Solid	1600	1.2	0.84
Marble	Solid	2500	2	0.88
Plastic board	Solid	1050	0.5	0.837

Many factors should be assured to guarantee a long lifetime of SHSMs such as thermal and chemical stability (constant thermal properties, no chemical decomposition and no degradation) at high temperature gradient and whatever the number of loops (charging/discharging). According to Klein et al. [43] storage substances should be good thermal conductors with low cost and should have larger specific heat and density and ability for operating at appropriate temperature range. Figure 6 displays the average volumetric specific heat capacity vs. the thermal diffusivity for the most available SHSMs [18].

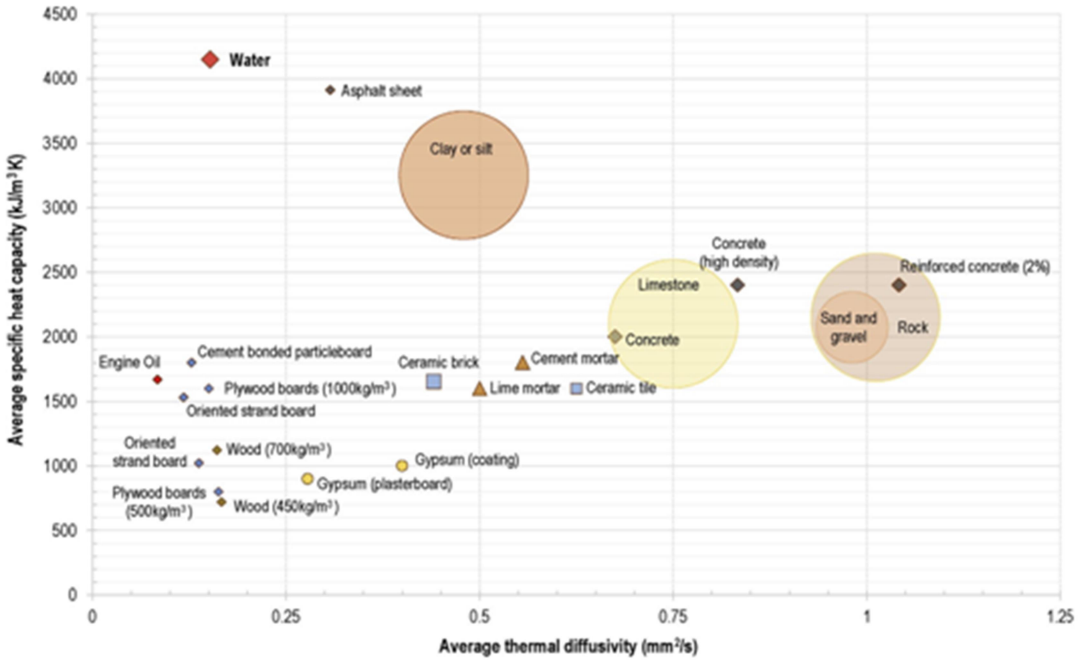

Figure 6. The most available and common SHSMs [18].

Today the available SHSMs (either liquids or solids) for engineering purposes exceed 150.000 substances [29, 32]. Among liquid form SHSMs, water is the most mature material due to its availability, non toxic, low cost and high specific heat capacity [29]. Almendros-Ibáñez et al. [44] performed a review study on different techniques of solar energy storage in particle beds. The focus is on two different particle methods: Packed and fluidized beds. They revealed that the use of SHSMs increases the efficiency of solar collectors. In addition, they indicated that SHSMs in liquid form have higher specific heat capacity than solid forms (e.g. rock). However, some issues limit the use of liquids such as the high-cost liquid storage infrastructures and heat exchangers [18, 45, 46, 47], the risk of leakages and the storage reservoirs (hot and cold) occupy large areas. On the other hand, for the use of solids, the main drawbacks are the low density, the high investment cost for storage units operation and maintenance and the risk of self-discharge (in the long-term) [18].

2.2 Sensible heat storage in porous media

SHS mode consists of a storage material (SHSM), container of the SHSMs (e.g. tank) and inlet/outlet devices [48]. Containers play two roles at once: they retain SHSMs and prevent thermal leakages and losses. Among the tools used in this storage method, the SHS in porous medium is the most preferred solution. This section describes some case studies found in literature in which porous SHSMs are applied in SHS systems. Tanks saturated with porous solid SHSMs are used in numerous industrial and building applications such as power generation and heating [3]. Such a residential heating application using a porous packed bed storage tank is portrayed in figure 7 [3]. In this system, the working fluid (e.g. air) transports the heat from the collector to the tank. The hot fluid transverses the gaps between the solid SHSMs (e.g., rock or sand) which leads to an increase in the temperature of particles during daytime. The quantity of the stored sensible heat inside the reservoir is retrieved during nighttime (discharging process should be held). The main parameters that influence the SHS system performance are the type and flow rate of the working fluid and the porosity of the reservoir [3, 48].

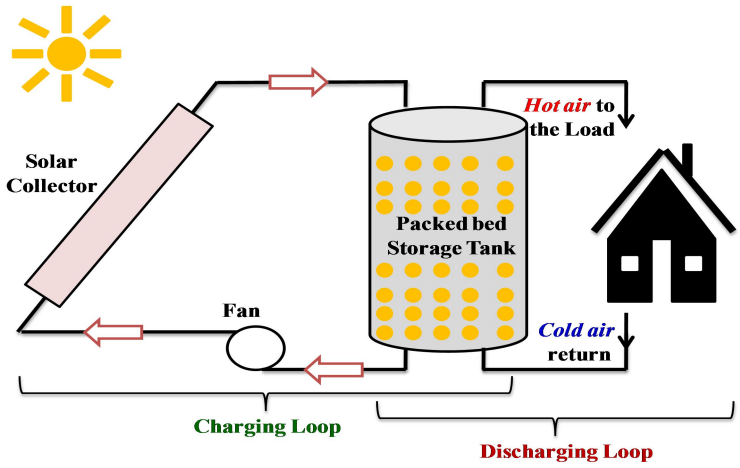

Figure 7. Heating application: Porous packed bed SHS system [3].

On such a topic, a huge range of investigations in literature have dealt with SHS in various porous units. Indeed, among the various characteristics of a sensible storage medium, the porosity effect, which is another crucial feature, is discussed in this subsection. To address this subject, Mabrouk et al. [49] developed a numerical model to study the effect of pore density parameter (PPI) for $\varepsilon = 0.9$ on a SHS unit. The system was subjected to forced convection and then it was compared with a LHS unit. They recommended a porous matrix such as metal foam to optimize the energetic and exergetic efficiencies. The authors stated that increasing PPI (=60) for high porosity value (=0.9) reduces the energy losses for sensible heat systems and so, increases the quality stored. In another study, Amami et al. [50] explored the charging and discharging process enhancement in a porous SHS duct maintained under

forced pulsating flow. They tested three porosities (0.6, 0.7 and 0.8) for the porous medium and estimated its thermal performance. The results disclosed that with the porosities increasing, the quantity of the stored sensible energy is improved, and then the quality (exergetic efficiency) drastically grew. For example, the energetic efficiency was increased from 31% to 68.2% with the porosity increase from 0.6 to 0.8, respectively for a given pulsating amplitude (=0.55) of a pulsating flow. Thus, the same was found for the exergetic efficiency which is raised from 32.4% (for $\varepsilon = 0.6$) to 67% (for $\varepsilon = 0.8$). In short, for pulsating or non-pulsating flow, the porosity effect did not change. Following the work of Elouali et al. [45], four physical models were performed through numerical simulations to describe the packed bed thermal behavior for sensible heat storage. The air represents the heat transfer fluid (HTF). The influence of the porosity parameter over the packed bed during the charging and discharging periods is taken into account and discussed. It was noted that a decrease in the bed porosity leads to an enhancement in the packed bed thermal storage capacity as well as an increase in the interstitial heat transfer area between HTF and solid particles. Furthermore, an increase in the porosity slows down the charging process. Thus, different attractive advantages of porous structure have been reported in the literature to optimize SHS devices. For instance, Kasaeian et al. [51] presented a review of numerous models to simulate complicated physics of nanofluid flow in a porous medium. They gathered details about the main features of a porous structure integrated into thermal systems such as heat exchangers and ducts. They stated that the use of porous matrix enlarges the specific interfacial area between porous structure and working fluid which causes a greater heat transfer rate. In addition, they indicated that such a technique plays a vital role to ameliorate thermal efficiency of the system. Therefore, Sheremet et al. [52] conducted a numerical analysis of natural convection in a concentric horizontal annulus filled with a porous structure saturated by Cu-water nanofluid. It turned out that decreasing the porosity ($\varepsilon \prec 0.5$) augments the thermal conductivity of the medium but, they did not notice any effect in fluid flow and heat transfer. However, increasing the porosity ($\varepsilon \succ 0.5$) intensifies the convective flow and increases the thermal conductivity. A year earlier, Sheremet et al. [53] numerically examined the thermal behavior of a square cavity composed of solid porous medium (aluminum foam and glass balls). Effect of morphological parameters of pores such as porosity (=0.3, 0.5 and 0.8) was studied. The authors noted that for a larger porosity value, the local and average Nusselt number is minimal. So, the porosity parameter significantly affects the heat transfer rate. In another work of Amami et al. [54] published in 2014, a proposed porous unit was used for storing sensible heat. By findings, they demonstrated that the use of porous medium with high permeability and low thermo-physical properties improves performance of the TES unit

deemed. Moreover, low thermal conductivity and capacity ratios between working fluid and porous medium leads to the increase of temperature and amount of stored sensible energy. Heap et al. [55] discussed the influence of the porosity of the volcanic rocks and magma (SHSMs). They indicated that an increase in the porosity causes a decrease in the rock density and compressive strength and an increase of the deformability of rocks. Therefore, low porosity of rocks is recommended. Besides, Dhifaoui et al. [56] conducted an experimental study of SHS performance of a vertical porous bed composed of glass beads and air and heated with a constant heat flow.

3. Latent heat storage (LHS) method

By definition, latent heat storage is based on the amount of energy absorbed or released when re-forming the phase structure of a phase change material (PCM) from one physical state to another during melting, solidification, gasification and liquefaction phenomena [19, 28, 57, 58]. At the start of the charging process, the latent heat storage material (PCM) temperature changes as it absorbs the thermal energy. When the PCM temperature reaches the specific range then, the material begins to experience a phase change as it stores the heat. However, during the discharging period, the PCM switches to its initial state as it releases the thermal energy. Unlike SHS, the phase transition process takes place at a constant or nearly constant temperature which corresponds to the PCM physical state change temperature [19, 58]. The heat storage capacity (Q) of a LHS system usually comprises two parts of sensible heat (before and after the phase transition) and a latent heat part (during the phase transition) [3, 19, 28, 59]:

$$Q = \underbrace{\int_{T_1}^{T_m} mc_p dT}_{Sensible\ heat} + \underbrace{m\Delta h}_{Latent\ heat} + \underbrace{\int_{T_m}^{T_2} mc_p dT}_{Sensible\ heat} \tag{3}$$

where, the mass (m), specific heat capacity (c_p) and temperature (T) are the properties of the PCM. Δh is its latent heat. The subscripts 1, 2 and m define the initial, final and melting temperature, respectively.

During the phase change operation, the temperature remains roughly constant with small volume changes, which makes the phenomenon simple and safe. Solid -liquid and/or liquid-solid phase transitions are the most commonly transformations in use. The typical diagram of LHS is illustrated in Figure 8 (e.g. solid to liquid and liquid to solid phase changes) [3, 29].

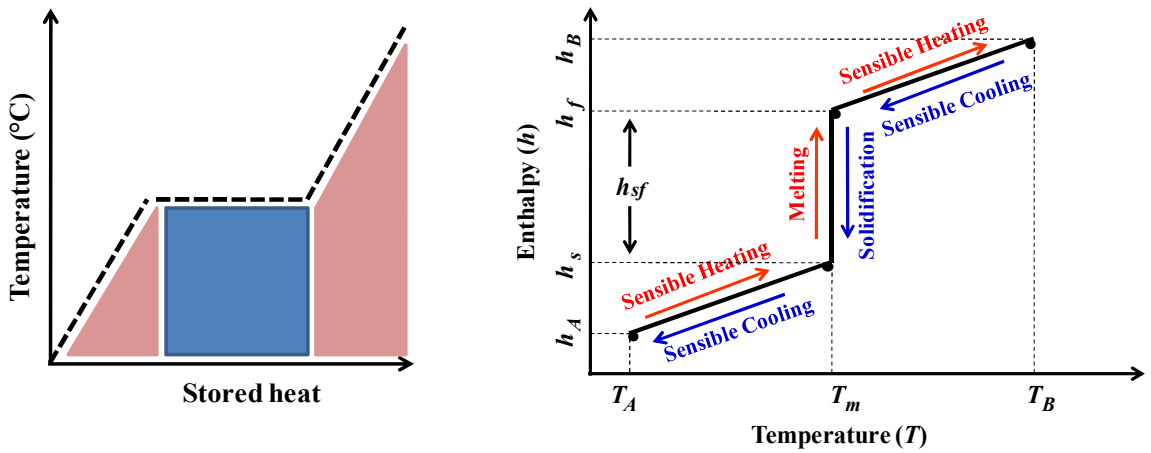

Figure 8. Diagram of enthalpy-temperature change during latent heat storage [3, 29].

As seen, PCMs store two forms of heat: sensible heat when the PCMs temperature is outside the range of phase change temperature and latent heat when the materials reach the phase change temperature.

Practically speaking, the different forms of phase change in LHS are as follows: solid–solid, solid–liquid, liquid-solid, solid–gas, gas-solid, liquid–gas and gas-liquid.

During the case of solid-solid transformation, the PCM undergoes a structure change. Therefore, the material stores the heat as its crystalline structure changes the form [35, 60]. Generally, these phase transition phenomena are characterized by small latent heat and volume changes as compared to solid-liquid processes. Among the promising solid-solid PCMs: organic solids such as pentaglycerine, pentaerythritol, Li2SO4 and KHF2 [60, 61]. Their main advantages are: less rigorous requirements of the reservoir, no leakage, more flexible conception and no need for encapsulation method [62, 63].

Yet, during the solid-gas and liquid gas transformations, a large amount of latent heat can be acquired, but it requires more stringent containers owing to the large volume change during these processes. Therefore, their applications for the thermal comfort of the buildings are not a suitable solution [64].

Compared to solid–gas and liquid–gas transformations, Solid–liquid PCMs have smaller latent heat and volume change. Thus, solid–liquid phase transition takes place at a narrow temperature range, while PCMs store a relatively important amount of latent heat with small volume changes. Consequently, these phase change processes (solid-liquid) are economically competitive with other LHS solutions [64].

On another aspect, the advantages of LHS mode over SHS one are listed as below:

- The PCMs phase-change enthalpy is 100 to 200 times more than sensible heat.
- According to Sharma et al. [60] LHS materials (PCMs) have a storage density 5 to14 times higher than that of SHS materials.

- The LHS method takes place in an almost isothermal way unlike the SHS process in which the temperature of SHS materials is too high.
- According to Tatsidjodoung et al. [35] to store the same quantity of heat, SHS devices using rocks (resp. water) requires 3 times (resp. 1.5 times) more volume than LHS units using paraffin wax.
- Seasonal overheating problems may not arise for LHS systems due to the low mass of PCMs.

However, there are many drawbacks related to LHS materials. Low thermal conductivity (which is mostly between 0.2 W/(mK) and 0.7 W/(mK)), thermal stability of PCMs under long-term cycles, supercooling, subcooling and phase segregation issues of PCM (e.g. salt hydrates), tools of heat transfer enhancement and cost are some of the LHS problems that are under investigation until now [3, 59, 65-69].

The problems of supercooling and phase segregation are encountered for the following PCM: salt hydrates. During the cooling process, the temperature of the substance drops below the melting range (T_{PCM} □ $T_{melting}$) without starting solidification mode. Thus, a nucleation phenomenon starts which leads to a sudden increase in temperature to the melting point. Figure 9 depicts the supercooling of a PCM [3]. The dispersion of nucleation agents into the PCM, an incomplete melting procedure (during charging period), PCM containers with insulated parts (named cold fingers), the insertion of impurities into the PCM and the application of some fields such as vibration, magnetic, electric and ultrasound are the several solutions to resolve the supercooling.

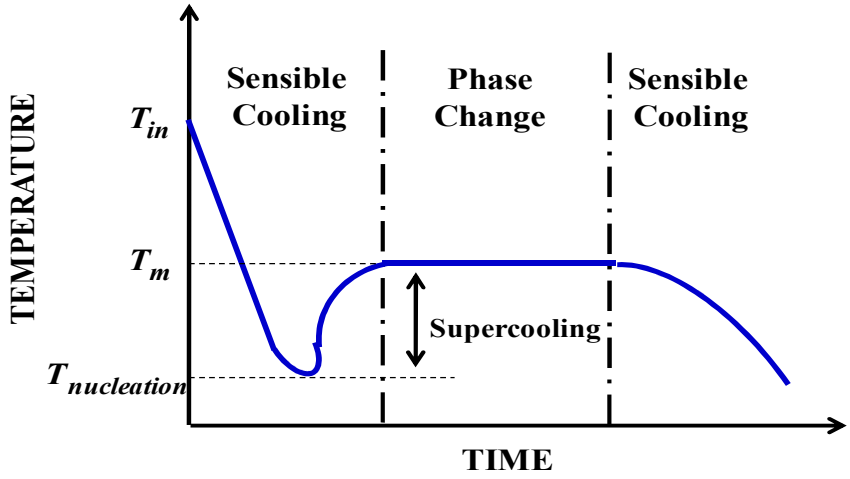

Figure 9. The supercooling phenomenon [3].

Phase segregation represents another crucial difficulty of salt hydrates. This problem represents a separation of the homogenous PCM (salt hydrates /water) which causes an accumulation of the dense salt at the bottom of the container as seen in figure 10 [3].

Therefore, the segregated PCM loses the desired characteristics and it cannot be used in an LHS application. In this context, thickening agents are the most widely used solutions to avoid phase segregation.

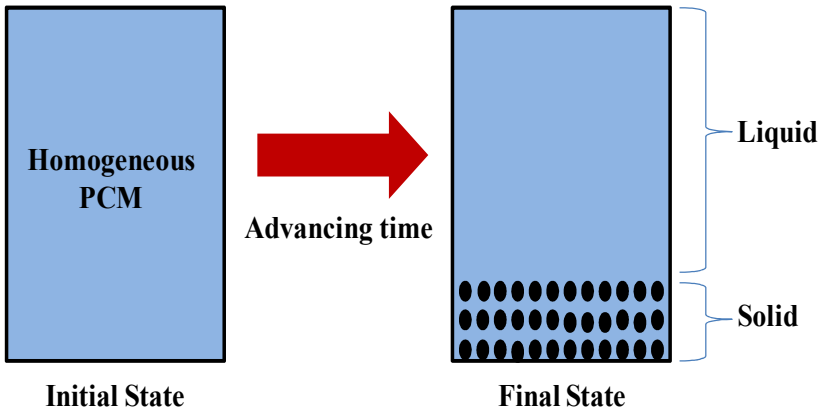

Figure 10. The phase segregation [3].

The primary components of an LHS system are as follows [3]:

- PCM: The thermal storage medium that performs a phase transition taking into account the working temperature range of the application.
- Heat transfer fluid (HTF): The material that transfers the heat from the source to the PCM. Operating conditions, characteristics and path of the HTF have an effect on the system performances.
- PCM container: The PCMs are impregnated inside containers to prevent leakages. PCM containers are adequately designed to allow better heat transfer between the PCM and the HTF.

3.1 Latent heat storage materials (PCM)

PCM appears as the most critical component of an LHS system, and it should satisfy some requirements to enhance energy storage density and ensure thermal stability under long and/or short-term loops. The main thermo-physical, kinetics, chemical, economical and environmental characteristics desired for the selection of a proper PCM are listed according to Nomura et al. [70] and Sharma et al. [60] as follows:

For thermal properties, PCM should possess a phase transformation temperature corresponding to the operating temperature of the LHS application. In addition, it should have large latent heat and specific heat in order to reduce the volume of the latent heat store. Furthermore, PCM with high thermal conductivity is recommended to assist phase transition and interstitial heat transfer between HTF and PCMs.

For physical properties, PCM should exhibit large density, small volume changes and low vapor pressure during the phase transition process while respecting the operating temperature range in order to limit the containment issues.

For kinetics properties, the phenomena of subcooling and supercooling must be prevented and a sufficient crystallization rate should be obtained.

For chemical properties, PCMs should be compatible with materials of the application. They should retain their chemical stability for long-term cycles (no degradation and chemical decomposition). Moreover, the latent heat storage material should be non-toxic, non-flammable, non corrosive and non-explosive substance. In addition, charging and discharging periods should be fully completed.

For economical properties, low cost and widely available PCMs are in demand.

For environmental properties, PCMs should be non-polluting and recyclable substances. They should have low environmental impact. However, each type of PCMs has its own characteristics, which complicates the response to all the criteria.

Based on the change in the physical state of the material, PCMs comprise different categories: solid– solid PCMs, solid–liquid PCMs, solid–gas PCMs and liquid–gas PCMs. The solid–liquid PCMs are involved in this section. They fall into three classes: organic, inorganic and eutectics as shown in figure 11 [3, 20, 25, 71-73].

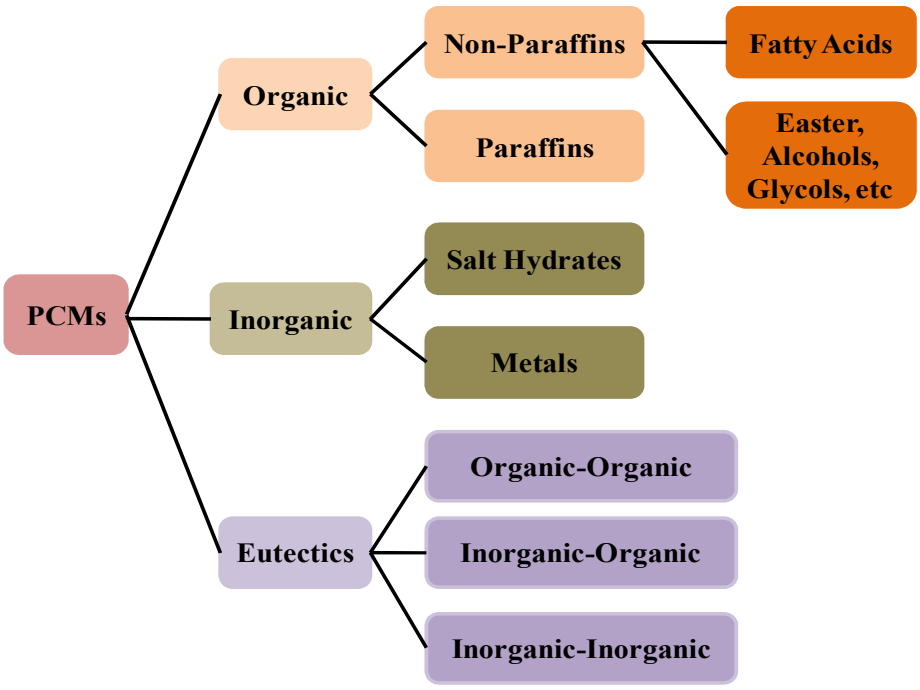

Figure 11. Classification of solid-liquid PCMs [3, 20, 25, 71-73].

A comparison of these various groups of PCMs is gathered in Table 5 below [25, 73].

Table 5. Benefits and drawbacks of different types of PCMs [25, 73].

Classification	**Benefits**	**drawbacks**
Organic PCMs	No subcooling No supercooling No phase segregation Large storage capacity High latent heat Recyclable substances Fatty acids and alcohols are renewable substances Available for all temperature range Compatible with other materials	Low thermal conductivity (0.2 W/m K) Flammable Large volume change Paraffins are non-renewable substances
Inorganic PCMs	High thermal conductivity (0.5 W/m K) High latent heat Storage capacity 2× Storage capacity of organic PCMs Small volume change Available and cheap	Supercooling Corrosion Salts can exhibit chemical instability
Eutectics	No segregation High storage density Adjustable phase transition temperature	Lack of test data for certain thermo-physical characteristics Same drawbacks of pure organic or inorganic PCMs

The use of PCMs has been expanded in various industrial sectors such as textiles, satellites, telecommunications and medicine thanks to the change in their physical states. For melting temperatures less than 15°C, PCMs are related to air conditioning and extreme cooling applications where operating temperature corresponds to that of melting. However, for melting temperatures larger than 90°C, PCMs are used to prevent a sudden increase in temperature that causes fires [74-77]. Figure 12 outlines the melting enthalpy vs. the melting temperature for some existing PCMs [73, 77-79]. From this figure, it can be pointed out that the potential PCMs for building applications are paraffin, fatty acids, salt hydrates and eutectic mixtures [73].

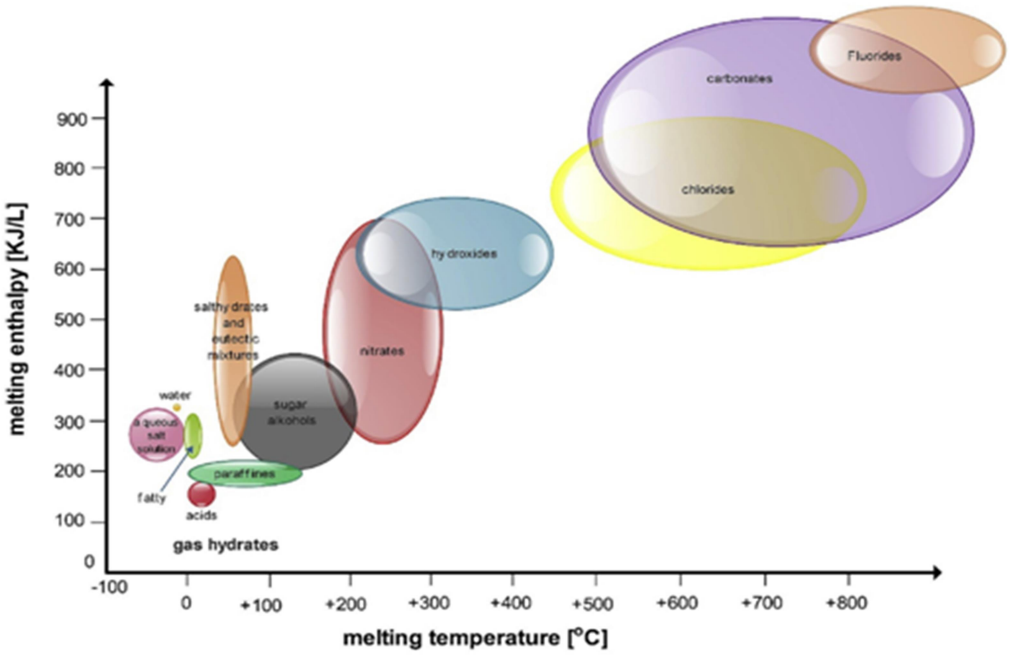

Figure 12. Melting enthalpy vs. melting temperature for some PCMs [73, 77-79].

From an energy consumption point of view, PCMs are widely applied in building applications with 40% energy consumption and industrial sectors with 55% energy consumption. The importance of these materials will be doubled when we focus on the recycling role and optimization of energy consumption in energy management [80, 81]. Indeed, all scientific efforts in buildings are giving comfortable conditions in the living environment for human comfort. These efforts are related not only by high costs and the consumption of available PCMs but also leads to environmental pollution and destruction of the energy sources. Energy consumption management figures as a novel way to limit energy consumption and pollutants of the environment [82-85]. In recent years, PCMs and energy storage technologies are among the tools that have become increasingly important in buildings energy management. For instance, the integration of PCMs into the different walls of a residential home leads to the following: in the east and west walls, an energy-saving about 29% is obtained and in the north and south walls, an energy-saving about 19% is achieved [86]. For this purpose, Faraj et al. [80] reviewed the literature on TES with focus on PCMs for building applications such as cooling, heating and hybrid applications. The two categories: active and passive systems are presented. They gave a summary of the used PCMs in each process, their characteristics and their incorporation techniques. It was concluded that the use of PCMs reduces energy consumption for heating, ventilating, and air-conditioning applications in the active system and ceilings in the passive one. They indicated that the main disadvantage in the application of PCMs for cooling systems is the incomplete solidification process at night. Another review on the use of PCMs for cooling building applications was

carried out by Souayfane et al. [90]. Several cooling applications based on PCM integration were discussed such as solar cooling system, free cooling, evaporative and radiative cooling systems, air conditioning systems, and PCMs active and passive systems application in building envelopes. The authors dealt with the selection criteria of PCMs and concluded that the incorporation of PCMs reduces energy consumption while thermal comfort is maintained. In addition, it causes a decrease in temperature fluctuations. However, many disadvantages have been pointed out in PCM applications such as low convective heat transfer coefficients of considerable portions of used PCM, incomplete cycle of PCM solidification process at night, and limited interstitial heat transfer between PCM and HTF (air). Therefore, active systems can solve the problem of low convective heat transfer. It was affirmed that paraffin was the most widely employed in cooling applications.

Several studies have reported that organic solid-liquid PCMs are the most extensively used substances where paraffin waxes represent about 27% of PCMs application, 57% for eicosane and 10% for other organic PCMs [77, 87-89]. Indeed, figure 13 exhibits the relationship between the properties of PCMs and the performance of LHS devices. As seen from this figure and through different investigations published in literature on this theme, PCMs has a strong influence on the thermal performances of LHS systems. [3].

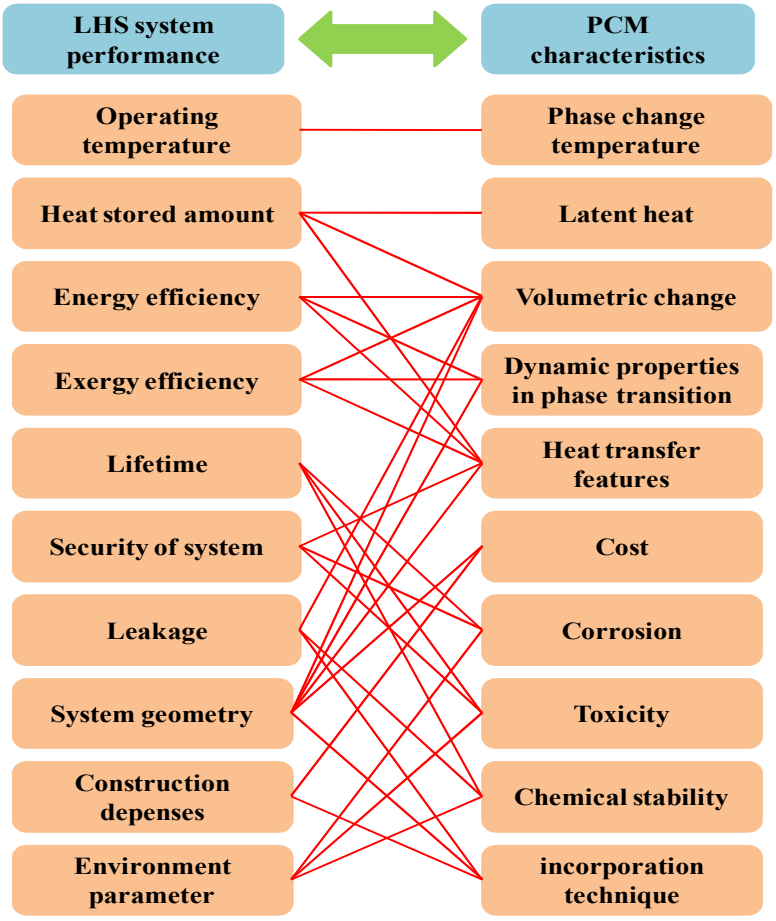

Figure 13. Influence of PCMs on performance of LHS system [3].

Otherwise, a PCM is appropriate for applications if it retains its properties after a number of cycles repeated, that is, if it exhibits a good cycling stability. This is called long-term stability [91]. Another important aspect, which overshadows all other qualifications, is economics. A PCM should be estimated with a reasonable price and its availability on the market [60, 82, 92].

PCMs can be integrated into applications by six main incorporation techniques: (1) Direct PCMs integration (where liquid or powdered PCMs (such as gypsum, concrete, plaster...) are mixed with other materials), (2) incorporation into porous structures through pores of materials, (3) shape stabilization, (4) macroencapsulation technique, (5) microencapsulation method and (6) nanoencapsulation approach [80]. Encapsulation technique helps to increase the interstitial surface area, prevent thermal losses and limit the direct exposure of PCMs to the environment. Besides, in some cases this method is employed to ameliorate the thermal conductivity or to retain the PCM morphology during the phase transformation. Generally, the capsules (containers) are fabricated of a polymer or a metal [73, 93-96]. Encapsulation technology can be classified into three methods according to the encapsulated PCM size ($D_{encapsulated\ PCM}$). If $D_{encapsulated\ PCM} \succ 1000\mu m$, it is macroencapsulated PCM, if $1\mu m \prec D_{encapsulated\ PCM} \prec 1000\mu m$, it is microencapsulated PCM, and if $D_{encapsulated\ PCM} \prec 1000nm$, it is nanoencapsulated PCM [93-95].

To the best of our knowledge, the microencapsulation method was first conducted by Barret K Green in 1950 [97]. Nowadays, this method plays a crucial role in building and textile sectors for thermal regulation. On the other hand, the first experimental study on the solid-liquid phase-change heat transfer of porous shape stabilized-PCM was developed by Weaver and Viskanta in 1986 [98]. They used water and glass as PCM and porous matrix, respectively. Figure 14 shows different methods to integrate PCMs [20, 99, 100].

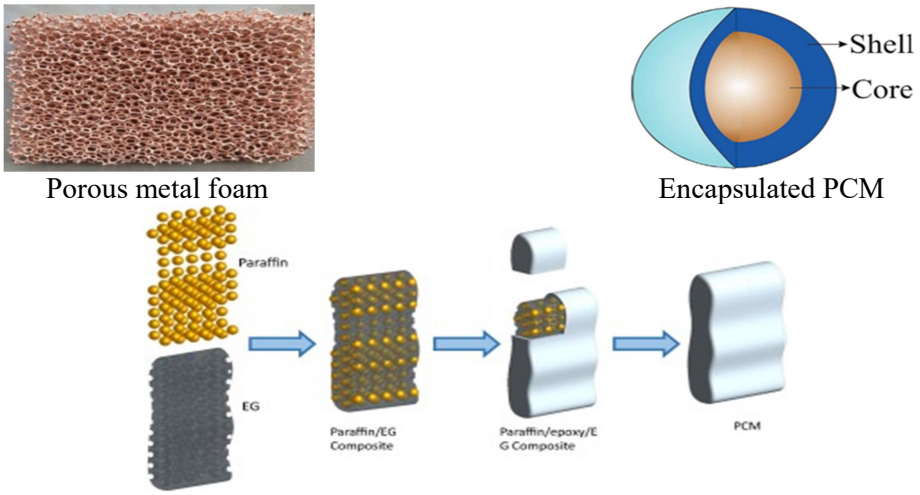

Porous metal foam

Encapsulated PCM

Shape-stabilized PCM

Figure 14. Techniques of PCM incorporation [20, 99, 100].

3.2 Latent heat storage in porous medium

Nevertheless, most pure PCMs suffer from the issue of low thermal conductivity ($\approx 0.1 Wm^{-1}K^{-1}$), which limits its use in many domains [101]. Three main solutions are proposed to enhance thermal conductivity:

- The first method is to make a composite of PCM with porous matrix such as metal foam or expanded graphite [102].
- The second solution consists of adding metallic spheres, screens, fins and wools to form a new PCM with enhanced thermal conductivity [103, 104].
- The final technique is the implementation of nano-materials [105-107].

Porous supports can be classified in terms of their pore size as macroporous ($\succ 50\,nm$), mesoporous ($2-50\,nm$), microporous ($\prec 2\,nm$) and hierarchical porous (from macro to micro) matrices [108]. Figure 15 shows the most used porous supports [109]. Different categories of these supports have varying characteristics and roles: metal foams, typical macroporous supports, have high thermal conductivity and thus are employed as heat delivery promoters owing to their large interstitial surface area. Meso and microporous supports exhibit a great guest-host interaction and consequently prevent leakage. In hierarchical porous forms, macropores store PCMs in a cavity, mesopores supply transport routes and micropores exert capillary force to block PCMs movement [110].

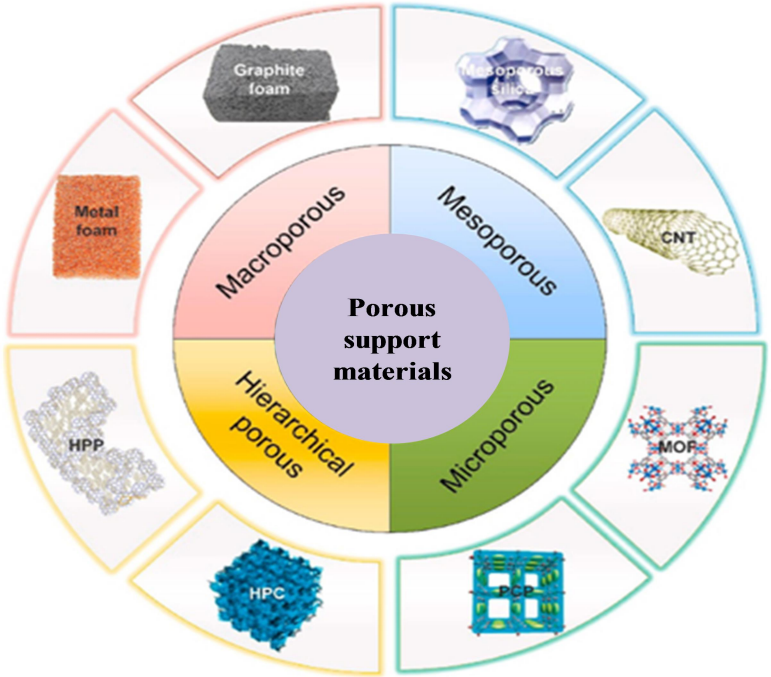

Figure 15. Porous support materials 109].

This section keeps focus on the impregnation of PCMs with porous structure. In this method, a porous medium is a form of material either fabricated (copper, aluminum...) or

natural (graphite, metal foam...) that comprises a solid matrix with interconnected or disconnected voids called pores, where PCMs are integrated to realize latent heat storage. High thermal conductivity of the porous structure and large interstitial surface areas inside porous material are beneficial in improving heat transfer rate in the system. When the pores are at nano- or microscale, PCMs can retain their original form without any leakage during phase transition due to capillary and surface tension forces (shape-stable composite PCMs) [70, 111]. Performance enhancement depends on the morphology and properties of the structure such as porosity, pore density and thermal conductivity [112, 113]. In the same research axis, Mabrouk et al. [114] numerically investigated the phase change process of a PCM in a porous open-ended channel filled with metal foam with three different porosities 0.5, 0.7 and 0.9. The laminar fluid flow was subjected to forced convection and tested for two Reynolds numbers (Re) 200 and 400. It was found that the melting rate intensifies as the porosity decreases (=0.5) and Re number (=400) increases. Moreover, the thermal performance improves significantly with low porosity values. The same authors in another work [115] carried out a two dimensional numerical simulation on steady and incompressible fluid flow in a rectangular duct. They analyzed the pore morphological parameters such as pore per inch (PPI) density (=10, 30 and 60) and porosity (=0.7, 0.8 and 0.9) of a metal foam/paraffin composite in order to explore the improvement effects of these parameters on heat transfer mechanisms during the phenomena of melting/solidification. By findings, they demonstrated that increasing Re (=400) with large PPI and porosity (60 and 0.9) reduces the melting time while it is slowed down for low PPI and porosity (10 and 0.7). In the light of this subject, Yang et al. [116] proposed a novel LHS system filled with porous metal foams with positive and negative gradients in pore parameters in order to ameliorate the thermal performances. They established both numerical and physical models to address this problem. They found that a 17.9% reduction in time of complete melting process can be obtained with the positive gradient concept of porosity while a 35.7% increase with the negative design can be achieved. Furthermore, positive gradients in porosity of 0.89–0.95–0.98 are recommended to decrease the melting time by 21.1%. Li et al. [117] developed a physical and numerical model to examine the effect of metal foam porosity and nanoparticle concentration on an LHS device where PCMs are embedded so as to solve the PCM low thermal conductivity problem. Authors pointed out that a reduction of 83.7/88.2% in melting/solidification time is achieved with the addition of 95% porous metal foam while a decrease of 25.9/28.2% is obtained by adding 5% copper nanoparticles. Sardari et al. [118] focused on the copper metal foams' porosity effect on the melting process. It was found that low porosity value of copper metal foam improves the system performance than that high value. However, the pore size has no

effect. Yang et al. [119] conducted an experimental and numerical survey on the solidification performance of PCMs impregnated into metallic structure. Effect of two porosities (0.93 and 0.97) and two pore densities (8 and 30) was investigated. Results indicated that the complete solidification time for porous matrix with a porosity value of 0.93 and 0.97 can be reduced by 87.5% and 76.7%, respectively. In addition, metal foam efficiently enhances the PCM composite thermal conductivity while at low porosity, the melting/solidification rates increase. Zhang et al. [120] constructed an experimental and numerical test on the behavior of copper foam/paraffin composite during melting phenomenon of PCMs. Compared to pure paraffin, the melting rate is dramatically enhanced owing to the great thermal conductivity of copper foam. However, the local thermal non-equilibrium condition (LTNE) prevails between solid and fluid phases. On the other hand, the porosity effect of the aluminium metal foam on an LHS unit was experimentally reported by Atal et al. [121]. They pointed out that the small porosity values could reduce the phase transition time owing to the high thermal conductivity of metal foam.

Several papers have been published in this context. Therefore some of them have been cited above. The porous matrix configuration, such as porosity and pore density, has a salient impact on the phase transition heat transfer mechanisms of PCM composite. Researchers have carried out many experiments and numerical studies to explore it. They illustrated that the small porosity value enhances the phenomenon, seeing that the decrease in porosity indicates a large volume of high thermal conductivity in porous structure, thereby increasing the whole heat conductivity capacity of the system. In contrast, the pore size effect is variable according to research type. However, the decrease in pore size ameliorated the thermal performance of system in the studies of Zhao et al. [65] and Mallow et al [122], while it showed a negative effect in the researches of Li et al. [123] and Allen et al. [124].

4. Latent heat storage (LHS) versus sensible heat storage (SHS)

Using the bibliometric analysis method, Gabeza et al. [27] reported that, up to 2021, more than 27.016 papers related to TES topic were published in literature. Where, 2907 documents related to SHS are available in literature while the LHS theme has a record number of 12.152 papers published. Table 6 tabulates a comparison between the SHS and LHS techniques: working principle, advantages, most used materials and application domains [5, 60, 109].

Table 6. Comparison between SHS and LHS techniques [5, 60, 109].

	Working principle	Benefits	Materials	Application fields
SHS	Temperature change (Increase/Decrease)	Inexpensive Simple operation	Water, rock, concrete ...	solar applications: Concentrated solar power (CSP) Plants or desalination Building heating
LHS	Phase change (Solid-Liquid)	Large storage density Large latent heat Stable temperature	Paraffins, salt hydrates, metallics …	Solar applications Building heating/cooling Heat pump Thermal control Industrial waste heat storage

In a comprehensive review by Zhao et al. [28], the difference between SHS and LHS in terms of technical parameters is analyzed. It is noteworthy that the heat storage density of LHSMs $2\times$ that of SHSMs which reflects the large amount of stored energy in LHS devices. Table 7 summarizes the most important technical parameters of these two TES types [28].

Table 7. Comparison of technical parameters of SHS and LHS [28].

	Heat storage density	Storage period	Heat transmission interval	Technical maintenance
SHS	$\approx 50\,kWhm^{-3}$ $\approx 0.02-0.03\,kWhKg^{-1}$	Limited	Short	Uncomplicated
LHS	$\approx 100\,kWhm^{-3}$ $\approx 0.05-0.1\,kWhKg^{-1}$	Limited	Short	Complicate

Another critical paper on the employment of PCMs for cooling applications in buildings was published by Faraj et al. [80]. The authors show a comparison between SHSMs and PCMs. It turned out that LHSMs store between 5 and 14 times more energy than SHSMs [125], where the storage mass of rock $15\times$ ($13\times$) that of inorganic PCM (organic PCM). However, the relative storage volume of rock is 11 times (about 9 times) larger than that of inorganic PCM (organic PCM).

5. Lattice Boltzmann simulation of sensible and latent heat storage

Although experimental studies can exhibit “directly interpretable” findings of the phenomenon during PCMs phase transition and sensible storage, yet, they take a long time

and cannot portray all detailed flow and heat transfer properties, like the flow and energy fields. Moreover, a high cost makes it possible to experimentally examine all the factors influencing the complex phase transition mechanism of composite PCMs in porous structure [126, 127] and heat transfer process during sensible heat storage in porous medium. The numerical simulation represents a relevant tool to address the complicated problems and thereby, a great number of numerical investigations have been conducted [128]. In general, the numerical simulation methods for heat transfer process for the mechanisms deemed in this paper can be divided in two approaches: representative elementary volume (REV)-scale approach and pore-scale approach [129]. The two classes are schematized in figure 16.

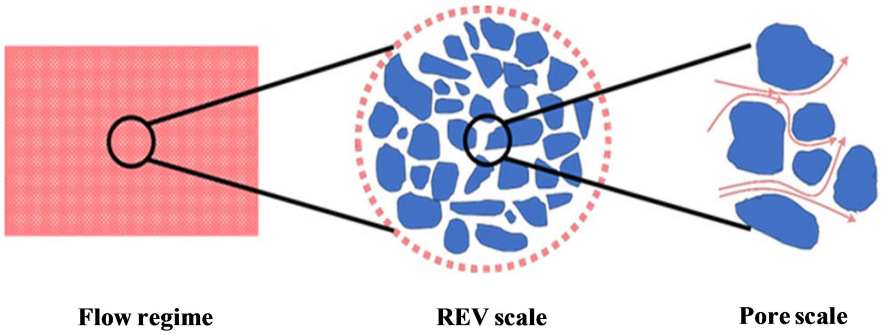

Figure 16. REV scale and pore scale approaches [130].

Among several computational fluid dynamics (CFD) methods, Lattice Boltzmann Method (LBM) has the robust capacity to simulate complicated physics (such as complex boundaries and geometry, heat transfer...), a large number of research utilize LBM to handle the REV-scale and pore-scale simulations of heat transfer mechanisms in porous medium, particularly the complicated phase change heat transfer phenomenon [131]. The Lattice Boltzmann method (LBM) appears as a relatively new numerical solution which is particle distribution-based and uses a simple kinetic model [132]. The principle of this approach is that particle distribution functions are employed to discretize the flow. Compared with other CFD methods, it has suitable advantages such as simple computation procedure, parallelizability, ability to simulate complicated geometries [132,133]. The first LBM application was proposed by McNamara et al. [134] in 1988 for handling fluid flow. However, the first LB application for fluid flow through a random porous medium was conducted by Succi et al. [135] in 1989. Recently, it is employed to analyze the phase change process and sensible storage phenomenon in porous medium [49, 136]. The pore-scale simulation treats the real porous structure as the computational domain while the REV-scale method adopts the porous computational domain as a uniformly mixed medium where statistical parameters (e.g. porosity, permeability, effective thermal conductivity) are used to characterize the porous

support. Therefore, Table 8 summarizes the main characteristics of applying LBM method at the REV scale and pore scale approaches to simulate the heat transfer mechanisms in porous structure (either during phase change phenomenon or sensible storage process).

Table 8. REV-scale versus pore-scale.

	REV-scale	**Pore-scale**
Principle	Volume average simulation (domain is considered as a uniform mixture)	Direct simulation
Advantages	Simple programming less computation requirements Large size of computation domain	Exhibit local information Exhibit interstitial heat transfer mechanism in pores
Disadvantages	Less reflect of transport mechanisms in pores	Limited computer resources Small size of computation domain Large computation requirements of porous matrix geometric Complex programming
Assumptions	Thermo-physical properties of fluid, PCM (if it is phase change phenomenon) and porous matrix are constant, homogeneous and isotropic The fluid flow and the liquid PCM are incompressible Porous matrix is rigid	
Computational domain [137, 138]	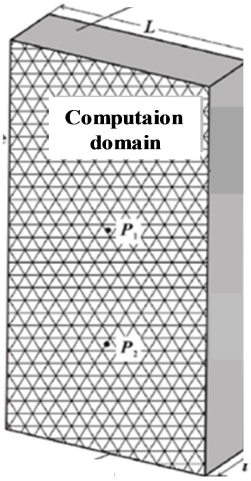	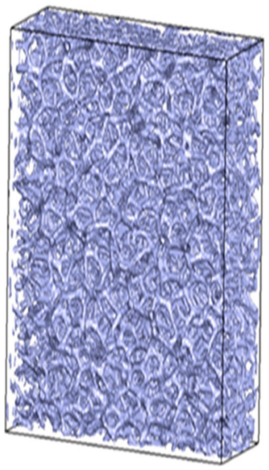
Momentum equation [109, 114]	Semi-empirical models are added to account the presence of porous structure $\frac{\partial \vec{u}}{\partial t}+\left(\vec{u}.\nabla\right)\left(\varepsilon^{-1}\vec{u}\right)=-\nabla\left(\varepsilon p\right)+\nu_f\nabla^2\vec{u}+\varepsilon.\vec{F}$ $\vec{F}=-\left(\frac{\nu_f}{K}+\frac{F_\varepsilon}{\sqrt{K}}\left\|\vec{u}\right\|\right)\vec{u}-g\beta\left(T-T_{ref}\right)$	No need to semi-empirical models because it handles the real pore structure $\frac{\partial \vec{u}}{\partial t}+\left(\vec{u}.\nabla\right)\vec{u}=-\frac{\nabla\left(p\right)}{\rho_f}+\nu_f\nabla^2\vec{u}+\vec{F}$ $\vec{F}=-g\beta\left(T-T_{ref}\right)$

Energy equation [109, 114]	**For solid phase** $\varepsilon\left(\rho C_p\right)_f\left(\frac{\partial T_f}{\partial t}+\vec{u}.\nabla T_f\right)=\nabla.\left(\lambda_{eff,f}\nabla T_f\right)$ $+h_{sf}a_{sf}\left(T_s-T_f\right)-\varepsilon\rho_f L_a\frac{\partial\Gamma}{\partial t}$ **For liquid phase** $\left(1-\varepsilon\right)\left(\rho C_p\right)_s\frac{\partial T_s}{\partial t}=\nabla.\left(\lambda_{eff,s}\nabla T_s\right)+h_{sf}a_{sf}\left(T_f-T_s\right)$	**For solid phase** $\frac{\partial\left(\rho_p H\right)}{\partial t}+\nabla.\left(\rho_f C_p u T_f\right)=\nabla.\left(\lambda_f\nabla T\right)$ $H=C_p T_f+f_l L$ **For liquid phase** $\frac{\partial\left(\rho C_p T\right)_s}{\partial t}=\nabla.\left(\lambda_s\nabla T\right)$
Flow field [137, 139]	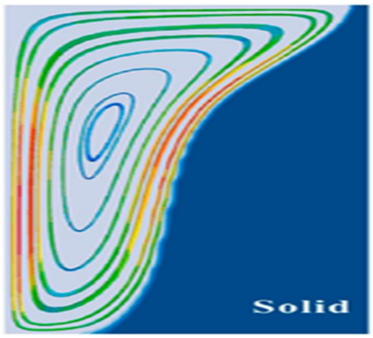 **F=0.0171**	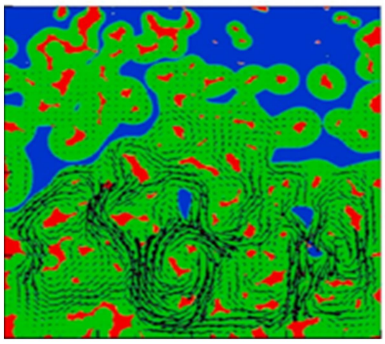 **F=0.04**
Temperature field [120, 140]	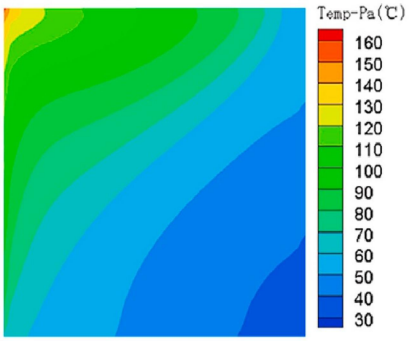 **4000s**	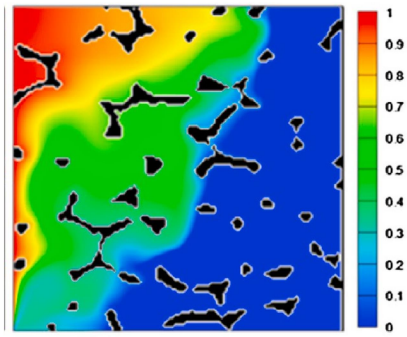 **F=0.06**
Solid-liquid interfaces [120, 140]	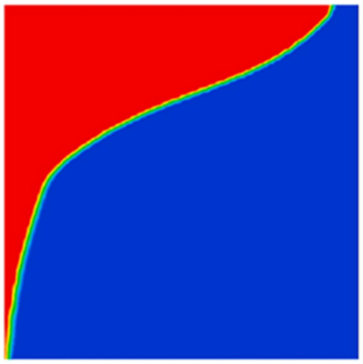	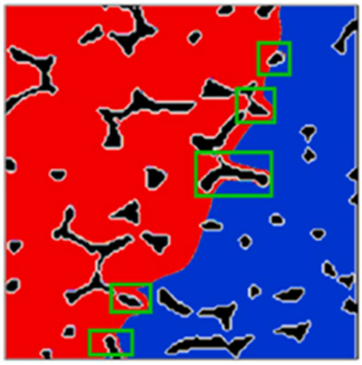

The effect of pore support is shown through a comparison of solid/liquid interfaces. As this comparison depicts, at the pore-scale method, the phase interface presents a zig-zag form with parallel parts to the skeleton, while these details cannot be seen in REV-scale simulation. On the other hand, as seen from the figures of the temperature field, the isotherm simulated by the REV approach was smoother than that by the pore scale method. In the pore scale simulation, many parallel parts to the skeleton interface appeared (usually the same trends) indicating the

effect of the body porous forces on the temperature distribution. The high thermal conductivity of the porous structure causes an irregular interface due to the non-uniform pore distribution. Generally, the LBM at the pore-scale or REV-scale method can simulate the overall heat transfer phenomenon in porous media, for instance a complex phase change phenomenon.

Lattice Boltzmann equations (LBEs) are classified in single relaxation time (SRT) model (known as Bhatnagar-Gross-Krook (BGK) model) and multiple relaxation time (MRT) model [130, 133]. The latest was proposed by d'Humières et al. [141] while the SRT model was proposed by Guo et al. [142]. The difference between these two models is in the collision term. More details can be found in Zhang et al. [109].

6. Conclusion

The current paper introduced a review on advanced research study in the scientific community regarding the application of sensible energy storage materials and phase change materials as sensible and latent energy storage strategies used in industrial and buildings sectors. Two application aspects were discussed: sensible heat storage process in porous medium and phase transition phenomenon in porous supports. Numerical method: lattice Boltzmann method is reviewed to handle these mechanisms. Presented literature was divided in two approaches in each numerical aspect based on the LBM: REV scale and pore scale methods. The reviewed articles were exhibited and their findings were analyzed. A summary of the used SHSMs and PCMs in porous matrices with their several characteristics are presented. Numerical simulations of the phase change heat transport problems using LBM are included. It was revealed that:

- Through a Bibliometric analysis published in the literature, amongst all the TES methods, LHS category appears to be the most pertinent technique investigated.
- SHS and LHS systems are most widely used in different applications owing to their high availability. However, most TCHS devices are not commercially available except in a small range of applications, due to their unstable lifetime and high prices.
- SHS method was strongly used in solar applications where water is the most mature material owing to its low cost and high specific heat capacity. Porosity is one of the main parameters that influence the SHS system performance.
- Pure PCMs suffer from their low thermal conductivity. They can be integrated into applications by six main incorporation modes where the impregnation of PCMs with porous

structure appears as the most relevant solution due to the high thermal conductivity of porous matrices.

- A comparison between SHSMs and PCMs shows that PCMs store between 5 and 14 times more energy than SHSMs in a smaller relative storage volume compared with that of sensible materials.
- LBM at the pore-scale and REV scale approaches presents great potential for the simulation of phase change phenomenon and sensible storage in porous medium owing to its transient inherence and robust ability to handle complicated physics. However, in the pore scale simulation, a detailed description can be captured.

Particular focus must be paid to optimization works relating to PCMs and SHSMs thermophysical, mechanical and geometrical characteristics. Two main research gaps were identified. The first important research gap is related to the low pertinence of environmental analysis and the second research gap is referred to the low techno-economic analysis. These analyzes play a key role in the commercialization of the investigated devices and the optimization of their utilization.

References

[1] Xu, H., Wang, N., Zhang, C., Qu, Z., Cao, M. (2020). Optimization on the melting performance of triplex-layer PCMs in a horizontal finned shell and tube thermal energy storage unit. Appl. Therm. Eng., 176, 115409.

[2] DeLong, J. P., Burger, O. (2015). Socio-economic instability and the scaling of energy use with population size. PloS one, 10 (6), e0130547.

[3] Dincer, I., Ezan, M. A. (2018). Heat storage: A unique solution for energy systems. Springer.

[4] Sarbu, I., Sebarchievici, C. (2016). Solar heating and cooling systems: Fundamentals, experiments and applications. Academic Press.

[5] Cabeza LF, editor (2015). Advances in thermal energy storage systems. Woodhead Publishing Series in Energy.

[6] Stutz, B., Le Pierrès, N., Kuznik, F., Johannes, K., Del Barrio, E. P., Bedecarrats, J. P., Gibout, S., Marty, P., Zalewski, L., Soto, J., Mazet, N. , Olives, R., Bezian, J. J., Minh, D. P. (2017). Storage of thermal solar energy. C. R. Phy., 18 (7-8), 401-414.

[7] Arce, P., Medrano, M., Gil, A., Oró, E., Cabeza, L. F. (2011). Overview of thermal energy storage (TES) potential energy savings and climate change mitigation in Spain and Europe. Appl. Energy, 88(8), 2764-2774.

[8] IRENA (2020), Innovation Outlook: Thermal Energy Storage, International Renewable Energy Agency, Abu Dhabi.

[9] Calderón, A., Barreneche, C., Hernández-Valle, K., Galindo, E., Segarra, M., Fernández, A. I. (2020). Where is Thermal Energy Storage (TES) research going?–A bibliometric analysis. Sol. Energy, 200, 37-50.

[10] Ibrahim, H., Ilinca, A., Perron, J. (2008). Energy storage systems—Characteristics and comparisons. Ren. Sust. energy Rev., 12(5), 1221-1250.

[11] Dahash, A. Ochs, F., Janetti, M. B., Streicher, W. (2019). Advances in seasonal thermal energy storage for solar district heating applications: A critical review on large-scale hot-water tank and pit thermal energy storage systems. Appl. Energy, 239, 296-315.

[12] Guo, F., Yang, X., Xu, L., Torrens, I., Hensen, J. (2017). A central solar-industrial waste heat heating system with large scale borehole thermal storage. Procedia Eng., 205, 1584-1591.

[13] Persson, J., Westermark, M. (2013). Low-energy buildings and seasonal thermal energy storages from a behavioral economics perspective. Appl. energy, 112, 975-980.

[14] Reed, A. L., Novelli, A. P., Doran, K. L., Ge, S., Lu, N., McCartney, J. S. (2018). Solar district heating with underground thermal energy storage: Pathways to commercial viability in North America. Ren. Energy, 126, 1-13.
[15] International Renewable Energy Agency (IRENA) (2013). The Energy Technology Systems Analysis Programme (ESTAP): Technology Brief E17, International Energy Agency (IEA).
[16] Navarro, L., De Gracia, A., Niall, D., Castell, A., Browne, M., McCormack, S. J., Griffiths, P., Cabeza, L. F. (2016). Thermal energy storage in building integrated thermal systems: A review. Part 2. Integration as passive system. Ren. Energy, 85, 1334-1356.
[17] Navarro, L., De Gracia, A., Colclough, S., Browne, M., McCormack, S. J., Griffiths, P., Cabeza, L. F. (2016). Thermal energy storage in building integrated thermal systems: A review. Part 1. active storage systems. Ren. Energy, 88, 526-547.
[18] Lizana, J., Chacartegui, R., Barrios-Padura, A., Valverde, J. M. (2017). Advances in thermal energy storage materials and their applications towards zero energy buildings: A critical review. Appl. Energy, 203, 219-239.
[19] Romdhane, S. B., Amamou, A., Khalifa, R. B., Said, N. M., Younsi, Z., Jemni, A. (2020). A review on thermal energy storage using phase change materials in passive building applications. J. Build. Eng., 101563.
[20] Rathore, P. K. S., Shukla, S. K. (2019). Potential of macroencapsulated PCM for thermal energy storage in buildings: A comprehensive review. Constr. Build. Mater., 225, 723-744.
[21] Hauer, A. Bayern, Z. (2011). Storage technology issues and opportunities. Workshop on Energy Storage: Issues and Opportunities, France, Paris.
[22] Calderón, A., Barreneche, C., Hernández-Valle, K., Galindo, E., Segarra, M., Fernández, A. I. (2020). Where is Thermal Energy Storage (TES) research going?–A bibliometric analysis. Sol. Energy, 200, 37-50.
[23] Borri, E., Tafone, A., Zsembinszki, G., Comodi, G., Romagnoli, A., Cabeza, L. F. (2020). Recent trends on liquid air energy storage: a bibliometric analysis. Appl. Sci., 10 (8), 2773.
[24] Tarragona, J., de Gracia, A., Cabeza, L. F. (2020). Bibliometric analysis of smart control applications in thermal energy storage systems. A model predictive control approach. J. Energy Storage, 32, 101704.
[25] Cárdenas-Ramírez, C., Jaramillo, F., Gómez, M. (2020). Systematic review of encapsulation and shape-stabilization of phase change materials. J. Energy Storage, 30, 101495.

[26] Mustapha, A. N., Onyeaka, H., Omoregbe, O., Ding, Y., Li, Y. (2021). Latent heat thermal energy storage: A bibliometric analysis explicating the paradigm from 2000–2019. J. Energy Storage, 33, 102027.
[27] Cabeza, L. F., de Gracia, A., Zsembinszki, G., Borri, E. (2021). Perspectives on thermal energy storage research. Energy, 231, 120943.
[28] Zhao, Y., Zhao, C. Y., Markides, C. N., Wang, H., Li, W. (2020). Medium-and high-temperature latent and thermochemical heat storage using metals and metallic compounds as heat storage media: A technical review. Appl. Energy, 280, 115950.
[29] De Gracia, A., Cabeza, L. F. (2015). Phase change materials and thermal energy storage for buildings. Energy Build., 103, 414-419.
[30] Chandel, S. S., Agarwal, T. (2017). Review of current state of research on energy storage, toxicity, health hazards and commercialization of phase changing materials. Ren. Sust. Energy Rev., 67, 581-596.
[31] Lin, Y., Alva, G., Fang, G. (2018). Review on thermal performances and applications of thermal energy storage systems with inorganic phase change materials. Energy, 165, 685-708.
[32] Fernández, A., Martínez, M., Segarra, M., Martorell, I., Cabeza, L. F. (2010). Selection of materials with potential in sensible thermal energy storage. Sol. Energy Mater. Sol. cells, 94 (10), 1723-1729.
[33] Kalaiselvam, S., Parameshwaran, R. (2014). Thermal energy storage technologies for sustainability: systems design, assessment and applications. Elsevier.
[34] Ståhl, F. (2009). Influence of thermal mass on the heating and cooling demands of a building unit. Chalmers Tekniska Hogskola (Sweden).
[35] Tatsidjodoung, P., Le Pierrès, N., Luo, L. (2013). A review of potential materials for thermal energy storage in building applications. Ren. Sust. Energy Rev., 18, 327-349.
[36] González-Roubaud, E., Pérez-Osorio, D., Prieto, C. (2017). Review of commercial thermal energy storage in concentrated solar power plants: Steam vs. molten salts. Renewable Ren. Sust. Energy Rev., 80, 133-148.
[37] Myers Jr, P. D., Goswami, D. Y. (2016). Thermal energy storage using chloride salts and their eutectics. Appl. Therm. Eng., 109, 889-900.
[38] Elashmawy, M. (2020). Improving the performance of a parabolic concentrator solar tracking-tubular solar still (PCST-TSS) using gravel as a sensible heat storage material. Desalination, 473, 114182.
[39] Koçak, B., Fernandez, A. I., Paksoy, H. (2020). Review on sensible thermal energy storage for industrial solar applications and sustainability aspects. Sol. Energy, 209, 135-169.

[40] Ashby, M.F. (2005). Materials Selection in Mechanical Design, 3rd ed., Elsevier, Oxford.

[41] Ashby, M. F., Shercliff, H., Cebon, D. (2018). Materials: engineering, science, processing and design. Butterworth-Heinemann.

[42] Ayyappan, S., Mayilsamy, K., Sreenarayanan, V. V. (2016). Performance improvement studies in a solar greenhouse drier using sensible heat storage materials. Heat Mass Transf., 52 (3), 459-467.

[43] Klein, P., Roos, T. H., Sheer, T. J. (2014). Experimental investigation into a packed bed thermal storage solution for solar gas turbine systems. Energy Procedia, 49, 840-849.

[44] Almendros-Ibáñez, J. A., Fernández-Torrijos, M., Díaz-Heras, M., Belmonte, J. F., Sobrino, C. (2019). A review of solar thermal energy storage in beds of particles: Packed and fluidized beds. Sol. Energy, 192, 193-237.

[45] Elouali, A., Kousksou, T., El Rhafiki, T., Hamdaoui, S., Mahdaoui, M., Allouhi, A., Zeraouli, Y. (2019). Physical models for packed bed: Sensible heat storage systems. J. Energy Storage, 23, 69-78.

[46] Pelay, U., Luo, L., Fan, Y., Stitou, D., Rood, M. (2017). Thermal energy storage systems for concentrated solar power plants. Ren. Sust. Energy Rev., 79, 82-100.

[47] Kumar, A., Kim, M. H. (2017). Solar air-heating system with packed-bed energy-storage systems. Ren. Sust. Energy Rev., 72, 215-227.

[48] Gil, A., Medrano, M., Martorell, I., Lázaro, A., Dolado, P., Zalba, B., Cabeza, L. F. (2010). State of the art on high temperature thermal energy storage for power generation. Part 1—Concepts, materials and modellization. Ren. Sust. Energy Rev., 14 (1), 31-55.

[49] Mabrouk, R., Naji, H., Dhahri, H. (2021). Numerical Investigation of Metal Foam Pore Density Effect on Sensible and Latent Heats Storage through an Enthalpy-Based REV-Scale Lattice Boltzmann Method. Processes, 9 (7), 1165.

[50] Amami, B., Rabhi, R., Dhahri, H., Mhimid, A. (2017). Numerical thermodynamic analysis of heat storage porous duct under pulsating flow using lattice Boltzmann method. Int. J. Exergy, 22 (4), 376-395.

[51] Kasaeian, A., Daneshazarian, R., Mahian, O., Kolsi, L., Chamkha, A. J., Wongwises, S., Pop, I. (2017). Nanofluid flow and heat transfer in porous media: a review of the latest developments. Int. J. Heat Mass Transf., 107, 778-791.

[52] Sheremet, M. A., Pop, I. (2015). Natural convection in a horizontal cylindrical annulus filled with a porous medium saturated by a nanofluid using Tiwari and Das' nanofluid model. Eur. Phy. J. Plus, 130 (6), 1-12.

[53] Sheremet, M. A., Grosan, T., Pop, I. (2015). Free convection in a square cavity filled with a porous medium saturated by nanofluid using Tiwari and Das' nanofluid model. Transp. Porous Media, 106(3), 595-610.
[54] Amami, B., Dhahri, H., Mhimid, A. (2014). Viscous dissipation effects on heat transfer, energy storage, and entropy generation for fluid flow in a porous channel submitted to a uniform magnetic field. J. Porous Media, 17 (10).
[55] Heap, M. J., Xu, T., Chen, C. F. (2014). The influence of porosity and vesicle size on the brittle strength of volcanic rocks and magma. Bull. Volcanol., 76 (9), 1-15.
[56] Dhifaoui, B., Jabrallah, S. B., Belghith, A., Corriou, J. P. (2007). Experimental study of the dynamic behaviour of a porous medium submitted to a wall heat flux in view of thermal energy storage by sensible heat. Int. J. Therm Sc, 46 (10), 1056-1063.
[57] Tian, Y., Zhao, C. Y. (2013). A review of solar collectors and thermal energy storage in solar thermal applications. Appl. Energy, 104, 538-553.
[58] Mahlia, T. M. I., Saktisahdan, T. J., Jannifar, A., Hasan, M. H., Matseelar, H. S. C. (2014). A review of available methods and development on energy storage; technology update. Ren. Sust. Energy Rev., 33, 532-545.
[59] Prasad, D. R., Senthilkumar, R., Lakshmanarao, G., Krishnan, S., Prasad, B. N. (2019). A critical review on thermal energy storage materials and systems for solar applications. AIMS Energy, 7(4), 507-526.
[60] Sharma, A., Tyagi, V. V., Chen, C. R., Buddhi, D. (2009). Review on thermal energy storage with phase change materials and applications. Ren. Sust. Energy Rev., 13 (2), 318-345.
[61] Garg, H. P., Mullick, S. C., Bhargava, A. K. (1985). Solar thermal energy storage. Dordrecht: Reidel Publishing Company.
[62] Pillai, K. K., Brinkworth, B. J. (1976). The storage of low grade thermal energy using phase change materials. Appl. Energy, 2 (3), 205-216.
[63] Alva, G., Lin, Y., Fang, G. (2018). An overview of thermal energy storage systems. Energy, 144, 341-378.
[64] Hasnain, S. M. (1998). Review on sustainable thermal energy storage technologies, Part I: heat storage materials and techniques. Energy Convers. Manag., 39 (11), 1127-1138.
[65] Zhao, C. Y., Lu, W., Tian, Y. (2010). Heat transfer enhancement for thermal energy storage using metal foams embedded within phase change materials (PCMs). Sol. energy, 84 (8), 1402-1412.
[66] Dincer I, Rosen MA. (2002). Thermal energy storage. Systems and applications. Chichester (England): John Wiley & Sons.

[67] Kimura, H., Kai, J. (1988). Mixtures of calcium chloride hexahydrate with some salt hydrates or anhydrous salts as latent heat storage materials. Energy Convers. Manag, 28 (3), 197-200.

[68] Abhat, A. (1983). Low temperature latent heat thermal energy storage: heat storage materials. Sol. Energy, 30 (4), 313-332.

[69] Jegadheeswaran, S., Pohekar, S. D. (2009). Performance enhancement in latent heat thermal storage system: a review. Ren. Sust. Energy Rev., 13 (9), 2225-2244.

[70] Nomura, T., Okinaka, N., Akiyama, T. (2010). Technology of latent heat storage for high temperature application: a review. ISIJ International, 50 (9), 1229-1239.

[71] Khadiran, T., Hussein, M. Z., Zainal, Z., Rusli, R. (2016). Advanced energy storage materials for building applications and their thermal performance characterization: A review. Ren. Sust. Energy Rev, 57, 916-928.

[72] Memon, S. A. (2014). Phase change materials integrated in building walls: A state of the art review. Ren. Sust. Energy Rev., 31, 870-906.

[73] Zhou, D., Zhao, C. Y., Tian, Y. (2012). Review on thermal energy storage with phase change materials (PCMs) in building applications. Appl. Energy, 92, 593-605.

[74] Wuttig, M., Yamada, N. (2007). Phase-change materials for rewriteable data storage. Nat. Mater., 6 (11), 824-832.

[75] Zhang, W., Mazzarello, R., Wuttig, M., Ma, E. (2019). Designing crystallization in phase-change materials for universal memory and neuro-inspired computing. Nat. Rev. Mater., 4 (3), 150-168.

[76] Yancheshme, A. A., Allahdini, A., Maghsoudi, K., Jafari, R., Momen, G. (2020). Potential anti-icing applications of encapsulated phase change material–embedded coatings; a review. J. Energy Storage, 31, 101638.

[77] Rostami, S., Afrand, M., Shahsavar, A., Sheikholeslami, M., Kalbasi, R., Aghakhani, S., Shadloo, M. S., Oztop, H. F. (2020). A review of melting and freezing processes of PCM/nano-PCM and their application in energy storage. Energy, 211, 118698.

[78] Dieckmann, J. H. (2006). Latent heat storage in concrete. University of Kaiserslautern, Germany.

[79] Sarbu, I., Dorca, A. (2019). Review on heat transfer analysis in thermal energy storage using latent heat storage systems and phase change materials. Int. J. Energy Res., 43 (1), 29-64.

[80] Faraj, K., Khaled, M., Faraj, J., Hachem, F., Castelain, C. (2020). Phase change material thermal energy storage systems for cooling applications in buildings: A review. Ren. Sust. Energy Rev., 119, 109579.

[81] Akeiber, H., Nejat, P., Majid, M. Z. A., Wahid, M. A., Jomehzadeh, F., Famileh, I. Z., Calautit, J. K., Hughes B. R., Zaki, S. A. (2016). A review on phase change material (PCM) for sustainable passive cooling in building envelopes. Ren. Sust. Energy Rev., 60, 1470-1497.

[82] Cabeza, L. F., Castell, A., Barreneche, C. D., De Gracia, A., Fernández, A. I. (2011). Materials used as PCM in thermal energy storage in buildings: A review. Ren. Sust. Energy Rev., 15 (3), 1675-1695.

[83] Battisti, A., Persiani, S. G., Crespi, M. (2019). Review and mapping of parameters for the early stage design of adaptive building technologies through life cycle assessment tools. Energies, 12 (9), 1729.

[84] Fabiani, C., Pisello, A. L., Barbanera, M., Cabeza, L. F., Cotana, F. (2019). Assessing the potentiality of animal fat based-bio phase change materials (PCM) for building applications: an innovative multipurpose thermal investigation. Energies, 12 (6), 1111.

[85] Alam, M., Zou, P. X., Sanjayan, J., Ramakrishnan, S. (2019). Energy saving performance assessment and lessons learned from the operation of an active phase change materials system in a multi-storey building in Melbourne. Appl. Energy, 238, 1582-1595.

[86] Arivazhagan, R., Geetha, N. B., Sivasamy, P., Kumaran, P., Gnanamithra, M. K., Sankar, S., Loganathan, G. B., Arivarasan, A. (2020). Review on performance assessment of phase change materials in buildings for thermal management through passive approach. Mater. Today: Proceedings, 22, 419-431.

[87] Umair, M. M., Zhang, Y., Iqbal, K., Zhang, S., Tang, B. (2019). Novel strategies and supporting materials applied to shape-stabilize organic phase change materials for thermal energy storage–A review. Appl. Energy, 235, 846-873.

[88] Kenisarin, M. M. (2014). Thermophysical properties of some organic phase change materials for latent heat storage. A review. Sol. Energy, 107, 553-575.

[89] Zhang, N., Yuan, Y., Cao, X., Du, Y., Zhang, Z., Gui, Y. (2018). Latent heat thermal energy storage systems with solid–liquid phase change materials: a review. Adv. Eng. Mater., 20(6), 1700753.

[90] Souayfane, F., Fardoun, F., Biwole, P. H. (2016). Phase change materials (PCM) for cooling applications in buildings: A review. Energy Build., 129, 396-431.

[91] Ferrer, G., Solé, A., Barreneche, C., Martorell, I., Cabeza, L. F. (2015). Review on the methodology used in thermal stability characterization of phase change materials. Ren. Sust. Energy Rev., 50, 665-685.

[92] Khudhair, A. M., Farid, M. M. (2004). A review on energy conservation in building applications with thermal storage by latent heat using phase change materials. Energy Convers. Manag., 45 (2), 263-275.

[93] Shchukina, E. M., Graham, M., Zheng, Z., Shchukin, D. G. (2018). Nanoencapsulation of phase change materials for advanced thermal energy storage systems. Chem. Soc. Rev., 47 (11), 4156-4175.
[94] Al Shannaq, R., Farid, M. M. (2015). Microencapsulation of phase change materials (PCMs) for thermal energy storage systems. In Advances in Thermal Energy Storage Systems (pp. 247-284). Woodhead Publishing.
[95] Liu, C., Rao, Z., Zhao, J., Huo, Y., Li, Y. (2015). Review on nanoencapsulated phase change materials: preparation, characterization and heat transfer enhancement. Nano Energy, 13, 814-826.
[96] Liu, L., Alva, G., Huang, X., Fang, G. (2016). Preparation, heat transfer and flow properties of microencapsulated phase change materials for thermal energy storage. Ren. Sust. Energy Rev., 66, 399-414.
[97] Umair, M. M., Zhang, Y., Iqbal, K., Zhang, S., Tang, B. (2019). Novel strategies and supporting materials applied to shape-stabilize organic phase change materials for thermal energy storage–A review. Appl. Energy, 235, 846-873.
[98] Weaver, J. A., Viskanta, R. (1986). Freezing of water saturated porous media in a rectangular cavity. Int. Comm. Heat Mass Transf., 13 (3), 245-252.
[99] Wang, Z., Situ, W., Li, X., Zhang, G., Huang, Z., Yuan, W., Yang, C., Yang, C. (2017). Novel shape stabilized phase change material based on epoxy matrix with ultrahigh cycle life for thermal energy storage. Appl. Therm. Eng., 123, 1006-1012.
[100] Xiao, X., Zhang, P., Li, M. (2013). Preparation and thermal characterization of paraffin/metal foam composite phase change material. Appl. Energy, 112, 1357-1366.
[101] Huang, X., Chen, X., Li, A., Atinafu, D., Gao, H., Dong, W., Wang, G. (2019). Shape-stabilized phase change materials based on porous supports for thermal energy storage applications. Chem. Eng. J., 356, 641-661.
[102] Zhang, H. L., Baeyens, J., Degrève, J., Cáceres, G., Segal, R., Pitié, F. (2014). Latent heat storage with tubular-encapsulated phase change materials (PCMs). Energy, 76, 66-72.
[103] Ling, Z., Zhang, Z., Shi, G., Fang, X., Wang, L., Gao, X., Fang, Y., Xu, T. Wang, S., Liu, X. (2014). Review on thermal management systems using phase change materials for electronic components, Li-ion batteries and photovoltaic modules. Ren. Sust. Energy Rev., 31, 427-438.
[104] Khodadadi, J. M., Fan, L., Babaei, H. (2013). Thermal conductivity enhancement of nanostructure-based colloidal suspensions utilized as phase change materials for thermal energy storage: a review. Ren. Sust. Energy Rev., 24, 418-444.

[105] Sarkar, J., Ghosh, P., Adil, A. (2015). A review on hybrid nanofluids: recent research, development and applications. Ren. Sust. Energy Rev., 43, 164-177.
[106] Şahan, N., Fois, M., Paksoy, H. (2015). Improving thermal conductivity phase change materials—A study of paraffin nanomagnetite composites. Sol. Energy Mater. Sol. Cells, 137, 61-67.
[107] Zhai, X. Q., Wang, X. L., Wang, T., Wang, R. Z. (2013). A review on phase change cold storage in air-conditioning system: Materials and applications. Ren. Sust. Energy Rev., 22, 108-120.
[108] Feng, D., Feng, Y., Qiu, L., Li, P., Zang, Y., Zou, H., Yu, Z., Zhang, X. (2019). Review on nanoporous composite phase change materials: Fabrication, characterization, enhancement and molecular simulation. Ren. Sust. Energy Rev., 109, 578-605.
[109] Zhang, S., Feng, D., Shi, L., Wang, L., Jin, Y., Tian, L., Li, Z., Wang, G., Zhao, L., Yan, Y. (2021). A review of phase change heat transfer in shape-stabilized phase change materials (ss-PCMs) based on porous supports for thermal energy storage. Ren. Sust. Energy Rev., 135, 110127.
[110] Gao, H., Wang, J., Chen, X., Wang, G., Huang, X., Li, A., Dong, W. (2018). Nanoconfinement effects on thermal properties of nanoporous shape-stabilized composite PCMs: A review. Nano Energy, 53, 769-797.
[111] Zhao, Y., Zhao, C. Y., Markides, C. N., Wang, H., Li, W. (2020). Medium-and high-temperature latent and thermochemical heat storage using metals and metallic compounds as heat storage media: A technical review. Appl. Energy, 280, 115950.
[112] Mesalhy, O., Lafdi, K., Elgafy, A., Bowman, K. (2005). Numerical study for enhancing the thermal conductivity of phase change material (PCM) storage using high thermal conductivity porous matrix. Energy Convers. Manag., 46(6), 847-867.
[113] Alva, G., Liu, L., Huang, X., Fang, G. (2017). Thermal energy storage materials and systems for solar energy applications. Ren. Sust. Energy Rev., 68, 693-706.
[114] Mabrouk, R., Naji, H., Dhahri, H., Hammouda, S., Younsi, Z. (2020). Numerical investigation of porosity effect on a PCM's thermal performance in a porous rectangular channel via thermal lattice Boltzmann method. Int. Comm. Heat Mass Transf., 119, 104992.
[115] Mabrouk, R., Naji, H., Dhahri, H., Younsi, Z. (2020). Insight into Foam Pore Effect on Phase Change Process in a Plane Channel under Forced Convection Using the Thermal Lattice Boltzmann Method. Energies, 13 (15), 3979.
[116] Yang, X., Wei, P., Wang, X., He, Y. L. (2020). Gradient design of pore parameters on the melting process in a thermal energy storage unit filled with open-cell metal foam. Appl. Energy, 268, 115019.

[117] Li, Z., Shahsavar, A., Al-Rashed, A. A., Talebizadehsardari, P. (2020). Effect of porous medium and nanoparticles presences in a counter-current triple-tube composite porous/nano-PCM system. Appl. Therm. Eng., 167, 114777.
[118] Sardari, P. T., Mohammed, H. I., Giddings, D., Gillott, M., Grant, D. (2019). Numerical study of a multiple-segment metal foam-PCM latent heat storage unit: Effect of porosity, pore density and location of heat source. Energy, 189, 116108.
[119] Yang, X., Bai, Q., Zhang, Q., Hu, W., Jin, L., Yan, J. (2018). Thermal and economic analysis of charging and discharging characteristics of composite phase change materials for cold storage. Appl. Energy, 225, 585-599.
[120] Zhang, P., Meng, Z. N., Zhu, H., Wang, Y. L., Peng, S. P. (2017). Melting heat transfer characteristics of a composite phase change material fabricated by paraffin and metal foam. Appl. Energy, 185, 1971-1983.
[121] Atal, A., Wang, Y., Harsha, M., Sengupta, S. (2016). Effect of porosity of conducting matrix on a phase change energy storage device. Int. J. Heat Mass Transf., 93, 9-16.
[122] Mallow, A., Abdelaziz, O., Graham, S. (2018). Thermal charging performance of enhanced phase change material composites for thermal battery design. Int. J. Therm. Sci., 127, 19-28.
[123] Li, W. Q., Qu, Z. G., He, Y. L., Tao, W. Q. (2012). Experimental and numerical studies on melting phase change heat transfer in open-cell metallic foams filled with paraffin. Appl. Therm. Eng., 37, 1-9.
[124] Allen, M. J., Bergman, T. L., Faghri, A., Sharifi, N. (2015). Robust heat transfer enhancement during melting and solidification of a phase change material using a combined heat pipe-metal foam or foil configuration. J. Heat Transf., 137 (10).
[125] Devaux, P., Farid, M. M. (2017). Benefits of PCM underfloor heating with PCM wallboards for space heating in winter. Appl. Energy, 191, 593-602.
[126] De Schampheleire, S., De Jaeger, P., De Kerpel, K., Ameel, B., Huisseune, H., De Paepe, M. (2016). How to study thermal applications of open-cell metal foam: Experiments and computational fluid dynamics. Materials, 9 (2), 94.
[127] Al-Abidi, A. A., Mat, S. B., Sopian, K., Sulaiman, M. Y., Mohammed, A. T. (2013). CFD applications for latent heat thermal energy storage: a review. Ren. Sust. Energy Rev., 20, 353-363.
[128] Agyenim, F., Hewitt, N., Eames, P., Smyth, M. (2010). A review of materials, heat transfer and phase change problem formulation for latent heat thermal energy storage systems (LHTESS). Ren. Sust. Energy Rev., 14 (2), 615-628.

[129] Liu, Q., Feng, X. B., He, Y. L., Lu, C. W., Gu, Q. H. (2019). Three-dimensional multiple-relaxation-time lattice Boltzmann models for single-phase and solid-liquid phase-change heat transfer in porous media at the REV scale. Appl. Therm. Eng., 152, 319-337.
[130] He, Y. L., Liu, Q., Li, Q., Tao, W. Q. (2019). Lattice Boltzmann methods for single-phase and solid-liquid phase-change heat transfer in porous media: A review. Int. J. Heat Mass Transf., 129, 160-197.
[131] Ma, Q., Chen, Z., Liu, H. (2017). Multiple-relaxation-time lattice Boltzmann simulation for flow, mass transfer, and adsorption in porous media. Phys. Rev. E, 96 (1), 013313.
[132] Li, Q., Luo, K. H., Kang, Q. J., He, Y. L., Chen, Q., Liu, Q. (2016). Lattice Boltzmann methods for multiphase flow and phase-change heat transfer. Progress in Energy and Combustion Science, 52, 62-105.
[133] Gao, D., Chen, Z. (2011). Lattice Boltzmann simulation of natural convection dominated melting in a rectangular cavity filled with porous media. Int. J. Therm. Sci., 50 (4), 493-501.
[134] McNamara, G. R., Zanetti, G. (1988). Use of the Boltzmann equation to simulate lattice-gas automata. Phys. Rev. let., 61 (20), 2332.
[135] Succi, S., Foti, E., Higuera, F. (1989). Three-dimensional flows in complex geometries with the lattice Boltzmann method. *EPL (*Europhysics Letters), 10 (5), 433.
[136] Luo, K., Yao, F. J., Yi, H. L., Tan, H. P. (2015). Lattice Boltzmann simulation of convection melting in complex heat storage systems filled with phase change materials. Appl. Therm. Eng., 86, 238-250.
[137] Yang, X., Bai, Q., Guo, Z., Niu, Z., Yang, C., Jin, L., Lu, T. J., Yan, J. (2018). Comparison of direct numerical simulation with volume-averaged method on composite phase change materials for thermal energy storage. Appl. Energy, 229, 700-714.
[138] Li, X., Zhu, Z., Xu, Z., Ma, T., Zhang, H., Liu, J., Wang, X., Wang, Q. (2019). A three-dimensional pore-scale lattice Boltzmann model for investigating the supergravity effects on charging process. Appl. Energy, 254, 113507.
[139] Ren, Q., He, Y. L., Su, K. Z., Chan, C. L. (2017). Investigation of the effect of metal foam characteristics on the PCM melting performance in a latent heat thermal energy storage unit by pore-scale lattice Boltzmann modeling. Numer. Heat Transf., Part A: Appl., 72 (10), 745-764.
[140] Li, X., Ma, T., Liu, J., Zhang, H., Wang, Q. (2018). Pore-scale investigation of gravity effects on phase change heat transfer characteristics using lattice Boltzmann method. Appl. Energy, 222, 92-103.

[141] d'Humières, D., Shizgal, B. D. (1992). Rarefied gas dynamics: theory and simulations. The American Institute of Aeronautics and Astronautics, 450-458.
[142] Guo, Z., Zhao, T. S. (2002). Lattice Boltzmann model for incompressible flows through porous media. Phys. Rev. E, 66 (3), 036304.

Chapter 2

Lattice Boltzmann simulation of forced convection melting of a composite phase change material with heat dissipation through an open-ended channel

Abstract

This paper performs a numerical analysis of time-dependent forced convection heat transfer in an open-ended straightchannel filled with a metal structure and paraffin as a phase change material (PCM). The steady two-dimensional governing equations, based on the Darcy-Brinkmann-Forchheimer (DBF) model and the two-energy transport equations (i.e. local thermal non-equilibrium, LTNE) at the representative elementary volume (REV) scale in their dimensionless forms, have been simulated using the thermal single relaxation time (T-SRT) Lattice Boltzmann Method (LBM) with three distribution functions to handle the fluid, and temperatures of the fluid and solid phases. Effects of Reynolds number ($100 \le \mathrm{Re} \le 600$), Eckert number ($0 \le Ec \le 10$), porosity ($0.1 \le \varepsilon \le 0.8$) on dynamic and thermal fields, entropy generation, and energy and exergy efficiencies of the considered system are examined. The relevance of these parameters is highlighted and discussed during the charging (melting) and discharging (solidifying) processes. Interestingly, it can be stated that small porosities promptly accelerate these two processes due to high thermal conductivity of the metal foam/PCM composite, and improve energy and exergy efficiencies of the system, whatever *Re* for the very low porosity values (0.4 and 0.6). In addition, streamlines, isotherms and melt front (phase field) are exhibited for this parameters range.

Based on the findings obtained, it is concluded that, in the context of laminar forced convection melting of a composite PCM with heat dissipation in a porous PCM-filled channel, 1) there is a critical Reynolds number for which the storage energy is optimal and whose quality is improved using both the porosity and the effects of viscous dissipation, and 2) the proposed approach's potential and the in-house code flexibility implemented are demonstrated.

1. Introduction

Recently, porous supports are increasingly used in thermal and chemical systems (TCS) because of many advantages provided such as heat transfer rate increasing, temperature homogenization, increasing heat flux absorption, and thermal insulation. Thereby, they are becoming passive cooling enhancers increasingly persuasive. Likewise, convective flows can constitute a cooling activator since they increase convective thermal transport. In addition, the use of porous media associated with phase change materials (PCMs) have emerged as an

attractive way for storing/releasing sensible heat. The many processes targeted and their application covers many sectors such as, cement, desalination equipment, thermal insulation, electronic chips cooling, solar collectors, solar absorbers, food processing, drying processes, air-condionning, water treatment, shale gas production, oil recovery, and so on.

It is now well known that thermal energy storage systems (TESS) have huge potential for an economic use of thermal equipment and large-scale energy substitution. Of all the TESS available, the most interesting is the latent heat thermal energy systems (LHTES). The thermal energy storage reduces the time gap between supply and demand, improves the energy systems performance and helps conserve energy.This storage can be achieved by using several heat kinds (sensible, thermochemical or latent). Among these types, latent heat energy storage (LHES) via PCMs is the most preferred and widely used method at present.PCMs benefit greatly from this type of being able to be stored or released over a tiny temperature range.Paraffin, an organic PCM, continues to attract interest in terms of research and use. However, its low thermal conductivity is its main drawback that hinders the heat conduction within it and, hence, decreases its effectiveness. Thereby, metal foams have been deployed to remedy this weakness.

It should be noted that open metal foams have become a backing material to enhance heat transfer due to their large surface area/volume ratio and high thermal conductivity, making them widely used for heat transfer enhancement applications during solid-liquid phase change. The Thermal conductivity can be further enhanced in many ways by adding high thermal conductivity materials such as metal foaming [1, 2], porous graphite [3], carbon nanofibre [4], internal fins [5,6] to cite a few, and nanoparticles [7, 8] for shaping new composite PCMs.

Deng et al. [9] studied the melting behavior of a PCM in a porous metallic foam. They examined the effects of many parameters including porosity and fractal dimension on the melting heat transfer while verifying their model experimentally. They demonstrated that the interstitial heat transfer at the PCM/matrix interface for melting behaviors is crucial. Atal et al. [10] conducted an experimental and numerical study of a thermal energy storage device in a shell and tube arrangement containing paraffin wax and metal foam of different porosity (77% and 95%). They found that the metal foam affected the speed of the charging-discharging cycle and that the numerical simulation corroborated the measurements.Wang et al. [11] experimentally studied heat storage performance (of a Li-ion battery) of paraffin and an aluminum/PCM (paraffin) foam composite. They stated that such a composite material has a good cooling effect during the discharging cycle. In addition, they pointed out that the effective thermal conductivity of the composite is extremely superior to that of pure paraffin

and that the melting time has been mitigated by about 25%. Cui et al. [12] experimentally investigated paraffin's heat charging process filling a high porosity copper foam. They showed that the metal foam addition allowed to further harmonize the thermal field while reducing the charging time. In addition to experimental studies, numerical studies have been and continue to be conducted to handle fluid flows and heat transfers in porous media. These studies are often based on traditional methods, such as the finite difference methods (FDM), finite volume methods (FVM), finite element methods (FEM), and direct numerical methods (DNM). From its beginnings, the lattice Boltzmann method (LBM) appeared as an alternative method because of its physical potential to incorporate advanced algorithms, to be parallelizable and easy to implement. Furthermore, interest in such a method has been steadily increasing since it grew out of lattice gas models in the late 1980s. The LBM being by nature explicit, it is more suitable for GPU (Graphics Processing Unit) to handle computations via the nVIDIA's compute unified device architecture (CUDA) technique because of its simple parallelism, which proven to reduce computation time compared to traditional CPU simulation. Thereby, it has become very useful for handling many physical and engineering problems 13], and for modeling physical phenomena involving complex boundary conditions and multiphasic interfaces [14]. Furthermore, Zhang et al. [15] successfully applied the LBM using a double-distribution function (DDF) thermal model to investigate gaz flow condensation in micro-channel typified by a boundary temperature jump. They highlighted its ability to handle the temperature jump at the gas-solid interface in the microchannel.

At the representative elementary volume (REV) scale, Krishnan et al. [16] numerically studied the natural convection transient melting of a PCM embedded in a metal matrix and occuring in a rectangular enclosure under local thermal non-equilibrium (LTNE) condition using a two-temperature model. They have pointed out that the foam reduces the overheating during the unsteady state, despite a lower melt volume fraction at steady state. Hu et al. [17] examined the heat transfer behavior of a PCM/metal foam system using a direct numerical simulation (DNS) and a two temperature models (one- and two temperature equations) based on LTE and LTNE assumptions. They stated that the effective thermal conductivity of the PCM/micro-foam structure is a key parameter to well-match the temperature profiles and liquid PCM volume fraction of the two simulations.Chen et al. [18] numerically examined the PCM (wax) melting behavior in metal foams at the REV scale with experimental support. They pointed out that these are able to enhance the PCM heat transfer during the melting using a double population LBM. Tao et al. [19] conducted an LBM simulation of latent heat storage (LHS) performance of metal foams/composite PCM (CPCM). They targeted effects of the pore density and porosity on PCM-temperature, dynamic field, PCM melting rate, and

thermal energy storage (TES) capacity. Wu et al. [20] proposed and widely validated a novel multiple relaxation times (MRT)-LBM with double distributions functions to simulate transient melting problems in porous media at REV scale. Zhu et al. [21] analyzed the energy storage efficiency of an embeddded PCM in graduated porous finned metal foams using both LBM and FVM approaches. They stated that key parameters as the metal fin thickness, metal foam porosity gradient and pore number could reduce the total melting time and enhance greatly the energy storage performance.

The open-ended straightchannel incorporating a porous medium (here copper foam) and PCM-filled may be a template of LHTES. It is therefore this model, where a convective flow with heat transfer under the LTNE constraint occurs, which is investigated numerically via a SRT-LBM approach. It is also to address the low thermal conductivity role of PCMs when used alone whose disadvantage is to slow down the thermal energy charging and discharging rates.

Up to the authors' knowledge, the topics on TESS almost often dealt with natural convection. Thereby, our mainly aim here is to numerically investigate forced convection in an open-ended channel filled with a metal structure and paraffin via the LBM. The forced flow for both charging and discharging cycles is generated by the Brinkman-Forchheimer extended Darcy model under the LTNE assumption. In addition, energy and exergy analyzes are also achieved by assessing the performance behavior and efficiency of the LHTES herein considered via charging/discharging (melting/solidification) cycles' energy balance.

Furthermore, according to our review, it would appear that Al-Sumaily et al. [22, 23] are among the rare authors to have addressed a forced flow convection in a channel with or without non-zero average pulsatile upstream flow. Explicitly these authors have dealt the convective flow over a circular cylinder mounted either in an empty two-dimensional channel or filled with porous media under the LTNE assumption. Note that in their study, there is fully no PCM. They concluded that the use of porous media promotes much better heat transfer improvement than can be achieved with pulsed flow. In addition, they showed that the porous particles alter significantly the unsteady dynamic and thermal fields inside the channel, sometimes suppressing the wake behind the cylinder.

Through the non-exhaustive literature thereby browsed, it appears that the LBM simulation of forced convection melting of a PCM incorporated in a metal structure with energy dissipation remains scarce. This is the main reason for fulfilling such a study.

Indeed, for several years now, the LBM, a mesoscopic CFD method, has become an outstanding numerical method for convective fluid flows with and without heat transfer in any form (conduction, convection, phase change, radiation, etc.). Different from traditional CFD

methods that numerically handle Navier-Stokes and energy equations, it is based on the fluid particle clusters evolution on a finite lattice an even at the REV level. It is increasingly used to address various complex flows such as convective flows and transport in porous media,improvement of heat transfers in porous media by sensible or latent heat via a PCM. Such flows are ubiquitous in many contexts, and their numerical handling with such a method has become one of the most popular topics in engineering. It should be noted that in recent decades, the LBM approach has been successfully applied to many fluid dynamics heat transfer problems, including fluid flows in porous medium, thermal flows with and without phase change thanks to the simple form of the governing equations regarded(mesoscopic kinetic equations, local spatio-temporal processing, straightforward parallelism, ability to handle complex boundaries conditions, and easy grid generation) compared to conventional CFD approaches (finite volumes (FVM), finite elements methods (FEM) and others).

In general, an LBM consists of a regular lattice with particles set residing on the lattice nodes. In this work, the single relaxation time approach (SRT-LBM), also known as BGK-LBM, has been used in which a set of discrete temperature velocity and temperature distribution functions evolve at each time step via a streaming step followed by a collision in that order.

The remainder of this paper is organized as follows. After the literature review (*Section 1*), the problem statement, related governing equations along with appropriate boundaries conditions (BCs) to be solved via the numerical simulation are presented in Section 2. Afterwards, the entropy generation and the thermal performances through energy and exergy balances of the considered system are briefly reported in Section 3. The numerical method of solution is outlined and validated in Section 4. Thereafter, Section 5 presents and comments investigations of our predictions. Finally, Section 6 completes the paper with the main findings, which are drawn from numerical simulations.

2. Problem statement, conjectures and mathematical model

2.1 Problem statement

The flow under consideration and the coordinate system are schematically depicted in Figure 1. It involves anopen-ended straight channel embedding a porous medium (copper foam) which is filled with paraffin as a PCM. Its height and length, as well as the boundary conditions (BCs) considered are illustrated. As seen, the channel entrance is hot at the isothermal temperature of T_h, while its exit is cold at the isothermal temperature of T_C. The top and bottom walls are thermally insulated. The outlet conditions are assumed to be fully developed. In other words, Neumann BCs are imposed. In addition, the hot fluid (T_h) enters

the channel at an uniform velocity U_i. It should be noted that the melting point of the PCM is T_m and that at the initial time, the left temperature is raised to T_h ($T_h > T_m$) thereby melting the PCM.

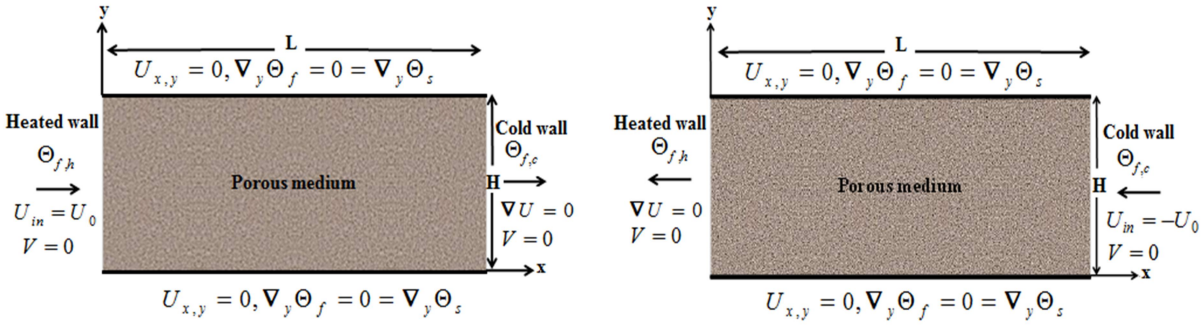

(a) *Charging case* (b) *Discharging case*

Figure 1. Physical model sketch, x and y denotingstreamwise and wall-normal directions, respectively.

2.2 Key conjectures

The following assumptions are considered through the present study to simplify the problem as follows: Steady state, two-dimensional laminar flow of fluid and liquid paraffin, and neglected natural convection and radiation (Forced convection predominates). Further, the fluid is Newtonian and viscous while satisfying the Boussinesq approximation. The thermo-physical properties of the solid porous matrix and the fluid are homogeneous and isotropic. Given the differences between the thermo-physical properties of paraffin and copper foam, the LTNE assumption stands during the transient heat transfer process; further details can be found in Nield and Bejan [24], to cite a few.

2.3 Governing equations

For handling laminar flow through the porous medium with melting, the DBF model (generalized Navier-Stokes equations) and the energy transport equations (at the REV) given by Eqs. (1)-(4) are considered in their dimensionless forms. These are [21-23]:

•Equations of fluid dynamics

To analyze the forced convection of PCM embedded in the metal foam, the dimensionless governing equations are adopted as following

$$\nabla \cdot \vec{U} = 0 \tag{1}$$

$$\frac{\partial \vec{U}}{\partial \tilde{t}} + \left(\vec{U}.\nabla\right)\left(\varepsilon^{-1}\vec{U}\right) = -\nabla\left(\varepsilon P\right) + Re^{-1}\nabla^2\vec{U} + \varepsilon.\vec{F} \tag{2}$$

Noted that, in the case of a solid matrix free channel, these equations reduce to the usual Navier-Stokes equations by taking $\varepsilon = 1$ and infinite Da (see relationship (5) hereafter).

•Equations of heat transfer.

To quantitatively analyze the energy stored in the composite, two equation models are used in this study. These reflect transient heat exchanges between the metal foam and the PCM. Such models can be written as

$$\frac{\partial \Theta_f}{\partial \tilde{t}} + U.\nabla \Theta_f = \frac{1}{Re.Pr}\nabla.\left(\frac{\lambda_{eff,f}}{\lambda_f}\nabla\left(\frac{\Theta_f}{\varepsilon}\right)\right) + Kr.\frac{Bi}{Re.Pr}\left(\frac{\Theta_s - \Theta_f}{\varepsilon}\right) - \frac{1}{Ste}\frac{\partial \Gamma}{\partial \tilde{t}} + \tilde{\Phi} \tag{3}$$

$$\frac{\partial \Theta_s}{\partial \tilde{t}} = \frac{Kr}{Rc}\frac{1}{Re.Pr}\nabla.\left(\frac{\lambda_{eff,s}}{\lambda_s}\nabla\left(\frac{\Theta_s}{1-\varepsilon}\right)\right) - \frac{Kr}{Rc}.\frac{Bi}{Re.Pr}\left(\frac{\Theta_s - \Theta_f}{1-\varepsilon}\right) \tag{4}$$

In Eqs. (1)-(4), $\vec{U}$ and$P$are the volume-averagedvelocity and pressure over the computational cell. ε and $\vec{F}$ denote the porous medium's porosity and the total force due to its presence and other external forces. Θ_f and Θ_s , are the fluid and porous medium temperatures, and Γ and $\tilde{\Phi}$ are the PCM liquid fraction and the viscous dissipation, respectively.

Note that here, the governing energy Eqs. (3)-(4) are written for the PCM (fluid phase) and metal foam (solid phase) separately. Similarly, the temperature equation of the fluid phase (3) reduces to the standard fluid temperature equation when $Bi = 0$.

The total body force induced by the porous matrix (metal foam) and other external force fields can be expressed as [16]

$$\vec{F} = -\left(\frac{1}{Re\,Da} + \frac{F_\varepsilon}{\sqrt{Da}}\left\|\vec{U}\right\|\right)\vec{U} \tag{5}$$

F_ε being the inertial coefficient also called the Forchheimer coefficient.

The relationship for the viscous dissipation within the the system can be written as follows [25,26], to mention a few.

$$\tilde{\Phi} = \varepsilon.Ec\left\{\frac{1}{Da.Re} + \frac{F_\varepsilon}{\sqrt{Da}}\left\|\vec{U}\right\|\right\}\left\|\vec{U}\right\|^2 + Ec.Re^{-1}\left\{2\left[\left(\frac{\partial U}{\partial X}\right)^2 + \left(\frac{\partial V}{\partial Y}\right)^2\right] + \left(\frac{\partial U}{\partial Y} + \frac{\partial V}{\partial X}\right)^2\right\} \tag{6}$$

Based on Ergun's empirical relationships [27], F_ε and K can be written as

$$F_\varepsilon = 0.068 \text{ for metal foams, } F_\varepsilon = 1.75\left(150\varepsilon^3\right)^{-0.5} \text{ for a spherical particles packed bed} \tag{7}$$

$$\text{and } K = \varepsilon^3 d_p^2 / \left[150\left(1-\varepsilon\right)^2\right] \tag{8}$$

K being the porous medium permeability.

It should be noted that the viscous heat dissipation effect is controlled by the Brinkman number, i.e. $Br = Ec \times Pr$ and that the DBF model have been extensively reviewed, notably

by Niel and Bejean [24] and Ingham and Pop [28], to name a few, and the aforementioned expressions (7)-(8) have been derived via an empirical fit.

It appears that the forced convection heat transfer problem governed by Eqs. (1)-(4) is characterized by the following key dimensionless parameters

$$Da = K / H^2, Pr = \nu_f / \alpha_f, Re = U_{in} H / \nu_f, Rc = (\rho C_p)_s / (\rho C_p)_f, Kr = \lambda_s / \lambda_f,$$
$$Bi = h_{sf} a_{sf} H^2 / \lambda_s, Ste = C_{pf}(T_h - T_m) / La, Ec = U_{in}^2 / C_f \Delta T_{ref} \quad (9)$$

In point of fact, to deal with the physical problem, the following dimensionless variables have used in deriving Eqs. (1)-(4)

$$(X,Y) = (x,y)/H, (U,V) = (u,v)/U_{in}, P = p/\rho U_{in}^2, \tilde{t} = tU_{in}/H, \Theta = T - T_c / \Delta T_{ref},$$
$$\Delta T_{ref} = T_h - T_c \quad (10)$$

In the present investigtion, the interfacial heat transfer coefficient h_{sf} and the specific surface area a_{sf} are computed from the following empirical correlations [29]

$$h_{sf} = 0.76.Re_d^{0.4} Pr^{0.37} \lambda_f / d_f \quad for \quad 1 \le Re_d \le 40 \quad (11)$$

with $d_f = 1.18\left((1-\varepsilon)/3\pi\right)^{1/2} d_p$, $Re_d = Re\, d_p / (\varepsilon H)$

and $a_{sf} = 3\pi d_f (1 - e^{-(1-\varepsilon)/0.004}) / (0.59 d_p)^2, with\ d_p = 22.4x10^{-3} / \omega \quad (12)$

The liquid fraction Γ is computed using the following relationship from the enthalpy method [30], to name a few:

$$\Gamma = \begin{cases} 0 & T < T_m - \Delta T \\ \dfrac{T - T_m + \Delta T}{2\Delta T} & if \quad T_m - \Delta T < T < T_m + \Delta T \\ 1 & T > T_m + \Delta T \end{cases} \quad (13)$$

Recall that the porous channel is filled with solid PCM whose melting temperature is T_m, and $2\Delta T$ is the melting temperature range.Initially, bothmetal foamand paraffin are atequilibrium at temperature T_0 and the entire channel is at the low temperature T_C.

•Boundary and initial conditions (BCs & IC)

In the charging case, the dimensionless Bcs and IC are expressed asfollows:

- $U = 1$; $V = 0$; $\Theta_{f,h} = 1$, at $X = 0$ and $0 \le Y \le 1$ (inlet);
- $\nabla_X U = 0$; $V = 0$; $\Theta_{f,c} = 0$ at $X = L/H$ and $0 \le Y \le 1$ (outlet);
- $U = 0$; $V = 0$ and $\nabla_y \Theta_{f,h} = \nabla_y \Theta_{f,s} = 0$ at $0 \le X \le L/H$ and $Y = 1$ (top);
- $U = 0$; $V = 0$ and $\nabla_y \Theta_{f,h} = \nabla_y \Theta_{f,s} = 0$ at $0 \le X \le L/H$ and $Y = 0$ (bottom);
- $U = 0$; $V = 0$ and $\Theta_f = 0$ at $\tilde{t} = 0$ for $0 \le X \le L/H$ and $0 \le Y \le 1$ (IC).

It is worth reiterating that the above Eqs. (1)-(4) along these BCs and IC are the mathematical model for investigating the steady forced convective flow in a porous media with phase change under LTNE.

3. Entropy generation and thermal performance through energy and exergy balances

3.1 Entropy generation

The TES optimization has often been achieved by scrutinizing the entropy generation arising in these systems. Moreover, the entropy generation is closely linked to the irreversibilities that prevail there. As such, it has become a useful measure of their extent. These are generated through fluid friction and heat transfer due to viscous dissipation and temperature gradients, respectively. Thereby, herein, the entropy generation, based on the LTNE conjecture for the porous media fluid and solid phases, can be set forth via a dimensionless number (Ns), called entropy generation number. It can be split into two terms as follows (Torabi et al. [31])

$$Ns = Ns_f + Ns_s \tag{14}$$

Ns_f and Ns_s being the dimensionless entropy generation for the fluid and solid phases, respectively.Note that the smaller such a number, the better the performance of the system considered. The two numbers just mentionedcan be read as follows [31] according to the previously mentioned dimensionless parameters (see relationships (9) - (10)):

$$\begin{aligned} Ns_f = & \underbrace{\frac{\varepsilon}{(\Theta_f + \Pi)^2}\left[\left(\frac{\partial \Theta_f}{\partial X}\right)^2 + \left(\frac{\partial \Theta_f}{\partial Y}\right)^2\right]}_{\textit{entropy generation due to heat transfer}} + \underbrace{\frac{\varepsilon.Ec.Pr}{\left(\Theta_f + \Pi\right)}\left(\frac{1}{Da} + \frac{Re.F_\varepsilon}{\sqrt{Da}}\left\|\vec{U}\right\|\right)\left\|\vec{U}\right\|^2}_{\textit{entropy generation due to Darcy-Brinkmann-Forchheimer force}} \\ & + \underbrace{\frac{Ec.Pr}{\left(\Theta_f + \Pi\right)}\left[2\left(\left(\frac{\partial U}{\partial X}\right)^2 + \left(\frac{\partial V}{\partial Y}\right)^2\right) + \left(\frac{\partial U}{\partial Y} + \frac{\partial V}{\partial X}\right)^2\right]}_{\textit{entropy generation due to viscous dissipation}} \\ & + \underbrace{\frac{Bi.Kr(\Theta_s - \Theta_f)}{\Theta_f + \Pi}}_{\textit{entropy generation due to heat exchange between phases in porous media}} \end{aligned} \tag{15}$$

$$Ns_s = \frac{(1-\varepsilon)Kr}{\left(\Theta_s + \Pi\right)^2}\left[\left(\frac{\partial \Theta_s}{\partial X}\right)^2 + \left(\frac{\partial \Theta_s}{\partial Y}\right)^2\right] - \frac{Bi.Kr(\Theta_s - \Theta_f)}{\Theta_s + \Pi} \tag{16}$$

where $\Pi \left(= T_c / \Delta T_{ref}\right)$ is a dimensionless temperature.

It is worthnoting that, according to authors' best knowledge, studies on convective flows in porous open-ended channels saturated with a PCM and generating heat, remain scarce or evennonexistent.

3.2 Energy efficiency

The assessment of the performance, behavior and efficiency of the LHTES can be achieved via the charging/discharging (melting/solidifying) cycles' energy balance as follows (e.g., see [32, 33])

For the charging process, one can write:

Energy input - Energy loss = Energy accumulation (*stored*) (17)

An energy balance for the storing cycle

Energy accumulation (*stored*) = - *Energy loss* (18)

So, the energy efficiency for the charging cycle can be taken as

$$\eta_{charging} = E_{accumulation} / E_{input} \tag{19}$$

An energy balance for the discharging cycle allows to write out

Energy accumulation (stored) = - (Energy recovered + Energy loss) (20)

Thus, an energy balance for the discharging cycle can be given as

$$\eta_{discharging} = E_{recovered} / E_{accumulation} \tag{21}$$

The overall energy efficiency (global) can be defined as the products of the energy efficiency of the charging, and discharging phases [32, 34, 35]

$$\eta = \prod_i \eta_i = \eta_{charging} \times \eta_{discharging} = 100 \times \left(E_{recovered} / E_{input} \right) \tag{22}$$

where $E_{recovered}$ and E_{input} are respectively characterized the energy recovered from the system during the discharging period and the energy input to the system during the charging period which are explained as the corresponding expressions

$$E_{input} = \dot{m} C_{p,f} \Delta T_{f,charging} + E_{diss,charging} + E_{latent,charging} \tag{23}$$

$$E_{recovered} = \dot{m} C_{p,f} \Delta T_{f,discharging} + E_{diss,discharging} + E_{latent,discharging} \tag{24}$$

where $E_{latent} \left(= \dot{m}_f \, C_{p,f} \times La \right)$ is the latent energy during the process of phase change [19] and E_{diss} is the dissipation energy which [33]

$$E_{diss} = \iint \tilde{\Phi} dS \tag{25}$$

More details on this analysis can be found in [19, 32-34], to name a few.

3.3 Exergy efficiency

In terms of exergy, the exergy efficiency can be assessed by performing an exergy balance during the charging (*melting*) and discharging (*solidification*) processes. Exergy balances and associated efficiency can be provided via Eqs. (26) - (32):

For the charging process, one can write:

Exergy input - Exergy output - Exergy consumption = Exergy accumulation (stored) (26)

For stored period, the exergy balance can be expressed as [32]

Exergy accumulation (stored) = - (Exergy loss + Exergy consumption) (27)

Thereby, the exergy efficiency for charging period is expressed as

$$\psi_{charging} = Ex_{stored} / Ex_{input} \tag{28}$$

An exergy balance can be written for the discharging period as

-(Exergy recovered + Exergy loss) - Exergy consumption =Exergy accumulation (stored) (26)

So, the exergy efficiency for discharging period is defined as

$$\psi_{discharging} = Ex_{recovered} / Ex_{stored} \tag{29}$$

So, the overal exergy efficiency (global) for the whole system is given asthe products of the exergy efficiency of the charging, and discharging phases [32]

$$\psi = \psi_{charging} \times \psi_{discharging} = 100 \times \left(Ex_{recovered} / Ex_{input} \right) \tag{30}$$

where $Ex_{recovered}$ and Ex_{input} are respectively characterized the exergy recovered from the system during the discharging period and the exergy input to the system during the charging period which are explained as the corresponding expressions:

$$Ex_{input} = \dot{m} C_{p,f} \left(T_{f,in} - T_{f,out} \right)_{charging} - T_0 \dot{m} C_{p,f} Ln \left(\frac{T_{f,in}}{T_{f,out}} \right)_{charging} \tag{31}$$

$$Ex_{recovered} = \dot{m} C_{p,f} \left(T_{f,out} - T_{f,in} \right)_{discharging} - \dot{m} C_{p,f} Ln \left(\frac{T_{f,out}}{T_{f,in}} \right)_{discharging} \tag{32}$$

For more details on this approach (Exergy's balance and efficiency), the interested reader can refer to Refs. [32, 33, 35, 36], to name a few.

4. Numerical method of solution

To numerically solve the above equations' system (see *Sub-section 2.3*), we chose the LBM, which is now considered and reviewed in detail in the literature. Indeed, in the last few decades, such a method has become an outstanding numerical method for fluid flows. It handles the evolution of fluid particle clusters that propagate on a regular lattice to neighboring particles while redistributing their moments over the collision process. Since

then, it has been significantly improved, so that many problems can now be tackled. It is more and more used to successfully simulate various complex flows, such as flows in a porous medium with and without heat transfer. Unless stated up, recall the main advantages of such a method, namely its simplicity, its efficient implementation for parallel computing and its ability to deal with complex geometries and/or boundary conditions of any type.

The LBM at the pore scale or at REV is ideally suited for handling transport processes and heat transfer in porous media whose pores may have a complex geometry. Overall, when dealing with transport phenomena in porous media, there are two main classes, namely the pore scale approach [18, 19, 21, 37, 38], etc.and the REV approach [39, 40]. Though the first category seems to be a simplest tool, it may have weak points in terms of geometry and computational domain size (especially, large domains). Thereby, the second category is often preferred. However, initially, the REV-scale LBM did not consider the change process phase. Note that the mathematical modeling of such problem remains a challenging task because of its nonlinear nature and the porous structure complexity. In addition to this lack, almost all previous LB models for forced convection in porous media are based on a single energy equation because of the invoked local thermal equilibrium (LTE) condition. Thereby, we aim here to apply such an approach to simulate the problem of forced convection melting in a porous medium at the REV scale in the LTNE situation where the viscous dissipation is taken into account. Such a condition reflects the temperature difference between the porous medium and the PCM.

To achieve this study, we lean on a three density functions (TDF) method to simulate the dynamic field, the PCM's thermal field and that of the solid matrix. In other words, the velocity field and thermal fields within the PCM and solid matrix are handled separately using a specific distribution function [20, 39, 41].

4.1 Lattice Boltzmann equation for fluid flow

As previously mentioned, a thermal LBM with three distribution functions is here considered to simulate the phase change with convection in a porous medium at the REV scale to address the above governing equations with appropriate BCs et ICs.

The continuity and momentum Eqs. (1)-(2) are modeled by the modified BGK-LBE (lattice Boltzmann equation) based on the SRT approximation. Thereby, the density distribution function [39, 42] for the velocity can be written as follows:

$$f_i\left(x+e_i\delta t,t+e_i\delta t\right)-f_i\left(x,t\right)=-\delta t\omega_i\left[f_i\left(x,t\right)-f_i^{eq}\left(x,t\right)\right]+\delta tF_{e_i} \tag{33}$$

Here $\omega_i\,(=1/\tau_v)$ is the single relaxation collision frequency, $\tau_v\,(=3\nu+0.5)$ being the dimensionless relaxation time; e_i isthe discrete velocity in direction i, $f_i(x,t)$ is the density

distribution function with velocity e_i at position x and time t, δt is the time increment,and $f_i^{eq}(x,t)$ is the equilibrium distribution function (EDF), which for the D2Q9 (*Qb denotes b velocity directions in nD space*) modelcan be defined as

$$f_i^{eq} = \rho w_i \left[1 + \frac{e_i u}{c_s^2} + \frac{uu : \left(e_i e_i - c_s^2 I \right)}{2 c_s^4 \varepsilon} \right] \tag{34}$$

where w_i is the weight, c_s $(= c/\sqrt{3})$ is the sound speed and I is the unit tensor. For the D2Q9 lattice model adopted here, w_i are set as: $w_0 = 4/9$, $w_{1,4} = 1/9$ and $w_{5,8} = 1/36$. The so-called D2Q9-discret velocity model is given as

$$e_i = \begin{cases} (0,0) \\ c\left[\cos\left((i-1)\pi/2 \right), \sin\left((i-1)\pi/2 \right) \right], i = 1-4 \\ \sqrt{2} c\left[\cos\left((2i-9)\pi/4 \right), \sin\left((2i-9)\pi/4 \right) \right], i = 5-8 \end{cases} \tag{35}$$

where c $(= \delta x / \delta t)$ is the lattice speed, δx and δt being the lattice spacingand time step, respectively. The discrete force term F_{ei} inEq. (33) can be expressed as [43]

$$F_{ei} = F \left(e_i - u \right)^2 f_i^{eq} / RT_0 \tag{36}$$

The macroscopic fluid variables, density ρ and velocity u, are obtained from the distribution functions moments as follows

$$\rho = \sum_i f_i \,,\; u = \sum_i f_i e_i / \rho + \delta t F_{e_i} / 2 \tag{37}$$

It should be pointed out that the numerical implementation of the BGK-LBE (Eqs. 33) is achieved via two steps, viz. collision and streaming (advection) steps

$$f_i^* (x,t) = f_i (x,t) - \delta t \omega_i \left[f_i (x,t) - f_i^{eq} (x,t) \right] + \delta t F_{e_i} \tag{38}$$

$$f_i \left(x + e_i \delta t, t + e_i \delta t \right) = f_i^* (x,t) \tag{39}$$

$f_i^* (x,t)$ being the post-collision distribution function.

4.2 Lattice Boltzmann equation for solid-liquid phase change

Still here, the Boltzmann model on the BGK-LBMlattice for solid-liquid phase change prevails to simulate the melting process in LHTES with metal foams. Therefore, the following temperature evolution equations for solving the Eqs. (3) and (4)are considered as follows [19, 44, 45]

$$\begin{aligned} g_{f,i} \left(x + e_i \delta t, t + \delta t \right) - g_{fi} (x,t) = & -\omega_{T,f} \left(g_{fi} (x,t) - g_{fi}^{eq} (x,t) \right) \\ & + \left(1 + \delta t \partial_t / 2 \right) \delta t S r_{i,f} + \delta t f_i (x,t) q_i \end{aligned} \tag{40}$$

$$g_{si}\left(x+e_i\delta t,t+\delta t\right)-g_{si}\left(x,t\right)=-\omega_{T,s}\left(g_{si}\left(x,t\right)-g_{si}^{eq}\left(x,t\right)\right)+\left(1+\delta t\partial_t/2\right)\delta tSr_{i,s} \tag{41}$$

where the subscripts f and s denote the fluid and solid phases, respectively. Here, $g_{f,i}$ and $g_{f,i}^{eq}$ are the temperature distribution function and the equilibrium temperature distribution function, respectively. Sr_i is the discrete source term and $\omega_{T,f;s}\left(=1/\tau_{T,f;s}\right)$ is the single relaxation collision frequency for temperature distribution function, $\tau_{T,f;s}$ being the dimensionless relaxation timesset as[45]

$$\tau_{T,f}=3\alpha_{e,f}/(\delta tc^2)+0.5 \tag{42}$$

$$\tau_{T,s}=3\alpha_{e,s}/(\delta tc^2)+0.5 \tag{43}$$

with $\alpha_{e,f}=k_{e,f}/\left(\varepsilon(\rho C_p)_f\right)$ and $\alpha_{e,s}=k_{e,s}/\left((1-\varepsilon)(\rho C_p)_s\right)$ pointing out PCM (in the fluid state) and solid matrix effective diffusivities, respectively.

According to Shi et al. [46], the internal heat production q_i (source term) associated with the viscous heat dissipation can be stated as:

$$q_i=-\left(f_i-f_i^{eq}\right)\left(e_i-u\right)\left(e_i-u\right):\nabla u \tag{44}$$

To match the energy Eqs. (3) - (4) with the LB Eqs. (40) - (41), appropriate equilibrium distribution functions (EDFs) and discrete source terms ($Sr_{i,f;s}$) have to be provided. So, the EDFs g_{fi}^{eq} and g_{si}^{eq} are expressed respectively as

$$g_{fi}^{eq}=w_iT_f\left(1+\frac{e_iu}{\varepsilon c_s^2}\right) \tag{45}$$

$$g_{si}^{eq}=w_iT_s \tag{46}$$

As for the source terms $Sr_{i,f}$ and $Sr_{i,s}$, they are given by the following [45]

$$Sr_{i,f}=w_i\left(\frac{La}{C_{p,f}}\left[\frac{\gamma(t+\delta t)-\gamma(t)}{\delta t}\right]+\frac{h(T_s-T_f)}{\varepsilon(\rho C_p)_f}\right) \tag{47}$$

$$Sr_{i,s}=w_i\frac{h(T_s-T_f)}{(1-\varepsilon)(\rho C_p)_s} \tag{48}$$

The average temperatures of the fluid and the solid matrix are found as follows

$$T_f=\sum g_{fi} \tag{49}$$

$$T_s=\sum g_{si} \tag{50}$$

It is to be noted thatthe implementation of BCs is of great importance for the simulation via the LBM approach. Thereby, the conditions specified above (see *Sub-section 2.3*) have been

converted to the mesoscopic level in terms of distribution functions f_i and g_i. Here, it is the usual bounce-back condition that has been applied to all solid walls, thereby being located with a good approximation between the last "fluid" node and the first "solid" point. For more details on this approach, see the Refs. [47, 48], to name a few.

4.3 Validation and grid independency

Numerical outcomes need to be independent for the grid used. Hence, the grid study is performed before validating. Thereby, simulations have been performed for a *Re* number of 200 using several (six) grids, viz. 320×80, 400×100, 460×115, 480×120, 500×125 and 550×130. Figure 2 shows dimensionless solid temperature (Θ_s) profiles vs. the transverse distance X at $Y=0.5$ for $Pr=50, Bi=0.1, Ste=1, Kr=10^{+3}, Rc=1, Ec=5$ and $\varepsilon=0.5$. As shown the difference between the first and second grid (320×80 and 400×100) is 14.3% that is reduced to 7% compared with third grid (460×115). As seen, the last three grids are closer to each other exhibiting a maximum discrepancy of 0.6%, thereby indicating that the solution becomes independent of grid size at 480x120 for the case dealt. This size is a best trade-off between accuracy and computation time. So, from now on, it is adopted for subsequent computations.

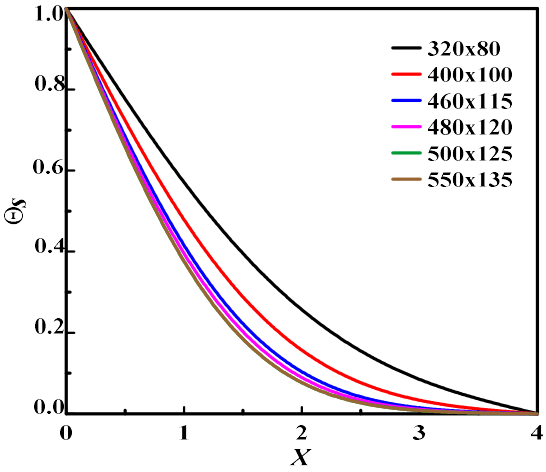

Figure 2. Mesh independency test of dimensionless solid temperature (Θ_s) profiles for $Re=200$ at Y=0.5 with $Pr=50, Bi=0.1, Ste=1, Kr=10^{+3}, Rc=1, Ec=5$ and $\varepsilon=0.5$.

It is now well accepted that any simulation requires prior validation withnumerical and/or experimental results available in the literature. Thereby, to validate the accuracy of the BGK-LBM adopted here, the numerical results were first compared with results of Kim et al. [49] who had numerically dealtthe steady and pulsatileforced convective flow in a porous medium filled channel. Figure 3 depicts the velocity profiles vs. the transverse coordinate Y atsection $X=0.5$ while exhibiting the Darcy number effect. It is shown that our preliminary simulations (for validation) are in good agreement with results of Ref. [49].

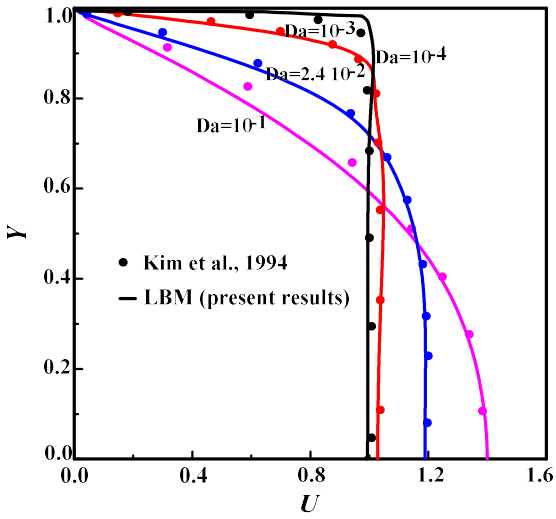

Figure 3. U-velocity profilesvs. dimensionless transverse distance at X=0.5(fully-developed region) for $Re = 50$ and $Pr = 0.7$. Comparison with Kim et al.' results [49].

To further support this validation, other results were compared to those reported by Abdedou et al. [50] who addressed the problem of forced convection heat transfer in a 2D planar channel filled with a saturated porous medium where an internal heat release takes place.

Based on our preliminaries simulations, figure 4 presents the dimensionless solide-to-fluide temperature difference ($\Theta_f - \Theta_s$), also called the LTNE intensity, vs. the transverse distance at two axial positions, viz. X=0.14 and X=0.5. It can be seen that the LTNE intensity decreases in the tranverse direction. In addition, the figure compares such a LTNE intensity showing that our results are matched well with Abdedou al.'s predictions [50], while already validating the LTNE assumption issued, which will be further confirmed in the following section (see, e.g., Figures. 8, 9, and 10 a).

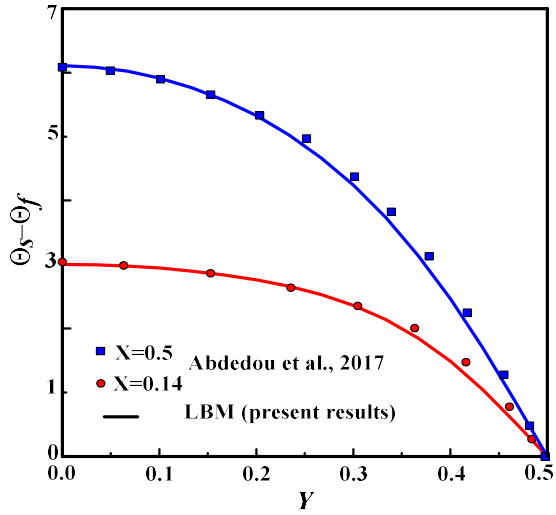

Figure 4. LTNE intensity, $\Theta_s - \Theta_f$, vs.dimensionless transverse distance at two axial sections for $Da = 10^{-4}, Bi = 0.01, Re = 100 = Rq$ and $Kr = 1$. Comparison with results of Ref. [50].

Through these figures, we can state that our results corroborate those chosen for the preliminary validation. To sum up, from these comparisons, it appears that the numerical approach provides satisfactory results, thereby supporting us as to the reliability of our in-house code implemented.

5. Results and discussion

The numerical solution method described up (see Sub-section 4.2 and 4.3) has been applied to numerically handle the considered problem, viz. the steady forced convective flow in a porous medium filled channelwith phase change under LTNE. In this work, the numbers of Prandtl, Biot, Stephan, Darcy, thermal conductivity ratio, and heat capacity ratio were held fixed to $Pr = 50, Bi = 0.1, Ste = 1, Da = 10^{-3}, Kr = 10^{3}, Rc = 1$, respectively. Unless otherwise stated, all computations reported in this study were performed with a uniform grid composed of 480x120 cells. Recall that velocity and temperatures fields are computed via a TDF method, one for the dynamic field and the other two for the liquid and solid phases.

5.1 Reynolds effect on the U-velocity

Figure 5 portrays the Reynlods number effects on the *U*-velocity during the charging and discharging process at $X = 0.5$. The following parameters have been considered to silence their effects: $Pr = 50, Kr = 10^{+3}, Rc = 1, Bi = 0.1, Da = 10^{-3}, Ec = 0$ and $\varepsilon = 0.6$. As can be seen, these profiles become closer to each other when the *Re* number exceeds 200. In other words, the velocity becomes stabilized at these *Re* values, thereby exhibiting almost similar profiles.This can be explained by the fact that high Re numbers reduce the viscous resistance offered to the fluid in the presence of a porous medium low porosity. Therefore, a decrease in the porosity of the metal foam prevents (brakes) the circulation of the fluid and, then, exhibits almost closer velocity profiles.

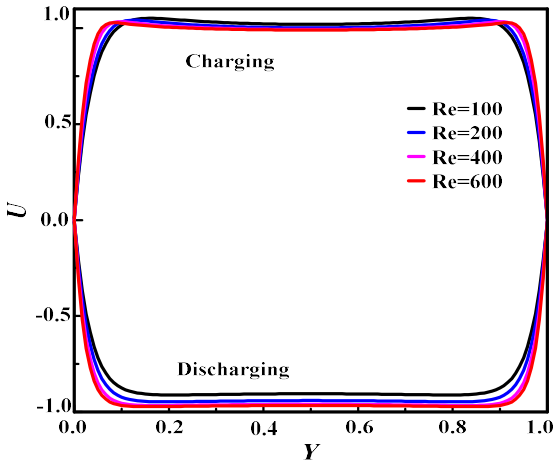

Figure 5. Reynolds number effects on *U*-velocity during charging and discharging processes at X =0.5 using $Pr = 50, Kr = 10^{+3}, Rc = 1, Bi = 0.1, Da = 10^{-3}, Ec = 0$ and $\varepsilon = 0.6$.

Figure 6 displays the *U*-contours plots for different *Re* numbers during the charging process. Interestingly, it is found that, at $Re = 100$, the flow field exhibits a nearly elliptic vortex in the channel due to the higher thermal conductivity ratio which improves the circulation intensity in the porous medium. As *Re* increases from 200 to 600, the flow field presents the same structure while showing two strong counter-rotating vortices due to the internal heat rise in the channel core. So, it can be concluded that at the inlet, the flow is not fully developed due to the presence of two elliptical vortices which disappear from 1/3 of the channel. From this, it appears that, a large number Re leads to a fully developed flow while minimizing and adjusting the flow recirculation when the permeability of the porous medium is lower.

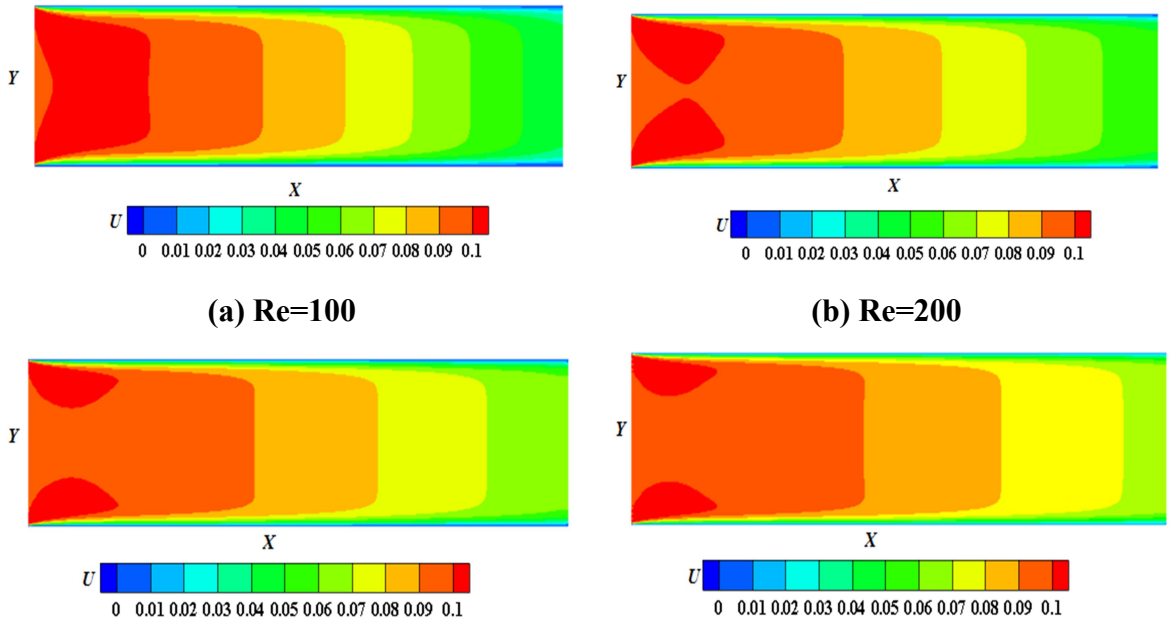

(a) Re=100 **(b) Re=200**

(c) Re =400 **(d) Re = 600**

Figure 6. Reynolds number effect on *U*-contours duringthe chargingprocesswith $Pr = 50, Kr = 10^{+3}, Rc = 1, Bi = 0.1, Da = 10^{-3}, Ec = 0$ and $\varepsilon = 0.6$.

The panel in figure 7 shows the *U*-contours plots during the discharging process as the Reynolds number increases from 100 to 600. As in the previous case, it can be noted that the profiles have similar shapes and that, for the considered *Re* range, the discharging cycle is performed rapidly as the *Re* number rises with a slight core increase of the two elliptical vortices due to the cold entry of the flow in the opposite direction. Note that the *Re* number's increase yields a flow acceleration and the formation of two contra-rotating vortices which are reduced compared to the same during charging period. This is due to the lower internal heat rise at the channel core end.

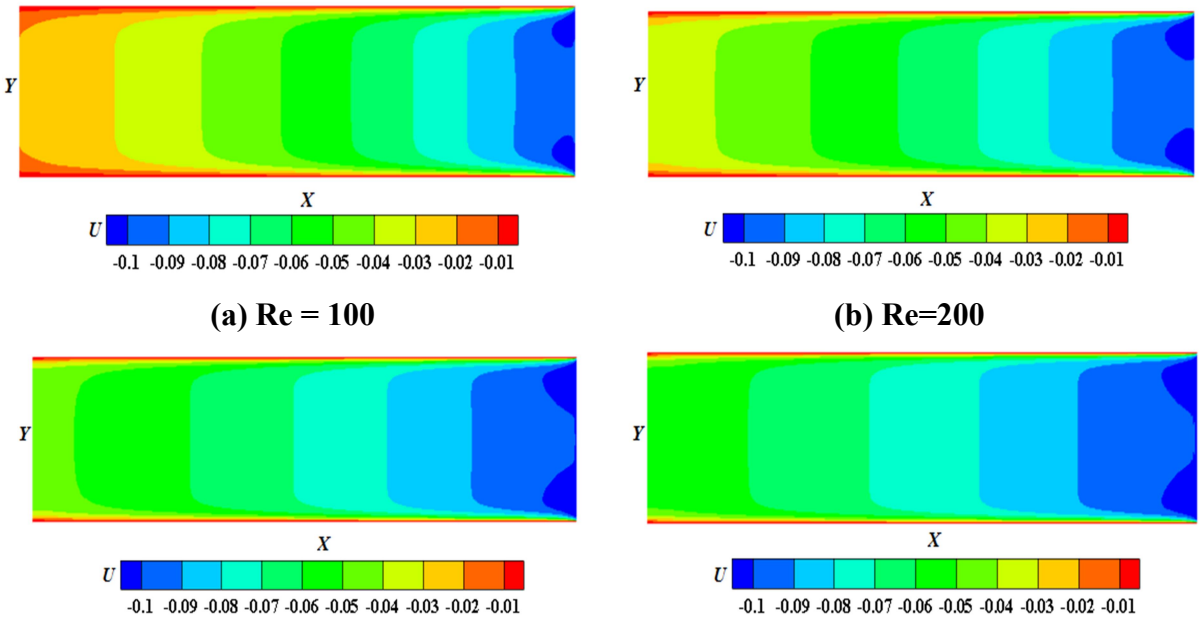

(a) Re = 100 **(b) Re=200**

(c) Re=400 **(d) Re=600**

Figure 7. Reynolds number effect on U-contours during the discharging processwith $Pr = 50, Kr = 10^{+3}, Rc = 1, Bi = 0.1, Da = 10^{-3}, Ec = 0$ and $\varepsilon = 0.6$.

5.2 Reynolds number effect on temperature and LTNE intensity

Figure 8 shows the temperature contours, Θ_f and Θ_s, for four Re numbers, viz., $Re = 100, 200, 400$ and 600 during the charging process without viscous dissipation ($Ec = 0$). It is explicitly demonstrated that the heat propagation is very slow at $Re = 100$ for fluid phase temperature (Θ_f) compared with that of the solid phase temperature (Θ_s). However, for fairly large Reynolds numbers (200 - 600), the heat propagation accelerates indicating that the forced convection prevails in the channel because of the porous medium higher thermal conductivity which contributes to the heat transfer acceleration for high Re's values. It can be stated that during the charging process, the solid phase extracts heat from the fluid thanks to the high thermal conductivity. This trend is pronounced as Re increases. Besides, it appears, undeniably, from this figure that the hypothesis $\Theta_s \neq \Theta_f$ (the LTNE assumption) emitted is effective everywhere in the channel except at the entry and at the exit where rather it is the local thermal equilibrium (LTE) which takes place.

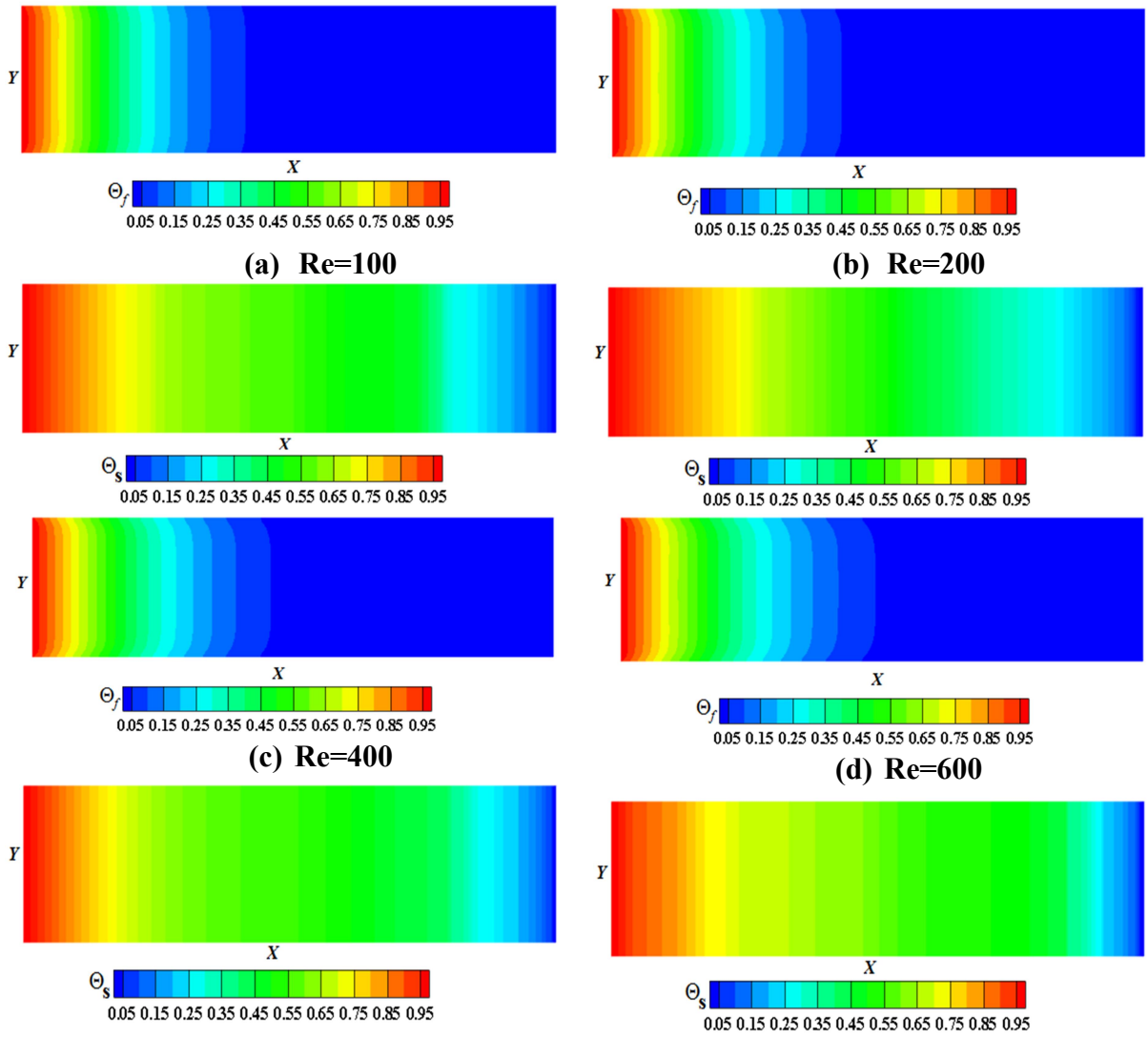

Figure 8. Reynolds number effect on *U*-contours during the discharging process with $Pr = 50, Kr = 10^{+3}, Rc = 1, Bi = 0.1, Da = 10^{-3}, Ec = 0$ and $\varepsilon = 0.6$.

During the discharging process without viscous dissipation $(Ec = 0)$, Figure 9 shows the temperature contours for the four *Re*-values considered herein. The Reynolds number effect is clearly seen. Compared to the previous figure (Fig. 8), and as expected, the same behavior is observed with heat propagation in the opposite direction, the fluid flow being reversed. In other words, the spread of cold heat clearly increases with Reynolds number for Θ_f due to the high thermal conductivity ratio.During the discharge period, the paraffin changes phase, releasing each amount of heat to the solid. Therefore, the *Re* influence is pronounced in the fluid phase having a different temperature distribution compared to the solid phase because of a low interstitial heat transfer. Once more, the LTNE hypothesis ($\Theta_s \neq \Theta_f$) adopted remains valid for the two processes (charging and discharging) in the entire canal except at its entry and exitwhere the LTE occurs.

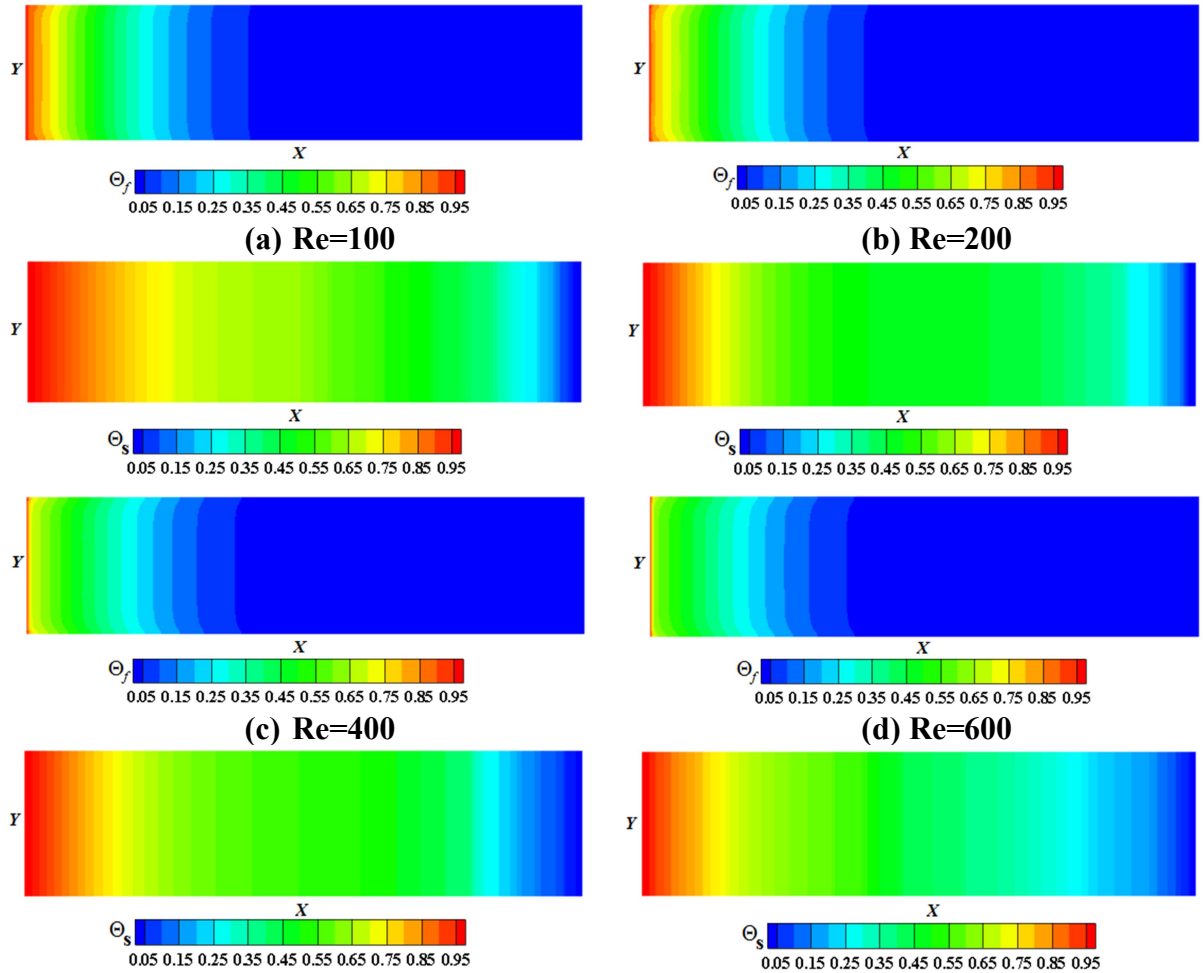

Figure 9. Reynolds number effect on temperature contours (Θ_f, Θ_s) during the discharging process with $Pr = 50, Kr = 10^{+3}, Rc = 1, Bi = 0.1, Da = 10^{-3}, Ec = 0$ and $\varepsilon = 0.6$.

The fluid and solid temperature distribution (Θ_f and Θ_s) during charging and discharging processes vs. the streamwise coordinate at Y= 0.5 (fully developed section) is depicted in figure 10 for different Eckert ($Ec = 0, 1, 5, 10$) and Reynolds numbers ($Re = 100, 200, 400, 600$) while setting the other parameters.It is worth noting that figure 10 a shows the solid and PCM Θ-evolvement without viscous dissipation ($Ec = 0$), while Figures 10 b-c-d demonstrate the viscous dissipation contribution ($Ec \neq 0$) for the fluid phase. A careful review of this figure clearly shows the Eckert number's effecton Θ_f as shown in Eq. 6. Note that the solid temperature profile (Θ_s) exhibits a linear profile for both the charging and discharging processes. This is different from those of the fluid, which depend on the *Re* number. Such a difference is due to the dominant convective heat transfer of the system. During the charging process, the fluid temperature increases with the Reynolds number and then drops rapidly in the channel. It turns out that when *Re* increases, this rise goes on until the second half of the channel. As for the discharging process, the temperature rises very fast over a short distance regardless of Reynolds and Eckert numbers (except for $Ec = 0$) and then gradually decreases.

In other words, during the two processes, the fluid temperature evolves separately (i.e. without any symmetry), the fluid being hot (respectively cold) in the charging phase (respectively in the discharging phase). It appears that the increase of Eckert number generates a significant increase of Θ_f in charging and discharging processes, the viscous dissipation (see Eq. 6) being a heat generating source. It is obvious that at the channel inlet and outlet, the fluid and solid temperatures are equal. Likewise, a close review of figure 10 a, shows that the hypothesis $\Theta_s \neq \Theta_f$ is well set up.

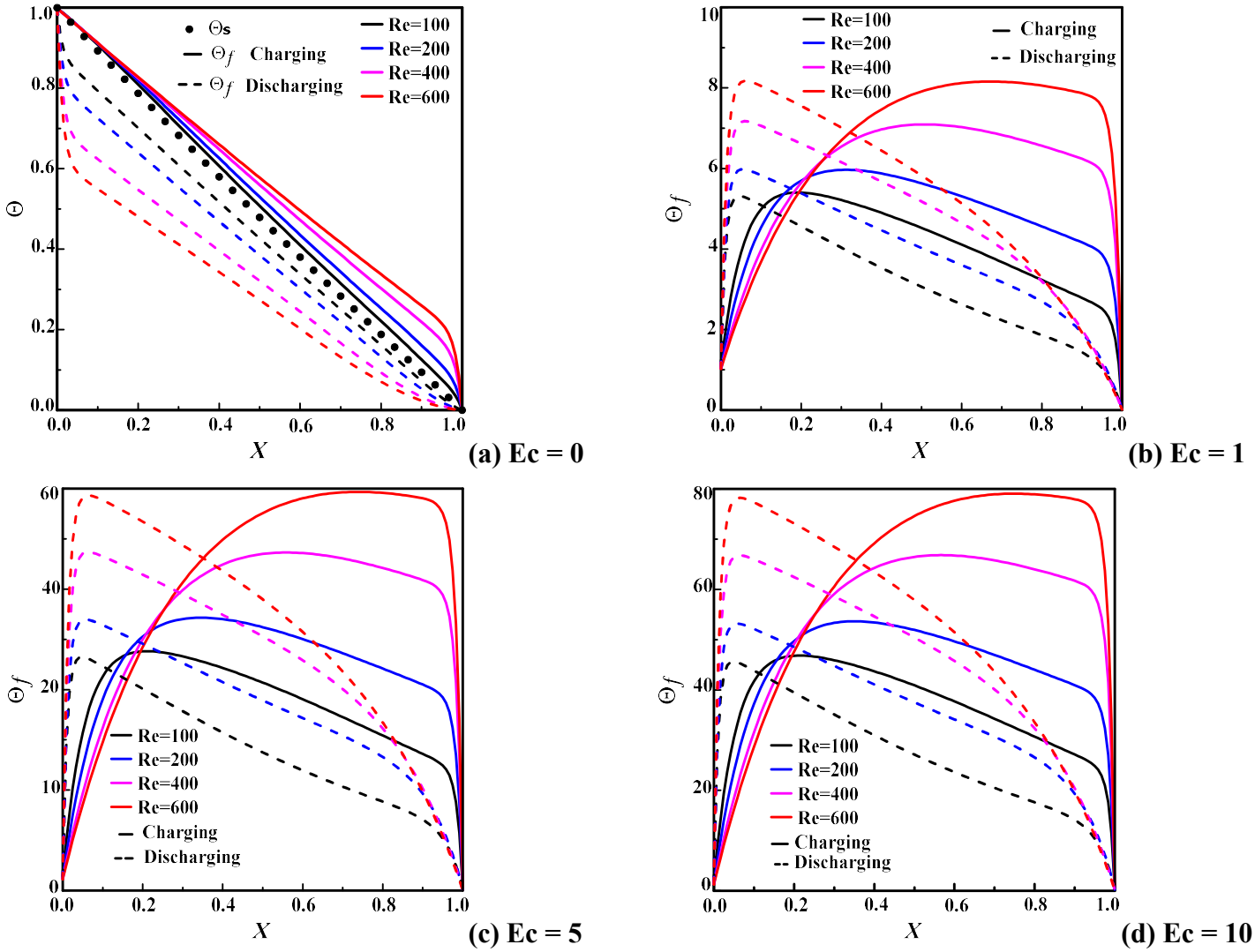

Figure 10. Dimensionless fluid (PCM) and solid temperature (Θ_f, Θ_s) vs. the streamwise distance at Y = 0.6 for different Re numbers with $Pr = 50, Kr = 1000, Rc = 1, Bi = 0.1, Da = 10^{-3}, Ste = 1$ and $\varepsilon = 0.6$ for charging and discharging processes: Eckert number effect.

5.3 Liquid fraction and melt front

Figure 11 presents the time-wise variation of the liquid fraction (Γ). In addition, it brings out Reynolds and medium porosity's effectsat $Pr = 50, Kr = 10^3, Rc = 1, Bi = 0.1, Da = 10^{-3}$ and $Ste = 1$. As shown, the melting rate increases promptly with the Reynolds number to sharply

drop during a short time period, regardless of the porosity herein considered. In other words, the fusion accelerates for this porosities range. Note that the moving solid-liquid phase interface is implicitly tracked via the liquid fraction when solving the PCM energy equation (Eq. (3)). As can be seen, the melting rate increases with *Re* number during the charging process due to the viscosity decrease and subsequently the friction. Besides, high Reynolds numbers accelerate the phase change during the discharging process. In other words, the *Re* number increase promotes the process in short time with a low porosity ($\varepsilon \leq 0.8$).

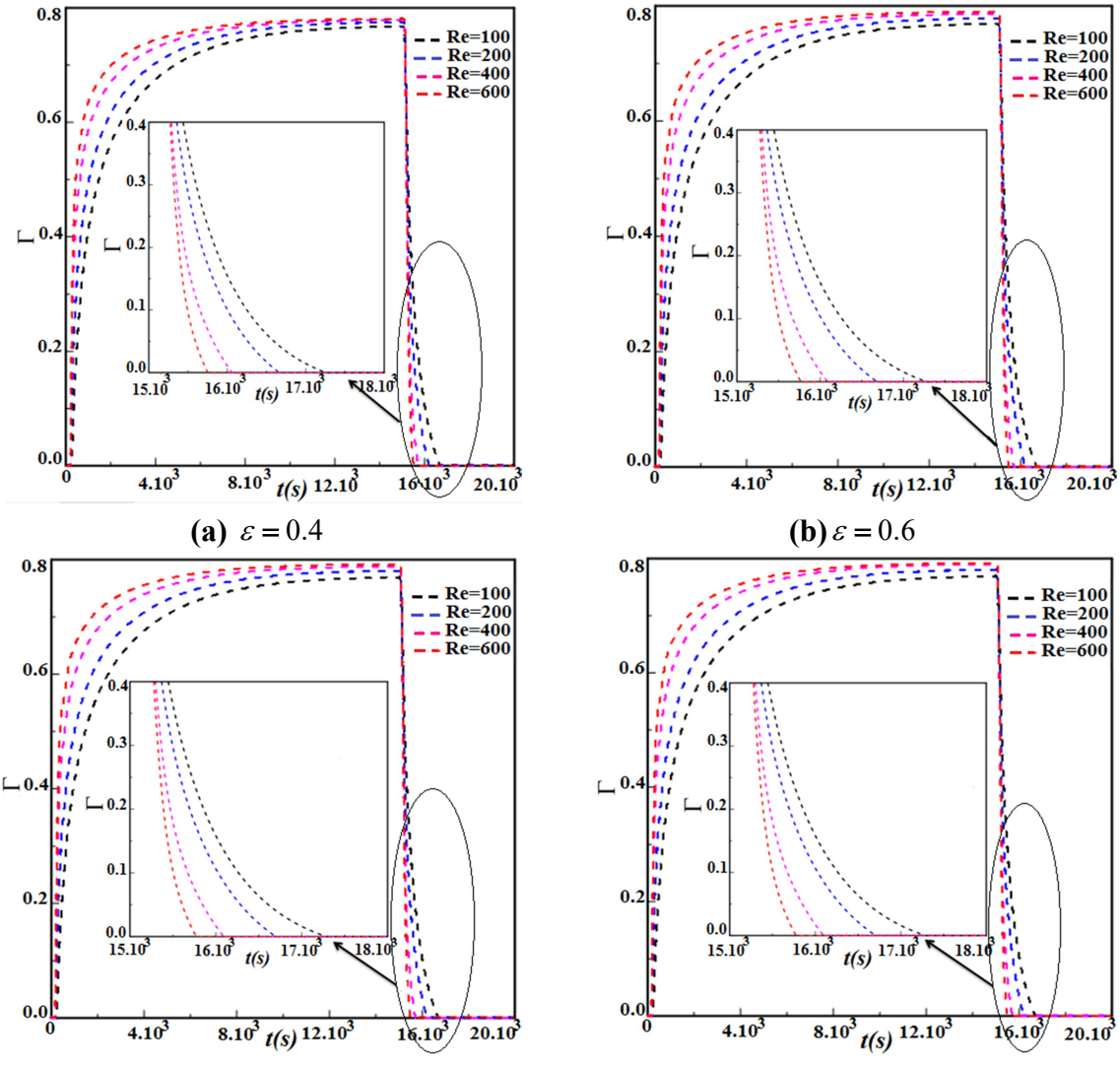

Figure 11. Temporal evolution of the predicted liquid fraction (Γ) for different *Re* numbers and medium porosities with $Pr = 50, Kr = 10^{+3}, Rc = 1, Bi = 0.1, Da = 10^{-3}$ and $Ste = 1$.

Figure 12 portrays the melt front (phase field) at various times and for three Reynolds numbers ($Re = 2\times10^2, 4\times10^2, 6\times10^2$) in the charging process ($Ec = 0$, *i.e. without dissipation*) keeping the other parameters fixed. As time goes by and as Reynolds number rises up, the melt front (phase field) advances forward in the channel due to forced convection with high thermal conductivity of the metal foam that rapidly conveys the hot fluid

downstream, thereby accelerating the melting. As shown, the melt front variation moves slowly, and, thereby the complete PCM fusion will held long after (a longer time not indicated here) even with a *Re* number up to 600, which is due to the insufficient heat generated in the channel (no viscous dissipation). This implies that the viscous dissipation absence further slows the melting at low *Re* numbers.

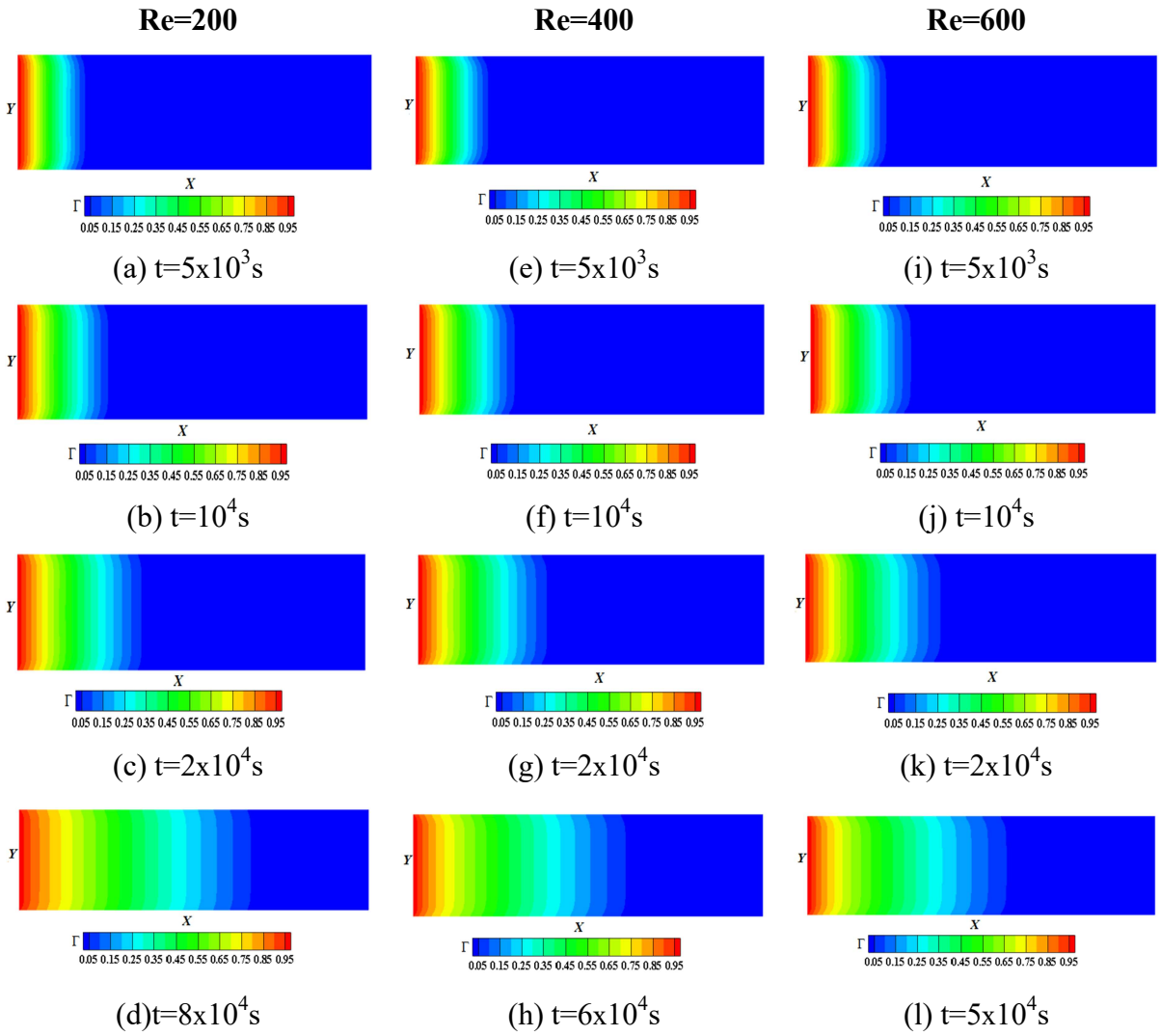

Figure 12. Melt front (phase field) at various time and for three Reynolds numbers in the charging process with $Pr = 50, Kr = 10^{+3}, Rc = 1, Bi = 0.1, Da = 10^{-3}, Ec = 0$ and $\varepsilon = 0.6$.

The phase change interface evolvementunder the convective flow effect is illustrated in figure 13 at various times and for different values of $Re = 100, 200, 400$ and 600 in the charging process with $Pr = 50, Kr = 10^{+3}, Rc = 1, Bi = 0.1, Da = 10^{-3}, Ec = 1$ and $\varepsilon = 0.6$. It is worth recalling that here, $Ec = 1$ indicating that there is dissipation. To better understand the legend exhibited, it should be noted that a contour value of 1 (*red zone*) corresponds to the melted PCM and 0 (*blue zone*) to the solid PCM, while the other colors depict the PCM's mushy zone. At low Reynolds ($Re = 100$ and 200) and at the first instants, the interface is nearly vertical except in the walls vicinity. With the time elapse, it thickens while promptly

advecting downstream showing a sudden change with a pick due to the viscous forces which generate a heat source inside the canal allowing PCM to absorb the heat released to achieve the melting phase during charging process. Therefore, the forced convection greatly improves the melting rise for low porosity. At the last instants, the PCM melts at a much quicker rate, and the red zone fills up most of the channel, indicating a near-complete melting. At large Reynolds numbers ($Re > 200$), it can be stated that the front progression is much faster while being more distorted (especially near walls) because of the convection and insulation cohabitation.

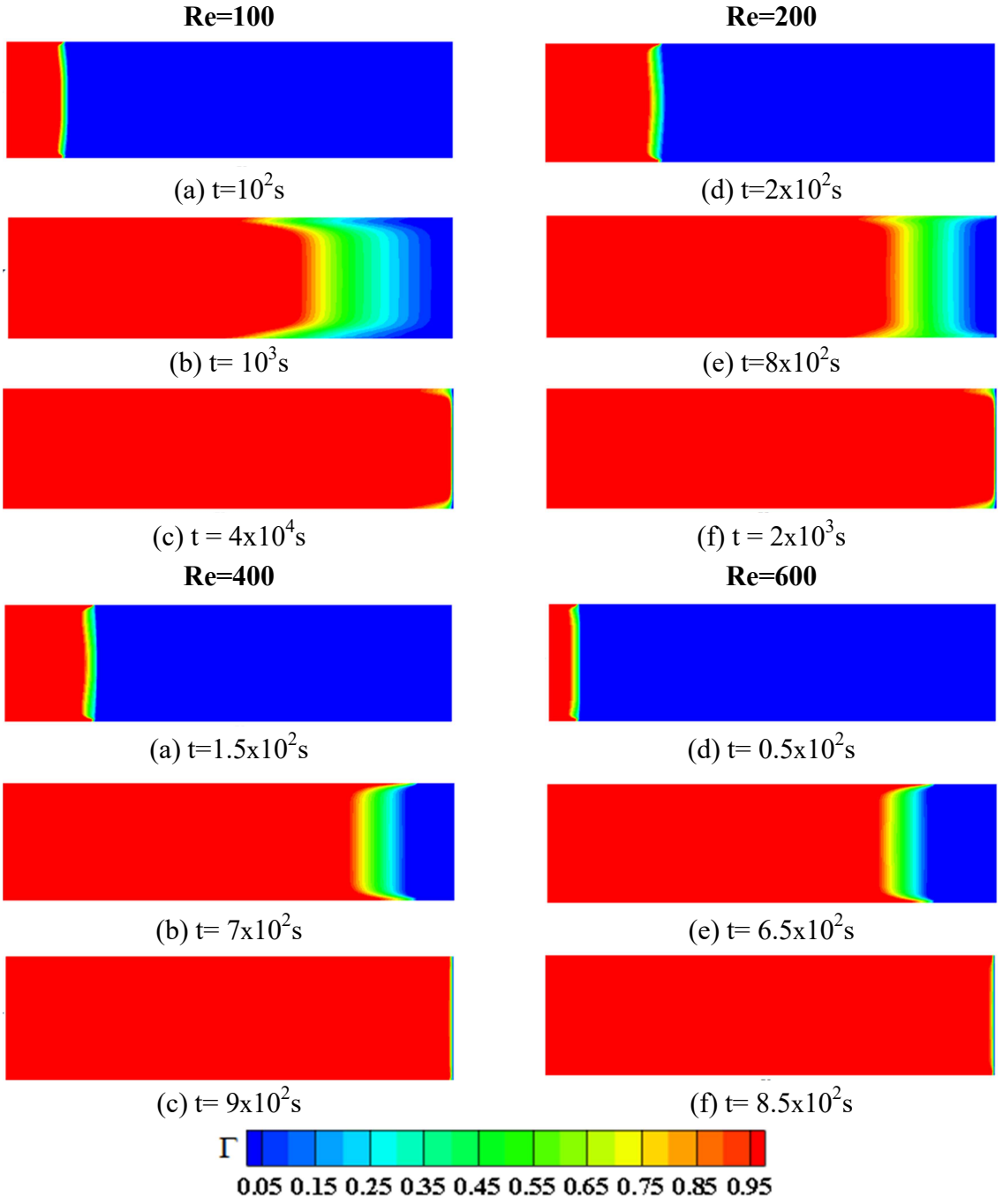

Figure 13. Melt front (phase field) at various times and for various Reynolds numbers in the charging process with $Pr = 50, Kr = 10^{+3}, Rc = 1, Bi = 0.1, Da = 10^{-3}, Ec = 1$ and $\varepsilon = 0.6$.

5.4 Entropy generation and thermal performance

To assess the irreversibility in the system, we opted for the entropy generation number (Ns), which states dimensionless entropy generation rate in a system. For charging and discharging processes, the Ns number is plotted (see figure 14) vs. the dimensionless streamwise distance, X for different Reynolds ($Re = 100, 200, 400, 600$), and Eckert numbers covering cases with $(Ec \neq 0)$ and without dissipation $(Ec = 0)$ while setting the other parameters.

With a fixed and non-zero Eckert number, as Reynolds increases, Ns varies significantly from $X \approx 1/5$ (the channel length's one-fifth) during the charging process. The higher the Re , the higher Ns is near the channel exit indicating that large Reynlods numbers accentuate the irreversibilities. So, to reduce the irreversibility input, a fluid with high viscosity (lower Re) should be used. Moreover, Ns being proportional to Ec (see relationship (15)), the increase of the latter generates that of Ns due to friction heating (viscous effects) which induces the fluid amplification. Furthermore, during the charging process, the impact of the Ec number involves that the generation of entropy goes from a minimum value (0) to a maximum one just at the exit of the channel to cancel itself just at the exit of the channel, and vice versa for the discharge period. The minimum can be explained by the low velocities and temperature gradients which prevail at the entry and which rise while advecting downstream, thereby, showing that fluid friction irreversibly dominates the the entropy generation rate. Likewise, as Re increases, the PCM fusion speed up via the heat transfer, and thereby increases the number Ns, thus the entropy generation. Looking more closely at figure 14, it turns out that Ns is rather controlled by the Brinkman number, namely $Br = Ec \times Pr$. However, during the discharging process, Ns increases slightly with Re and Ec while remaining low compared to the charging case. As for the case without dissipation $(Ec = 0)$, Ns exhibits the same variations while remaining sharply negligible suggesting that irreversibilities might neglected compared to the case with dissipation $(Ec \neq 0)$.

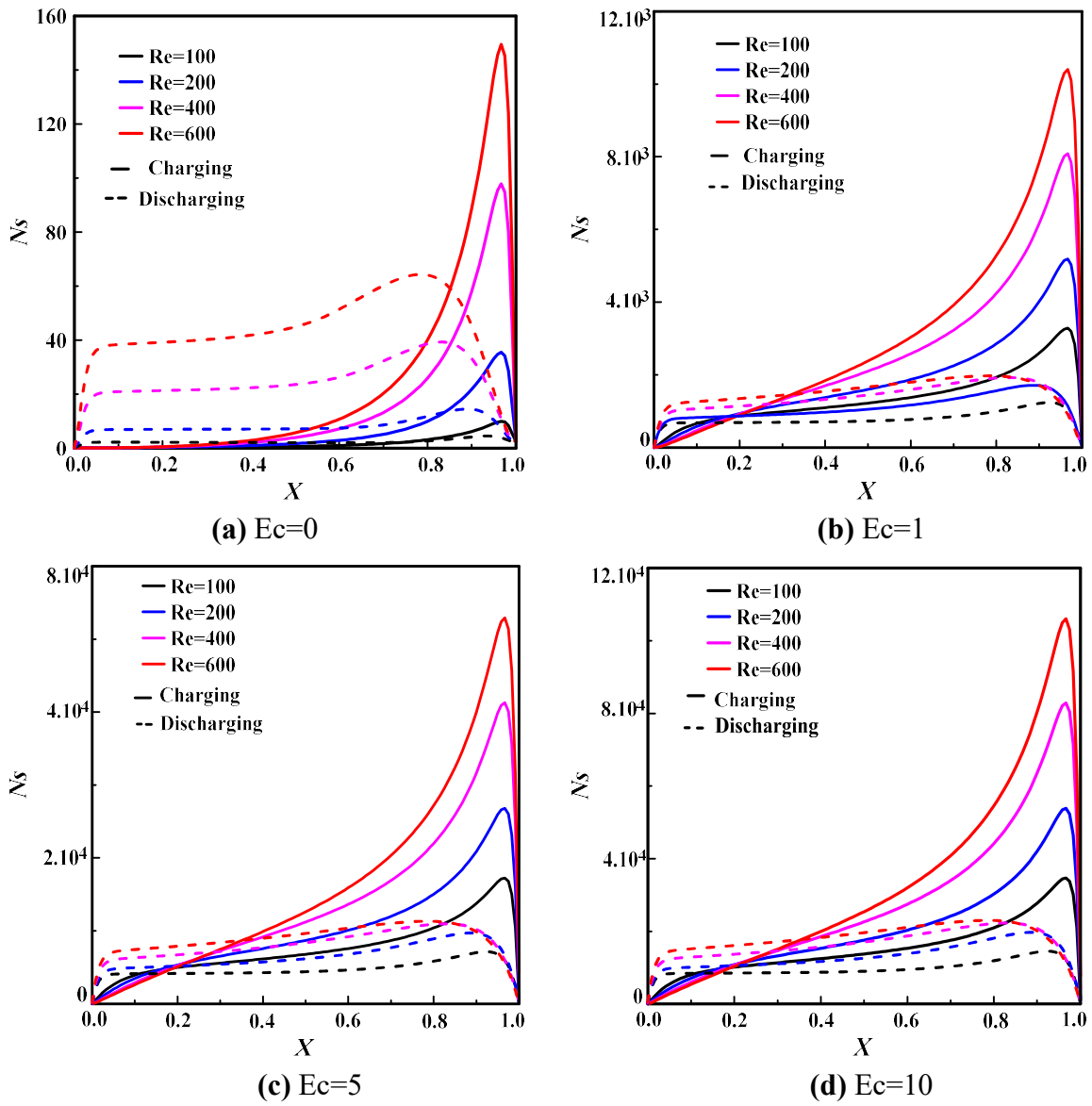

Figure 14. Streamwise evolution of the entropy generation rate (*Ns*) for different Reynolds and Eckert numbers at Y=0.5 with $Pr = 50, Kr = 10^{+3}, Rc = 1, Bi = 0.1, Da = 10^{-3}, Ste = 1$ and $\varepsilon = 0.6$ during charging and discharging processes.

Figure 15 presents the energetic efficiency (η) evolution vs. *Re* for different *Ec* and different porosities during charging and discharging processes. It can be seen that an increase in the number of *Re* greatly improves η for ε = 0.4-0.6, whereas for ε = 0.7-0.8, η increasesvery slightly, reaches a maximum for *Re* close to 400, and then decreases. It turns out that during the charging process, the increase in *Re* rises the heat transfer between the solid and fluid phases, thereby increasing the stored energy. As for the discharge process, an increase in *Re* promotes the transfer of heat stored in the solid matrix to the cold fluid while improving the discharge efficiency. For both processes, there is critical Re value around 400 for which the energy stored is optimal independently of the viscous dissipation effects for porosity higher than 0.6. For low porosity value, the optimal energy stored is achieved for a lower critical Reynolds number (around 150) while being strongly affected by the Eckert

number. In addition, it appears that when the porosity of the structure increases, the energy efficiency decreases due to the low conductivity of the PCM compared to that of the structure having a low porosity (compared to a standard structure) and in the event of low interstitial heat transfer between the fluid and solid phases, thereby leading to the energy loss. Moreover, the *Ec* rise, which is linked to that of the viscous dissipation and the heat released quantity, is accompanied by an increase in the energy efficiency of the system.

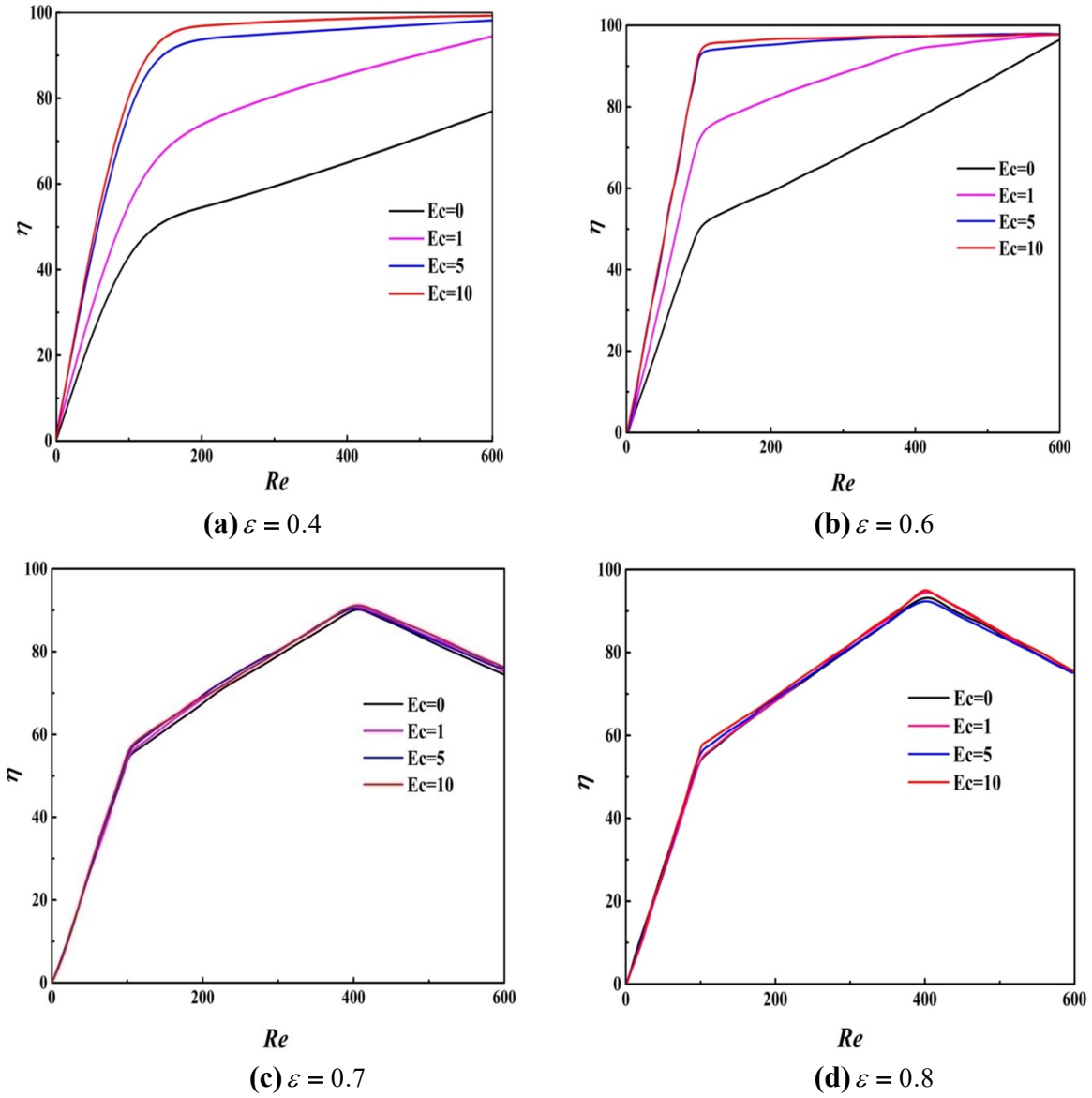

(a) $\varepsilon = 0.4$ **(b)** $\varepsilon = 0.6$

(c) $\varepsilon = 0.7$ **(d)** $\varepsilon = 0.8$

Figure 15. Energetic efficiency (η) vs. Re for different Eckert numberswith $Pr = 50, Kr = 10^{+3}, Rc = 1, Bi = 0.1, Da = 10^{-3}$ and $Ste = 1$.

Figure 16 depicts the exergetic efficiency (Ψ) evolution vs. *Re* for different Eckert numbers and different porosities during charging and discharging processes. By examining figures.16 a-b, we can state that for, ε = 0.4-0.6, Ψ increases with *Re* and *Ec* (0-10). This increase improves heat exchange between the two phases and, with low porosity, mitigates the entropy generation, the thermal conductivity of paraffin being low. However, for a high ε

(0.7 and 0.8), the exergy efficiency increases, reaching its maximum for a *Re* about 400 and then decreases. Note that for the ε-highest values (0.7 and 0.8) considered herein, the *Ec* effect starts to be felt regardless of *Re* (see figures. 16 c-d). Likewise, it turns out that at these values, Ψ is lower regardless of *Re* and *Ec* numbers. It can also be noted that, according to *E*c and *Re*, the quality of the stored energy is greatly improved for a porosity of less than 0.7.

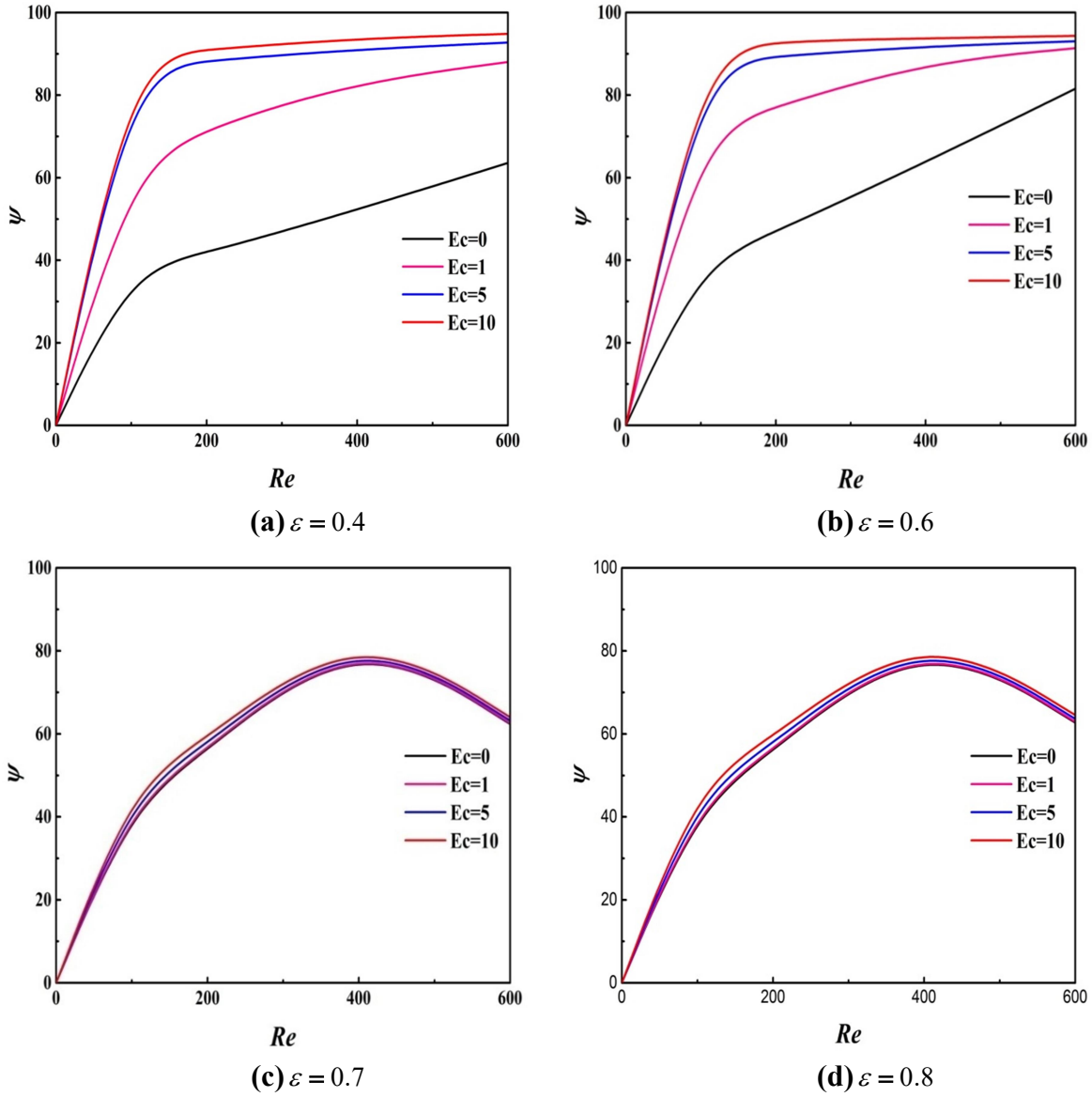

Figure 16. Exergetic efficiency (Ψ) vs. Re for different Eckert numbers with $Pr = 50, Kr = 10^{+3}, Rc = 1, Bi = 0.1, Da = 10^{-3}$ and $Ste = 1$.

6. Conclusion

The aim of this work is to present numerical study on convective flow heat transfer in a two-dimensional open-ended channel filled with a composite porous medium (copper foam/PCM (paraffin)) under the LTNE condition. The dimensionless transport equations are numerically solved using a thermal BGK-LBM with three density functions. Beforehand, a

mesh testing procedure has been performed to grantee the present solution independency. Streamlines, isotherms, the melt front visualization, the entropy generation rate, and energetic and exergetic efficiencies in the channel are produced to illustrate the pattern of the flow and heat fields, the melt front progress, and the system storage capacity through suitable parameters such as the Reynolds and Eckert numbers during the charging (melting) and discharging (solidifying) processes. The Reynolds number considered ranges from $Re = 100$ up to 600 to avoid transient and turbulent states. Based on the simulation results, our main findings can be drawn as follows

•As Re increases, the flow field exhibits strong eddies due to the internal heat rise within the channel.

• During the charging process without viscous dissipation ($Ec = 0$), the propagation of heat is very slow at low Re ($= 100$). However, for fairly large Reynolds numbers ($200 - 600$), the heat propagation accelerates indicating a strong forced convection downstream. As for the discharging process, the spread of cold heat increases with increasing Reynolds number.

•The melting rate increases with Re to sharply drop for a short time period, regardless of the porosity.In addition, it turns out that small porosities promptly accelerate both the chargingand dischargingprocesses due to high thermal conductivity of the metal foam/PCM composite, and improve energy and exergy efficiencies of the system whatever Re for the very low values of porosity (0.4 and 0.6).

•There is a critical Reynolds number for which the storage energy is optimal and whose quality is improved using both the porosity and the effects of viscous dissipation.

•At large Reynolds number, the front progress is much faster while being more distorted (especially near walls) due to convection and insulation of the solid walls.

•At a fixed and non-zero Ec and as Re increases, the entropy generation number (Ns) varies significantly from one fifth of the channel length during the charging process.

•The Ec increase, related to that of the viscous dissipation, is accompanied by an increase in the energy efficiency of the system for low porosity' values regardless of Re. However, for larger porosity' values, the increase continues until Re about 400 and then decreases

•The energetic exergy is lower at high porosity values (0.7 and 0.8) whatever Re and Ec.

To sum up, the findings evidence the potential of the current method for laminar forced convection melting/solidification of a composite phase change material with heat dissipation in a porous PCM-filled channel for Re number up to 600.

References

[1] Zhao, C. Y., Lu, W., Tian, Y. (2010). Heat transfer enhancement for thermal energy storage using metal foams embedded within phase change materials (PCMs). Sol. energy, 84 (8), 1402-1412.

[2] Tian, Y., Zhao, C. Y. (2011). A numerical investigation of heat transfer in phase change materials (PCMs) embedded in porous metals. Energy, 36 (9), 5539-5546.

[3] Py, X., Olives, R., Mauran, S. (2001). Paraffin/porous-graphite-matrix composite as a high and constant power thermal storage material. Int. J. Heat Mass Transf., 44 (14), 2727-2737.

[4] Elgafy, A., & Lafdi, K. (2005). Effect of carbon nanofiber additives on thermal behavior of phase change materials. Carbon, 43 (15), 3067-3074.

[5] Zhang, Y., Faghri, A. (1996). Heat transfer enhancement in latent heat thermal energy storage system by using the internally finned tube. Int. J. Heat Mass Transf., 39 (15), 3165-3173.

[6] Shatikian, V., Ziskind, G., Letan, R. (2005). Numerical investigation of a PCM-based heat sink with internal fins. Int. J. Heat Mass Transf., 48 (17), 3689-3706.

[7] Ho, C. J., Gao, J. Y. (2009). Preparation and thermophysical properties of nanoparticle-in-paraffin emulsion as phase change material. Int. Comm. Heat Mass Transf., 36 (5), 467-470.

[8] Yang, Y., Luo, J., Song, G., Liu, Y., Tang, G. (2014). The experimental exploration of nano-Si3N4/paraffin on thermal behavior of phase change materials. Thermochim. Acta, 597, 101-106.

[9] Deng, Z., Liu, X., Zhang, C., Huang, Y., Chen, Y. (2017). Melting behaviors of PCM in porous metal foam characterized by fractal geometry. Int. J. Heat Mass Transf., 113, 1031-1042.

[10] Atal, A., Wang, Y., Harsha, M., Sengupta, S. (2016). Effect of porosity of conducting matrix on a phase change energy storage device. Int. J. Heat Mass Transf., 93, 9-16.

[11] Wang, Z., Zhang, Z., Jia, L., Yang, L. (2015). Paraffin and paraffin/aluminum foam composite phase change material heat storage experimental study based on thermal management of Li-ion battery. Appl. Therm. Eng., 78, 428-436.

[12] Cui, H. T. (2012). Experimental investigation on the heat charging process by paraffin filled with high porosity copper foam. Appl. Therm. Eng., 39, 26-28.

[13] Xu, A., Shi, L., Zhao, T. S. (2017). Accelerated lattice Boltzmann simulation using GPU and OpenACC with data management. Int. J. Heat Mass Transf., 109, 577-588.

[14] Chen, S., Doolen, G. D. (1998). Lattice Boltzmann method for fluid flows. Annu. Rev. Fluid Mech., 30 (1), 329-364.

[15] Zhang, C., Deng, Z., Chen, Y. (2014). Temperature jump at rough gas–solid interface in Couette flow with a rough surface described by Cantor fractal. Int. J. Heat Mass Transf., 70, 322-329.

[16] Krishnan, S., Murthy, J. Y., Garimella, S. V. (2005). A two-temperature model for solid-liquid phase change in metal foams. J. Heat Transf., 127, 995-1004

[17] Hu, X., Wan, H., Patnaik, S. S. (2015). Numerical modeling of heat transfer in open-cell micro-foam with phase change material. Int. J. Heat Mass Transf., 88, 617-626.

[18] Chen, Z., Gao, D., Shi, J. (2014). Experimental and numerical study on melting of phase change materials in metal foams at pore scale. Int. J. Heat Mass Transf., 72, 646-655.

[19] Tao, Y. B., You, Y., He, Y. L. (2016). Lattice Boltzmann simulation on phase change heat transfer in metal foams/paraffin composite phase change material. Appl. Therm. Eng., 93, 476-485.

[20] Wu, W., Zhang, S., Wang, S. (2017). A novel lattice Boltzmann model for the solid–liquid phase change with the convection heat transfer in the porous media. Int. J. Heat Mass Transf., 104, 675-687.

[21] Zhu, F., Zhang, C., Gong, X. (2017). Numerical analysis on the energy storage efficiency of phase change material embedded in finned metal foam with graded porosity. Appl. Therm. Eng., 123, 256-265.

[22] Al-Sumaily, G. F., Nakayama, A., Sheridan, J., Thompson, M. C. (2012). The effect of porous media particle size on forced convection from a circular cylinder without assuming local thermal equilibrium between phases. Int. J. Heat Mass Transf., 55 (13-14), 3366-3378.

[23] Al-Sumaily, G. F., Thompson, M. C. (2013). Forced convection from a circular cylinder in pulsating flow with and without the presence of porous media. Int. J. Heat Mass Transf., 61, 226-244.

[24] Nield, D. A., Bejan, A. (2013). Convection in Porous Media. 4th editon. *New York:* Springer-Verlag.

[25] Ting, T. W., Hung, Y. M., Guo, N. (2015). Entropy generation of viscous dissipative nanofluid flow in thermal non-equilibrium porous media embedded in microchannels. Int. J. Heat Mass Transf., 81, 862-877.

[26] Rabhi, R., Amami, B., Dhahri, H., Mhimid, A. (2016). Entropy generation for an axisymmetric MHD flow under thermal non-equilibrium in porous micro duct using a modified lattice Boltzmann method. J. Magn. Magn. Mater., 419, 521-532.

[27] Ergun, S. (1952). Fluid flow through packed columns. Chem. Eng. Prog., 48, 89-94.

[28] Ingham, D. B., Pop, I. (2005). Transport Phenomena in Porous Media, 1st Edition, Elsevier Science: Oxford, UK.

[29] Joshi, V., Rathod, M. K. (2019). Constructal enhancement of thermal transport in metal foam-PCM composite-assisted latent heat thermal energy storage system. Numer. Heat Transf., Part A: App., 75 (6), 413-433.
[30] Zhao, W., France, D. M., Yu, W., Kim, T., Singh, D. (2014). Phase change material with graphite foam for applications in high-temperature latent heat storage systems of concentrated solar power plants. Ren. Energy, 69, 134-146.
[31] Torabi, M., Karimi, N., Peterson, G. P., Yee, S. (2017). Challenges and progress on the modelling of entropy generation in porous media: a review. Int. J. Heat Mass Transf., 114, 31-46.
[32] Dincer, I., & Rosen, M. A. (2011). Thermal Energy Storage: Systems and Applications, 2nd ed., John Wiley & Sons.
[33] Amami, B., Rabhi, R., Dhahri, H., Mhimid, A. (2017). Numerical thermodynamic analysis of heat storage porous duct under pulsating flow using lattice Boltzmann method. Int. J. Exergy, 22 (4), 376-395.
[34] Hänchen, M., Brückner, S., Steinfeld, A. (2011). High-temperature thermal storage using a packed bed of rocks–heat transfer analysis and experimental validation. Appl. Therm. Eng., 31 (10), 1798-1806.
[35] Rosen, M. A. (2001). The exergy of stratified thermal energy storages. J. Sol. Energy. 71 (3), 173-185.
[36] Erek, A., Dincer, I. (2008). An approach to entropy analysis of a latent heat storage module. Int. J. Therm. Sci., 47 (8), 1077-1085.
[37] Zhang, Z., Cheng, J., He, X. (2017). Numerical simulation of flow and heat transfer in composite PCM on the basis of two different models of open-cell metal foam skeletons. Int. J. Heat Mass Transf., 112, 959-971.
[38] Xu, A., Zhao, T. S., Shi, L., & Xu, J. B. (2018). Lattice Boltzmann simulation of mass transfer coefficients for chemically reactive flows in porous media. J. Heat Transf., 140 (5).
[39] Guo, Z., Zhao, T. S. (2005). A lattice Boltzmann model for convection heat transfer in porous media. Numer. Heat Transf., Part B, 47 (2), 157-177.
[40] Seta, T., Takegoshi, E., Okui, K. (2006). Lattice Boltzmann simulation of natural convection in porous media. Math. Comput. Simul., 72 (2-6), 195-200.
[41] Gao, D., Tian, F. B., Chen, Z., Zhang, D. (2017). An improved lattice Boltzmann method for solid-liquid phase change in porous media under local thermal non-equilibrium conditions. Int. J. Heat Mass Transf., 110, 58-62.

[42] Yehya, A., Naji, H., Zalewski, L. (2019). Experimental and numerical characterization of an impure phase change material using a thermal lattice Boltzmann method. Appl. Therm. Eng., 154, 738-750.
[43] Amami, B., Dhahri, H., Mhimid, A. (2014). Viscous dissipation effects on heat transfer, energy storage, and entropy generation for fluid flow in a porous channel submitted to a uniform magnetic field. J. Porous Media, 17(10).
[44] Bin, D., Bao-Chang, S., Guang-Chao, W. (2005). A new lattice Bhatnagar–Gross–Krook model for the convection–diffusion equation with a source term. Chin. Phys. Lett., 22 (2), 267.
[45] Gao, D., Chen, Z., Chen, L. (2014). A thermal lattice Boltzmann model for natural convection in porous media under local thermal non-equilibrium conditions. Int. J. Heat Mass Transf., 70, 979-989.
[46] Shi, Y., Zhao, T. S., Guo, Z. L. (2004). Thermal lattice Bhatnagar-Gross-Krook model for flows with viscous heat dissipation in the incompressible limit. Phys. Rev. E, 70 (6), 066310.
[47] Mezrhab, A., Moussaoui, M. A., Jami, M., Naji, H., Bouzidi, M. H. (2010). Double MRT thermal lattice Boltzmann method for simulating convective flows. Phys. Lett. A, 374 (34), 3499-3507.
[48] Moussaoui, M. A., Mezrhab, A., Naji, H. (2011). A computation of flow and heat transfer past three heated cylinders in a vee shape by a double distribution MRT thermal lattice Boltzmann model. Int. J. thermal Sci., 50 (8), 1532-1542.
[49] Kim, S. Y., Kang, B. H., Hyun, J. M. (1994). Heat transfer from pulsating flow in a channel filled with porous media. Int. J. Heat Mass Transf., 37 (14), 2025-2033.
[50] Abdedou, A., Bouhadef, K., Bennacer, R. (2017). Forced convection in a self heating porous channel: Local thermal nonequilibium model. Therm. Sci., 21(6 Part A), 2419-2429.

Chapter 3

Numerical investigation of metal foam pore density effect on sensible and latent heats storage through an enthalpy-based REV-scale lattice Boltzmann method

Abstract

In this work, a steady forced convection heat transfers in an open-ended channel incorporating a porous medium filled either with a phase change material (PCM; case 1) or with water (case 2) has been studied using a thermal lattice Boltzmann method (TLBM) at the representative elementary volume (REV) scale. The set of governing equations includes the dimensionless generalized Navier-Stokes equations and the two energy model transport equations based on local thermal non-equilibrium (LTNE). The enthalpy-based method is employed to cope with phase change process. The pores per inch density ($10 \le PPI \le 60$) effects of the metal foam on the storage of sensible and latent heat were studied during charging/discharging processes at two Reynolds numbers (*Re*) of 200 and 400. The significant outcomes are discussed for the dynamic and thermal fields, the entropy generation rate (*Ns*), the LTNE intensity, and the energy and exergy efficiencies under the influence of *Re*. It can be stated that increasing the PPI improves the energy and exergy efficiencies of the latent heat model, reduces energy losses and improves the stored energy quality. Likewise, at a moderate Re (=200), a low PPI (= 10) would be suitable to reduce the system irreversibility during the charging period, while a high value (PPI = 60) might be advised for the discharging process. As becomes clear from the obtained findings, PPI and porosity are relevant factors. In concluding, this paper further provides a first analysis of entropy generation during forced convection to improve the energy efficiency of various renewable energy systems.

1. Introduction

Energy penury ranks is one factor of global attention limiting universal economic development. Thereby, over the years, thermal energy storage system (TESS) technology has been widely developed to cut energy loss and the gap between energy demand and supply [1]. This burgeoning development of large-scale energy storage devices began upon renewable and clean energies discovery. These units (systems) are established using thermochemical heat, sensible heat and/or latent heat. To bridge the spatio-temporal gap between energy production and demand in industrial facilities such as solar power where cyclical fluctuations may be involved, latent heat storage (LHS) technologies are increasingly being used adopting phase change materials (PCMs). There are mainly two types of sensible and latent thermal energy storage systems (S/L-TESSs) [2]. These are devices that store energy by heating a

storage medium. In latent thermal energy storage systems, the base media is made up of a PCM. This is because PCMs can store thermal energy with low temperature variations while involving few volume, which is very cost effective in many thermal energy applications. Among the commonly used PCMs is paraffin which has many advantages such as high latent heat, non-toxicity and chemical stability. However, it also has drawbacks such as low thermal conductivity. Therefore, the use of open-cell PCM-filled metal foams is a possible action that can be implemented to improve thermal conductivity and hence heat transfer.

Medrano et al. [2] noted the advantages and disadvantages of these storage systems based on experimental results of storage units in concentrated solar power (CSP) plants. Besides, Kuravi et al. [3] discussed the storage design, methodologies and performance of different thermal energy storage systems incorporated in the CPS plants. Mohan et al. [4] reviewed sensible energy storage media (supports) with molten salt maintained at a temperature above 600 °C. They mainly kept a focus on thermal properties, cost and corrosion. These are the thermal energy storage systems with sensible and latent heat (SHTESS and LHTESS) using porous materials that are the subject of this numerical investigation. On such a topic, a huge range of studies have dealt with sensible heat storage in different units. Thereby, Elouali et al. [5] performed physical models to assess the packed bed thermal performance for sensible heat storage during charging/discharging processeswhere air is the heat transfer fluid (HTF) and noted that a decrease in the bed porosity enhances the thermal capacity storage and drops the charging period. To store sensible heat, Dhifaoui et al. [6] experimentally examined the thermal behaviour of a vertical porous bed composed of glass beads and air and heated with a constant heat flow. They stated that the system efficiency rises with the stored heat quantity when the outlet temperature drops for a given volume owing to the average permeability factor. Yang et al. [7] experimentally investigated the effect of an open-cell metal foam embedded into paraffin (PCM) on a thermal shell-and-tube unit response during charging process. They found that the involvement of open-cell metal foam can greatly enhance the thermal energy storage efficiency while shortening the melting time compared to a pure PCM. Amami et al. [8] numerically investigated the thermodynamic behaviour of porous unit of sensible heat storage maintained under forced convective pulsating flow. They found that the exergy efficiency rate of the storage system is lower than the energy efficiency regardless the parameters deemed. Lafdi et al. [9] carried out an experimental test of the same criterions' effects on the phase change heat transfer of wax/Aluminium foam composite. They observed that increasing pore size and porosity intensifies heat transfer and speeds up the steady state achievement.

Ren et al. [10, 11] numerically investigated the effect of metal foam characteristics on the PCM melting performance in a LHTES unit by pore-scale lattice Boltzmann approach. They found that the metal foams considered greatly improved the PCM heat transfer capacity compared to nanoparticles. Younsi and Naji [12] developed a finite volume (FV)-based model to assess the thermal behaviour of brick walls with embedded PCMs using an enthalpy-porosity approach. They noted that such a process can both reduce maximum temperatures by up to 3 ° C and smooth out daily fluctuations. Sardari et al. [13] numerically reported the porosity and pore size effects of metal foams on the PCM melting evolvement and found that lowering porosity improves the system performance and reduces the melting time compared to a pure PCM. However, they did not notice any effect of the metal pore size. Tao et al. [14] investigated both the PPI density and porosity effects of metal foams on PCM melting rate, heat storage capacity and heat storage density under conduction and natural convection. By findings, they demonstrated of an optimum porosity's existence which mitigates the fusion time while improving the latent heat storage (LHS) rate performance. Mabrouk et al. [15] performed a numerical analysis of steady forced convection heat transfer in an open-ended straight channel filled with a metal foam and PCM (paraffin) embedded in its pores. They demonstrated that the quantity and quality of stored energy is influenced by key parameters such as Reynolds (Re) and Eckert (Ec) numbers and porosity.

As an alternative numerical method for solving the problems of fluid flow and heat transfer, the lattice Boltzmann method (LBM) based on the Boltzmann equation in statistical mechanics has been developed rapidly in recent decades. From the evolution of particles clusters (sets) dynamics, the macroscopic quantities (density, velocity, temperature, etc.) are recovered. In addition, in view of the success achieved, it has been extended to simulate transport phenomena in multiphase systems where the heat transfer occurs between different media, e.g., porous media filled or not with PCM. In this context, the characterization of flow, heat and mass transfers at pore level in porous structures, and the effect demonstration of the insert in composite material through key parameters such as porosity was the first coveted. Likewise, increasingly, the approach with dual (or even triple) distribution functions [14, 16, 17] have been adopted for the different media involved. By adding additional terms to reflect the porous medium existence, PCM and the transport phenomena involved, TLBM has been shown to be able to deal with such problems. To sum up, several works [18-20] demonstrated that over the years, LBMs have become leading approaches in modeling fluid-fluid and fluid-solid interactions within complex geometric structures, such as porous materials.

It is worth noting that the nature of many problems in engineering, materials science, mechanics, electronics, etc. is rather multi-scale. In addition, the study of open channel

transport phenomena filled with paraffin-saturated metal foam under forced convection is a macro/mesoscale problem. In addition, when a PCM is impregnated into porous materials, the local thermal non-equilibrium (LTNE) approach is commonly used with which separate energy equations are solved for the fluid and the porous (solid) media. For such a problem, the use of traditional numerical approaches at the macro level (finite volume and element methods, etc.) even associated with the Darcy-Brinkmann-Forchheimer (DBF) steady flow and two-equation energy models based on LTNE may ignore some details related to local mesoscale transport. These are the reasons that led us to consider the TLBM method at the representative elementary volume (REV) scale instead of the pore scale TLBM approach since it requires the knowledge and simulation of details in terms of geometry which can be tedious. Simply stated, the pore scale TLBM approach often deals with small computational domains due to the huge computational resources involved and difficulties in achieving good numerical precision with non-prohibitive computing costs [14, 21, 22] to name a few. Thereby, due to its origin and intrinsic computational efficiency, the REV-TLBM method has become a safe approach that can deal with a large number of academic or engineering issues including saturated porous media or not with PCMs often encountered in heat transfer devices.

This present work is dedicated to a numerical study of the following innovative aspects:1) use of an enthalpy-based TLBM with triple distribution functions at the REV scale, 2) investigation of the metal foam pore density effect on sensible and latent heats storage under steady forced convection, and 3) analysis of steady flow, entropy generation rate (Ns), the LTNE intensity, and energy and exergy efficiencies of the considered system under influence of the Reynolds number (Re) during the charging and discharging processes.

The remainder of this paper is arranged to starts with the problem statement and governing equations followed by the TLBM simulation of hydrodynamic flow and heat transfer where the implementation of boundary conditions in LBM is presented, as well as the validation of available results. Next, the following section is vowed to the findings presentation and their comment. Finally, the major conclusions of this work are provided as a closure section.

2. Problem statement, assumptions and governing equations

This section deals with the presentation of the computation domain, the simplifying assumptions, and the governing dimensionless equations formulation to be handled numerically with appropriate boundary conditions. This paper proposes a numerical investigation of the fluid dynamics and heat transfer in an open-ended channel incorporating a

porous medium filled either with a PCM (case 1) or with water (case 2) which constitute two phases.

2.1 Physical models

Before introducing the models deemed, it should be mentioned that the main objective targeted here concerns thermal energy storage units dealing specifically with latent and sensitive thermal storage. The channel heat exchanger (storage tank) is an excellent example [23]. Moreover, open cell metal foams saturated with different filling media (such as paraffin, water, air, and oil) can be found in many thermal and other applications such as solar energy production, drying in porous media, energy storage units, refrigeration, nuclear power and other fields (see [23] to name a few).

A simple schematic view of the under study forced convection problem is depicted in figure 1. Based on the semi-infinite approximation along the Z-axis, the computational domains are two-dimensional straight channel whose horizontal walls are adiathermic, impermeable and non-slip. They are of length and height L and H and are filled with a porous metal foam including paraffin as PCM impregnated in its pore space (latent heat; case 1) or the same metal foam saturated with liquid water (sensible heat; case 2). Note that the charging process starts with a hot temperature $T_{f,h}$ and a uniform velocity $u_{in}(=U_0)$ (west), while the discharging process begins at cold temperature $T_{f,c}$ ($< T_{f,h}$) and velocity $-u_{in}$ (east). It is very useful to point out that in the first case (Figure 1 a), the thermal input condition is well set so that the PCM can start to melt ($T_{f,h} > T_m$), while in the second case (figure 1 b), water keeps its liquid state.

It should also be pointed out that water is commonly used for heat exchange (cooling) during its advection (flow) and that paraffin is widely picked out in thermal management of buildings, heat recovery, heating, ventilation and air conditioning (HVAC), healthcare and electronics.

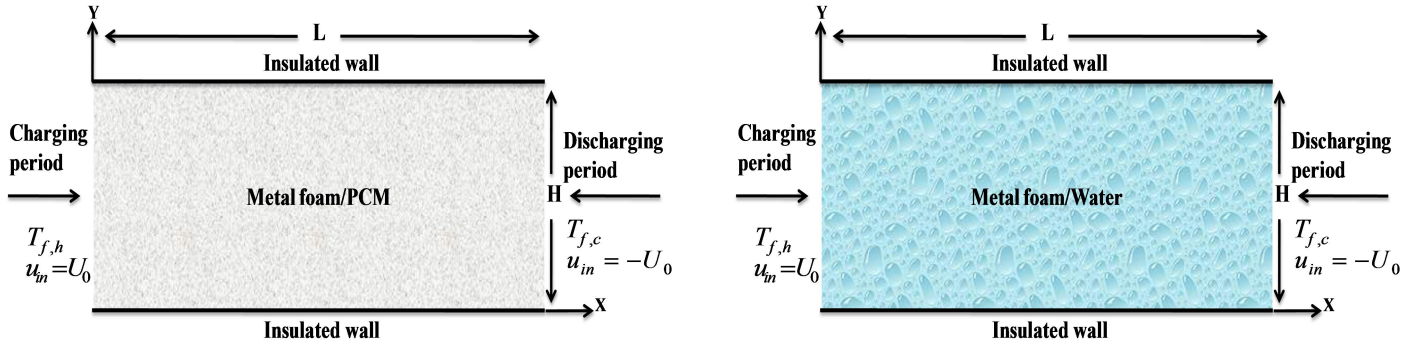

Figure 1. Configuration sketch of flow through a straight channel filled with metallic foam impregnated with PCM (a) or water (b) along with imposed boundary conditions: (**a**) Latent heat (case 1); (**b**) Sensible heat (case 2).

2.2 Computational assumptions

The heat transfer involved in porous composite media (metal foam/PCM or metal foam/liquid can prove to be very complicated, including heat transfer by convection between the metal foam and the liquid PCM or the liquid deemed, the thermal conduction between metal foam and solid PCM, etc. Thereby, to simplify, establish and then handle numerically the mathematical model considered, the following assumptions were initially set out: Forced convection flow prevailing throughout the channel (natural convection and radiation are neglected) is laminar and steady. The volumetric expansion of the PCM is skipped, and the working fluid (air) is assumed to be Newtonian, incompressible and viscous. Liquid paraffin (case 1) and water (case 2) due to its easy access, low cost and stability are presumed viscous, incompressible, while shaping a second metal foam phase for which the LTNE assumption is involved [24]**.** The thermo-physical properties of the components moving in the channel are constant, homogeneous and isotropic within the temperature and Reynolds numbers ranges considered. Thereby, the DBF model was adopted here to model and investigate the convective fluid flow in two porous media (cases 1 and 2) at Reynolds numbers of 200 and 400 under the LTNE assumption.

All the governing equations are handled via a REV enthalpy-TLBM method approach. It is interesting to point out already that the phase change and heat transfer are solved numerically through our built in-house code developed for the aim seeked.

2.3 Governing equations

To simulate fluid flow and convective heat transfer (latent and/or sensitive) within a channel impregnated with a porous medium, we consider the generalized Navier-Stokes equations associated with two transport equations of energy (model known as LTNE) at the REV scale. Such a model includes the melting term and the nonlinear DBF terms of the mean resistance, where applicable.

Based on the above assumptions up-stated, the governing equations (Eqs. (3)- (6)) for the steady two-dimensional forced convection flow in porous channels can be written with the following dimensionless variables or numbers at the REV scale as [24-26]:

$$\begin{aligned}&(X,Y)=(x,y)/H,(U,V)=(u,v)/U_0,P=p/\rho U_0^2,\ \tilde{t}=tU_0/H,\ \Theta=(T-T_c)/(T_h-T_c),\\&\Delta T_{ref}=T_h-T_c;\end{aligned} \tag{1}$$

$$\begin{aligned}&Da=K/H^2,\ Pr=\nu_f/\alpha_f,\ Re=U_0H/\nu_f,\ Rc=(\rho C_p)_s/(\rho C_p)_f,\ Kr=\lambda_s/\lambda_f,\\&Bi=h_{sf}a_{sf}H^2/\lambda_s,\ Ste=C_{pf}(T_h-T_m)/L_a,\ Ec=U_0^2/\left(C_{pf}\Delta T_{ref}\right).\end{aligned} \tag{2}$$

which lead to following governing equations:

$$\nabla \cdot \vec{U} = 0 \tag{3}$$

$$\frac{\partial \vec{U}}{\partial \tilde{t}} + \left(\vec{U}.\nabla\right)\left(\varepsilon^{-1}\vec{U}\right) = -\nabla\left(\varepsilon P\right) + \frac{1}{Re}\nabla^2\vec{U} \underbrace{-\varepsilon\left(\frac{1}{Re\,Da} + \frac{F_\varepsilon}{\sqrt{Da}}\left\|\vec{U}\right\|\right)\vec{U}}_{\vec{F}} \tag{4}$$

$$\frac{\partial \Theta_f}{\partial \tilde{t}} + \vec{U}.\nabla\Theta_f = \frac{1}{Re.Pr}\nabla.\left(\frac{\lambda_{e,f}}{\lambda_f}\nabla\left(\frac{\Theta_f}{\varepsilon}\right)\right) + Kr.\frac{Bi}{Re.Pr}\left(\frac{\Theta_s - \Theta_f}{\varepsilon}\right) + III + \tilde{\Phi} \tag{5}$$

$$\frac{\partial \Theta_s}{\partial \tilde{t}} = \frac{Kr}{Rc}\frac{1}{Re.Pr}\nabla.\left(\frac{\lambda_{e,s}}{\lambda_s}\nabla\left(\frac{\Theta_s}{1-\varepsilon}\right)\right) - \frac{Kr}{Rc}.\frac{Bi}{Re.Pr}\left(\frac{\Theta_s - \Theta_f}{1-\varepsilon}\right) \tag{6}$$

Under the following dimensionless initial and boundary conditions (I-BCs):

- $U = 0$; $V = 0$ and $\Theta_f = 0 \;\forall\; X$ and Y (IC);
- $U = 1$; $V = 0$; $\Theta_{f,h} = 1$, at $X = 0$ and $0 \le Y \le 1$ (the channel inlet);
- $\nabla_X U = 0$; $V = 0$; $\Theta_{f,c} = 0$ at $X = L/H$ and $0 \le Y \le 1$ (the channel outlet);
- $U = 0$; $V = 0$ and $\nabla_y \Theta_{f,h} = \nabla_y \Theta_{f,s} = 0$ at $0 \le X \le L/H$ and $Y = 1$ (upper wall);
- $U = 0$; $V = 0$ and $\nabla_y \Theta_{f,h} = \nabla_y \Theta_{f,s} = 0$ at $0 \le X \le L/H$ and $Y = 0$ (lower wall).

where $\vec{U}$, P, Θ_f, Θ_s, ε, F_ε, $\tilde{\Gamma}$, λ, $\tilde{\Phi}$ and λ_e are the velocity vector filed, the pressure, the fluid and porous medium temperatures, copper porosity, the geometric coefficient appearing in the total force due to porous media and other external forces, the PCM's liquid fraction, the thermal conductivity, the viscous dissipation and equivalent thermal conductivity, respectively. Here a_{sf} and h_{sf} (see relationship (2)) are the porous matrix specific surface and the local interfacial heat transfer coefficient between copper and paraffin. Subscripts f and s denote, respectively, the fluid and solid phases. It is worth noting that Eq. (6) reflects heat transfer in porous media, while Eq. (5) involves the second phase (PCM) or water in the first and second cases).

As paraffin was selected as the PCM for the numerical computations, the values of its main properties within the temperature and *Re* numbers ranges deemed are reported in Table 1.

Table1. Thermo-physical properties of PCM [14].

Density, $\rho(kg.m^{-3}.s^{-1})$	785.02
Thermal conductivity, $\lambda(W.m^{-1}.K^{-1})$	0.2
Specificheatcapacity, $C_p(kJ.kg^{-1}.K^{-1})$	2850.0
Latent heat, $L_a(J.kg^{-1})$	102.1
Dynamic viscosity coefficient, $\mu(kg.m^{-1}.s^{-1})$	3.65×10^{-3}
PCM melting temperature, $T_m(K)$	54.0
Thermal expansion coefficient, $\beta(K^{-1})$	3.085×10^{-4}

The source term (III) and the last term of Eq. (5) pointing out, respectively, the melting term (which takes into account the rate of latent heat stored/released) and the PCM's viscous dissipation which can be expressed as follows [15]:

$$\mathrm{III} = \left\{ \begin{array}{ll} -\dfrac{1}{\mathrm{Ste}}\dfrac{\partial \tilde{\Gamma}}{\partial \tilde{t}} & \text{for the case 1} \\ 0 & \text{for the case 2} \end{array} \right\} \tag{7}$$

$$\tilde{\Phi} = \varepsilon.\mathrm{Ec}\left\{\frac{1}{\mathrm{Da}.\mathrm{Re}} + \frac{F_\varepsilon}{\sqrt{\mathrm{Da}}}\left\|\vec{U}\right\|\right\}\left\|\vec{U}\right\|^2 + \frac{\mathrm{Ec}}{\mathrm{Re}}\left\{2\left[\left(\frac{\partial \vec{U}}{\partial X}\right)^2 + \left(\frac{\partial \vec{V}}{\partial Y}\right)^2\right] + \left(\frac{\partial \vec{U}}{\partial Y} + \frac{\partial \vec{V}}{\partial X}\right)^2\right\} \tag{8}$$

In Eq. (5), the relationship between the liquid fraction $\tilde{\Gamma}$ and the temperature T (see relationship (7)) is here solved by the method-based enthalpy. Thereby, $\tilde{\Gamma}$ in pore space is defined as [27]:

$$\tilde{\Gamma} = \begin{cases} 0 & \Theta < \Theta_s \\ \dfrac{\Theta - \Theta_s}{\Theta_l - \Theta_s} & \text{if} \quad \Theta_s \le \Theta \le \Theta_l \\ 1 & \Theta > \Theta_l \end{cases} \tag{9}$$

where, Θ_s and Θ_l are the fully solid and fully liquid PCM (paraffin) temperatures, respectively.

It should be recalled that this quantity is nil for the metallic foam/water (second case). In fact, a $\tilde{\Gamma}$-value is assigned to each cell indicating the liquid fraction within such a cell.

To close Eqs. (3), (4), (5) and (6), some parameters such as a_{sf}, h_{sf}, λ_e, F_ε and K have to be determined. To estimate the quantities a_{sf} and h_{sf}, the following correlations were involved [28-30]:

$$a_{sf} = 3\pi d_f (1 - e^{-(1-\varepsilon)/0.004}) / 0.59 / d_p^2 \tag{10}$$

$$\text{with } d_f = 1.18\left((1-\varepsilon)/3\pi\right)^{1/2} d_p \text{ and } d_p = 22.4\times10^{-3}/\omega \tag{11}$$

$$h_{sf} = \begin{cases} 0.76.\mathrm{Re}_d^{0.4}\,\mathrm{Pr}^{0.37}\,\lambda_f / d_f & 1 \le \mathrm{Re}_d \le 40 \\ 0.52.\mathrm{Re}_d^{0.5}\,\mathrm{Pr}^{0.37}\,\lambda_f / d_f & \text{for} \quad 40 \le \mathrm{Re}_d \le 10^3 \\ 0.26.\mathrm{Re}_d^{0.6}\,\mathrm{Pr}^{0.37}\,\lambda_f / d_f & 10^3 \le \mathrm{Re}_d \le 2.10^5 \end{cases} \tag{12}$$

where, $\mathrm{Re}_d\left(=d_f U_{in}/\varepsilon\nu_f\right)$, d_f, d_p and ω being the pore Reynolds number, the ligament diameter, the pore size, and pores density, respectively.

Likewise, the thermal properties of the metallic foam such as λ_e can be correlated under the LTNE assumption as follows [13, 31, 32]:

$$\lambda_e = 1/\left[\sqrt{2}(R_A + R_B + R_C + R_D)\right] \tag{13}$$

where

$$R_A = 4\sigma / \left[(2e^2 + \pi\sigma(1-e)\lambda_s + (4 - 2e^2 - \pi\sigma(1-e))\lambda_f \right] \tag{14}$$

$$R_B = (e-2\sigma)^2 / \left[(e-2\sigma)e^2\lambda_s + (2e - 4\sigma - (e-2\sigma)e^2)\lambda_f \right] \tag{15}$$

$$R_C = (\sqrt{2} - 2e) / \left[\sqrt{2}\pi\sigma^2\lambda_s + (2 - \sqrt{2}\pi\sigma^2)\lambda_f \right] \tag{16}$$

$$R_D = 2e / \left[e^2\lambda_s + (4 - e^2)\lambda_f \right] \tag{17}$$

$$\text{with } e = 0.16 \text{ and } \sigma = \left(\sqrt{2}(2 - \frac{3\sqrt{2}}{4}e^3 - 2\varepsilon) / (\pi(3 - 2\sqrt{2}e - e)) \right)^{1/2} \tag{18}$$

$$\text{So, } \lambda_{e,f} = \lambda_e \big|_{\lambda_s = 0} \text{ and } \lambda_{e,s} = \lambda_e \big|_{\lambda_f = 0} \tag{19}$$

As the relationships between permeability (K), form drag coefficient (F_ε) (see relationship (2) and Eq. (4)), and pore space are generally described by empirical correlations, these quantities were computed here with the following correlations [28-30]:

$$F_\varepsilon = 2.12 \times 10^{-3} (1-\varepsilon)^{-0.132} (d_f / d_p)^{-1.63} \tag{20}$$

$$K = 7.3 \times 10^{-4} d_p^2 (1-\varepsilon)^{-0.224} (d_f / d_p)^{-1.11} \tag{21}$$

2.4 Entropy generation

For the problem deemed here, the dimensionless entropy generation rate (Ns) is reflected by the entropy generation due to heat transfer induced by local temperature gradients and the generation entropy due to fluid friction resulting from viscous effects in the fluid and at fluid-solid interfaces which, under the LTNE conjecture, it can be expressed as [15, 33]:

$$Ns = Ns_f + Ns_s \tag{22}$$

with

$$\begin{aligned} Ns_f = & \underbrace{\frac{\varepsilon}{(\Theta_f + \Pi)^2}\left[\left(\frac{\partial \Theta_f}{\partial X} \right)^2 + \left(\frac{\partial \Theta_f}{\partial Y} \right)^2 \right]}_{\text{entropy generation due to heat transfer}} + \underbrace{\frac{\varepsilon.Ec.Pr}{(\Theta_f + \Pi)} \left(\frac{1}{Da} + \frac{Re.F_\varepsilon}{\sqrt{Da}} \left\| \vec{U} \right\| \right) \left\| \vec{U} \right\|^2}_{\text{entropy generation due to Darcy-Brinkmann-Forchheimer force}} \\ & + \underbrace{\frac{Ec.Pr}{(\Theta_f + \Pi)} \left[2 \left(\left(\frac{\partial \vec{U}}{\partial X} \right)^2 + \left(\frac{\partial \vec{V}}{\partial Y} \right)^2 \right) + \left(\frac{\partial \vec{U}}{\partial Y} + \frac{\partial \vec{V}}{\partial X} \right)^2 \right]}_{\text{entropy generation due to viscous dissipation}} \\ & + \underbrace{\frac{Bi.Kr(\Theta_s - \Theta_f)}{\Theta_f + \Pi}}_{\text{entropy generation due to heat exchange between phases in porous media}} \end{aligned} \tag{23}$$

$$Ns_s = \frac{(1-\varepsilon)Kr}{(\Theta_s + \Pi)^2} \left[\left(\frac{\partial \Theta_s}{\partial X} \right)^2 + \left(\frac{\partial \Theta_s}{\partial Y} \right)^2 \right] - \frac{Bi.Kr(\Theta_s - \Theta_f)}{\Theta_s + \Pi} \tag{24}$$

$\Pi \left(= T_c / \Delta T_{ref} \right)$ being the dimensionless temperature.

The average rate of entropy generation within the porous channel can be assessed numerically as [34]:

$$Ns_{av} = \frac{1}{S}\int_S Nsdxdy \tag{25}$$

To assess the thermal energy efficiency and the quality of the stored energy of the systems under consideration, two parameters are important, i.e., overall energy and exergy efficiencies.

2.5 LHTESs' energy and exergy efficiencies

The latent and sensible thermal energy systems' efficiency can be rated via the first thermodynamic law and the overall energy efficiency during the two processes (charging/discharging). From this, the overall energy efficiency (η) can be defined as follows [15, 35-37]:

$$\eta = \eta_{charging} \times \eta_{discharging} = 100 \times \left(E_{recovered} / E_{input} \right) \tag{26}$$

$$\text{where, } \eta_{charging} = E_{accumulation} / E_{input} \quad \text{and} \quad \eta_{discharging} = E_{recovered} / E_{accumulation} \tag{27}$$

with

$$E_{input} = \dot{m} C_{p,f} \Delta T_{f,charging} + E_{diss,charging} + E_{latent,charging} \tag{28}$$

$$E_{recovered} = \dot{m} C_{p,f} \Delta T_{f,discharging} + E_{diss,discharging} + E_{latent,discharging} \tag{29}$$

$E_{latent}\left(= \dot{m}_f C_{p,f} \times La \right)$ and $E_{diss} = \iint \tilde{\Phi} dS$ being the latent energy of PCM (which concerns only the case1) [14] and the dissipation energy [15], respectively. More details on the notion of LHTESS' energy efficiency are provided, e.g., in [15].

For any LHTES system, the overall exergy efficiency (ψ), which allows to qualify the quality of the energy stored, can be defined as [15, 35, 38, 39]:

$$\psi = \psi_{charging} \times \psi_{discharging} = 100 \times \left(Ex_{recovered} / Ex_{input} \right) \tag{30}$$

$$\text{where } \psi_{charging} = Ex_{stored} / Ex_{input} \text{ and } \psi_{discharging} = Ex_{recovered} / Ex_{stored} \tag{31}$$

with Ex_{stored} = (Exergy loss + Exergy consumption) .

As for $Ex_{recovered}$ and Ex_{input} , they are respectively the exergy recovered during the discharging period and the exergy input to the system during the charging period whose expressions can be given as follows (see Refs. [15, 35, 38, 39] to name a few):

$$Ex_{input} = \dot{m} C_{p,f} \left(T_{f,in} - T_{f,out} \right)_{charging} - T_0 \dot{m} C_{p,f} Ln\left(T_{f,in} / T_{f,out} \right)_{charging} \tag{32}$$

$$Ex_{recovered} = \dot{m} C_{p,f} \left(T_{f,out} - T_{f,in} \right)_{discharging} - \dot{m} C_{p,f} Ln\left(T_{f,out} / T_{f,in} \right)_{discharging} \tag{33}$$

3. Computational approach and validation

The LBM is the proper implementation of the Boltzmann equation to solve fluid flow, heat transfer, and other transport problems. It is based on statistical particles distribution evolution of a lattice gas whose density represents the physical quantities to be modelled, such as momentum, temperature, etc. So, the dynamic and thermal fields of the problem deemed here can be solved using an evolution equation of the density distribution function. So, an enthalpy porosity TLBM method at REV scale [17] is adopted here to handle the governing equations (Eqs. (3) - (6)) associated with suitable boundary and initial conditions. It is coupled with a local thermal non-equilibrium (LTNE) technique to assess the phase change in PCM infused with metallic foam or the heat transfer with water.

3.1 Thermal lattice Boltzmann formulation

Explicitly, the TLBM consists on handling the propagation of fictive fluid particles on a lattice x at time t with finite discrete distribution velocities. Thereby, the fluid macroscopic properties (density, velocity, temperature, etc.) can be computed via the discrete Boltzmann equation using weighted averages or moments of the particle distribution. As in this work, the LTNE assumption has been presumed, three distribution functions (TDF) constitute the key ingredient of this approach (commonly referred to as the SRT-LBM due to the simple modeling of the collision term), viz., $f_i(x,t)$ (for the dynamic field) and $g_{i,f,s}(x,t)$ (for the two thermal fields). So, the LBM discrete generalized governing equations (Eqs. (34) - (36)) with a force term are expressed as [14, 40]:

$$\underbrace{f_i\left(x+e_i\delta t,t+e_i\delta t\right)-f_i\left(x,t\right)}_{\text{streaming}}=-\delta t\underbrace{\left(f_i\left(x,t\right)-f_i^{eq}\left(x,t\right)\right)}_{\text{collision term}}/\tau_v+\delta t.\underbrace{\vec{F}_{e_i}}_{\text{force term}} \tag{34}$$

$$\begin{aligned}\underbrace{g_{f,i}\left(x+e_i\delta t,t+\delta t\right)-g_{f,i}\left(x,t\right)}_{\text{streaming}}=&-\underbrace{\left(g_{f,i}\left(x,t\right)-g_{f,i}^{eq}\left(x,t\right)\right)/\tau_{T,f}}_{\text{collision term}}\\&+\underbrace{\left(1+\delta t\partial_t/2\right)\delta tSr_{i,f}+\delta tf_i\left(x,t\right)q_i}_{\text{source terms}}\end{aligned} \tag{35}$$

$$\underbrace{g_{s,i}\left(x+e_i\delta t,t+\delta t\right)-g_{s,i}\left(x,t\right)}_{\text{streaming}}=-\underbrace{\left(g_{s,i}\left(x,t\right)-g_{s,i}^{eq}\left(x,t\right)\right)/\tau_{T,s}}_{\text{collision term}}+\underbrace{\left(1+\delta t\partial_t/2\right)\delta tSr_{i,s}}_{\text{source term}} \tag{36}$$

where $\tau_v\,(=3\nu+0.5)$ (Eq.(34)) is the dimensionless collision time for velocity, and $\tau_{T,f;s}$ (Eqs. (35) and (36)) are the dimensionless collision times for temperatures which are computed as follows [40 - 42]:

$$\tau_{T,f}=3\alpha_{e,f}/(\delta tc^2)+0.5 \quad \text{with} \quad \alpha_{e,f}=\lambda_{e,f}/\left(\varepsilon(\rho C_p)_f\right) \tag{37}$$

$$\tau_{T,s}=3\alpha_{e,s}/(\delta tc^2)+0.5 \quad \text{with} \quad \alpha_{e,s}=\lambda_{e,s}/\left((1-\varepsilon)(\rho C_p)_s\right) \tag{38}$$

δt, $c\,(=\delta x/\delta t=1;\delta x=\delta t)$ and $\alpha_{e,f,s}$ being the lattice time step, the streaming speed and the effective diffusivity, respectively. Note that the left-hand term (LHT) of the above equations represents the free-streaming part, while the first right-hand term (RHT) represents the collision relaxation part towards a local thermodynamic equilibrium state.

Since it is the D2Q9 model which is presumed here as a lattice with nine velocities, the local equilibrium distribution functions (LEDFs) $f_i^{eq}(x,t)$ and $g_{i,f;s}^{eq}$ are modeled as by considering the porosity effects:

$$f_i^{eq}=\rho w_i\left(1+\frac{\vec{e}_i.\vec{u}}{c_s^2}+\frac{\vec{u}\otimes\vec{u}:\left(\vec{e}_i\otimes\vec{e}_i-c_s^2I\right)}{2c_s^4\varepsilon}\right) \tag{39}$$

$$g_{f,i}^{eq}=w_iT_f\left(1+e_iu/(\varepsilon c_s^2)\right)\ \text{and}\ \ g_{s,i}^{eq}=w_iT_s \tag{40}$$

$c_s\ (=c/\sqrt{3})$ being the lattice sound speed, and $\vec{e}_i$ and w_i are the particle streaming velocity and the equilibrium weighting coefficients in the model which are expressed, respectively, as follows

$$\vec{e}_i=\begin{cases}0\vec{i}+0\vec{j}, & i=0\\ c\left(\cos\theta_i\vec{i}+\sin\theta_i\vec{j}\right),\ \theta_i=(i-1)\pi/2 & i=1,2,3,4\\ \sqrt{2}c\left[\cos\theta_i\vec{i}+\sin\theta_i\vec{j}\right],\ \theta_i=(2i-9)\pi/4 & i=5,6,7,8\end{cases} \tag{41}$$

and

$$w_i=\begin{cases}4/9 & i=0\\ 1/9 & i=1,2,3,4\\ 1/36 & i=5,6,7,8\end{cases} \tag{42}$$

Since the density and the velocity obtained via the distributions f_i and f_i^{eq} must coincide, these weights satisfy isotropy constraints, e.g., $\sum_i w_i=1$ and $\sum_i e_iw_i=0$.

The last term $\overrightarrow{F_{e_i}}$ (Eq. (34)) [14, 40, 41] and the source terms $Sr_{i,f;s}$ [40, 41] and q_i [43] (Eqs. (35)- (36)) are computed as follows

$$\overrightarrow{F_{e_i}}=w_i\rho\left(1-\frac{1}{2\tau_v}\right)\left[\frac{\vec{e}_i.\vec{F}}{c_s^2}+\frac{\vec{u}.\vec{F}:\left(\vec{e}_i\vec{e}_i-c_s^2I\right)}{\varepsilon c_s^4}\right] \tag{43}$$

$$Sr_{i,f}=w_i\left(\frac{La}{C_{p,f}}\left[\frac{\gamma(t+\delta t)-\gamma(t)}{\delta t}\right]+\frac{h(T_s-T_f)}{\varepsilon(\rho C_p)_f}\right) \tag{44}$$

$$Sr_{i,s} = w_i \left(\frac{h(T_s - T_f)}{(1-\varepsilon)(\rho C_p)_s} \right) \tag{45}$$

$$q_i = -(f_i - f_i^{eq})(\vec{e}_i - \vec{u})(\vec{e}_i - \vec{u}) : \Delta\vec{u} \tag{46}$$

To be complete, the boundary conditions (BCs) regarding velocity and temperature must be specified. In the TLBM framework, the BCs for velocity and temperature pertain to the microscopic distribution functions f_i and g_i after the streaming process. In this work, the bounce-back boundary scheme proposed by Ladd [44] was picked out to get the no-slip velocity conditions at the upper and lower walls [16]. However, at the channel inlet, Dirichlet condition is adopted to obtain the unknown velocities [45, 46], while at the channel exit, the conditions commonly mentioned in the literature were used [47]. Within the present framework and on the basis of the references selected, the BCs dealing with velocity and temperature are gathered in Table 2 below.

Table 2. TLBM boundary conditions for velocity and temperature.

	Velocity BCs	**Thermal BCs**
Channel inlet	$\rho_{in} = \left(f_0 + f_2 + f_4 + 2\left(f_3 + f_6 + f_7\right)\right)/\left(1 - u_{in}\right)$ $f_1 = f_3 + 2\rho_{in}u_{in}/3$ $f_5 = f_7 + \rho_{in}u_{in}/6$ $f_8 = f_6 + \rho_{in}u_{in}/6$	$T_w = \Theta_h = 1$ $g_1 = T_w(w_1 + w_3) - g_3$ $g_5 = T_w(w_5 + w_7) - g_7$ $g_8 = T_w\left(w_8 + w_6\right) - g_6$
Channel outlet	$f_{3,n-1} = f_{3,n}$; $f_{7,n-1} = f_{7,n}$; $f_{6,n-1} = f_{6,n}$	$g_7 = -g_5$; $g_3 = -g_1$; $g_6 = -g_8$
Top wall	$f_{7,n} = f_{5,n}$; $f_{4,n} = f_{2,n}$; $f_{8,n} = f_{6,n}$	$g_{8,m} = g_{8,m-1}$; $g_{4,m} = g_{4,m-1}$; $g_{7,m} = g_{7,m-1}$
Bottom wall	$f_{6,n} = f_{8,n}$; $f_{2,n} = f_{4,n}$; $f_{5,n} = f_{7,n}$	$g_{6,0} = g_{6,1}$; $g_{2,0} = g_{2,1}$; $g_{5,0} = g_{5,1}$

The following relationships are then used to set the (local) macroscopic quantities (ρ, $\vec{u}$, T_f, T_s):

$$\rho = \sum_i f_i \; ; \; \rho\vec{u} = \sum_i f_i\vec{e}_i + \delta t\vec{F}/2 \; ; \; T_f = \sum g_{fi} \text{ and } T_s = \sum g_{si} \tag{47}$$

3.2 Validation

It should be stressed that our in-house code has already been validated [23]. However, before presenting and commenting on the results in the dedicated section, we ensured to further validate this via other previously published benchmarks.

For this ultimate validation, we compare the results obtained by the present thermal SRT-LBM with those of Ref. [48]. Figure 2 shows the comparison of the dimensionless velocity and temperature results generated by developed forced convection in a rectangular porous

channel differentially heated via its two lower and upper walls along the line X= 0.5 for three selected Da numbers of 0.01, 0.05 and 0.1, and under the LTE conjecture. As pointed in Figure 2 (a), the permeability increases with the Da number, thereby reducing the velocity profile flatness. As for the thermal field, it turns out that the viscous effects decrease when the Da number increases (Figure 2 (b)). As noted, our predictions corroborate these selected benchmarks. Furthermore, we support our findings with maximum errors (%), which are gathered in Table 3.

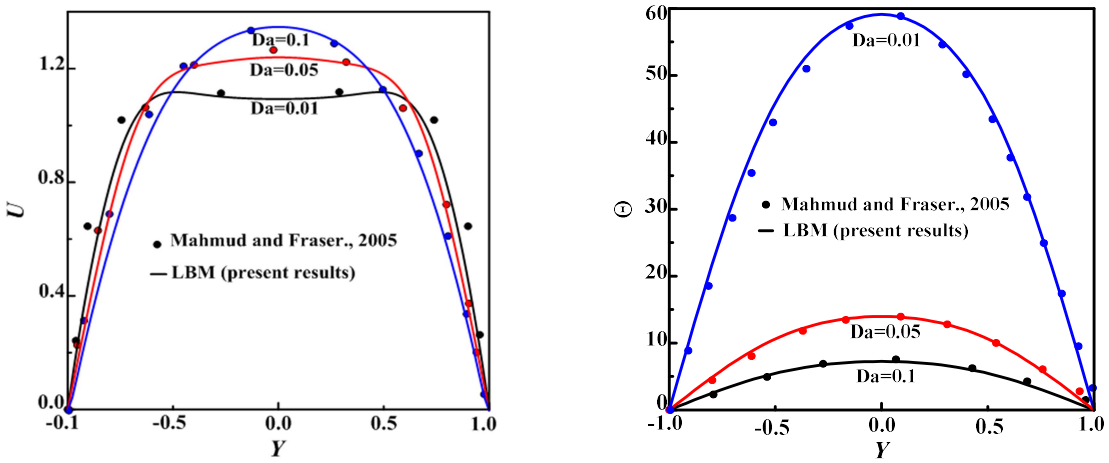

(**a**) (**b**)

Figure 2. U-velocity streamwise profiles (**a**) and temperature (**b**) set by three *Da* numbers. Comparison with Mahmud and Fraser' results [48].

Table 3. Model validation's (error %).

Da	*error (%)/*U *-velocity*	*error (%)/*Θ
0.01	2.01	0.81
0.05	1.18	0.47
0.1	1.15	0.42

4. Results and discussion

In this section, the numerical results from the model of considered equations are presented and commented, and the effect of the following parameters is studied on the fluid flow, heat transfer, LTNE intensity, entropy generation rate (Ns) and interfacial heat transfer: pore density ω ($10 \le \mathrm{PPI} \le 60$) and Reynolds number (200 and 400). Furthermore, it is worth stating that the in-house code has been implemented and amply benchmarked (see [15], to cite a few) at LESTE/National School of Engineers of Monastir in Tunisia and at LGCgE/Univ. Artois in France.

The effects of the pores density ω ($\mathrm{PPI} = 10, 30$ and 60) and the Re number (200 and 400) will be investigated in the following sections whereas the numbers of Prandtl, Stephan, Eckert

are kept fixed throughout this study. Explicitly, these numbers are set, respectively, to: $\mathrm{Pr}=50, \mathrm{Ste}=1, \mathrm{Ec}=0$ (for the case 1) and $\mathrm{Pr}=7.01, \mathrm{Ste}=0, \mathrm{Ec}=0$ (for the case 2).

4.1 PPI's effect on the LTNE intensity for both cases

The effect of pores density ω ($10 \le \mathrm{PPI} \le 60$) on the LTNE intensity are exhibited in figures 3 and 4 for Re = 200 and 400 during both charging and discharging processes. The results show that this parameter has a significant effect, especially at Re 400. As can be seen (figure 3), the LTE assumption could be adopted during the charging process for case 1 since $\mathrm{LTNE} < 0.05$ [49, 50], 0.05 being the limit value allowed so that the LTNE can be conjectured. This obviously cannot be evoqued for case 2 ($\mathrm{LTNE} > 0.05$) whatever PPI and Re. However, during the discharging process (figure 4), the LTNE intensity is secured for both cases while decreasing with increasing PPI regardless of Re.

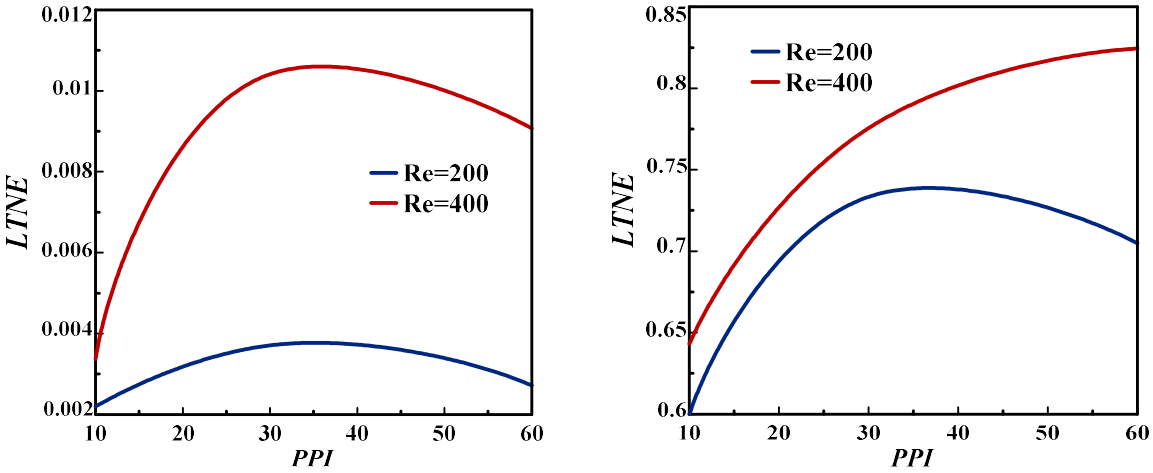

Figure 3. Pore density effect on LTNE intensity during charging process for $\varepsilon = 0.9$: (**a**) case 1; (**b**) case 2.

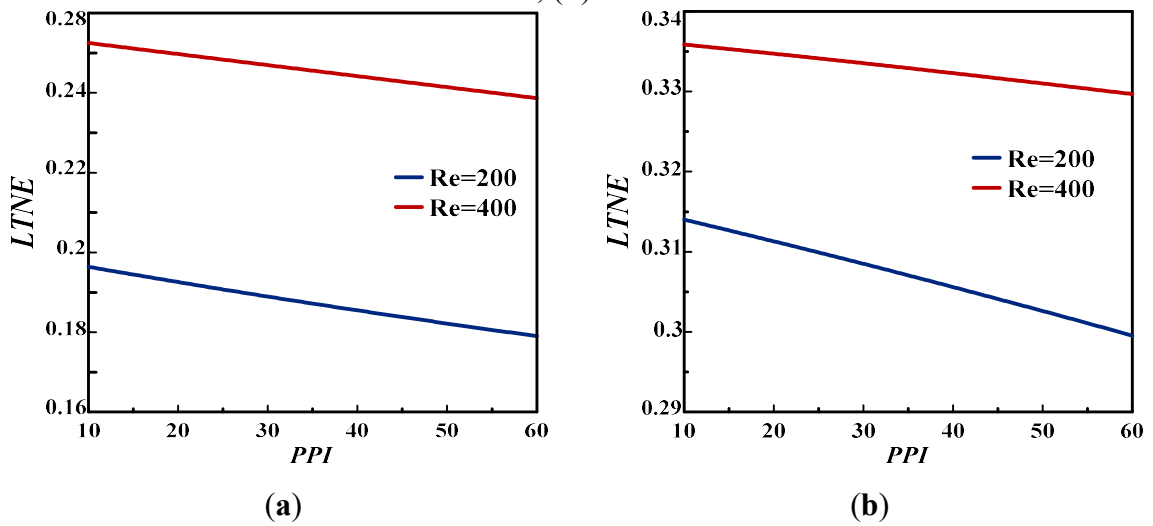

Figure 4. Pore density effect on LTNE intensity during discharging process for $\varepsilon = 0.9$: (**a**) case 1; (**b**) case 2.

4.2 PPI's effect on the dimensionless U-velocity and streamlines for both cases

Figures 5 and 6 exemplify the PPI's effect on U-velocity and streamlines for the two cases 1 and 2. During the charging process, it is clear from these figures that the velocity distribution displays an approximately similar shape in both cases. In addition, it appeared that the PPI increase flattens the velocity distribution indicating that the permeability (or Darcy number) inside the channel is decreasing.

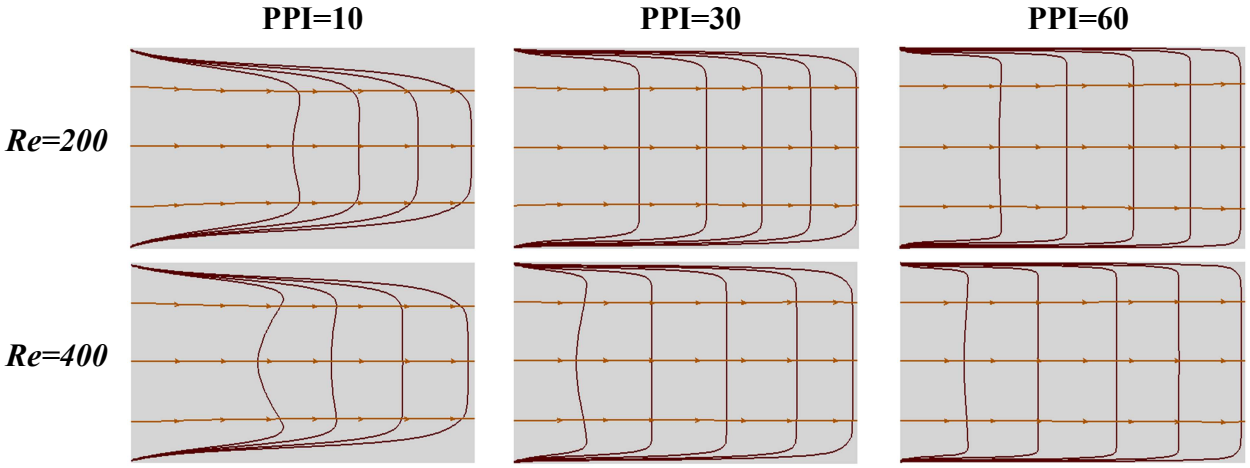

Figure 5. Pore density effect on U-contours and streamlines during charging process at $\varepsilon = 0.9$: case 1.

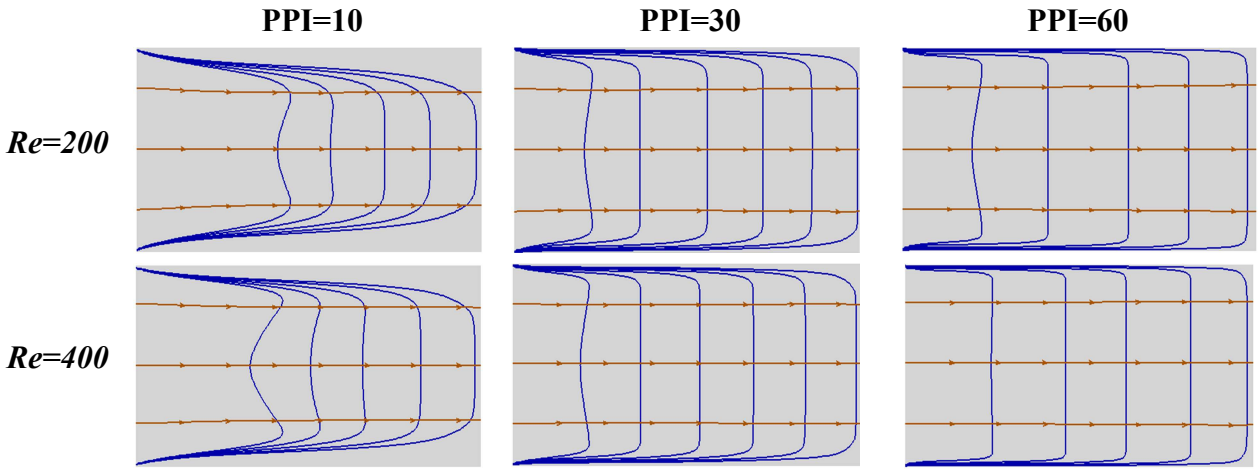

Figure 6. Pore density effect on U-contours and streamlines during charging process at $\varepsilon = 0.9$: case 2.

4.3 PPI's effect on the dimensionless intensity ($\Theta_s - \Theta_f$) for both cases

Figures 7 and 8 depict the PPI's effect on dimensionless intensity ($\Theta_s - \Theta_f$) during two processes for both cases. As can be seen, temperature profiles exhibit completely different shapes for latent and sensible heat cases. It is observed that, during the charging process, the temperature intensity decreases to X = 2/5 of the channel and then increases until it reaches its maximum near the channel exit before decreasing further due to the channel cold exit. This is because the temperature of the metal is higher than that of the paraffin in 2/5 of the channel due to the high thermal conductivity of the metallic foam, thereby revealing the dominance of

the forced convection. From there, the paraffin temperature rises faster than that of the foam (melting phase) to drop at the channel exit due to the forced convection weakness to the detriment somewhat of the particles thermal conduction, which is accentuated. In both cases, it appears that this effect remains slight regardless the process nature (loading or unloading). As for the second case under the charging process, the temperature constantly rises with the PPI and decreases at the channel end where the two temperatures equalize, implying that the LTE assumption can be cited between the foam and water. In addition, for this model (figure 8), the fluid temperature generally remains higher than that of the solid, indicating that it is the thermal conduction mode that predominates. Simply stated, an increase in the PPI value inhibits (hampers) forced convection. During the discharge process, the PPI has practically no effect in the second case, the profiles being very close to each other.

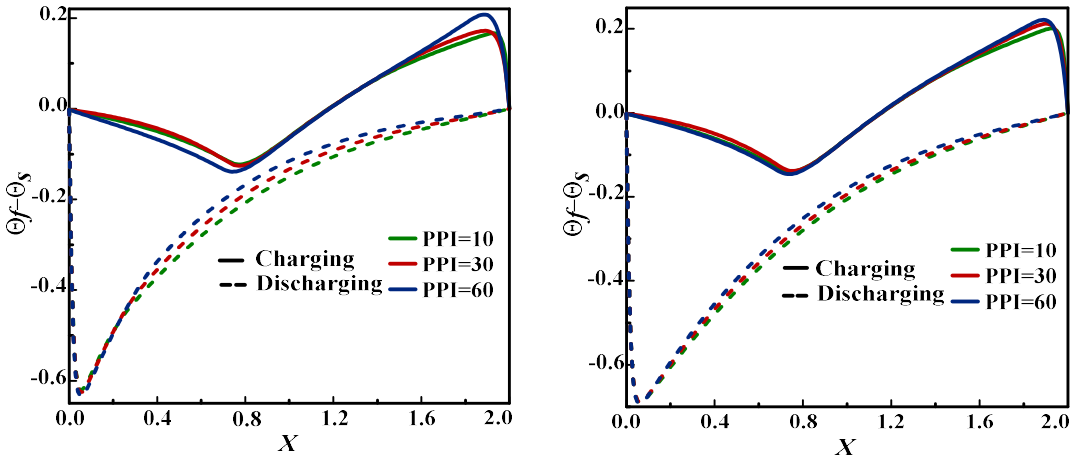

(**a**) (**b**)

Figure 7. Pore density effect on the dimensionless intensity during charging and discharging processes for $\varepsilon = 0.9$: case 1: (**a**) Re=200; (**b**) Re=400.

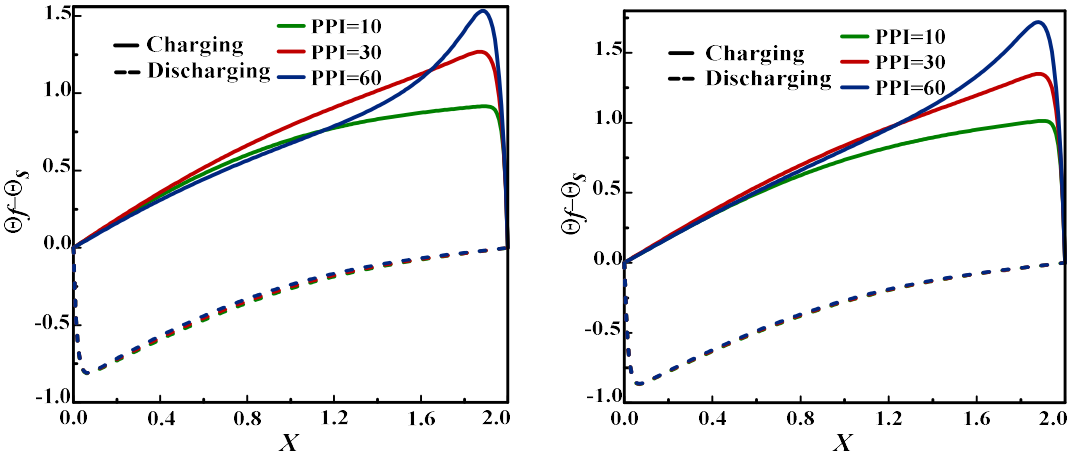

(**a**) (**b**)

Figure 8. Pore density effect on the dimensionless intensity during charging and discharging processes for $\varepsilon = 0.9$: case 2: (**a**) Re=200; (**b**) Re=400.

4.4 PPI's effect on the dimensionless entropy generation rate for both cases

When dealing with a system stability, estimating the irreversibility generated can prove propitious and serve as an indicator. Figures 9 and 10 outline the dimensionless entropy generation rate (Ns) during charging/discharging periods for both cases. As displayed in these figures, the entropy generation rate is usually the highest for a larger PPI (= 60) in both cases. Moreover, from Re of 400 and PPI of 60, the dimensionless entropy generation rate reaches its maximum, pointing that forced convection is the dominant mode. However, during the discharging process, and from halfway through the channel, Ns drops as the PPI increases since forced convection gradually gives way to conduction. Likewise, this rate is always higher (of the order of 10 times) in case 1 than in case 2. According to the amplitude of Ns, it appears that the sensible heat system is more stable than that with latent heat. To sum up, to reduce the irreversibility of the system, low values of the PPI and the Re number may be appropriate during the charging case, while a higher PPI may be helpful for the discharging case.

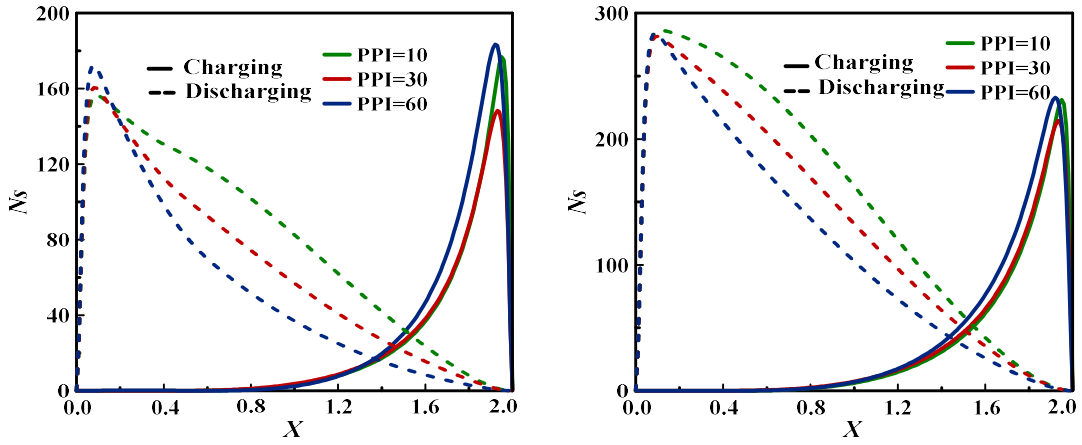

Figure 9. Pore density effect on the dimensionless entropy generation rate during charging and discharging processes for $\varepsilon = 0.9$: case 1: (**a**) Re=200; (**b**) Re=400.

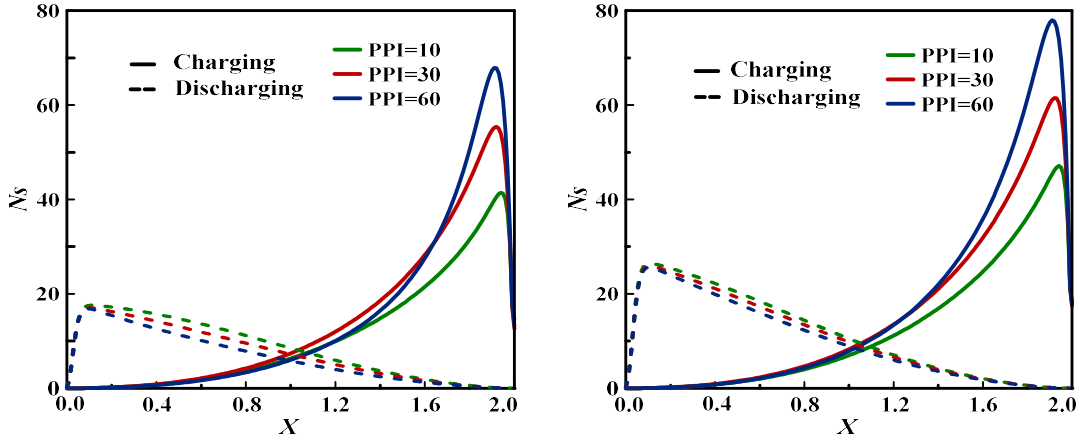

Figure 10. Pore density effect on the dimensionless entropy generation rate during charging and discharging processes for $\varepsilon = 0.9$: case 2: (**a**) Re=200; (**b**) Re=400.

The evolvement of the mean entropy generation rate (Ns_{av}) in the systems considered with the pores density ω is plotted in figures 11 and 12 at the selected Re numbers and for both processes. It may be noted that, during charging process, the average entropy raises with the PPI's for both models, while during discharging process, it drops when PPI increases. In addition, it should be noted that the sensible heat system's irreversibility is always lower compared to that of the latent heat system during the two periods.

According to the impacts up-discussed, it appears that for the two models, a high porosity (= 0.9) and a moderate or even low PPI must be sought to mitigate the system irreversibility during the charging process, while a larger PPI (= 60) would be suitable for the discharging process.

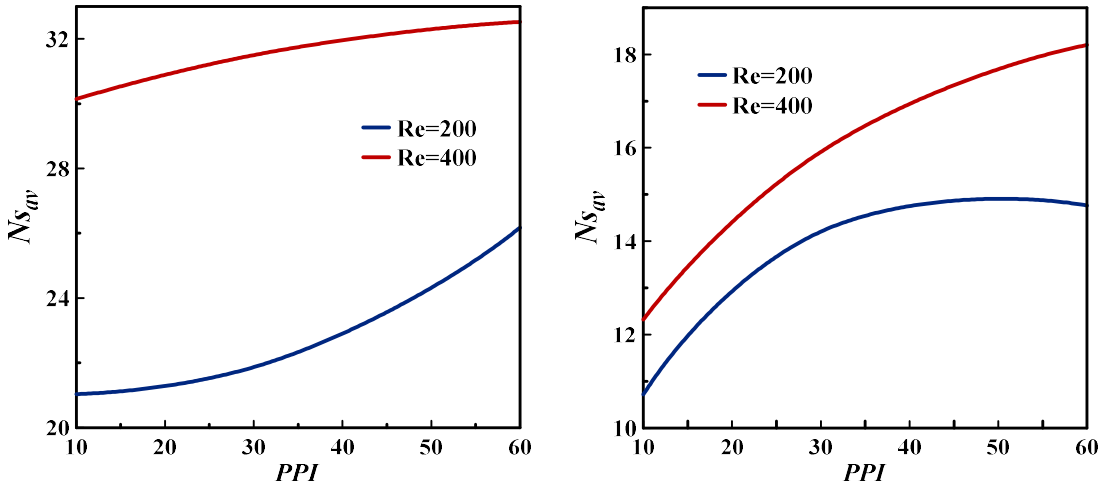

Figure 11. Pore density effect on the dimensionless average entropy generation rate during charging process for $\varepsilon = 0.9$: (**a**) case 1; (**b**) case 2.

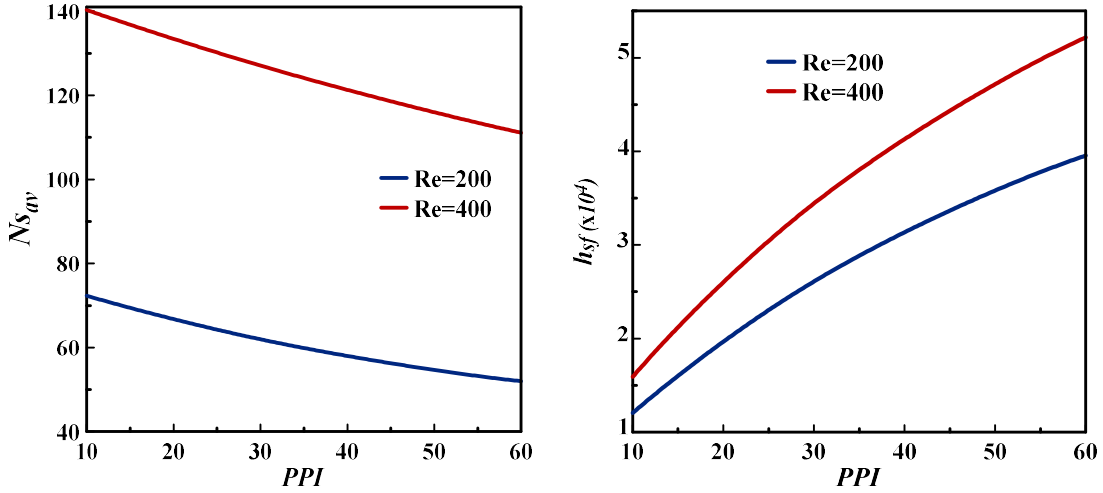

Figure 12. Pore density effect on the dimensionless average entropy generation rate during discharging process for $\varepsilon = 0.9$: (**a**) case 1; (**b**) case 2.

4.5 PPI's effect on the interfacial heat transfer coefficient (h_{sf}) for both cases

The analysis of PPI's effect on the interfacial heat transfer coefficient (h_{sf}) between the metal foam/paraffin on the one hand and the metal foam/water on the other is conducted on the basis of Eq. (12). Figure 13 compares this effect between the two considered cases. It can be seen that h_{sf} increases with the considered PPI and Re and reaches its maximum in both cases for high values of Re (= 400) and PPI (= 60). So, an increase in Re number improves the interfacial heat transfer coefficient which highlights the conduction of heat between solid and fluid particles. This demonstrates that the forced convection in the channel generates a significant heat transfer between the particles which contribute to rise the thermal conduction of the metallic foam. It can be stated that the h_{sf} 's values for the sensible heat are larger than those for latent heat due to the high intensity values between metal/water than those between metal/paraffin (this is in accordance with figures 3 and 4). Thereby, as h_{sf} increases, the solid and fluid phases converge for high PPI (= 60), and then the LTNE decreases in the overall system for this PPI's value.

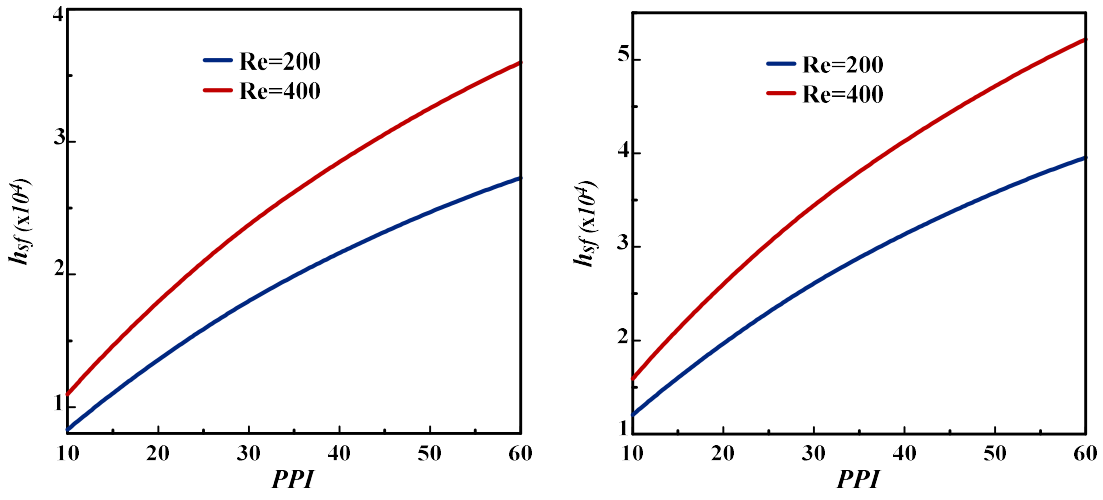

(**a**) (**b**)

Figure 13. Pore density effect on the interfacial hat transfer coefficient (h_{sf}) for $\varepsilon = 0.9$: (**a**) case 1; (**b**) case 2.

4.6 PPI's effect on the performance indicator for both cases

It is admitted that the systems assessment would be complete when the energy and exergy analyzes are estimated. So, to illustrate a performance indicator such as energy efficiency, figure 14 portrays the PPI's effect on the energy efficiency for the considered Re. It is found that the decrease in Re number enhances the performance of the two considered systems. During the processes of the first model (phase change phenomenon), the increase in PPI from 10 to 60 for $\varepsilon = 0.9$ improves the system performance (η) with an increase about 2% for

Re=200 and 400. However, for the second model (sensible heat), the overall energy efficiency decreases with 3.6% for Re=400 and 1.3% for Re=200 for the PPI's variation from 10 to 60. It may be noted that the LHTESSs are more useful than SHTESSs to pick up the maximum energy.

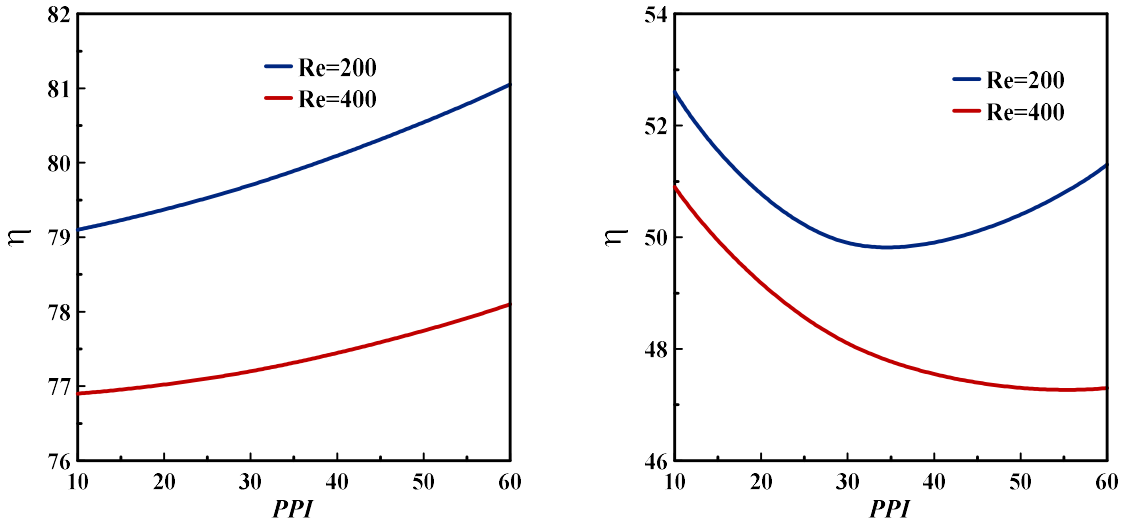

(**a**) (**b**)

Figure 14. Pore density effect on the energy efficiency (η) for $\varepsilon = 0.9$:(**a**) case 1; (**b**) case

It should be pointed out that systems exergy evaluation (including thermal losses) imparts the thermodynamic estimation of the energy stored quality because it considers the pros and cons of heat availability through these systems. As shown in figure 15, it can be seen that the Re decrease improves the exergy efficiency for the models considered due to the two systems irreversibility decrease (see figures 11 and 12). For the first model, the exergy efficiency increases from 29.1% (PPI = 10) to 50.3% (PPI = 6 0) with the PPI for Re = 200. However, for Re= 400, it increases from 21.5% (PPI=10) to 29.2% (PPI=60). Simply put, it can be stated that an increase in PPI promotes the rate of latent heat transfer and the melting process. As for the second model, the exergetic efficiency exhibited ascending profiles vs. the PPI's values, thereby, contradicting with the energetic analysis. This explains the significant thermal losses for low PPI's values ($PPI \leq 30$) for SHTESSs. In addition, as PPI increases ($PPI \geq 30$), the energy damage is reduced due to the system stability. To sum up, it turned out that the first model generally provided higher exergy efficiency than the second model.

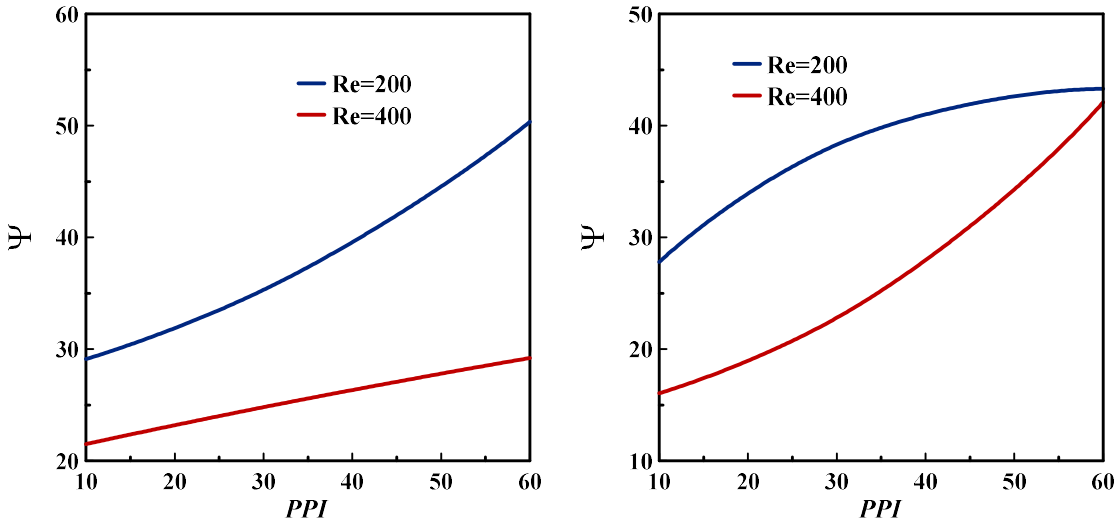

Figure 15. Pore density effect on the exergy efficiency for $\varepsilon = 0.9$: (**a**) case 1; (**b**) case 2.

4.7 PPI's effect on melting front and PCM temperature field (case 1)

The melting evolution and with the PCM temperature distribution are exhibited in figures 16 a - 16 c at Reynolds number (*Re*) of 200 .Note that the melt front mushy zone is highlighted with colors other than red and blue which point out the liquid and solid PCM regions, respectively. For $\varepsilon = 0.9$ (figures 16 a-16 c), the increase in PPI improves the heat transfer between PCM and metal foam and speeds up the melting time due to the metal foam permeability influence. However, the melting evolvement rises with PPI and becomes stronger for higher porosity (= 0.9) as presented in figures 16 a, 16 b and 16 c owing to the increase in metal foams heat transfer. More specifically, a higher PPI and porosity (60 and 0.9) improve the heat transfer between the PCM and the metal foam for Re = 200 while reducing the melting time.

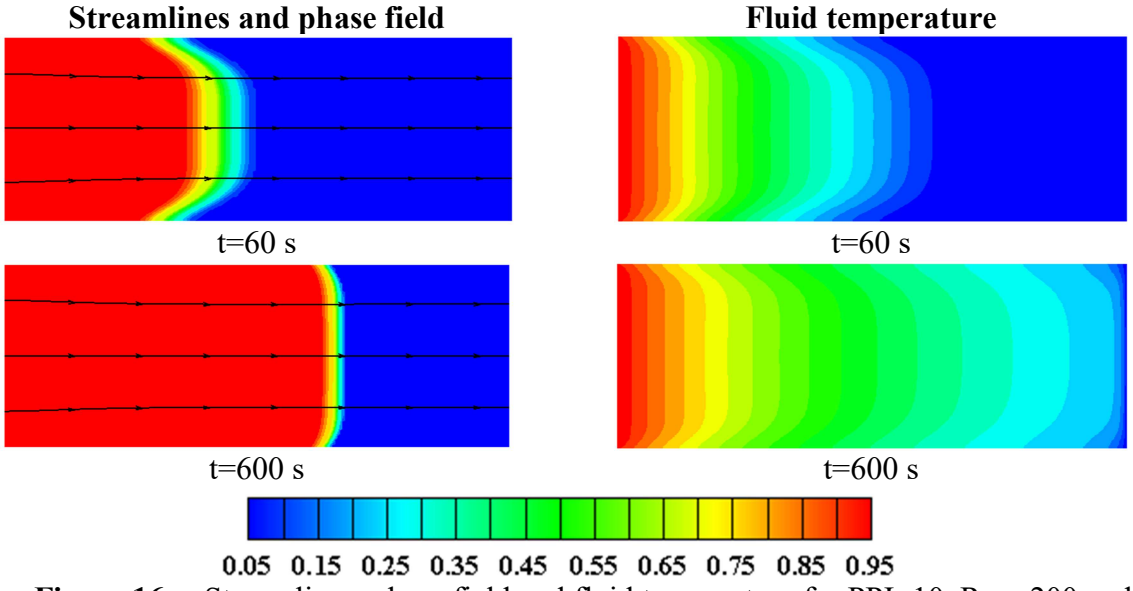

Figure 16 a. Streamlines, phase field and fluid temperature for PPI=10, Re = 200 and $\varepsilon = 0.9$ at two times: charging process.

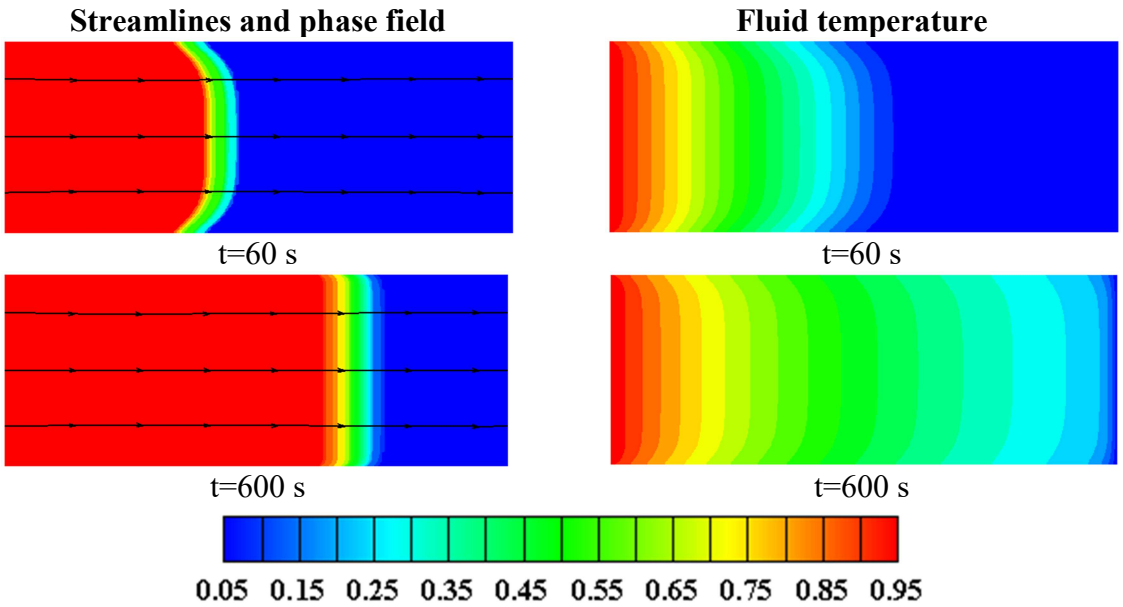

Figure 16 b. Streamlines, phase field and fluid temperature for PPI=30, Re = 200 and $\varepsilon = 0.9$ at two times: charging process.

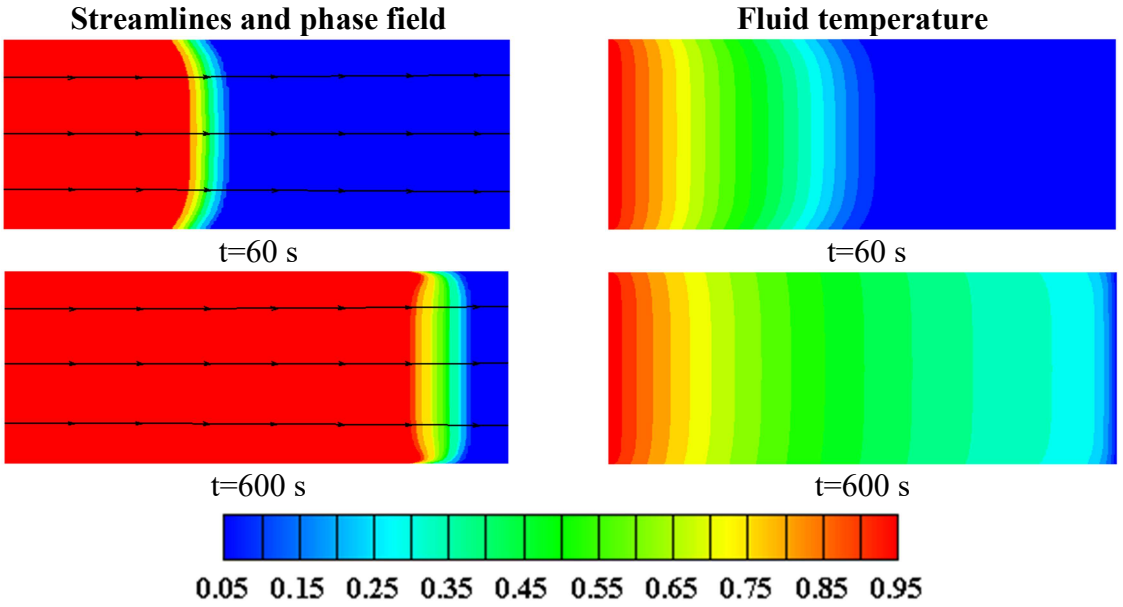

Figure 16 c. Streamlines, phase field and fluid temperature for PPI=60, Re = 200 and $\varepsilon = 0.9$ at two times: charging process.

The distribution of streamlines, flow, and temperature fields during the charging process at Re = 400 are depicted in figure 17 a–c, for the same values of PPI and porosity as shown in the previous figures, i.e., $10 \leq \text{PPI} \leq 30$ and $\varepsilon = 0.9$.

As for $\varepsilon = 0.9$ with a PPI of 60 (the largest value deemed here) (figure 17 a –c), the melting front advanced rapidly and melted the whole PCM in a short time just above 600 s (not illustrated here).

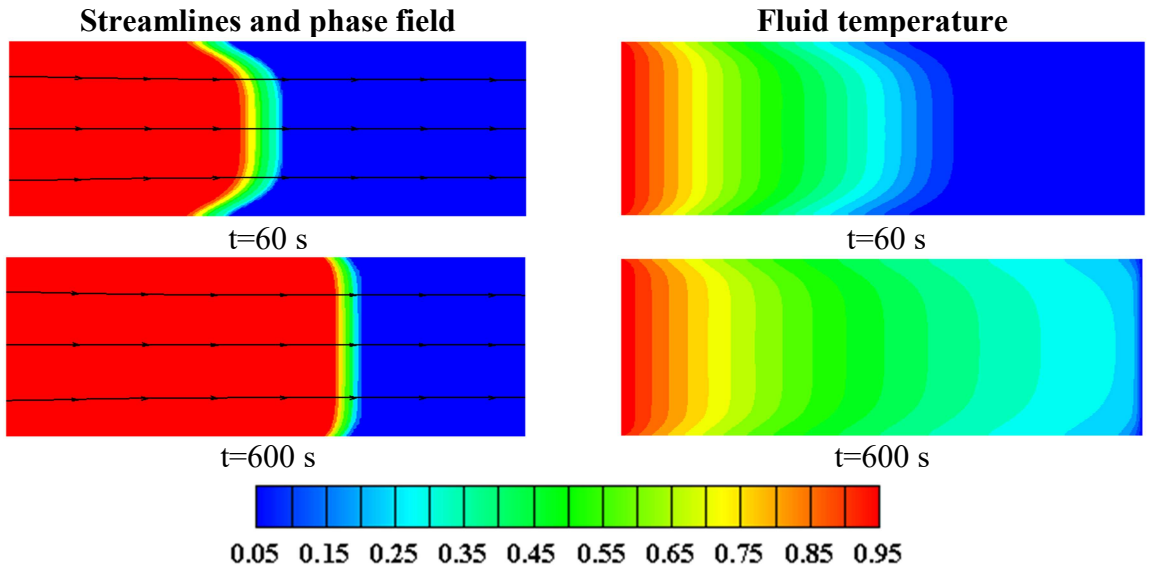

Figure 17 a. Streamlines, phase field and fluid temperature for PPI=10, Re= 400 and $\varepsilon = 0.9$ at two times: charging process.

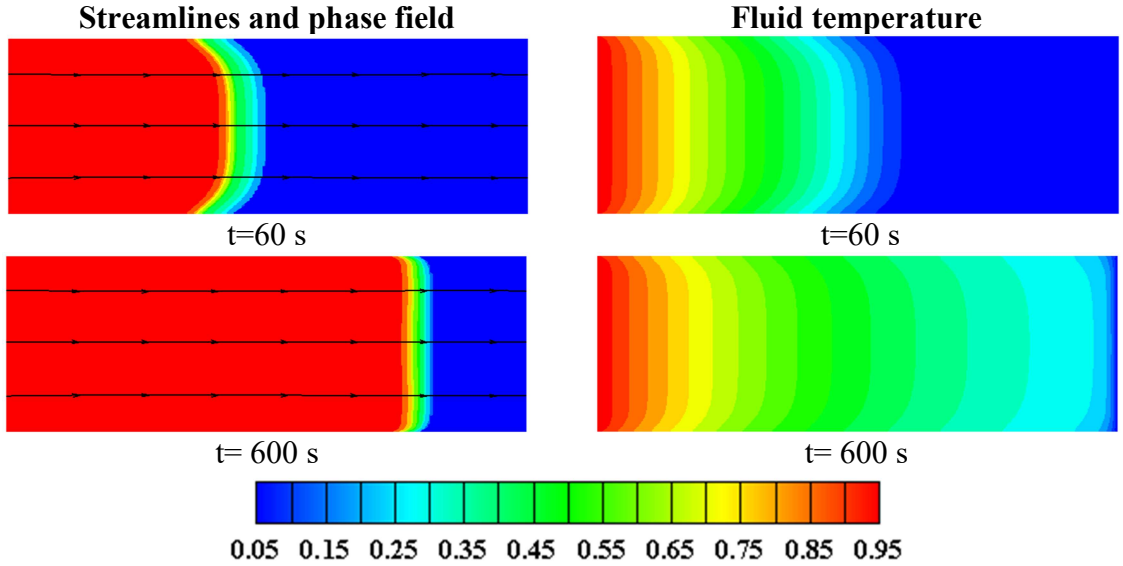

Figure 17 b. Streamlines, phase field and fluid temperature for PPI=30, Re= 400 and $\varepsilon = 0.9$ at two times: charging process.

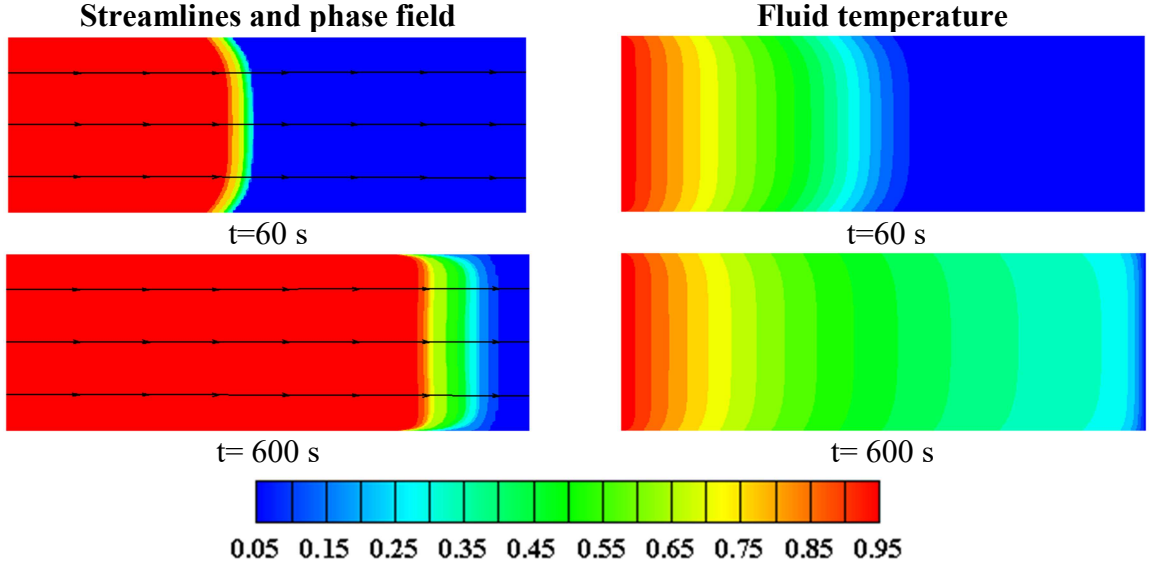

Figure 17 c. Streamlines, phase field and fluid temperature for PPI=60, Re = 400 and $\varepsilon = 0.9$ at two times: charging process.

5. Summary and Conclusions

The present study dealt with the metal foam pore density effect on sensible and latent heats storage through an enthalpy-based TLBM during charging/discharging processes at two *Re* numbers of 200 and 400. The porous medium effects at the REV-scale and based on the DBF model are incorporated in the equilibrium distribution functions and Boltzmann's equation. The investigation was performed in an open-ended channel incorporating a porous medium filled with either a PCM or water. Streamlines, velocity and thermal fields, LTNE intensity, entropy generation rate, interfacial heat transfer coefficient and performance indicators such as energetic and exergetic efficiencies were exhibited. These findings provided some insights into the targeted parameters effects.

From the results thereby obtained, it should be stated that the enthalpy-based REV-TLBM approach has a great potential in simulating the phase change in a porous medium under the flow steady conjecture and that LTNE constraint, during charging process, is not valid for the case 1, unlike the second. However, during discharging process, such an assumption proved to be valid for both systems while evolving inversely with the PPI variation. As far as the charging process concerns, increasing the PPI de-creases the permeability within the systems and thereby flattens the velocity shape. Furthermore, it raises the temperature intensity while mitigating the forced convection for both systems.

For the first case, forced convection prevails at the channel's beginning during the charging process followed by the conduction mode, while thermal conduction dominates almost everywhere in the second case. However, during the discharging period, the PPI variation is proportional to the temperature intensity for the first case but it has no effect in the second.

To improve the thermal performance of the cases deemed, the system irreversibility (in both cases) can be mitigated via a low PPI (= 10) during the charging process, while a high value (PPI = 60) can be advised during the discharging process. In addition, for both cases, the values of the energy and exergy efficiencies obtain an optimum value at low *Re* number. While, the intensification of PPI lessens energy losses for sensible heat systems and thereby to rise the stored energy quality.

To sum up, the obtained findings provide some novel implications on the simulation of phase change in a porous medium under steady flow with LTNE. Likewise, they can be useful in the design of LHTES and SHTES systems.

References

[1] Xu, H., Wang, N., Zhang, C., Qu, Z., Cao, M. (2020). Optimization on the melting performance of triplex-layer PCMs in a horizontal finned shell and tube thermal energy storage unit. Appl. Therm. Eng., 176, 115409.

[2] Medrano, M., Gil, A., Martorell, I., Potau, X., Cabeza, L. F. (2010). State of the art on high-temperature thermal energy storage for power generation. Part 2—Case studies. Ren. Sust. Energy Rev., 14 (1), 56-72.

[3] Kuravi, S., Trahan, J., Goswami, D. Y., Rahman, M. M., Stefanakos, E. K. (2013). Thermal energy storage technologies and systems for concentrating solar power plants. Prog. Energy Combust. Sci, 39 (4), 285-319.

[4] Mohan, G., Venkataraman, M. B., Coventry, J. (2019). Sensible energy storage options for concentrating solar power plants operating above 600° C. Ren. Sust. Energy Rev., 107, 319-337.

[5] Elouali, A., Kousksou, T., El Rhafiki, T., Hamdaoui, S., Mahdaoui, M., Allouhi, A., Zeraouli, Y. (2019). Physical models for packed bed: Sensible heat storage systems. J. Energy Storage, 23, 69-78.

[6] Dhifaoui, B., Jabrallah, S. B., Belghith, A., Corriou, J. P. (2007). Experimental study of the dynamic behaviour of a porous medium submitted to a wall heat flux in view of thermal energy storage by sensible heat. Int. J. therm. Sci., 46 (10), 1056-1063.

[7] Yang, X., Wei, P., Cui, X., Jin, L., He, Y. L. (2019). Thermal response of annuli filled with metal foam for thermal energy storage: an experimental study. Appl. Energy, 250, 1457-1467.

[8] Amami, B., Rabhi, R., Dhahri, H., Mhimid, A. (2017). Numerical thermodynamic analysis of heat storage porous duct under pulsating flow using lattice Boltzmann method. Int. J. Exergy, 22 (4), 376-395.

[9] Lafdi, K., Mesalhy, O., Shaikh, S. (2007). Experimental study on the influence of foam porosity and pore size on the melting of phase change materials. J.Appl. Phys., 102 (8), 083549.

[10] Ren, Q., He, Y. L., Su, K. Z., Chan, C. L. (2017). Investigation of the effect of metal foam characteristics on the PCM melting performance in a latent heat thermal energy storage unit by pore-scale lattice Boltzmann modeling. Numer. Heat Transf., Part A: App., 72(10), 745-764.

[11] Ren, Q., Meng, F., Guo, P. (2018). A comparative study of PCM melting process in a heat pipe-assisted LHTES unit enhanced with nanoparticles and metal foams by immersed boundary-lattice Boltzmann method at pore-scale. Int. J. Heat Mass Transf., 121, 1214-1228.
[12] Younsi, Z., Naji, H. (2020). Numerical simulation and thermal performance of hybrid brick walls embedding a phase change material for passive building applications. Jo.Therm. Anal. Calorim., 140 (3), 965-978.
[13] Sardari, P. T., Mohammed, H. I., Giddings, D., Gillott, M., Grant, D. (2019). Numerical study of a multiple-segment metal foam-PCM latent heat storage unit: Effect of porosity, pore density and location of heat source. Energy, 189, 116108.
[14] Tao, Y. B., You, Y., He, Y. L. (2016). Lattice Boltzmann simulation on phase change heat transfer in metal foams/paraffin composite phase change material. Appl. Therm. Eng., 93, 476-485.
[15] Mabrouk, R., Dhahri, H., Naji, H., Hammouda, S., Younsi, Z. (2020). Lattice Boltzmann simulation of forced convection melting of a composite phase change material with heat dissipation through an open-ended channel. Int. J. Heat Mass Transf., 153, 119606.
[16] Jourabian, M., Darzi, A. A. R., Toghraie, D., ali Akbari, O. (2018). Melting process in porous media around two hot cylinders: Numerical study using the lattice Boltzmann method. Physica A: Stat. Mech. App., 509, 316-335.
[17] Gao, D., Tian, F. B., Chen, Z., Zhang, D. (2017). An improved lattice Boltzmann method for solid-liquid phase change in porous media under local thermal non-equilibrium conditions. Int. J. Heat Mass Transf., 110, 58-62.
[18] Zhang, J., Yu, X., Tu, S. T. (2019). Lattice Boltzmann simulation on droplet flow through 3d metal foam. Processes, 7 (12), 877.
[19] Kuschel, M., Fitschen, J., Hoffmann, M., von Kameke, A., Schlüter, M., Wucherpfennig, T. (2021). Validation of Novel Lattice Boltzmann Large Eddy Simulations (LB LES) for Equipment Characterization in Biopharma. Processes, 9 (6), 950.
[20] Noori, S. S., Rahni, M. T., Taleghani, S. S. (2019). Multiple-relaxation time color-gradient lattice Boltzmann model for simulating contact angle in two-phase flows with high density ratio. Eur. Phys. J. Plus, 134 (8), 1-15.
[21] Bai, M., Chung, J. N. (2011). Analytical and numerical prediction of heat transfer and pressure drop in open-cell metal foams. Int. J. Therm. Sci., 50 (6), 869-880.
[22] Chen, L., Fang, W., Kang, Q., Hyman, J. D. H., Viswanathan, H. S., Tao, W. Q. (2015). Generalized lattice Boltzmann model for flow through tight porous media with Klinkenberg's effect. Phys. Rev. E, 91 (3), 033004.

[23] Dincer, I., & Ezan, M. A. (2018). *Heat storage:* A unique solution for energy systems. Springer.

[24] Nield, D. A., Bejan, A. (2013). Convection in Porous Media. 4th editon. Springer-Verlag: New York, NY, USA.

[25] Al-Sumaily, G. F., Thompson, M. C. (2013). Forced convection from a circular cylinder in pulsating flow with and without the presence of porous media. Int. J. Heat Mass Transf., 61, 226-244.

[26] Al-Sumaily, G. F., Nakayama, A., Sheridan, J., Thompson, M. C. (2012). The effect of porous media particle size on forced convection from a circular cylinder without assuming local thermal equilibrium between phases. Int. J. Heat Mass Transf., 55(13-14), 3366-3378.

[27] Ranjbaran, Y. S., Haghparast, S. J., Shojaeefard, M. H., Molaeimanesh, G. R. (2020). Numerical evaluation of a thermal management system consisting PCM and porous metal foam for Li-ion batteries. J. Therm. Anal. Calorim., 141 (5), 1717-1739.

[28] Joshi, V., Rathod, M. K. (2019). Constructal enhancement of thermal transport in metal foam-PCM composite-assisted latent heat thermal energy storage system. Numer. Heat Transf., Part A: Appl., 75 (6), 413-433.

[29] Chen, C. C., Huang, P. C., & Hwang, H. Y. (2013). Enhanced forced convective cooling of heat sources by metal-foam porous layers. International J.Heat Mass Transf., 58 (1-2), 356-373.

[30] Settar, A., Nebbali, R., Madani, B., Abboudi, S. (2015). Numerical investigation of convective heat transfer in a plane channel filled with metal foam under local thermal non-equilibrium. Mech. Ind., 16 (5), 504.

[31] Boomsma, K., Poulikakos, D. (2001). On the effective thermal conductivity of a three-dimensionally structured fluid-saturated metal foam. Int. J. Heat Mass Transf., 44(4), 827-836.

[32] Boomsma, K., Poulikakos, D. (2011). Corrigendum for the paper: K. Boomsma, D. Poulikakos,"On the effective thermal conductivity of a three-dimensionally structured fluid-saturated metal foam"[International Journal of Heat and Mass Transfer, 44 (2001) 827–836]. Int. J. Heat Mass Transf., 1 (54), 746-748.

[33] Torabi, M., Karimi, N., Peterson, G. P., Yee, S. (2017). Challenges and progress on the modelling of entropy generation in porous media: a review. Int. J. Heat Mass Transf., *114*, 31-46.

[34] Rabhi, R., Amami, B., Dhahri, H., Mhimid, A. (2016). Entropy generation for an axisymmetric MHD flow under thermal non-equilibrium in porous micro duct using a modified lattice Boltzmann method. J. Magn. Magn. Mater., 419, 521-532.

[35] Dinçer, I., Rosen, M. (2011). Thermal Energy Storage: Systems and Applications., 2nd edition, John Wiley &Sons.

[36] Rosen, M. A., Dincer, I. (2009). Efficiency assessment of glycol cold thermal energy storage and effect of varying environment temperature. Trans. Can. Soc. Mech. Eng., 33 (1), 119-130.

[37] Hänchen, M., Brückner, S., Steinfeld, A. (2011). High-temperature thermal storage using a packed bed of rocks–heat transfer analysis and experimental validation. Appl. Therm. Eng., 31 (10), 1798-1806.

[38] Rosen, M. A. (2001). The exergy of stratified thermal energy storages. Sol. Energy, 71 (3), 173-185.

[39] Erek, A., Dincer, I. (2008). An approach to entropy analysis of a latent heat storage module. Int. J. Therm. Sci., 47(8), 1077-1085.

[40] Gao, D., Chen, Z., Chen, L. (2014). A thermal lattice Boltzmann model for natural convection in porous media under local thermal non-equilibrium conditions. Int. J. Heat Mass Transf., 70, 979-989.

[41] Guo, Z., Zheng, C., Shi, B., Zhao, T. S. (2007). Thermal lattice Boltzmann equation for low Mach number flows: Decoupling model. Phys. Rev. E, 75 (3), 036704.

[42] Guo, Z., Zheng, C., Shi, B. (2002). Discrete lattice effects on the forcing term in the lattice Boltzmann method. Phys. Rev. E, 65 (4), 046308.

[43] Shi, Y., Zhao, T. S., Guo, Z. L. (2004). Thermal lattice Bhatnagar-Gross-Krook model for flows with viscous heat dissipation in the incompressible limit. Phys. Rev. E, 70 (6), 066310.

[44] Ladd, A. J. (1994). Numerical simulations of particulate suspensions via a discretized Boltzmann equation. Part 1. Theoretical foundation. J. Fluid Mech., 271, 285-309.

[45] Zou, Q., He, X. (1997). On pressure and velocity boundary conditions for the lattice Boltzmann BGK model. Phys. Fluids, 9 (6), 1591-1598.

[46] Kumar, C. S., Mohankumar, S., Geier, M., Pattamatta, A. (2017). Numerical investigations on convective heat transfer enhancement in jet impingement due to the presence of porous media using cascaded lattice Boltzmann method. Int. J. Therm. Sci., 122, 201-217.

[47] Mohamad, A. A. (2011). Lattice Boltzmann Method: Fundamentals and Engineering Applications with Computer Codes., 2nd edition, Springer-Verlag: London.

[48] Mahmud, S., Fraser, R. A. (2005). Flow, thermal, and entropy generation characteristics inside a porous channel with viscous dissipation. Int. J. Therm. Sci., 44 (1), 21-32.

[49] Abdedou, A., Bouhadef, K., Bennacer, R. (2017). Forced convection in a self heating porous channel: Local thermal nonequilibium model. Therm. Sci., 21 (6 Part A), 2419-2429.
[50] Al-Sumaily, G. F., Sheridan, J., Thompson, M. C. (2013). Validation of thermal equilibrium assumption in forced convection steady and pulsatile flows over a cylinder embedded in a porous channel. Int. Comm. Heat Mass Transf., 43, 30-38.

Chapter 4

Pulsating flow effects on phase change phenomenon in a porous channel using the Lattice Boltzmann method

Summary

In this work, a novel latent heat thermal energy storage (LHTES) system composed of porous metal foams with phase change material (PCM) subjected to pulsating fluid flow was proposed and it was compared to the previous studies. The effect of three porosities ε (=0.7, 0.8 and 0.9) and pulsating flow parameters namely pulsating amplitude, A (=0.1, 0.5 and 0.9), and Strouhal number, St (=0.5 and 1), were tested. Physical (two-dimensional governing equations of mass, momentum and energy) and numerical systems were exhibited to handle the melting/solidification phenomenon. The enthalpy-based thermal lattice Boltzmann method (TLBM) at the representative elementary volume (REV) scale is adopted for numerical simulations. The local thermal non equilibrium (LTNE) condition is computed and used. The outcomes revealed that small A (=0.1) accelerates the melting rate and the heat spread where forced convection acts the domain. In addition, low St (=0.5) during discharging process with larger A (=0.9), and during charging period with smaller A (=0.1) is useful to reduce the global irreversibility of the system. Moreover, a steady convective flow is recommended than pulsating one to improve the energetic and exergetic performances of the unit.

1. Introduction

Owing to technological progress to improve our life quality, energy demand and consumption have jumped substantially over the last years, ensuing a universal energy crisis and atmospheric pollution. Thus, renewable energy such as solar energy (sustainable energy) and energy recuperation (waste energy) were the propositions to overcome these axes. Nonetheless, irregularity and instability of these techniques nature require to be broached by using the so-called thermal energy storage (TES) systems. The latter have the benefit that can store energy (during charging) and release it (during discharging) as the needs. Hence, TES systems are classified into three models of sensible, latent, and thermo-chemical thermal energy storage. Owing to their much larger energy storage capacity, latent heat thermal energy storage systems (LHTESSs) have acquired much attention and been gainful options for economizing energy. Interest in LHTESSs has been developing promptly to secure a satisfactory improvement in heat transfer with minimum losses. In addition, LHTESSs have been a growing need in various engineering applications due to its small volume for large amount of storage without significantly temperature fluctuation [1] during the

charging/discharging process. In particular, one of the promising techniques for LHTESS using substances called phase change materials (PCMs) is the use of highly conductive metallic foams because of its high thermal conductivity that increases the heat exchange inside these systems and improves heat transfer process and PCMs thermal conductivity. Wherefore, metallic foams deemed as porous media containing PCMs represent the most noted enhancement schemes of the heat transfer due to its large specific surface area and its low cost [2]. Nowadays, one of the substantial insights into the study of phase change phenomenon is the use of porous medium with high thermal conductivity such as copper foam, aluminum foam, nickel foam... To address this problem, fundamental efforts have been made, for example in 2020, Mabrouk et al. [3] numerically investigated the melting behavior of a PCM in a porous metallic foam structure for three different porosities 0.5, 0.7 and 0.9. The system was maintained under forced convection and was studied for two Reynolds (Re) numbers (200 and 400). It was found that the small porosity (=0.5) speeds up the melting phenomenon and improves the thermal performance of the suggested concept while increasing Re number. The same authors in 2020 in an extra study [4] evaluated the efficiency of a unit containing phase change phenomenon melting/solidification of the paraffin integrated into porous metal foam during charging/discharging processes. Numerical tests estimated that for large Re (=600) for the porosities 0.4-0.6, the energetic and exergetic efficiencies were optimum while Eckert number (Ec) is high (=10). However, an increase in the metallic structure porosity: 0.7-0.8 reduced the charging/discharging efficiencies which reached its maximum for a critical Re (~400) regardless of Ec. With an analysis of the effect of pore morphological parameters (pore per inch (PPI) density and porosity) of a porous metallic configuration on the thermal performance of melting/solidification phenomenon, Mabrouk et al. [1] indicated that an increase in PPI (=60) at high porosity (0.8-09) drops the melting time for Re=400 while it is slowed down for the porosity 0.7. In another study in 2020, Zadeh et al. [5] surveyed the phase change transition in a circular thermal energy storage unit partially filled porous copper foam and nano-additives. The results reveal that an increase in the porosity improves latent heat capacity owing to the PCM volume rises. However, it slows down the melting speed and intensifies convection heat transfer. Zhang et al. [6] numerically analyzed the heat transfer enhancement of PCM melting/solidification through a combination of heat pipe-fins-copper foam (HP-Fin-CF). They reported that when the porosity of the HP-CF combination decreases, the heat transfer rate of phase change processes of PCM rises obviously when the PCM volume is fixed. Thus, they found the same when increase the number of fins. Nevertheless, this combination restricts strongly natural convection and strengthens conduction. A year earlier, Sardari et al. [7] studied the effect of

copper foam contained in a vertical latent heat storage unit on the phase transition of PCM. They used porous copper foams with various porosities and pore sizes and estimated its thermal performance. The results show that low porosities drastically improve the system performances and reduce the melting period by 85% than using pure PCM. However, the pore size change has no effect. In addition, natural convection has larger effect on the PCM only system which was suppressed in the presence of porous medium. Esapour et al. [8] presented a model of multi-tube heat exchanger based on a metal foam/PCM composite. They found that the melting time is reduced by 14% and 55% for the porosities 0.9 and 0.7, respectively. In short, porous metal foam insertion is more efficient during PCM solidification period than that of melting. Yang et al. [9] developed an experimental and numerical study on the PCM (water) solidification features impregnated into metal foam samples with different pore parameters such as porosity (0.93 and 0.97) and pore density (8 and 30 PPI) for cold storage system. They showed that the time interval of solidification process was reduced by 87.5% and 76.7% with porosities of 0.93 and 0.97, respectively compared with pure PCM. Furthermore, they demonstrated that porosity rather than pore density represents the key parameter that influenced and dominated heat transfer enhancement of the phenomenon.

Generally speaking, the phase change phenomenon of metallic foam/PCM composite has been investigated under the so-called local thermal non-equilibrium (LTNE) condition; two-temperature energy model or the local thermal equilibrium (LTE) condition; a single energy equation. Several focuses have been placed upon on explaining the effect of these hypotheses and their validity. Zhang et al. [10] conducted the temperature measurement of copper foam/paraffin through an experimental survey using infrared camera and numerical simulations by a commercially available CFD program Fluent 14.5. They found out that there existed a quite considerable temperature difference between copper foam and paraffin, which indicates that the use of LTNE model is more efficient to describe the heat transfer behavior. Yang et al. [11] built an analytical/numerical and experimental survey to explore the role of porous metal foam on PCM solidification mechanism for cold storage. The results showed that visualization of temperature difference between saturating PCM and metal foam was appeared when phase transition initiation, then it was negligible. Authors indicated that for low Stefan (Ste) numbers such as 0.22, LTE model was held and applicable. A numerical investigation was carried out by Buonomo et al. [12] to describe the melting evolution in a LHTES system using aluminum foam in LTE conjecture. Jourabian et al. [13] underlined the PCM melting mechanism in porous matrix around two hot cylinders under natural convection. The analysis was reported employing an LTE model. More recently, Mabrouk et al. [1, 3, 4] numerically pointed out the charging and discharging processes of an LHTESS. The studies

were provided considering an LTNE model. It was found that LTNE assumption is validated and prevailed for the melting and solidification of an embedded PCM into metallic porous media regardless the parameters deemed. Specifically, the LTNE intensity parameter plays a key role in numerical investigations to deal with phase change behavior in LHTESSs for cold and/or hot storage. The validity of this parameter must be calculated and depends on the geometric configuration of the model and physical variables deemed. For example focusing on the illustrated issue, Al-Sumaily et al. [14] have accomplished a numerical survey on the thermal equilibrium model validation in an open-ended porous channel maintained under forced convection. They reported that for the steady flow, higher fluid flow characteristics such as Reynolds and Prandtl (Pr) numbers have intensified the validity rages of the LTNE hypothesis. Furthermore, the increase in thermal properties of the porous structure such as Biot (Bi) number, thermal conductivity, porosity and particle diameter reduces the degree of the LTNE assumption. However, for the pulsating flow, it is revealed that the validity of the LTNE model decreases with the decrease of the pulsating frequency or the increase of the pulsating flow amplitude.

As indicted from the above discussion, porous metal foams play a crucial role in optimizing thermal performance of LHTES systems. Thereby, efforts have been continued to developing the manufacture mechanism of these systems. Nonetheless, pulsating flow has been given as a novel idea to explore its effect during melting/solidification process of PCM. Generally, studies that have been dealt with pulsating flow with LHTES systems are limited. Chang et al. [15] conducted an experimental test of a hybrid pin-fin channel with a pulsatile airflow input condition to measure the heat transfer enhancement (HTE) efficiency. The airflow was at the frequencies of 1/4, 1/6 and 1/12 Hz for $1500 \le Re \le 20000$ with a Strouhal (St) number range of $0.00028 \le St \le 0.017$. The results proved that the St increase reduced initially the pulsating flow's Fanning friction factors and the area-averaged time-mean Nusselt numbers and then they increased. In addition, it was found that the thermal performances were deteriorated by increasing the airflow pulsation period from 1/4 to 3/4. Including PCM to the horizontal cylinders of a heatsink filled with metal foam, Ghalambaz and Zhang. [16] developed a theoretical model to address the pulse heat load effect on the performance of the PCM's phase change mechanism. They showed that a heatsink with PCM gave a higher cooling power about four times more than that of pure external convection. Nevertheless, during pulse load, the heatsink efficiency was improved from 4 to 5. This increase was accompanied with a reduction of Bi number from 0.5 to 0.35. Afrouzi et al. [17] constructed a numerical survey using the Lattice Boltzmann Method (LBM) to deal with pulsating non-Newtonian flow circulating through a corrugated duct. Authors studied the

effect of the following parameters: $50 \le Re \le 200$, pulsating flow amplitude ($0 \le A_{pulse} \le 0.35$), and power law indices $0.6 \le n \le 1.4$ with fixed St (=0.25). They argued that the increase in A_{pulse} to 0.35 reinforced recirculation zones in the duct valley regions regardless Re. Therewith, decreasing the A_{pulse} unified the velocity profiles but its increase revealed large difference between these profiles regardless the flow regime deemed. Bayomy and Saghir [18] determined pulsating and steady flow (water) characteristics numerically and experimentally circulating through a heat skin composed of porous aluminum foam subjected to forced heat transfer. Parameters range deemed to deal with pulsating water were: frequency: 0.04-0.1Hz, amplitude: 297-1353 and heat flux: 8.5 - 13.8 W/cm2. They observed that the comparison between pulsating and steady flow denoted an increase in the average Nusselt number by 14% and a decrease in the uniformity index by 73% for pulsating flow. They also found that the average local temperature decreases with increasing the pulsating flow parameters and reducing heat flux. Incompressible steady and pulsating flow in a porous/not porous channel which was heated inside by a circular cylinder was simulated by Al-Sumaily and Thompson [19]. Although, they concluded that at larger Re number, porous media effect on heat transfer enhancement for the system deemed is more promoted than using pulsating flow. Dhahri et al. [20] deemed the effect of a forced pulsating fluid flow through a cylinder domain partially filled with porous structure. They have shown that higher pulsation frequency increases the pulsation amplitude in porous zone while it is reduced in fluid region. It is clear from the above discussion that pulsating flow affects each media according to phenomenon deemed. In this paper, the pulsating flow effects on phase change phenomenon (melting/solidification) in porous metal structure subjected to forced convection represents the innovation of this article.

Recently, lattice Boltzmann method (LBM) has been developed as a primordial numerical approach for handling complicate heat transfer and fluid dynamics phenomena, including PCM phase change process within porous structure with its complicated physics, etc [21]. Thereby, this technique is effective to handle the macroscopic and microscopic mechanisms of flow process inserted within porous media by adding an additional term in the lattice Boltzmann equation (LBE) characterizing drag forces, buoyancy, etc. [1]. On grounds of its mesoscopic nature, LBM stands at attention to the characteristic of a group of molecules directed at each lattice instead of following individually all the molecules such as molecular dynamics method which make LBM more tractable. On account of this, in this work, the LBM has been devoted to scrutinize the pulsating flow effects on phase change phenomenon in porous latent heat storage unit subjected to forced convection. Jiaung et al. [22] was the

first survey reported on simulating the heat conduction problem during phase change phenomenon using the enthalpy-based LBM. Years later, Huber et al. [23] developed the previous study [22] and successfully extended the LBM to couple melting mechanism and heat convection. In this context, Li et al. [21] used enthalpy-based LBM at pore-scale to investigate natural convection effects (gravity effects) on PCM solid–liquid phase change problems in porous metal structure. Owing to this study, they proved the reliability and the accuracy of the method. Therefore, Mabrouk et al. [1, 3, 4] introduced enthalpy-based LBM at the representative elementary volume (REV) scale to simulate the forced heat transfer convection enhancement during PCM melting/ solidification processes within porous metal unit of energy storage. Authors indicated the ability of this method to deal with this type of physical problems. Indeed, several works have been notably demonstrated the reliability of LBM for simulating different complex fluid flow problems with phase change phenomenon, see for example the studies of Tao et al. [2], Jourabian et al. [13], Gao et al. [24] etc., to name a few.

The works mentioned herein up on LHTES systems using metal foam are usually carried out under the steady flow condition. Howbeit, there is lack of oeuvres on LHTES systems with porous metal foam maintained under pulsating convective fluid flow effect. Thus, the main task is to throw light on pulsating flow effects on HTE of LHTES systems.

Indeed, in the present study, a REV-scale LBM is performed to copy with PCM melting/solidification phenomena in porous metal foam storage unit under different pulsating flow parameters to view the underlying processes. The porosity effect of the metal foam structure is adopted and the PCM/metal foam interactions were considered with LTNE condition and empirical models. Since, thermal and dynamic fields and PCM phase field are dependent on porosity structure and flow conditions imposed, the flow and heat transfer characteristics during paraffin phase change in porous metal unit are studied under different emerging parameters: two Strouhal numbers: 0.5 and 1, three pulsating amplitudes; A: 0.1, 0.5 and 0.9 and three porosities: 0.7, 0.8 and 0.9. In the next section; section 2, the geometric model, assumptions, governing equations and boundaries conditions are reported to explain the physical phenomenon. Afterwards, Section 3 presented performance indicators' equations as entropy generation and energy and exergy efficiencies. The LBM method explanation and code validation are outlined in section 4. Thereafter, in Section 5, simulations results are drawn and analyzed. Finally, findings are summarized and made in Section 6.

2. Simulation domain's presentation

2.1 Geometry presentation

The two-dimensional channel open at both ends comprises a porous metal matrix such as metal foam whose pores are completely filled with phase change material (PCM) such as paraffin represents the interest geometry for this study, as depicted in Figure 1. As seen, both top and bottom channel walls are thermally insulated, impermeable and no-slip. During the charging process (Figure 1 (a)), the fluid (air) enters the channel at high temperature T_h (red color) with the pulsating velocity $u(t) = U_0(1 + A\sin(wt))$ while causing the paraffin to begin to melt. Then, the PCM's volume will be reduced and consequently the fluid can continue its path until the east wall where it leaves at constant lower temperature T_c ($< T_h$) (cold temperature (blue color)). Inversely, during the discharge process (Figure 1 (b)), the air enters the channel from the east with the same exit temperature of the charging period T_c and the velocity $u(t) = -U_0(1 + A\sin(wt))$, and since the paraffin is in a liquid state, the fluid can flow more easily from the beginning to the end of the process. At this point, the liquid paraffin releases more heat energy and begins to solidify. So, the air heats up and set (force) a flow which leaves the channel (from the west wall) at hot temperature T_h.

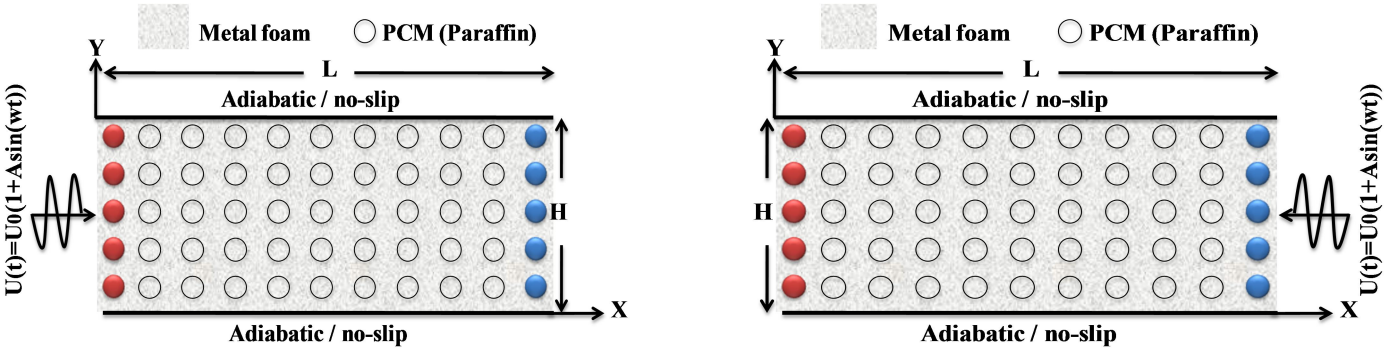

(a) Charging case **(b) Discharging case**

Figure 1. Physical sketch of the geometry

2.2 Assumptions Adopted

The assumptions adopted for this work are: forced convection predominates in the porous channel. The flow is assumed to be laminar ($\mathrm{Re} = 200$), Newtonian, unsteady and has a sufficiently low Mach number (Ma < 0.3) to satisfy the incompressibility limit of LBM [25]. The characteristic velocity u_0 is chosen to be 0,1 m/s. With the lattice sound speed c_s being $1/\sqrt{3}$, a Mach number of 0.17 is obtained, which fulfills the incompressibility condition ($Ma = \frac{u_0}{c_s} = \frac{0.1}{1/\sqrt{3}} = 0.17 \prec 0.3$). It is deemed to point out that the temperatures involved (and thereby, thermal exchanges between the phases) do not strongly affect the medium's thermo-

physical properties, they then remain constant, homogeneous and isotropic. Further, air and PCM (paraffin) in the liquid state are in LTNE with the solid matrix as proved in the results section (LTNE > 5%). In addition, the porous medium effect is incorporated through the governing equations homogenization at the REV scale. Thereby, the Darcy-Brinkmann-Forchheimer (DBF) model is used to handle the flow in the porous medium. For further details, one can cite Nield and Bejan [26].

It is well known that the method adopted (SRT-LBM) is subject to the condition of Courant-Friedrichs-Lewy (CFL) stability ($CFL < 1$). In the LBM framework, this number can be defined as follows [27]:

$$CFL_{LB} = Ma.c_s = 0.17/\sqrt{3} = 0.29 \tag{1}$$

Such a value demonstrates that the stability of the LBM method adopted to handle our simulations is preserved.

2.3 Mathematical formulation

For handling convective pulsatile flow through porous channel where melting phenomenon occurs, the generalized Navier-Stokes equations (DBF model) and the energy transport equations (LTNE model) at the REV scale are considered are considered in light of the assumptions adopted.

Thereby, the two-dimensional governing equations of mass, momentum and energy, respectively in their dimensionless forms are as follows [14, 19, 13]:

$$\nabla \cdot \vec{U} = 0 \tag{2}$$

$$\frac{\partial \vec{U}}{\partial \tilde{t}} + \left(\vec{U}.\nabla\right)\left(\varepsilon^{-1}\vec{U}\right) = -\nabla\left(\varepsilon P\right) + \frac{1}{Re}\nabla^2\vec{U} \underbrace{-\varepsilon\left(\frac{1}{Re\,Da} + \frac{F_\varepsilon}{\sqrt{Da}}\left\|\vec{U}\right\|\right)\vec{U}}_{\vec{F}} \tag{3}$$

$$\frac{\partial \Theta_f}{\partial \tilde{t}} + \vec{U}.\nabla\Theta_f = \frac{1}{Re.Pr}\nabla.\left(\frac{\lambda_{eff,f}}{\lambda_f}\nabla\frac{\Theta_f}{\varepsilon}\right) + \frac{Kr.Bi}{Re.Pr}\left(\frac{\Theta_s - \Theta_f}{\varepsilon}\right) - \frac{1}{Ste}\frac{\partial \Gamma}{\partial \tilde{t}} + \Phi \tag{4}$$

$$\frac{\partial \Theta_s}{\partial \tilde{t}} = \frac{Kr}{Rc}\frac{1}{Re.Pr}\nabla.\left(\frac{\lambda_{eff,s}}{\lambda_s}\nabla\frac{\Theta_s}{1-\varepsilon}\right) - \frac{Kr}{Rc}.\frac{Bi}{Re.Pr}\left(\frac{\Theta_s - \Theta_f}{1-\varepsilon}\right) \tag{5}$$

The dimensionless parameters governed in Eqs. (2)- (5) are given as:

$$\left(X,Y\right) = \frac{\left(x,y\right)}{H}, \left(U,V\right) = \frac{\left(u,v\right)}{U_0},\ P = \frac{p}{\rho U_0^2},\ \tilde{t} = \frac{tU_0}{H},\ \Theta = \frac{T - T_c}{\Delta T_{ref}},\ \Delta T_{ref} = T_h - T_c \tag{6}$$

$$Da=\frac{K}{H^2},\ \mathrm{Pr}=\frac{\nu_f}{\alpha_f},\ \mathrm{Re}=\frac{U_0 H}{\nu_f},\ Rc=\frac{(\rho C_p)_s}{(\rho C_p)_f},\ Kr=\frac{\lambda_s}{\lambda_f},\ Bi=\frac{h_{sf}a_{sf}H^2}{\lambda_s}$$
$$Ste=\frac{C_{pf}(T_h-T_m)}{La},\ Ec=\frac{U_0^2}{C_f\Delta T_{ref}},\ St=\frac{\breve{f}H}{U_0} \tag{7}$$

It is noteworthy that the subscripts f and s are used to distinguish the fluid (f) phase of the solid (s).

where, $\vec{U}$, P , Θ_f , Θ_s , ε , F_ε , Γ , λ , Φ and λ_{eff} are the velocity vector filed, the pressure, the fluid and porous medium temperatures, copper porosity,the geometric coefficient appearing in the total force due to porous media and other external forces, the PCM's liquid fraction, the thermal conductivity, the viscous dissipation and equivalent thermal conductivity, respectively. Also, La , a_{sf} and h_{sf} appearing in Eq. (7) are the PCM latent heat, the specific surface area of the porous matrix, and the local interfacial heat transfer coefficient between metal foam and paraffin, respectively.

In the last term of Eq. (3), the Forchheimer coefficient F_ε can be calculated as [28, 29]:

$$F_\varepsilon=2.12\times10^{-3}(1-\varepsilon)^{-0.132}(d_f/d_p)^{-1.63} \tag{8}$$

$$\text{where } d_f=1.18\left((1-\varepsilon)/3\pi\right)^{1/2}d_p \text{ and } d_p=22.4\times10^{-3}/\omega \tag{9}$$

here, d_f, d_p and ω are the ligament diameter, the pore size, and the pore density, respectively.

In Eq. (4), the last term points out the PCM's viscous dissipation which can be given as [4]:

$$\tilde{\Phi}=\varepsilon.Ec\left\{\frac{1}{Da.Re}+\frac{F_\varepsilon}{\sqrt{Da}}\left\|\vec{U}\right\|\right\}\left\|\vec{U}\right\|^2+\frac{Ec}{Re}\left\{2\left[\left(\frac{\partial\vec{U}}{\partial X}\right)^2+\left(\frac{\partial\vec{V}}{\partial Y}\right)^2\right]+\left(\frac{\partial\vec{U}}{\partial Y}+\frac{\partial\vec{V}}{\partial X}\right)^2\right\} \tag{10}$$

Likewise, the liquid fraction Γ appearing in the penultimate term of Eq. (4) is computed in our work using the enthalpy method as [30]:

$$\Gamma=\begin{cases}0 & \Theta<\Theta_s\\ \dfrac{\Theta-\Theta_s}{\Theta_l-\Theta_s} & \Theta_s\le\Theta\le\Theta_l\\ 1 & \Theta>\Theta_l\end{cases} \quad if \tag{11}$$

It should be noted that Θ_s and Θ_l represent the fully solid and liquid paraffin temperatures, respectively.

In Eq. (4) and (5), the effective thermal conductivity λ_{eff} can be determined under the LTNE conjecture as follows [7, 31, 32]:

$$\lambda_{eff} = \sqrt{2}(R_A + R_B + R_C + R_D)/2 \tag{12}$$

where

$$R_A = 4\sigma / \left[(2e^2 + \pi\sigma(1-e)\lambda_s + (4 - 2e^2 - \pi\sigma(1-e))\lambda_f \right] \tag{13}$$

$$R_B = (e-2\sigma)^2 / \left[(e-2\sigma)e^2\lambda_s + (2e - 4\sigma - (e-2\sigma)e^2)\lambda_f \right] \tag{14}$$

$$R_C = (\sqrt{2} - 2e) / \left[\sqrt{2}\pi\sigma^2\lambda_s + (2 - \sqrt{2}\pi\sigma^2)\lambda_f \right] \tag{15}$$

$$R_D = 2e / \left[e^2\lambda_s + (4 - e^2)\lambda_f \right] \tag{16}$$

with $e = 0.16$ and $\sigma = \left(\sqrt{2}(2 - \frac{3\sqrt{2}}{4}e^3 - 2\varepsilon) / (\pi(3 - 2\sqrt{2}e - e)) \right)^{1/2}$ (17)

So, $\lambda_{eff,f} = \lambda_{eff}\big|_{\lambda_s = 0}$ and $\lambda_{eff,s} = \lambda_{eff}\big|_{\lambda_f = 0}$ (18)

In Eq. (7), the permeability K appearing in Darcy number (Da) can be correlated as follows [28, 29]:

$$K = 7.3 \times 10^{-4} d_p^2 (1-\varepsilon)^{-0.224} (d_f / d_p)^{-1.11} \tag{19}$$

To close Eq. (7), the empirical quantities a_{sf} and h_{sf} appearing in Biot number (Bi) can be expressed, respectively as follows [28, 29]:

$$a_{sf} = 3\pi d_f (1 - e^{-(1-\varepsilon)/0.004}) / 0.59 / d_p^2 \tag{20}$$

$$h_{sf} = \begin{cases} 0.76.\mathrm{Re}_d^{0.4}\,\mathrm{Pr}^{0.37}\,\lambda_f / d_f & 1 \le \mathrm{Re}_d \le 40 \\ 0.52.\mathrm{Re}_d^{0.5}\,\mathrm{Pr}^{0.37}\,\lambda_f / d_f \quad for & 40 \le \mathrm{Re}_d \le 10^3 \\ 0.26.\mathrm{Re}_d^{0.6}\,\mathrm{Pr}^{0.37}\,\lambda_f / d_f & 10^3 \le \mathrm{Re}_d \le 2.10^5 \end{cases} \tag{20}$$

where $Re_d \left(= d_f U_0 / \varepsilon \nu_f \right)$ being the pore Reynolds number.

2.4 Boundary and initial conditions (BCs & IC)

Refering to Eq. (6) where the dimensionless variables are introduced, the dimensionless BCs and IC imposed on the considered computational domain (Figure 1) are presented as follows

During charging period,

IC: at $\tilde{t} = 0$

- $U = 0$; $V = 0$ and $\Theta_f = \Theta_c = 0$ for $0 \le X \le L/H$ and $0 \le Y \le 1$.

BCs: at $\tilde{t} \succ 0$

- $U(\tilde{t}) = 1 + A\sin(2\pi.St.\tilde{t})$; $V = 0$; $\Theta_{f,h} = 1$, at $X = 0$ and $0 \le Y \le 1$ (inlet);
- $\nabla_X U = 0$; $V = 0$; $\Theta_{f,c} = 0$ at $X = L/H$ and $0 \le Y \le 1$ (outlet);
- $U = 0$; $V = 0$ and $\nabla_y \Theta_{f,h} = \nabla_y \Theta_{f,s} = 0$ at $0 \le X \le L/H$ and $Y = 1$ (top);
- $U = 0$; $V = 0$ and $\nabla_y \Theta_{f,h} = \nabla_y \Theta_{f,s} = 0$ at $0 \le X \le L/H$ and $Y = 0$ (bottom);

During discharging period, the BCs are kept the same as charging process with an inverse pulsating flow $U(\tilde{t}) = -1 + A\sin(2\pi.St.\tilde{t})$.

3. Thermal performance

The thermal optimization is required for our system in order to determine and compare its performance with other systems such as that in the work of Mabrouk et al. [4].

3.1 Entropy generation

In general, the entropy generation rate is related to the system's irreversibility which is caused by two factors: the fluid friction irreversibility: FFI (viscous dissipation) and/ or the heat transfer irreversibility: HTI (temperature gradient). For the problem deemed in this work, the LTNE model is applied on the entropy generation to obtain the dimensionless form as follows [4, 33]:

$$Ns = Ns_f + Ns_s \tag{21}$$

where,

$$Ns_f = \underbrace{\frac{\varepsilon}{(\Theta_f + \Pi)^2}\left[\left(\frac{\partial \Theta_f}{\partial X}\right)^2 + \left(\frac{\partial \Theta_f}{\partial Y}\right)^2\right]}_{\textit{entropy generation due to heat transfer}} + \underbrace{\frac{\varepsilon.Ec.Pr}{\left(\Theta_f + \Pi\right)}\left(\frac{1}{Da} + \frac{Re.F_\varepsilon}{\sqrt{Da}}\left\|\vec{U}\right\|\right)\left\|\vec{U}\right\|^2}_{\textit{entropy generation due to Darcy-Brinkmann-Forchheimer force}}$$
$$+ \underbrace{\frac{Ec.Pr}{\left(\Theta_f + \Pi\right)}\left[2\left(\left(\frac{\partial \vec{U}}{\partial X}\right)^2 + \left(\frac{\partial \vec{V}}{\partial Y}\right)^2\right) + \left(\frac{\partial \vec{U}}{\partial Y} + \frac{\partial \vec{V}}{\partial X}\right)^2\right]}_{\textit{entropy generation due to viscous dissipation}} \tag{22}$$
$$+ \underbrace{\frac{Bi.Kr(\Theta_s - \Theta_f)}{\Theta_f + \Pi}}_{\textit{entropy generation due to heat exchange between phases in porous media}}$$

$$Ns_s = \underbrace{\frac{(1-\varepsilon)Kr}{\left(\Theta_s + \Pi\right)^2}\left[\left(\frac{\partial \Theta_s}{\partial X}\right)^2 + \left(\frac{\partial \Theta_s}{\partial Y}\right)^2\right]}_{\text{entropy generation due to heat transfer}} - \underbrace{\frac{Bi.Kr(\Theta_s - \Theta_f)}{\Theta_s + \Pi}}_{\text{entropy generation due to heat exchange between phases in porous media}} \tag{23}$$

here, $\Pi\left(= T_c / \Delta T_{ref}\right)$ is the dimensionless temperature.

The average entropy generation rate can be correlated as [3]:

$$Ns_{av} = \frac{1}{S}\int_S Ns\,dx\,dy \tag{24}$$

3.2 Energy efficiency

According to the first law of thermodynamics, the overall energy efficiency of the system deemed during charging/discharging periods is assessed as follows [4, 34, 35, 36]:

$$\eta = \prod_i \eta_i = \eta_{charging} \times \eta_{discharging} = 100 \times \left(E_{recovered} / E_{input}\right) \tag{25}$$

where, $\eta_{charging} = E_{accumulation} / E_{input}$ and $\eta_{discharging} = E_{recovered} / E_{accumulation}$ (26)

Thereby,

$$E_{input} = \dot{m} C_{p,f} \Delta T_{f,charging} + E_{diss,charging} + E_{latent,charging} \quad (27)$$

$$E_{recovered} = \dot{m} C_{p,f} \Delta T_{f,discharging} + E_{diss,discharging} + E_{latent,discharging} \quad (28)$$

where, $E_{latent}\left(= \dot{m}_f \, C_{p,f} \times La\right)$ [2] and $E_{diss}\left(= \iint \tilde{\Phi} dS\right)$ [4] being the latent and dissipation energy, respectively.

here, $E_{recovered}$ and E_{input} being the energy recovered during the discharging period and the energy input to the system during the charging period, respectively.

3.3 Exergy efficiency

According to the second law of thermodynamics, the global exergy efficiency of the system deemed denotes the stored energy quality which is evaluated as follows [4, 34, 37, 38]:

$$\psi = \psi_{charging} \times \psi_{discharging} = 100 \times \left(Ex_{recovered} / Ex_{input}\right) \quad (29)$$

where, $\psi_{charging} = Ex_{stored} / Ex_{input}$ and $\psi_{discharging} = Ex_{recovered} / Ex_{stored}$ (30)

and, $$Ex_{input} = \dot{m} C_{p,f} \left(T_{f,in} - T_{f,out}\right)_{charging} - T_0 \dot{m} C_{p,f} Ln\left(\frac{T_{f,in}}{T_{f,out}}\right)_{charging} \quad (31)$$

$$Ex_{recovered} = \dot{m} C_{p,f} \left(T_{f,out} - T_{f,in}\right)_{discharging} - \dot{m} C_{p,f} Ln\left(\frac{T_{f,out}}{T_{f,in}}\right)_{discharging} \quad (32)$$

here, $Ex_{recovered}$ and Ex_{input} being the exergy recovered during the discharging period and the exergy input to the system during the charging period, respectively.

4. Lattice Boltzmann Method (LBM)

In this study, the Thermal Lattice Boltzmann method (T-LBM) was chosen as the numerical approach for handling the equations system emerged in section 2. The LBM has been deemed among the powerful numerical methods for studying complex fluid flow, heat transfer, and complicated physics: dealing with complex boundaries, using parallel algorithms...etc [24]. Indeed, energy conservation was deemed in view of the significant results of thermal energy storage in many engineering applications. Briefly, the density distribution function (DDF) model is used to portray the evolution of fluid particle clusters towards neighboring sights at each time and position $(\vec{x}, t)$ with a discrete velocity $\vec{e}_i$. Based

on two essential sub-steps: streaming and collision (local thermodynamic equilibrium state), the particles propagation is performed. In addition, the LBM is able to successfully tackle physical phenomena in porous geometry with complex pore characteristics using two main categories that are the pore scale (1) and the representative elementary volume (REV) scale (2) [24]. To the best of our knowledge, the first approach is frequently averted owing to its weakness in terms of geometry and the computational domain [4, 24]. However, in this work, the second one has been adopted in which an additional term is added to the standard lattice Boltzmann equation (LBE) to highlight the presence of the porous medium. Thereby, the basic idea is that the fluid macroscopic fields such as dynamic and thermal (density, velocity, temperature, etc.) are computed via the discrete Boltzmann equation using three distribution functions owing to LTNE model presumed above. To cope with the present study, the forced convection melting phenomenon with viscous dissipation in a such porous geometry deemed under LTNE condition at the REV scale is manipulated via the generalized discrete governing equations LBM, viz., $f_i(\vec{x},t)$ (for the dynamic field) and $g_{i,f,s}(\vec{x},t)$ (for the PCM-solid metal temperature fields) as [24, 2]:

$$\underbrace{f_i\left(\vec{x}+\vec{e}_i\delta t,t+\vec{e}_i\delta t\right)-f_i\left(\vec{x},t\right)}_{streaming}=-\delta t\underbrace{\left(f_i\left(\vec{x},t\right)-f_i^{eq}\left(\vec{x},t\right)\right)}_{collision\ term}/\tau_v+\delta t.\ \underbrace{\vec{F}_{e_i}}_{force\ term} \tag{33}$$

$$\underbrace{g_{f,i}\left(\vec{x}+\vec{e}_i\delta t,t+\delta t\right)-g_{f,i}\left(\vec{x},t\right)}_{streaming}=-\underbrace{\left(g_{f,i}\left(\vec{x},t\right)-g_{f,i}^{eq}\left(\vec{x},t\right)\right)/\tau_{T,f}}_{collision\ term}+\underbrace{\left(1+\delta t\partial_t/2\right)\delta tSr_{i,f}+\delta tf_i\left(\vec{x},t\right)q_i}_{source\ terms} \tag{34}$$

$$\underbrace{g_{s,i}\left(\vec{x}+\vec{e}_i\delta t,t+\delta t\right)-g_{s,i}\left(\vec{x},t\right)}_{streaming}=-\underbrace{\left(g_{s,i}\left(\vec{x},t\right)-g_{s,i}^{eq}\left(\vec{x},t\right)\right)/\tau_{T,s}}_{collision\ term}+\underbrace{\left(1+\delta t\partial_t/2\right)\delta tSr_{i,s}}_{source\ term} \tag{35}$$

where, τ_v (Eq.(33)), $\tau_{T,f}$ (Eq.(34)) $\tau_{T,s}$ (Eq.(35)) being the dimensionless collision times for velocity, PCM and solid temperatures, respectively which are expressed as follows [24, 39]:

$$\tau_v=3\nu+0.5 \tag{36}$$

$$\tau_{T,f}=3\alpha_{e,f}/(\delta tc^2)+0.5\quad with\quad \alpha_{e,f}=\lambda_{e,f}/\left(\varepsilon(\rho C_p)_f\right) \tag{37}$$

$$\tau_{T,s}=3\alpha_{e,s}/(\delta tc^2)+0.5\quad with\quad \alpha_{e,s}=\lambda_{e,s}/\left((1-\varepsilon)(\rho C_p)_s\right) \tag{38}$$

δt , $c\,(=\delta x/\delta t=1;\delta x=\delta t)$ and $\alpha_{e,f,s}$ are the lattice time step, the streaming speed and the effective diffusivity, respectively.

It is worth mentioning that, among the advantages of using the thermal model D2Q9, one can cite the possibility of modeling non-isotropic thermal problems and the possibility of

canceling the dependence of thermal diffusivity on the advection velocity [40]. However, for thermal problems with isotropic diffusivity, the D2Q5 model can also be used (it is fully sufficient, faster and requires less memory than the D2Q9 model) [40].

The quantities $f_i^{eq}\left(\vec{x},t\right)$ (Eq. (33)) and $g_{i,f;s}^{eq}$ (Eqs. (34)-(35)) represent the local equilibrium distribution functions (*LEDFs*) for the dynamic and thermal fields, respectively, where the porous medium effects are taken into account as:

$$f_i^{eq} = \rho w_i \left(1 + \frac{\vec{e}_i.\vec{u}}{c_s^2} + \frac{\vec{u} \otimes \vec{u} : \left(\vec{e}_i \otimes \vec{e}_i - c_s^2 I \right)}{2c_s^4 \varepsilon} \right) \tag{39}$$

$$g_{f,i}^{eq} = w_i T_f \left(1 + \vec{e}_i \vec{u} / (\varepsilon c_s^2) \right) \qquad \text{and} \qquad g_{s,i}^{eq} = w_i T_s \tag{40}$$

where, the terms c_s $(= c/\sqrt{3})$, $\vec{e}_i$ and w_i denote the lattice sound speed, the discrete velocity in direction i, and the equilibrium weighting coefficients , respectively in the presumed model D2Q9 which are computed as follows:

$$\vec{e}_i = \left\{ \begin{array}{lll} 0\vec{i} + 0\vec{j}, & i = 0 & 4/9 \\ c\left[\cos\left((k-1)\pi/2 \right)\vec{i} + \sin\left((k-1)\pi/2 \right)\vec{j} \right], & i = 1,2,3,4 & 1/9 \\ \sqrt{2}c\left[\cos\left((2k-9)\pi/4 \right)\vec{i} + \sin\left((2k-9)\pi/4 \right)\vec{j} \right], & i = 5,6,7,8 & 1/36 \end{array} \right\} = w_i \tag{41}$$

To close the LBEs: Eqs. (33)- (35), the last quantities that indicates source terms such as $\overrightarrow{F_{e_i}}$ (Eq. (33)) [2], $Sr_{i,f;s}$ [24, 39] and q_i [41] (Eqs. (34)- (35)) are calculated, respectively as follows:

$$\overrightarrow{F_{e_i}} = w_i \rho (1 - \frac{1}{2\tau_v}) \left[\frac{\vec{e}_i.\vec{F}}{c_s^2} + \frac{\vec{u}.\vec{F} : \left(\vec{e}_i \vec{e}_i - c_s^2 I \right)}{\varepsilon c_s^4} \right] \tag{42}$$

$$Sr_{i,f} = w_i \left(\frac{La}{C_{p,f}} \left[\frac{\gamma(t+\delta t) - \gamma(t)}{\delta t} \right] + \frac{h(T_s - T_f)}{\varepsilon (\rho C_p)_f} \right) \qquad \text{and} \qquad Sr_{i,s} = w_i \left(\frac{h(T_s - T_f)}{(1-\varepsilon)(\rho C_p)_s} \right) \tag{43}$$

$$q_i = -(f_i - f_i^{eq})(\vec{e}_i - \vec{u})(\vec{e}_i - \vec{u}) : \Delta\vec{u} \tag{44}$$

LBM boundary conditions' implementation

It should be pointed out that in the LBM framework, the lattice Boltzmann boundary conditions (LB-BCs) regarding velocity and temperature are pertained to the unknown microscopic distribution functions f and g in the computational domain. However, for the velocity BCs, at the channel inlet, Dirichlet condition was picked out for two processes with $u_{in} = U_0(1 + A\sin(2\pi.St.\tilde{t}))$ for charging and $u_{in} = -U_0(1 + A\sin(2\pi.St.\tilde{t}))$ for discharging [14, 43]. At the top and bottom walls, the no-slip velocity conditions were expressed through the bounce-back boundary scheme proposed by Ladd [44, 13] and finally at the channel outlet,

the open-ended boundary conditions were adopted [45]. Thereby, for temperature BCs, the west thermal BCs correspond to a high temperature $\Theta_h (=1)$ and a low temperature $\Theta_c (=0)$, respectively, while the upper and lower walls are adiabatic (such as illustrated in sub-section 2.1).

The applied dynamic and thermal boundary conditions are depicted in Figure 2 and Table 1.

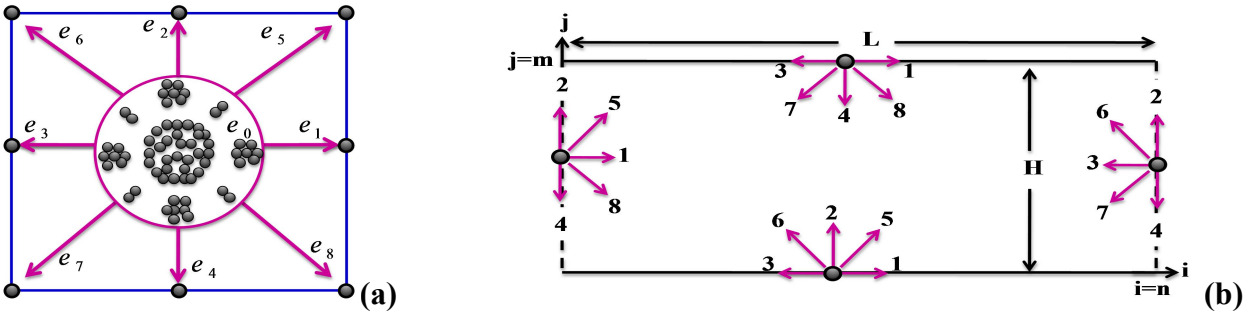

Figure 2. The distribution of the unknowns f and g in the computational domain according to the D2Q9 model.

Table. 1. TLBM- boundary conditions for charging and discharging cases.

	Velocity BCs	***Thermal BCs***
West wall	$\rho_{in}=\left(f_0+f_2+f_4+2\left(f_3+f_6+f_7\right)\right)/\left(1-u_{in}\right)$ $f_1=f_3+2\rho_{in}u_{in}/3$ $f_5=f_7+\rho_{in}u_{in}/6$ $\underbrace{f_8=f_6+\rho_{in}u_{in}/6}_{for\ charging\ case}$ $\underbrace{f_{1,n-1}=f_{1,n};\ \ f_{5,n-1}=f_{5,n};\ \ f_{8,n-1}=f_{8,n}}_{for\ discharging\ case}$	$T_w=\Theta_h=1$ $g_1=T_w(w_1+w_3)-g_3$ $g_5=T_w(w_5+w_7)-g_7$ $g_8=T_w\left(w_8+w_6\right)-g_6$
East wall	$\underbrace{f_{3,n-1}=f_{3,n};\ \ f_{6,n-1}=f_{6,n};\ \ f_{7,n-1}=f_{7,n}}_{for\ charging\ case}$ $\rho_{in}=\left(f_0+f_2+f_4+2\left(f_3+f_6+f_7\right)\right)/\left(1-u_{in}\right)$ $f_3=f_1+2\rho_{in}u_{in}/3$ $f_6=f_8+\rho_{in}u_{in}/6$ $\underbrace{f_7=f_5+\rho_{in}u_{in}/6}_{for\ discharging\ case}$	$T_w=\Theta_c=0$ $g_7=-g_5;\ \ g_3=-g_1;\ \ g_6=-g_8$
Top wall	$f_{7,n}=f_{5,n};\ \ f_{4,n}=f_{2,n};\ \ f_{8,n}=f_{6,n}$	$g_{8,m}=g_{8,m-1};\ \ g_{4,m}=g_{4,m-1};\ \ g_{7,m}=g_{7,m-1}$
Bottom wall	$f_{6,n}=f_{8,n};\ \ f_{2,n}=f_{4,n};\ \ f_{5,n}=f_{7,n}$	$g_{6,0}=g_{6,1};\ \ g_{2,0}=g_{2,1};\ \ g_{5,0}=g_{5,1}$

Validation of results

The present study is carried out using an in-house developed code. Therefore, a validation study is carried out to ensure the stability and accuracy of the code. To this purpose, the case discussed in Ref. [46] was considered. Figure 3 depicts the comparison with the results of Krishnan et al. [46] of the dimensionless fluid (Θ_f) and solid (Θ_s) temperatures evolution in a square cavity containing a porous metallic foam/PCM under natural convection.

As can be seen, this comparison confirms the reliability of the in-house code implemented.

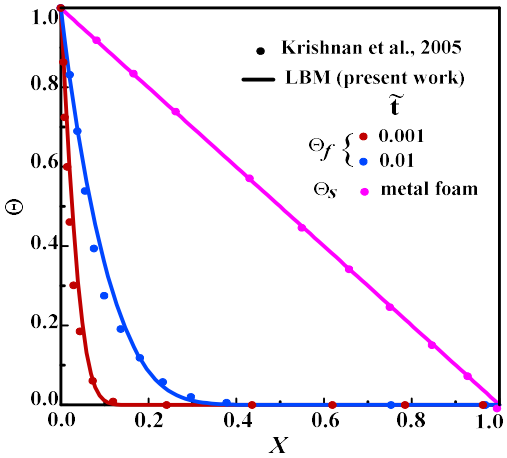

Figure 3. Dimensionless fluid and solid temperature evolution (Θ_f, Θ_s) vs. dimensionless streamwise distance X for null interstitial Nusselt number for $Da = 10^{-2}, Pr = 50, Ra = 10^6, Ste = 1$.

5. Results and discussion

In this section, the dynamic and thermal behavior on a three density distribution functions (LTNE condition) basis as well as the performance of the porous LHTES unit adopted herein are discussed. As highlighted above, a detailed numerical analysis using T-LBM approach at the REV scale will concern the PCM melting/solidification phenomenon subjected to pulsating convection flow.

First, a mesh control is presented for an accurate analysis and computational time gain of simulations. Next, the dynamic and thermal fields are described the PCM phase change phenomenon by considering the porosity (=0.7, 0.8 and 0.9), pulsating velocity effect (pulsating amplitude (A=0.1, 0.5 and 0.9) and Strouhal number (St=0.5 and 1)). Finally, an energy and exergy balance has been posted to qualify the pulsating velocity effects on the unit performance.

5.1 Strouhal number, St, and pulsating amplitude, A, effects on the LTNE intensity

As indicated in the present work, in the Sub -section 2.2 and 2.3 the LTNE condition is manifested between the solid and fluid phases (two dimensionless energy equations) and to prove this condition a criterion parameter LTNE defined as [3] that allows to justify the LTNE validity as:

$$LTNE = \sum_N \left| \Theta_s - \Theta_f \right| / N \tag{45}$$

where, $N = 480x120$ being the total number of nodes in the computation domain.

It is turned out that if $LTNE > 5\%$, it is the LTNE condition otherwise, it is the local thermal equilibrium (LTE) condition. So, based on this idea, Figure 4 illustrates the effects of St (0.5 and 1), pulsating amplitude, A ($0.1 \le A \le 0.9$), on the LTNE intensity for the three

porosities deemed (0.7, 0.8 and 0.9) for Re=200 during charging and discharging processes. It is clear that the LTNE is secured ($LTNE > 0.05$) for the discharging period regardless the parameters considered while decreasing with increasing A regardless of ε . Conversely, during the charging process, LTE condition could be taken into account ($LTNE \leq 0.05$) except for St=0.5 at A=0.9 whatever ε where LTNE occurs again.

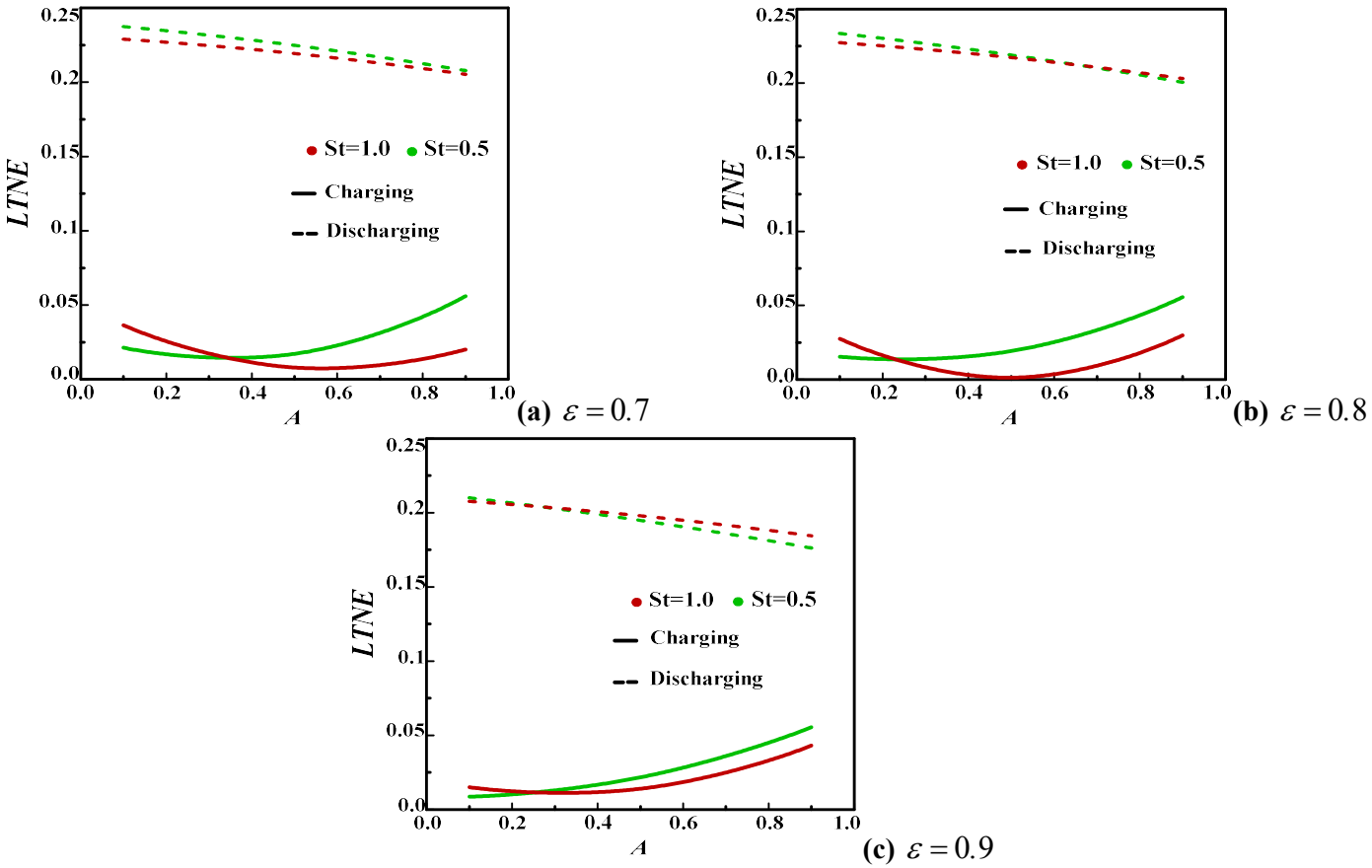

Figure 4. Strouhal number (St) effects on LTNE intensity vs. pulsating amplitude (A) during charging and discharging processes using $Pr = 50, Re = 200, Ec = 0$.

5.2 Strouhal number (St) and amplitude (A) effects on U-velocity

Figure 5 portrays the Strouhal number (St), amplitude (A) and porosity effects on the *U*-velocity vs. pulsation (w) during charging and discharging processes while attenuating the effect of the following parameters Pr (=50), Re (=200) and Ec (=0) numbers. As seen in the figure, during both periods charging and discharging, an increase in the pulsating amplitude (A) increases the velocity amplitudes. By contrast, the velocity amplitudes during charging process exceed usually that during discharging time. The primary reason is that during discharging process, the cold air traverses readily metal pores owing to the PCM liquid state. Likewise, it appeared that the porosity increase (=0.9) has a strong effect on such a pulsating velocity, thereby, amplifying the velocity amplitude for higher A (=0.9) and lower St (=0.5). It stands to reason that the forced convection is weak at high porosity value (=0.9) which slows down the pulsating velocity progress owing to the permeability of the metal medium

and its high thermal conductivity. So, the heat conduction prevails in the domain. As for A=0.1, and whatever the porosity, the U-velocity profile exhibits a small velocity amplitude during two periods charging/discharging, revealing the convection dominance.

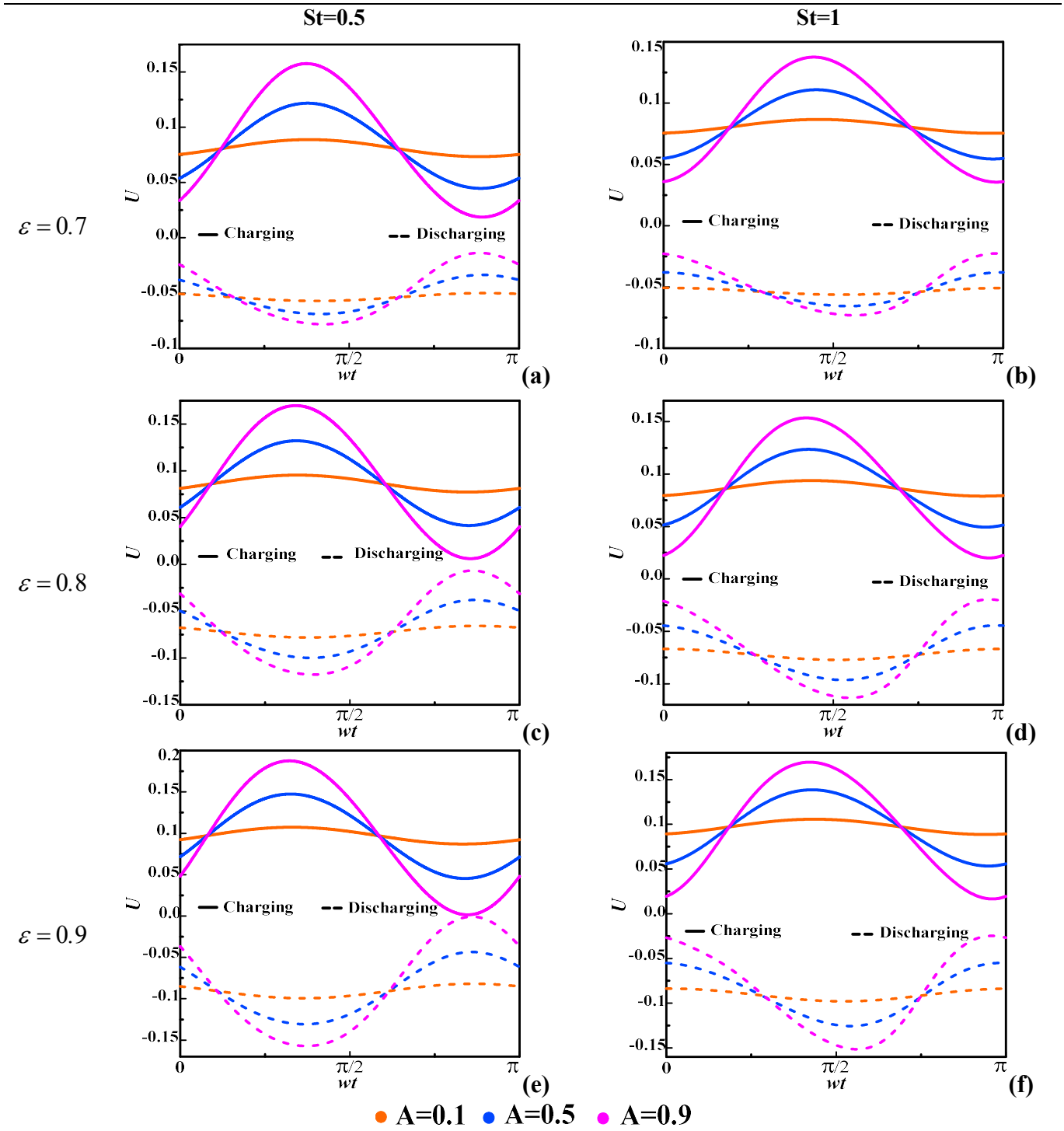

Figure 5. Strouhal number (St) and pulsating amplitude (A) effects on *U*-velocity vs. pulsation during charging and discharging processes at (X, Y) = (0.5, 0.5) using $Pr = 50, Re = 200, Ec = 0$.

Accordingly, for an accurate explication of the porosity, pulsating amplitude A and St effects on the phase change phenomenon, a U-contours based on the same analysis of variables as depicted in Figure 5 during charging period were considered. This is displayed in Figure 6. As shown in Figure 6 a, at low porosity (=0.7), the flow is developed from the

beginning to the end of the process regardless of A and St deemed, proving the convection role is important. However, as seen in Figure 6 b and 6 c, as the porosity increases (=0.8 and 0.9), the shape of U-contours were modified depending on A and St. For example in Figure 6 b, at St=1 and A=0.5, the flatness of the U-contour becomes lesser owing to the medium permeability. But, for the same porosity (=0.8) at high A (=0.9) and St (=1), the U contour becomes undeveloped in the channel's last fourth indicating the weakness of the convection in this region. Regarding Figure 6 c, for $\varepsilon = 0.9$, the permeability of the metal medium strongly affects the U- contours shapes by reducing the U flatness. Thereby, it starts to exhibit twisted forms for St=1 as increasing A (=0.5 and 0.9). It turned out that the convection rate mitigates at higher porosity (=0.9) value and St (=1) from the channel's last third for A=0.5 and from the middle region for A=0.9. It can be safely concluded that at lower A (=0.1) the convection acts the domain.

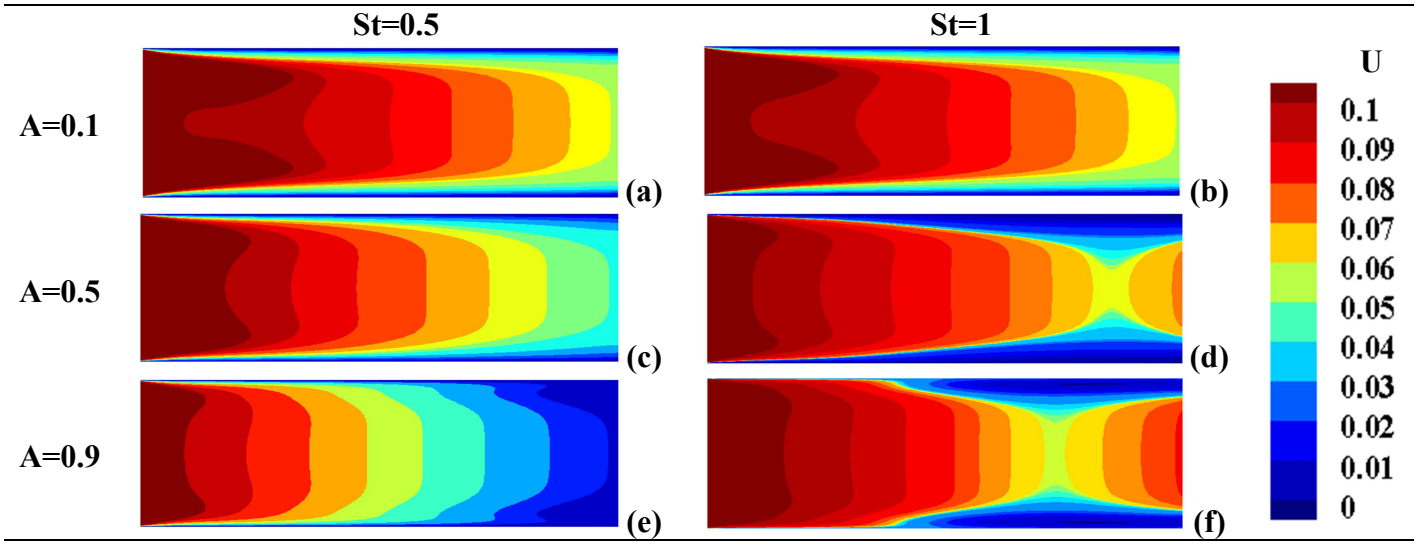

Figure 6 a. Strouhal number (St) and amplitude, A, effects on U contours during charging process using $Pr = 50, Re = 200, Ec = 0$ and $\varepsilon = 0.7$.

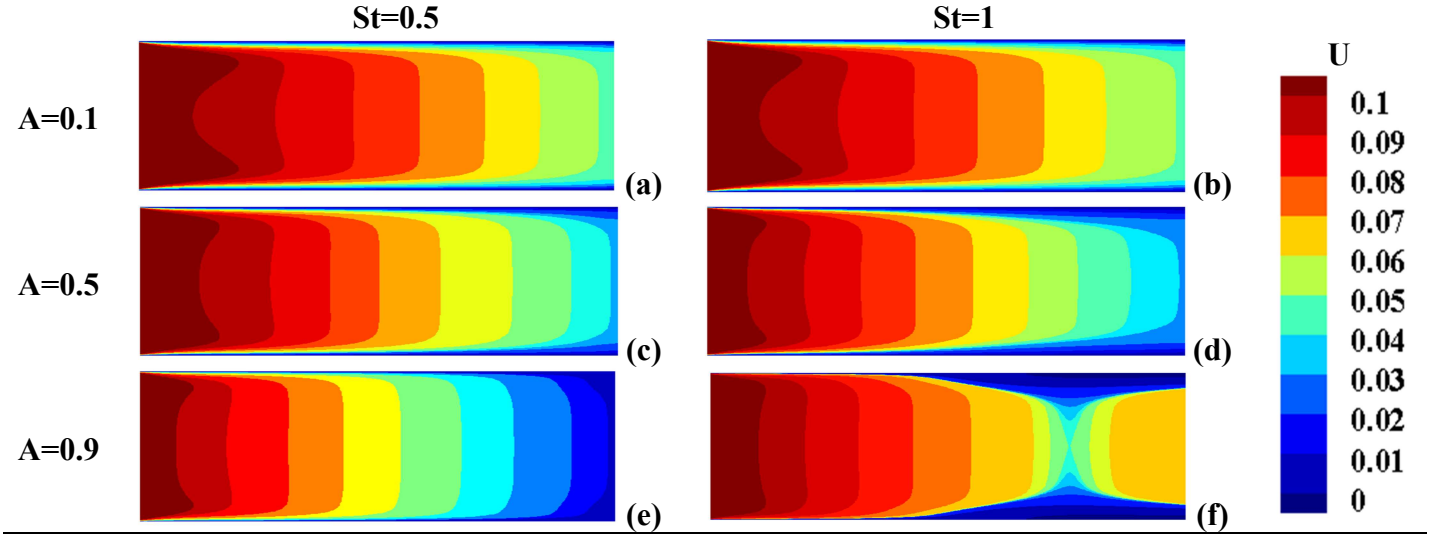

Figure 6 b. Strouhal number (St) and amplitude, A, effects on U contours during charging process using $Pr = 50, Re = 200, Ec = 0$ and $\varepsilon = 0.8$.

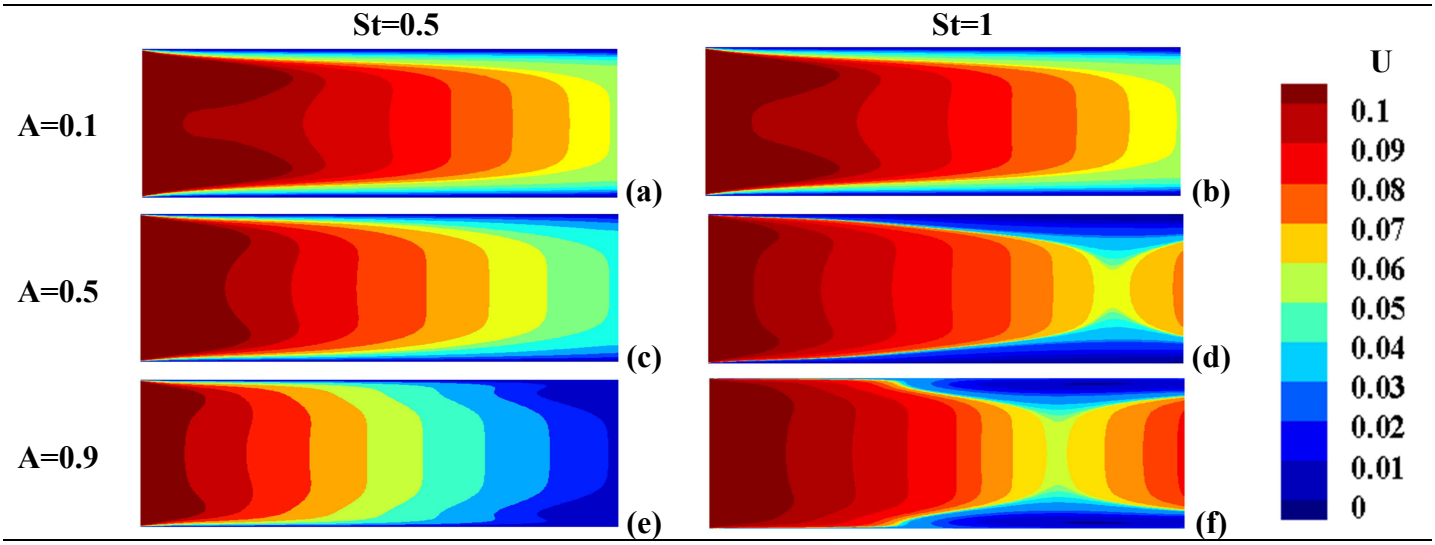

Figure 6 c. Strouhal number (St) and amplitude, A effects on U contours during charging process using $Pr = 50, Re = 200, Ec = 0$ and $\varepsilon = 0.9$.

5.3 Strouhal number and pulsating amplitude effects on solid-fluid difference temperature

In Figure 7, the effects of the porosity, pulsating amplitude and St deemed are reproduced on the temperature difference $(\Theta_f - \Theta_s)$ vs. the streamwise coordinate during charging and discharging processes. As shown, during charging period, at St=0.5 (Figure 7 a, c and e), the curves increases proportionally with the A increase, then they grow inversely proportional from a X_c-critical value ($X_c \approx 0.2$) where a maximum is reached depending on the porosity. However, at St=1 (Figure 7 b, d and f) and even in the same period, the curves behave in the same manner from a critical X_c of order of 0.05 then they are closer to each other at the exit region. This can be explained by the fact that for a larger A regardless of St and ε, forced convection is restricted owing to the porous metal foam characteristics; large specific surface area and thermal conductivity compared to the paraffin. Still in the same period, just at the beginning of the channel the heat convective transfer prevails (curves growth is proportional with A). On the other hand, when the fluid flow being reversed (discharging case), the difference between two temperatures increases proportional with A whatever the parameters varied (St and ε,). This demonstrates that at this case, the liquid PCM releases the thermal energy that has received during charging process, thereby, rising the interstitial heat transfer between solid and liquid phases due to the large heat exchange within the domain.

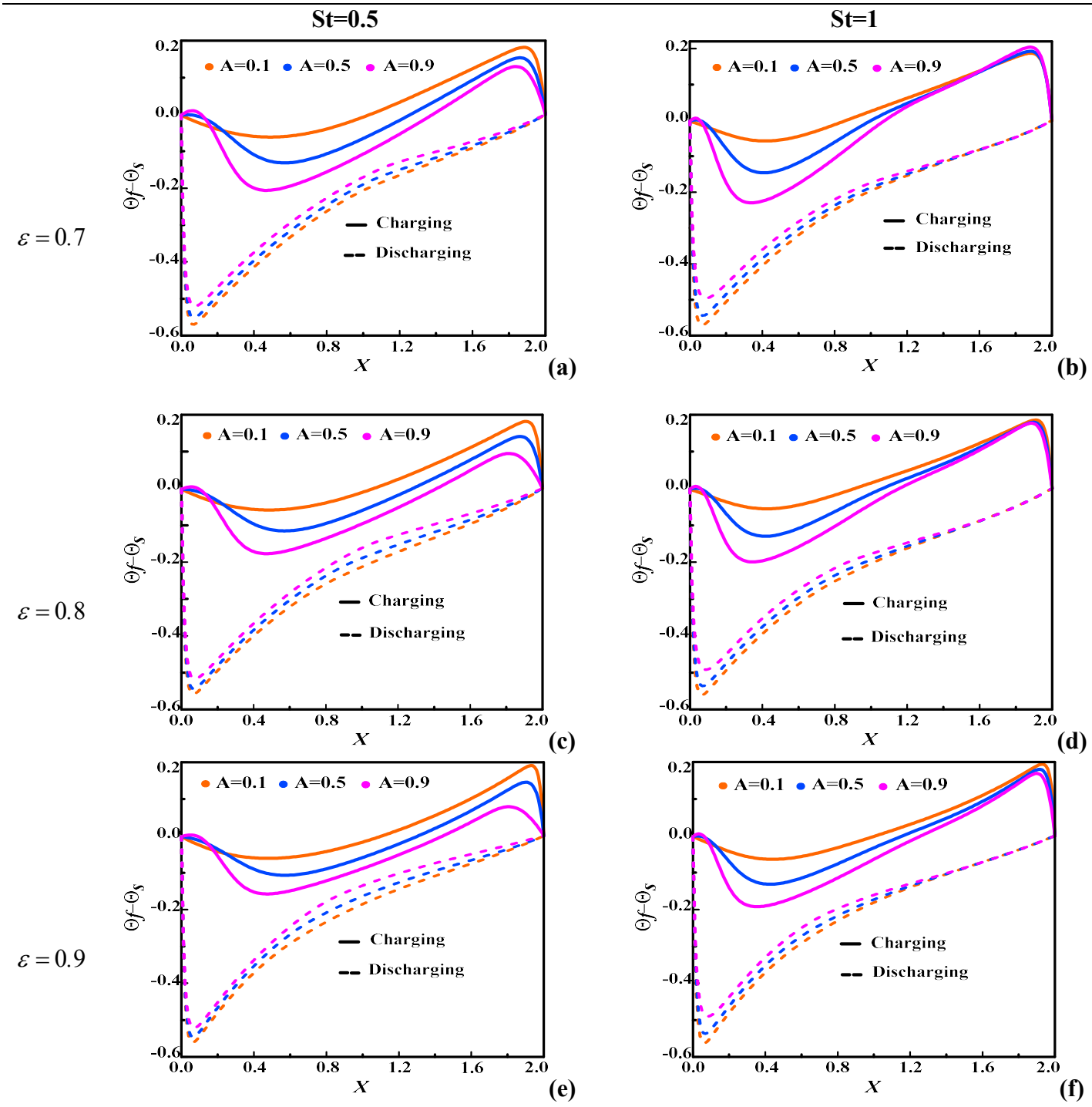

Figure 7. Strouhal number (St) and amplitude, A, effects on $\Theta_f - \Theta_s$ vs. the streamwise distance during charging and discharging processes at Y = 0.5 using $Pr = 50, Re = 200, Ec = 0$.

5.4 Strouhal number and pulsating amplitude effects on liquid fraction and melt front

Figure 8 portrays the pulsation-wise variation of the liquid fraction (Γ). In addition, it highlights pulsation amplitude (A), St and medium porosity's effects. It can be observed from this figure that the increase in A promotes the melting rate during charging process to sharply drop indicating the discharging period. It is obviously remarked that the same shape of liquid fraction is presented as in the work of Mabrouk et. al [4]. A comparison between two works

revealed that steady flow accelerates the melting rate than pulsatile flow. However, it can be noted from two works that the discharging time is very short, confirming that cold air can moves easily during this period and as mentioned-up the heat exchange increases, thereby, the PCM solidifies quickly. Also, as shown in this figure, the liquid fraction curves increase with decreasing the porosity. This demonstrates that medium permeability plays a crucial role in phase change process that strongly affects the interstitial heat transfer between phases. Besides, it was seen that decreasing St stabilizes the liquid fraction to reach its maximum. In other words, the PCM melting/solidification depend stoutly on flow features.

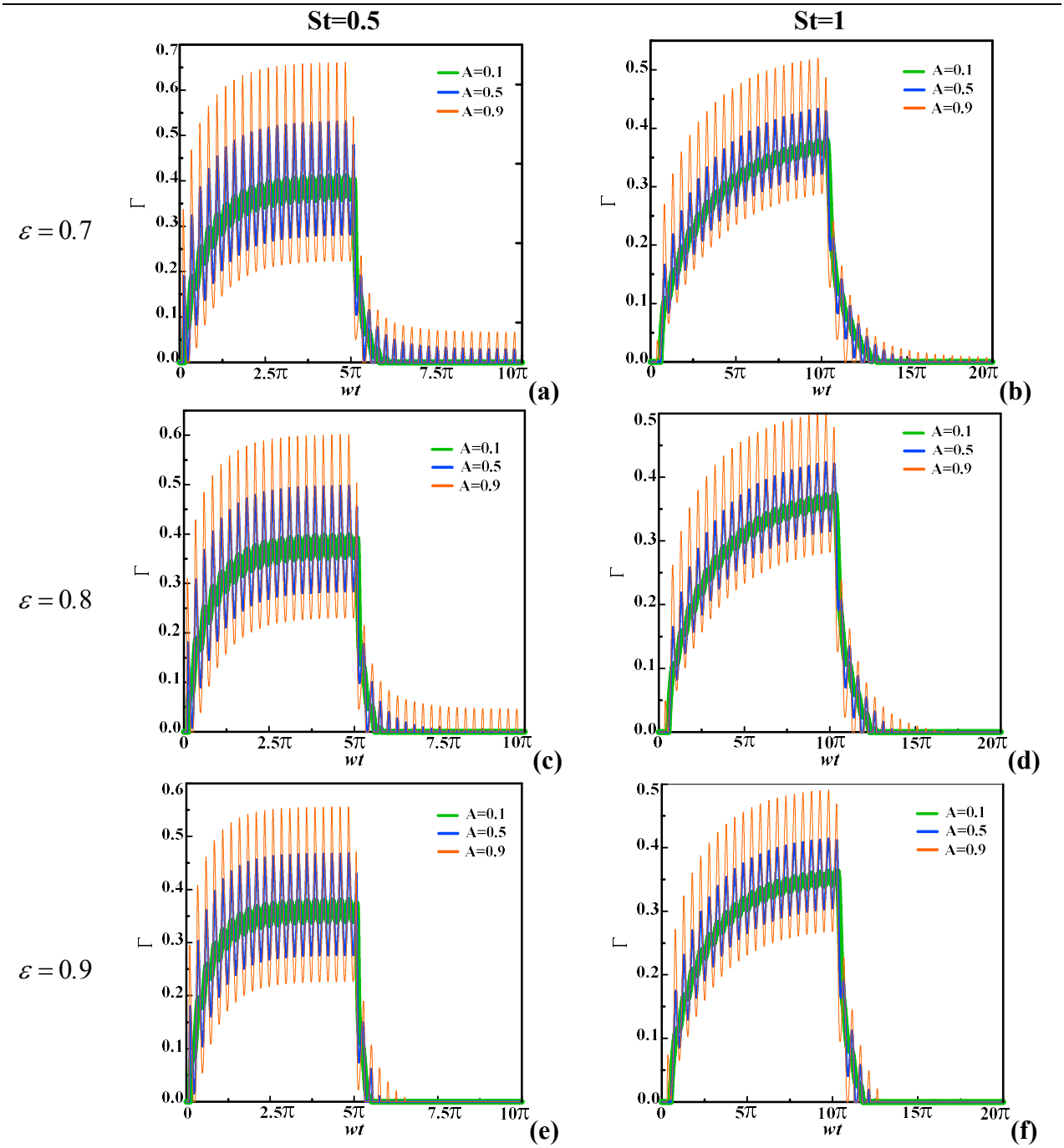

Figure 8. Strouhal number (St) and amplitude, A, effects on the local Γ vs. the pulsation using $Pr = 50, Re = 200, Ec = 0$.

The global phase field evolvement subjected to the convective pulsatile air flow effect is exhibited in figure 9 at three pulsating amplitudes, A, and two St as the previous figures for the three porosity values in the charging process. The red and blue zone indicated the liquid and solid paraffin parts respectively and between them is the mushy zone. A horizontal viewing shows that at lower St (=0.5), the front propagation advances faster which is proved in Figure 8. However, a vertical viewing points out that as A increases, the heat propagation decelerates as exhibited above in Figure 7 and explained the weakness of the forced convection. So, it can be stated that the melting phenomenon slows down for larger A and St whatever the porosity. For the same St, it can be seen that the quantity of molten paraffin is larger (the red zone is thickly) as A increases owing to the high local interstitial heat transfer between phases as presented in Figure 8.

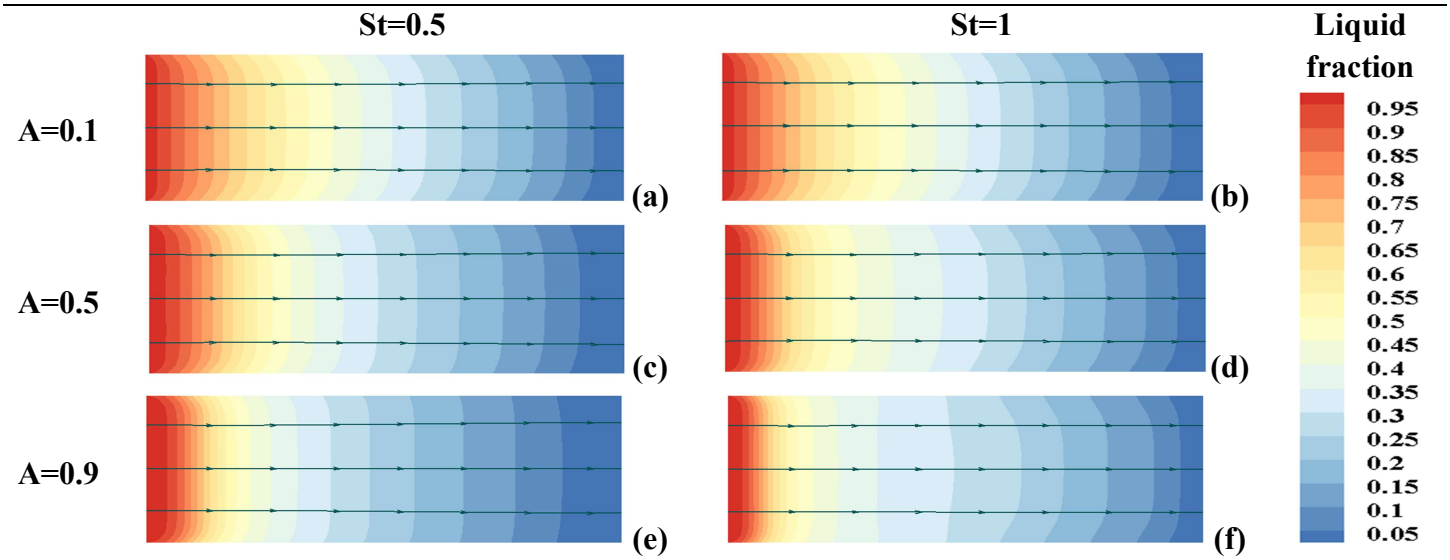

Figure 9 a. Strouhal number (St) and amplitude, A, effects on the phase field and streamlines during charging process using $Pr = 50, Re = 200, Ec = 0$ and $\varepsilon = 0.7$.

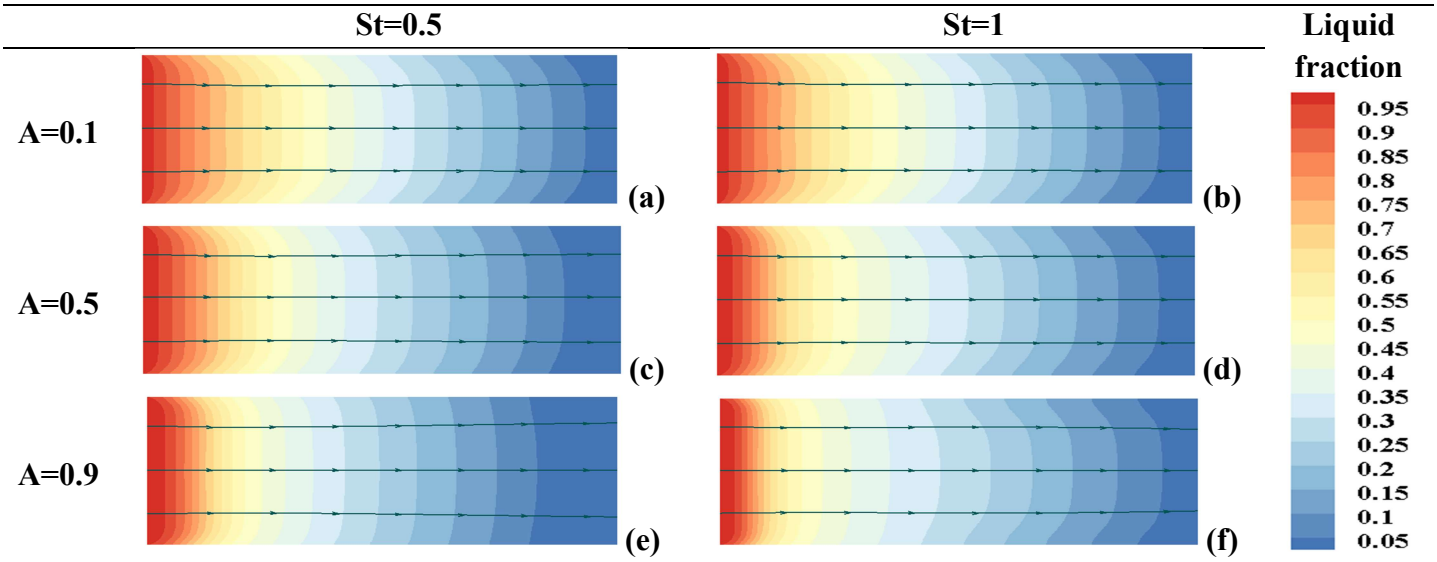

Figure 9 b. Strouhal number (St) and amplitude, A, effects on the phase field and streamlines during charging process using $Pr = 50, Re = 200, Ec = 0$ and $\varepsilon = 0.8$.

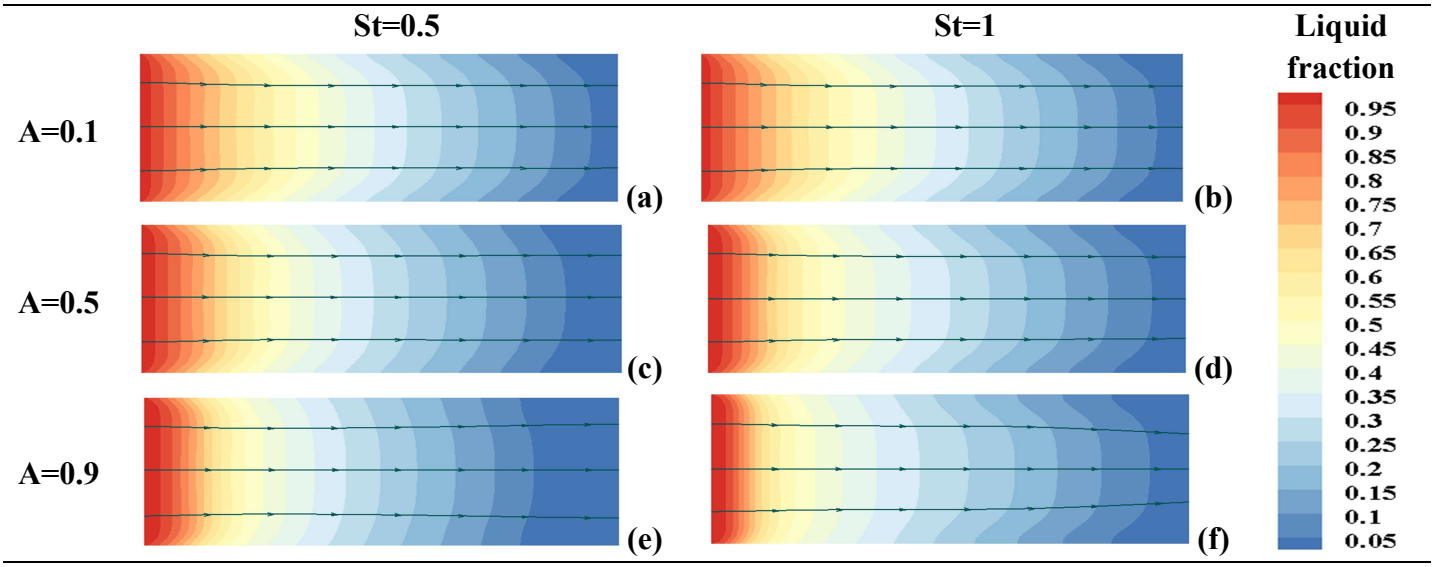

Figure 9 c. Strouhal number (St) and pulsating amplitude, A, effects on the phase field and streamlines during charging process using $Pr = 50, Re = 200, Ec = 0$ and $\varepsilon = 0.9$.

5.5 Strouhal number and pulsating amplitude effects on the average entropy generation rate

The entropy generation rate was the key parameter that represents and clarifies the system stability. To uncover the effect of the key parameters (A, St and porosity) of this study, Figure 10 outlines the dimensionless average entropy generation rate during charging/discharging periods. As displayed in figures 10. a, b and c, the average entropy generation rate (Ns_{av}) is always higher during discharging process than that during charging regardless of the porosity value. It turns out that the LHTES system is more stable during charging time because of the heat transfer irreversibility during PCM melting. In addition, it can be seen that the system irreversibility is slightly accented with the porosity variation, corroborating the larger thermal conductivity ratio and the interfacial heat transfer coefficient between two phases that favor the heat transferred. Furthermore, to reduce the irriversibilities of the system, low St is recommended for both processes and whatever A and ε values. Likewise, it can be remarked that during discharging period, Ns_{av} decreases with the A increase regardless of the porosity, but, increases slightly and proportionally with A during charging period. To sum up, low St (=0.5) with large A (=0.9) may be helpful for the system stability during discharging process, however, low A (=0.1) with low St (=0.5) may be useful during the charging period. To compare this study with that of Mabrouk et al. [3], the irreversibility of the system is slightly depending on the porosity regardless of the feature of the fluid flow (steady or pulsatile) owing to the heat transfer mode domination.

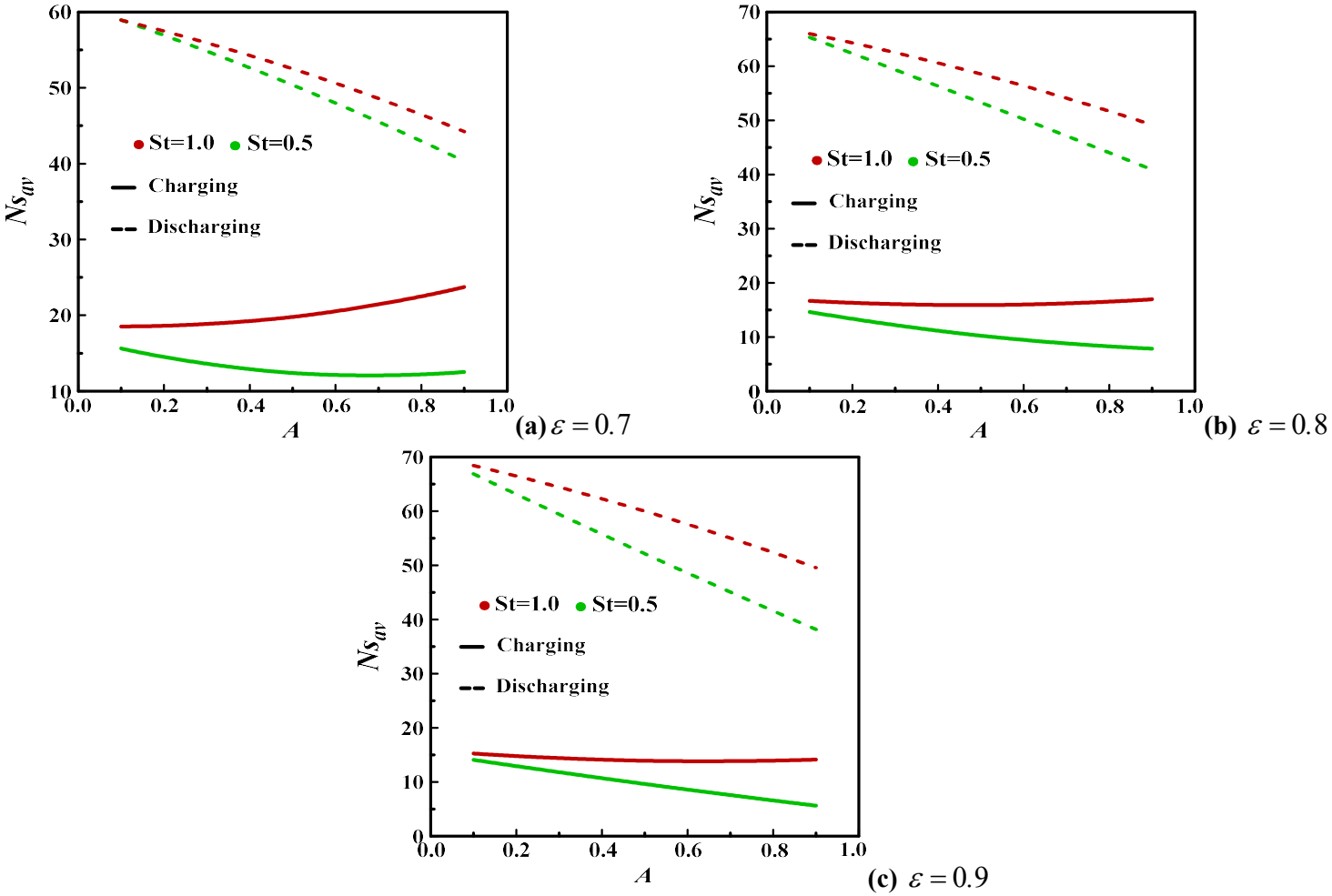

Figure 10. Strouhal number (St) and pulsating amplitude (A) effects on the average entropy, Ns_{av}, during charging and discharging processes using $Pr = 50, Re = 200, Ec = 0$.

5.6 Strouhal number, pulsating amplitude and porosity effects on the global energetic and exergetic efficiencies

To further explain the system assessment, energy and exergy analysis are plotted in figures 11 and 12. The evolution of the energetic efficiency (η) vs. ε for the three pulsating amplitude (A) values and two St is depicted in figure 11. It can be seen that a decrease in St (=0.5) enhances the performance of the system regardless of the porosity and A. Likewise, at low porosity values (=0.7), the overall energy efficiency is optimum and maximum regardless of A. Thereby, it appears that the same result is found out in this survey compared with that of Mabrouk et al. [4]. This can be explained by the fact that by decreasing the porosity of the metal structure, the interstitial heat transfer between the fluid and solid phases decreases, thereby, the energy stored reduces. However, as A increases, the system performance is greatly improves because of a higher portion of local molten PCM that absorbed and stored the energy. To compare this result with that of the work of Mabrouk et al. [4], it can be safely concluded that steady flow may be appropriates than pulsating flow owing to the instability inside the system.

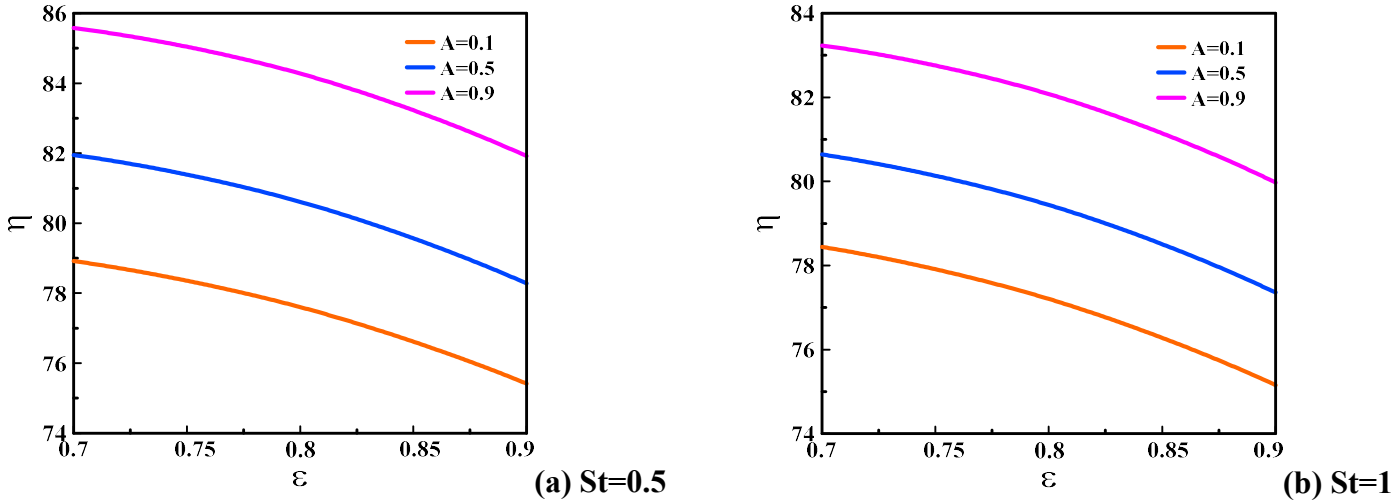

Figure 11. Strouhal number (St), pulsating amplitude (A) and porosity effects on global energetic efficiency using $Pr = 50, Re = 200, Ec = 0$.

It is admitted that the exergy evaluation of such a system is closer to the real efficiency seeing that energy losses are taken into account. Figure 12 portrays the exergetic efficiency (Ψ) evolution vs. ε for the three pulsating amplitude (A) values and the two St. As well as the first insight into this figure shows a limited and bass exergetic efficiency, where its maximum is closed in □ 22%. This revealed that the energy losses are enormous compared with the exergetic results in the Ref [4] and the above results. It was pleasantly expected that pulsating flow was strongly affected the melting/solidification phenomena in porous system than steady flow. Furthermore, from these figures, as St increases the energy losses decreases, except for A=0.1, which ameliorates the exergetic performances. As seen, at larger porosity value (=0.9), the exergetic efficiency reaches its maximum for A=0.5 and 0.9 whatever St. This demonstrated that by increasing the morphology of the metal structure (porosity), the PCM mass increases and hence, the latent heat stored augments. From the other side, it is shown that for St=0.5, the global exergetic efficiency increases inversely proportional with A regardless of the porosity, the same is seen for St=1 for $\varepsilon \leq 0.8$. Then, from ε □ 0.8 , the curves grow proportionally with A. It turned out that large St (=1) with high A value (=0.9) for high metal porosity (=0.9) reduces the heat loses and promotes the phase change phenomenon. It can be concluded that pulsating flow affected strongly the latent processes while the steady convective flow is more advantageous for LHTES system, more details can be found in Ref [4].

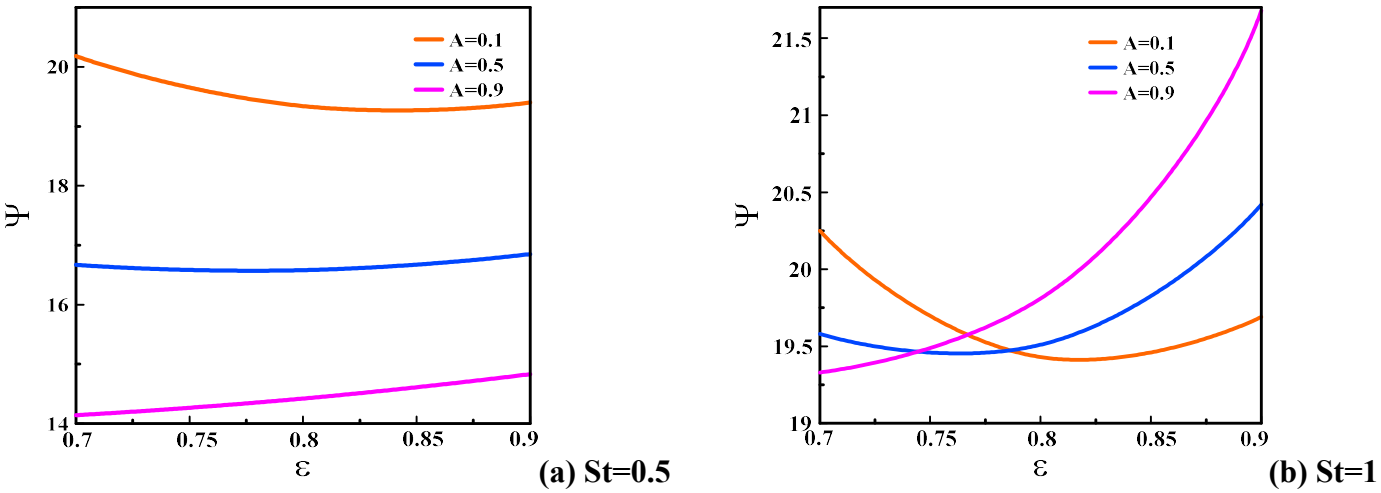

(a) St=0.5 **(b) St=1**

Figure 12. Strouhal number (St), pulsating amplitude (A) and porosity effects on global exergetic efficiency using $Pr = 50, Re = 200, Ec = 0$.

6. Conclusions

Melting and solidification processes of metal foam composite PCM were numerically examined. Enthalpy-based thermal lattice Boltzmann method was used to model the PCM's phase change features subjected to pulsating heat transfer in porous metallic domain. Dynamic and thermal development, entropy generation rate, melting front evolution and energetic and exergetic assessments of applying pulsating flow on porous LHTES system were estimated.

Main findings were drawn as below:

- The LTNE condition prevails during the discharging period regardless the parameters considered, unlike the charging process where it is valid only for St=0.5 at A=0.9 regardless of the porosity.
- During charging/discharging times, the smaller the pulsating amplitude (A), the more the forced convection mode acts the porous domain.
- High porosity value (=0.9) decelerates the pulsating velocity owing to the permeability of the medium.
- During the charging case, the temperature difference grows inversely proportional with A whatever St and porosity, but it increases proportionally with A for the discharging process because of the larger heat exchange within the domain.
- Small A value (=0.1) speeds up the melting phenomenon and the heat propagation regardless of the porosity and St.
- To reduce the irreversibility of the system, it is useful the use low St (=0.5) for discharging process with large A value (=0.9), and with small A value (=0.1) for charging period.

- The decrease of the porosity reduces the energetic efficiency, however it is improved with higher A and lower St. The interstitial heat transfer between phases strongly affected the energetic efficiency.
- The pulsating flow is responsible of a huge energy losses; limited exergy efficiency.

A comparison between this study and that of Mabrouk et al. [4] revealed the importance of applying a steady flow on LHTES system than pulsating flow.

References

[1] Mabrouk, R., Naji, H., Dhahri, H., Younsi, Z. (2020). Insight into Foam Pore Effect on Phase Change Process in a Plane Channel under Forced Convection Using the Thermal Lattice Boltzmann Method. Energies, 13 (15), 3979.

[2] Tao, Y. B., You, Y., He, Y. L. (2016). Lattice Boltzmann simulation on phase change heat transfer in metal foams/paraffin composite phase change material. Appl. Therm. Eng., 93, 476-485.

[3] Mabrouk, R., Naji, H., Dhahri, H., Hammouda, S., Younsi, Z. (2020). Numerical investigation of porosity effect on a PCM's thermal performance in a porous rectangular channel via thermal lattice Boltzmann method. Int. Comm. Heat Mass Transf., 119, 104992.

[4] Mabrouk, R., Dhahri, H., Naji, H., Hammouda, S., Younsi, Z. (2020). Lattice Boltzmann simulation of forced convection melting of a composite phase change material with heat dissipation through an open-ended channel. Int. J. Heat Mass Transf., 153, 119606.

[5] Zadeh, S. M. H., Mehryan, S. A. M., Ghalambaz, M., Ghodrat, M., Young, J., Chamkha, A. (2020). Hybrid thermal performance enhancement of a circular latent heat storage system by utilizing partially filled copper foam and Cu/GO nano-additives. Energy, 213, 118761.

[6] Zhang, C., Yu, M., Fan, Y., Zhang, X., Zhao, Y., Qiu, L. (2020). Numerical study on heat transfer enhancement of PCM using three combined methods based on heat pipe. Energy, 195, 116809.

[7] Sardari, P. T., Mohammed, H. I., Giddings, D., Gillott, M., Grant, D. (2019). Numerical study of a multiple-segment metal foam-PCM latent heat storage unit: Effect of porosity, pore density and location of heat source. Energy, 189, 116108.

[8] Esapour, M., Hamzehnezhad, A., Darzi, A. A. R., Jourabian, M. (2018). Melting and solidification of PCM embedded in porous metal foam in horizontal multi-tube heat storage system. Energy Convers. Manag., 171, 398-410.

[9] Yang, X., Bai, Q., Zhang, Q., Hu, W., Jin, L., Yan, J. (2018). Thermal and economic analysis of charging and discharging characteristics of composite phase change materials for cold storage. Appl. Energy, 225, 585-599.

[10] Zhang, P., Meng, Z. N., Zhu, H., Wang, Y. L., Peng, S. P. (2017). Melting heat transfer characteristics of a composite phase change material fabricated by paraffin and metal foam. Appl. Energy, 185, 1971-1983.

[11] Yang, X., Feng, S., Zhang, Q., Chai, Y., Jin, L., Lu, T. J. (2017). The role of porous metal foam on the unidirectional solidification of saturating fluid for cold storage. Appl. energy, 194, 508-521.

[12] Buonomo, B., Celik, H., Ercole, D., Manca, O., Mobedi, M. (2019). Numerical study on latent thermal energy storage systems with aluminum foam in local thermal equilibrium. Appl. Therm. Eng., 159, 113980.
[13] Jourabian, M., Darzi, A. A. R., Toghraie, D., ali Akbari, O. (2018). Melting process in porous media around two hot cylinders: Numerical study using the lattice Boltzmann method. Phys. A: Stat. Mech. App., 509, 316-335.
[14] Al-Sumaily, G. F., Sheridan, J., Thompson, M. C. (2013). Validation of thermal equilibrium assumption in forced convection steady and pulsatile flows over a cylinder embedded in a porous channel. Int. Comm. Heat Mass Transf., 43, 30-38.
[15] Chang, S. W., Cheng, T. H. (2021). Thermal performance of channel flow with detached and attached pin-fins of hybrid shapes under inlet flow pulsation. Int. J. Heat Mass Transf., 164, 120554.
[16] Ghalambaz, M., Zhang, J. (2020). Conjugate solid-liquid phase change heat transfer in heatsink filled with phase change material-metal foam. Int. J. Heat Mass Transf., 146, 118832.
[17] Afrouzi, H. H., Ahmadian, M., Moshfegh, A., Toghraie, D., Javadzadegan, A. (2019). Statistical analysis of pulsating non-Newtonian flow in a corrugated channel using Lattice-Boltzmann method. Phys. A: Stat. Mech. App., 535, 122486.
[18] Bayomy, A. M., Saghir, M. Z. (2016). Heat transfer characteristics of aluminum metal foam subjected to a pulsating/steady water flow: Experimental and numerical approach. Int. J. Heat Mass Transf., 97, 318-336.
[19] Al-Sumaily, G. F., Thompson, M. C. (2013). Forced convection from a circular cylinder in pulsating flow with and without the presence of porous media. Int. J. Heat Mass Transf., 61, 226-244.
[20] Hacen, D., Boughamoura, A., Nasrallah, S. B. (2006). Forced pulsating flow and heat transfer in a tube partially filled with a porous medium. J. Porous Media, 9 (1).
[21] Li, X., Ma, T., Liu, J., Zhang, H., Wang, Q. (2018). Pore-scale investigation of gravity effects on phase change heat transfer characteristics using lattice Boltzmann method. Appl. Energy, 222, 92-103.
[22] Jiaung, W. S., Ho, J. R., Kuo, C. P. (2001). Lattice Boltzmann method for the heat conduction problem with phase change. Numer. Heat Transf.: Part B: Fund. (2), 167-187.
[23] Huber, C., Parmigiani, A., Chopard, B., Manga, M., Bachmann, O. (2008). Lattice Boltzmann model for melting with natural convection. Int. J. Heat Fluid Flow, 29 (5), 1469-1480.

[24] Gao, D., Chen, Z., Chen, L. (2014). A thermal lattice Boltzmann model for natural convection in porous media under local thermal non-equilibrium conditions. Int. J. Heat Mass Transf., 70, 979-989.

[25] Kebriti, S., Moqtaderi, H. (2021). Numerical simulation of convective non-Newtonian power-law solid-liquid phase change using the lattice Boltzmann method. Int. J. Therm. Sci., 159, 106574.

[26] Nield, D. A., Bejan, A. (2013). Convection in Porous Media, 4th ed., Springer-Verlag, New York.

[27] Xu, A., Shi, L., Xi, H. D. (2019). Lattice Boltzmann simulations of three-dimensional thermal convective flows at high Rayleigh number. Int. J. Heat Mass Transf., 140, 359-370.

[28] Joshi, V., Rathod, M. K. (2019). Constructal enhancement of thermal transport in metal foam-PCM composite-assisted latent heat thermal energy storage system. Numer. Heat Transf., Part A: App., 75 (6), 413-433.

[29] Chen, C. C., Huang, P. C., Hwang, H. Y. (2013). Enhanced forced convective cooling of heat sources by metal-foam porous layers. Int. J. Heat Mass Transf., 58 (1-2), 356-373.

[30] Ranjbaran, Y. S., Haghparast, S. J., Shojaeefard, M. H., & Molaeimanesh, G. R. (2020). Numerical evaluation of a thermal management system consisting PCM and porous metal foam for Li-ion batteries. J. Therm. Anal. Calorim., 141(5), 1717-1739.

[31] Boomsma, K., Poulikakos, D. (2001). On the effective thermal conductivity of a three-dimensionally structured fluid-saturated metal foam. Int. J. Heat Mass Transf., 44(4), 827-836.

[32] Boomsma, K., Poulikakos, D. (2011). Corrigendum for the paper: K. Boomsma, D. Poulikakos,“On the effective thermal conductivity of a three-dimensionally structured fluid-saturated metal foam”[International Journal of Heat and Mass Transfer, 44 (2001) 827–836]. Int. J. Heat Mass Transf., 1 (54), 746-748.

[33] Torabi, M., Karimi, N., Peterson, G. P., Yee, S. (2017). Challenges and progress on the modelling of entropy generation in porous media: a review. Int. J. Heat Mass Transf., 114, 31-46.

[34] Dincer, I., Rosen, M. A. (2011). Thermal Energy Storage: Systems and Applications, 2nd ed., John Wiley & Sons.

[35] Rosen, M. A., Dincer, I. (2009). Efficiency assessment of glycol cold thermal energy storage and effect of varying environment temperature. Trans. Can. Soc. Mech. Eng., 33 (1), 119-130.

[36] Hänchen, M., Brückner, S., & Steinfeld, A. (2011). High-temperature thermal storage using a packed bed of rocks–heat transfer analysis and experimental validation. Appl. Therm. Eng., 31 (10), 1798-1806.
[37] Rosen, M. A. (2001). The exergy of stratified thermal energy storages. J. Sol. Energy, 71 (3), 173-185.
[38] Erek, A., & Dincer, I. (2008). An approach to entropy analysis of a latent heat storage module. Int. J. Therm. Sci., 47 (8), 1077-1085.
[39] Guo, Z., Zheng, C., Shi, B., Zhao, T. S. (2007). Thermal lattice Boltzmann equation for low Mach number flows: Decoupling model. Phys. Rev. E, 75 (3), 036704.
[40] Li, L., Mei, R., Klausner, J. F. (2017). Lattice Boltzmann models for the convection-diffusion equation: D2Q5 vs D2Q9. Int. J. Heat Mass Transf., 108, 41-62.
[41] Shi, Y., Zhao, T. S., Guo, Z. L. (2004). Thermal lattice Bhatnagar-Gross-Krook model for flows with viscous heat dissipation in the incompressible limit. Phys. Rev. E, 70 (6), 066310.
[42] Zou, Q., He, X. (1997). On pressure and velocity boundary conditions for the lattice Boltzmann BGK model. Phys. Fluids, 9 (6), 1591-1598.
[43] Kumar, C. S., Mohankumar, S., Geier, M., Pattamatta, A. (2017). Numerical investigations on convective heat transfer enhancement in jet impingement due to the presence of porous media using cascaded lattice Boltzmann method. Int. J. Therm. Sci., 122, 201-217.
[44] Ladd, A. J. (1994). Numerical simulations of particulate suspensions via a discretized Boltzmann equation. Part 1. Theoretical foundation. J. Fluid Mech., 271, 285-309.
[45] Mohamad, A. A. (2011). Lattice Boltzmann Method: Fundamentals and Engineering Applications with Computer Codes, Second edition, Springer-Verlag, London.
[46] Krishnan, S., Murthy, J. Y., Garimella, S. V. (2005). A two-temperature model for solid-liquid phase change in metal foams. J. Heat Transf., 127, 995-1004.

General conclusion

Due to the enormous consumption of thermal energy by humanity, any amelioration in thermal energy management operations can greatly meet the society requirements. Among the primordial tools in thermal energy management, thermal energy storage (TES) figures as the most important key. Thereby, this dissertation provides an overview of the state-of-the-art of TES technologies for a better understanding of different approaches related to this topic. A particular attention kept focus on sensible heat storage (SHS) and latent heat storage (LHS) methods. Therefore, the main object of this thesis is to find the new challenges in storing the sensible and latent energy through the use of porous metallic matrices, by using a numerical method: Lattice Boltzmann method (LBM).

The physical model with Cartesian coordinates system deemed in this report is the model considered to analyze physical phenomena. It was a two-dimensional laminar flow and heat transfer in an open-ended horizontal porous channel (metal foam) including either a phase change material (to deal with LHS process) or liquid water (to deal with SHS process) subjected to forced convection. To gain further insight into the effect of different relevant parameters on system thermal performances during charging/discharging cycles, The Darcy-Brinkmann-Forchheimer (DBF) unsteady flow model and the one with two temperature equations based on the local thermal non-equilibrium (LTNE) have been solved. The single relaxation time-thermal lattice Boltzmann method (SRT-TLBM) with triple distribution function (TDF) at the representative elementary volume (REV) scale has been employed to perform all numerical simulations.

In the first part of this thesis, the sensible and latent heat storage solutions using porous media strategy are reviewed from the aspect of the numerical T-LBM approach. It was highlighted that the porosity figures as one of the most significant parameters that greatly influences the performance of the SHS and LHS systems. In addition, it was indicated that phase change materials (PCMs) used in LHS devices store 5 to 14 times more energy than sensible heat storage materials (SHSMs) used in SHS systems. Moreover, LBM at the pore-scale and REV scale approaches presents a robust ability to handle these two TES mechanisms.

In fact, in the second part, a numerical study has been performed using the SRT-LBM at the REV scale. The open-ended straight channel is filled with a porous metal foam structure and paraffin as a PCM. The numerical outcomes obtained were used to investigate the porosity ($0.1 \le \varepsilon \le 0.8$), Reynolds number ($100 \le \mathrm{Re} \le 600$) and Eckert number ($0 \le Ec \le 10$) effects on dynamic and thermal fields, entropy generation and energy and exergy efficiencies of the considered system during the melting and solidifying processes of PCMs. Validations

of the TLBM code with relevant previous studies have shown good agreement. Furthermore, it was revealed that the decrease in the porosity accelerates the melting/solidifying phenomenon owing to the high thermal conductivity of the metal foam and improves energy and exergy efficiencies of the system. Besides, at large Re and Ec numbers, the melt front progression is much faster.

The third part of this thesis carried out a numerical investigation of the metal foam pore density effect ($10 \le PPI \le 60$) on sensible and latent heats storage using the SRT-TLBM approach at the REV scale. Two physical models have been investigated: an open-ended rectangular porous channel filled with metal foam saturated either with PCMs: paraffin (model 1; LHS unit) or with liquid water (model 2; SHS unit). Based on the findings presented, it was shown that to reduce the system irreversibility of the models deemed, low PPI value (= 10) is recommended during the charging process, while a high value (PPI = 60) should be used during the discharging period. However, the decrease in Re number improves the energy and exergy efficiencies for both models. In addition, the increase in PPI reduces energy losses for the SHS system and thereby, enhances the quality of the stored energy.

Finally, this dissertation performed a numerical assessment of the porosity (0.7, 0.8 and 0.9), pulsating amplitude (A=0.1, 0.5 and 0.9) and Strouhal number (St=0.5 and 1) effects on heat transfer under pulsating forced convection in an open-ended horizontal channel filled with a porous metal foam structure and a PCM. The results highlighted that small A value (=0.1) accelerates the melting phenomenon and the heat propagation whatever the porosity and St number. On the other hand, small porosity reduces the energetic efficiency. However, higher A and lower St enhance the thermal performances of the system. It was found that the pulsating flow parameters play a key role in increase or decrease of the energy losses.

Despite the huge results achieved in the field of SHS and LHS technologies, there are gaps in some areas of these topics. Thereby, some future recommendations in this topic are listed below:

- The two-dimensional physical model can be developed to a three dimensional model to accentuate further details.
- The SRT-TLBM approach can be extended to the MRT-LBM approach.
- The latent and sensible heat storage mechanisms can be developed in micro-porous systems.
- Detailed studies on the environmental effects of these systems are required.
- Economical studies and cycle life parameter of TES systems are required.

Nomenclature

A	Pulsating amplitude
a_{sf}	Specific solid-fluid interfacial area (m^{-1})
Be	Bejan number
Bi	Biot number, $Bi = h_{sf} a_{sf} H^2 / \lambda_s$
Br	Brinkmannumber, $Br = Pr.Ec$
c	Lattice speed ($m.s^{-1}$)
C_p	Specific heat capacity at constant pressure ($KJ.Kg^{-1}.K^{-1}$)
c_s	Sound speed ($m.s^{-1}$)
$\overline{\overline{D}}$	Strain tensor (s^{-1})
Da	Darcy number, $Da = K / H^2$
d_f	Ligament diameter (m)
d_p	Average pore diameter (m)
Ec	Eckert number, $Ec = Uo^2 / (C_f . \Delta T_{ref})$
e_i	Discrete velocity in direction *i*
F_ε	Forchheimer form coefficient
F	Body force per unit mass ($N.Kg^{-1}$)
F_{ei}	Discrete body force in direction *i* ($Kg.m^{-3}.s^{-1}$)
f_i, g_i	Distribution function in direction *i*
f_i^{eq}, g_i^{eq}	Equilibrium distribution function in direction *i*
$\breve{f}$	Pulsating frequency (Hz)
H	characteristic length scale (m)
h_{sf}	Interfacial heat transfer coefficient ($W.m^{-2}.K^{-1}$)
K	Porous medium permeability (m^2)
K_R	Thermal conductivity ratio, $K_R = \lambda_s / \lambda_f$
L_a	Latent heat ($J.Kg^{-1}$)
Ns	Entropy generation number
p	Pressure (Pa)
P	Dimensionless pressure
Pr	Prandtl number, $Pr = \nu_f / \alpha_f$
Re	Reynolds number, $Re = u_{in} H / \nu_f$
Re_d	Particle Reynolds number, $Re_d = \sqrt{U^2 + V^2}\, d_f / \varepsilon \nu_f$
Rc	Heat capacity ratio, $Rc = (\rho C_p)_s / (\rho C_p)_f$
Ste	Stefan number, $Ste = C_p (T_h - T_m) / L_a$
St	Strouhal number, $St = \breve{f} H / U_0$
T	Temperature (K)
T_m	PCM melting temperature (K)
Θ	Dimensionless temperature
t	Time (s)
u, v	Velocity ($m.s^{-1}$)
U, V	Dimensionless velocity
x, y	Cartesiancoordinates (m)

w	Pulsation (rad.s^{-1})
X, Y	Dimensionless coordinates
Greek symbols	
∇	Gradient operator
$\nabla.$	Divergence operator
∇^2	Laplacian operator
Δx	Lattice step
Δt	Time step
$\overline{\overline{\tau}}$	Stress tensor (Pa)
α	Thermal diffusivity ($m^2.s^{-1}$)
ε	Media porosity
η	Energy efficiency
λ	Thermal conductivity ($W.m^{-1}.K^{-1}$)
μ_f	Dynamic fluid viscosity ($Kg.m^{-1}.s^{-1}$)
Γ	PCM's melting fraction
ν	Kinematicviscosity ($m^2.s^{-1}$)
ω	Pore density (PPI)
ψ	Exergy efficiency
ρ	Density ($Kg.m^{-3}$)
$\tilde{t}$	Dimensionless time
τ	Dimensionless relaxation time
w_i	Weight coefficient in direction i
Superscripts/subscripts	
f	Fluid
s	Solid
h	Hot
m	Melting
o	Initial state
in	Inlet
out	Outlet
Ref	Reference